Studies on Nonlinear and Dynamic Soil Structure Interaction

by

Hesham Elhuni

A thesis
presented to the University of Waterloo
in fulfillment of the
thesis requirement for the degree of
Doctor of Philosophy
in
Civil Engineering

Waterloo, Ontario, Canada, 2023

Examining Committee Membership

The following served on the Examining Committee for this thesis. The decision of the Examining Committee is by majority vote.

External Examiner:	Sai Vanapalli Professor, Department of Civil Engineering University of Ottawa
Supervisor(s):	Dipanjan Basu Professor, Department of Civil & Environmental Engineering University of Waterloo
Internal Member:	Hassan Baaj Professor, Department of Civil & Environmental Engineering University of Waterloo
Internal Member:	Giovanni Cascante Professor, Department of Civil & Environmental Engineering University of Waterloo
Internal-External Member:	Hamid Jahed Professor, Department of Mechanical & Mechatronics Engineering University of Waterloo

Author's Declaration

I hereby declare that I am the sole author of this thesis. This is a true copy of the thesis, including any required final revisions, as accepted by my examiners.

I understand that my thesis may be made electronically available to the public.

Abstract

High-speed trains, excessive loads in moving trucks, and vibrating machines on foundations on soft ground can generate significant vibration and deformation in the subgrade (soil). Better understanding and realistic analysis of the interaction between railway tracks, pavements, and foundations and the supporting soil under moving and dynamic loads is necessary. Experimental investigations are always associated with large costs when simulating the loading conditions. Modeling dynamic soil-structure interaction problems is often associated with a high level of complexity and a large computational effort. Analytical modeling of these problems that results in accurate and reliable prediction of these soil structure interaction problems with a low computational cost and ease of use is a distinct advantage that can supplement the numerical modeling and experimental investigations.

In this research, a new computationally efficient but mathematically rigorous semi-analytical continuum model is developed for dynamic analysis of beams resting on layered poroelastic nonlinear soil deposit and subjected to dynamic loads. The proposed model is developed in stages in terms of the complexity of simulating the soil behaviour. First, the soil is simulated as a discrete two-parameter foundation in which the soil body is represented by mechanical springs with shear interactions. Subsequently, the soil is simulated as a linear and nonlinear continuum. Finally, the soil is simulated as a linear and nonlinear poroelastic continuum, For the continuum-based analysis, a simplified continuum approach was adopted in which the soil displacement field is expressed as a product of separable variables. The principle of virtual work was applied to obtain the governing differential equations that were solved partly analytically and partly numerically. The semi-analytical approach was found to be significantly faster than the corresponding full blown finite element analysis.

A significant contribution of this work is the simulation of the nonlinear and poroelastic response of soil in the semi-analytical framework, which otherwise require elaborate meshing by the users and high computational effort. A nonlinear hyperbolic stress-strain relationship is used to represent the soil nonlinearity. Biot's poroelastic theory is used to represent the poroelastic behaviour of soil. The nonlinear dynamic, nonlinear consolidation, and nonlinear poroelastic dynamic responses of the beams under moving and oscillating loads are obtained. It is envisaged that the methods developed in this thesis will provide more insights into the dynamic soil structure interaction problem, and will help in developing design aids.

Acknowledgements

I would like to express my gratitude to my supervisor, Prof. Dipanjan Basu, for his guidance, encouragement, and support throughout my Ph.D. research. I am grateful to the members of the Examining Committee who graciously consented to read and comment on my thesis: Professor Hassan Baaj, Professor Giovanni Cascante, Professor Hamid Jahed, and Professor Sai Vanapalli. In addition, I truly appreciate the support and the help from Professor Adil Al-Mayah; the graduate chair of the civil engineering department. Finally, I would also like to thank my mother, my wife and all my friends and family who supported me during my academic years. .

Dedication

Mom, this is for you. Thank you for the many sacrifices, prayers, and love!

Table of Contents

List of Figures

List of Tables

Chapter 1

Introduction

1.1 General

All structural and mechanical systems transmit their loads to the supporting soil through foundations. Modeling the interaction between foundations and soil is a key factor in the analysis of foundation-soil systems [15]. In the field of civil, structural, and geotechnical engineering, interaction between foundation elements and soil is often referred to as soil-structure interaction. The problem of a beam on elastic foundation (BOF) is a classical soil-structure interaction problem, and it is relevant to many disciplines in engineering related to roads, railroads, marine engineering, bio-mechanics, structural engineering, and geotechnical engineering [24].

Research related to soil dynamics have shown that high-speed trains, heavily loaded moving vehicles and vibrating machines on soft grounds can generate significant increase in vibration levels within the soil [13, 23, 26, 52]. These induced excessive vibrations can drive the supporting system (foundation and soil) to oscillate with large amplitudes at specific frequencies resulting in resonance, thereby endangering the infrastructure and humans. A better understanding and modeling of the interactive behavior between the foundations and supporting subgrade to capture such dynamic responses. Many of these problems can be modeled as beams vibrating on underlying soil and subjected to a variety of dynamic loads. Experimental investigation of such dynamic beam-soil interaction problems is usually associated with large cost and limitations in simulating all possible loading and soil conditions. In contrast, numerical studies are cost effective and relatively faster. However, studying dynamic soil-structure interaction problems using numerical methods in three dimensional (3-D) and two dimensional (2-D) computational frameworks is usually associ-

ated with a high level of complexity and large computational effort, particularly because of the nonlinearity exhibited by soil. Alternatively, a precise, simplified, and reliable analytical and semi-analytical modeling framework for dynamic beam-soil interaction analysis has a distinct advantage from computational efficiency and ease of use points of view.

Many soil spring models and soil continuum-based analytical and semi-analytical models have been proposed for the beam on foundation BOF theories used to investigate these soil structure interaction problems [22, 14, 259]. In the soil spring models, the beam is assumed to rest on a bed of soil springs – the springs represent the resistance offered by the underlying soil to beam displacement or motion. In the soil continuum models, the soil is assumed to behave as a continuum, often with a variety of simplified assumptions.

The existing models are often empirically based and lack rigour [220, 45]. For example, most BOF model does not account for the stress-strain nonlinearity of soil [227, 233, 102]. The spring-based models cannot represent the soil behaviour in its totality [242]. Most continuum based analytical models are complex and usually are used to investigate the effect of static loads with the assumption that soil behaves as linear elastic material [237, 25]. The modified Vlasov foundation model is relatively simple to interpret and has the potential to account for a variety of realistic soil behavior (e.g., nonlinearity and poroelasticity) that other analytical models does not have [219, 86]. However, a unified continuum-based analytical approach that can incorporate soil nonlinearity and poroelasticity and model the inertia-based dynamic interaction of beam with the soil is lacking in the literature [211, 217, 88].

In this thesis, the approach of modified Vlasov model is adopted to investigate the beam-soil interaction under a variety of static and dynamic loads and under a variety of soil conditions considering soil poroelasticity and nonlinearity. The proposed approach is developed in stages in terms of the complexity of simulating the soil behaviour. First, the soil is modeled using two-parameter spring model in which the soil offers resistance from compression and shear. Then, the model is improved by simulating the soil as a linear elastic continuum, defined with two elastic constants. The model is further enhanced by considering soil heterogeneity and material nonlinearity into the soil continuum. Appropriate nonlinear constitutive models for different soil types are incorporated into the model. Next nonlinear poroelasticity based on Biot's theory is introduced into the soil continuum so that long-term time-dependent consolidation settlement can be modeled for static loads. Finally, the inertia forces are incorporated into the nonlinear poroelastic model to capture the consolidation settlement of beams under dynamic loads.

In this chapter, a brief literature review is presented on the different aspects of the beam on foundation problem. A generic review is presented in this chapter with detailed topic-

specific reviews provided in subsequent chapters. Subsequently, the gaps in the literature is pointed out in this chapter followed by a description of the research objectives and tasks.

1.2 Spring-Based Mechanical Soil Models for BOF Problems

1.2.1 One-Parameter (Winkler) Model

The most fundamental and oldest model was proposed by Winkler (1867) [255] in which a local linear proportionality between the vertical ground displacement and the reaction from the soil was assumed. Thus, the surface soil displacement is directly proportional to the applied distributed load at that point and such a relationship is completely independent of the loads and/or displacements at other neighboring points in the soil. Thus, the soil is idealised as a bed of linear vertical closely-spaced springs [34, 107, 220, 245] in which the stiffness of the spring k_s characterize the compressive stiffness of the soil. This model is also sometimes called the one-parameter model. The model parameter k (which is the spring constant) is often related to the soil subgrade modulus [34, 98, 220, 45, 68, 104].

The mathematical representation of Winkler's model is given by Equation 1.1. This equation is used with the beam on foundation equation given by Equation 1.2. The deformation pattern of the model is shown in Figure 1.1. When both the equations are combined, the final differential equation is given by Equation 1.3.

$$q_s(x) = k_s w(x) \tag{1.1}$$

$$E_b I_b \frac{d^4 w}{dx^4} + q_s - q = 0 \tag{1.2}$$

$$E_b I_b \frac{d^4 w}{dx^4} + k_s w = q \tag{1.3}$$

where x is the horizontal distance (coordinate) along the beam, $q_s(x)$ is the contact pressure, k_s is the soil spring constant, $w(x)$ is the beam or soil surface displacement, $E_b I_b$ is the flexural rigidity of the beam, and $q(x)$ is the applied load.

The main deficiencies for this model are:

- The discontinuous behaviour of the surface displacement restricts the application of the model to non-cohesive soils in which the interaction between soil springs is not significant [95].
- The shear interaction between soil springs is neglected so that continuity of soil displacement beyond the loaded region is not maintained [9].
- The spring parameter is determined empirically using subgrade reaction modulus or otherwise with ad hoc assumptions [26].

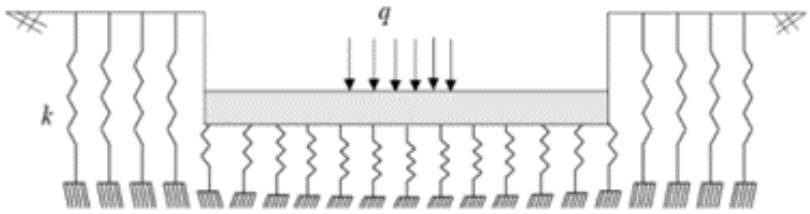

Figure 1.1: The deformation pattern of Winkler's foundation

1.2.2 The Two-Parameter Model (Pasternak Type Foundation)

A better idealization of the soil was proposed by Filonenko-Borodich (1945) [92] and Pasternak (1954) [177], in which the Winkler springs were connected following different idealizations. Pasternak (1954) [177] assumed a shear element connecting the springs while Filonenko-Borodich (1945) [92] assumed a thin elastic membrane with a constant tension connecting Winkler springs. Several other authors made several different assumptions [125, 267, 61, 66, 174]. The ensuing models had the same mathematical form and can be called two-parameter models in which two parameters k_s and t_s are used to represent the mechanical behaviour of soil. These models provide a continuity of soil displacement between the loaded and unloaded regions. The differential equation for all the two parameter models is given by

$$q_s(x) = k_s w(x) - 2t_s \frac{d^2 w(x)}{dx^2} \tag{1.4}$$

where t_s is the second parameter and can be interpreted in different ways depending on the model used. In this study, we interpret t_s as soil shear parameter because soil resistance arises from shear and compression, and k_s represents compressive (spring) resistance.

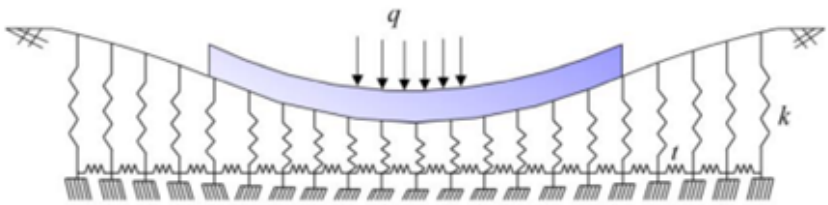

Figure 1.2: The deformation pattern of Pasternak foundation

1.2.3 Multi-Parameter Models

Kerr (1964) [125] presented a three-parameter model to describe elastic soils. The model consists of two horizontal layers of vertical springs separated by a shear strip layer and based on the work of Reissner (1958) [190] who proposed two layers of vertical springs interconnected by a horizontal shear layer. This model is too complicated because of excess parameters and are not widely used. Recent studies based on discrete soil models are summarized in Table 1.1.

1.3 Continuum Based Soil Models for BOF Problems

The main difficulty with the discrete models is that the spring parameters are often empirically determined and not accurate enough so that the resulting beam-soil responses are often not reliable. Moreover, springs cannot represent the actual mechanical behavior of soil. Therefore, the soil underneath the beams has been represented by several researchers as an elastic continuum characterized by the elastic constants, Young's modulus E, and Poisson ratio v. A variety of models have been developed based on the continuum approach.

Table 1.1: Summary of the literature map and the filled-research gaps for BOF models

Soil Model		**Solution form**	**Beam domain**		**Response**			**Soil behaviour**		**Soil material phase**	
			infinite	**finite**	**Static**	**SSD***	**TDD***	**Linear**	**Nonlinear**	**Soil porous**	
										Quasi static	**Dynamic**
Mechanical (Discrete springs)	One-Parameter (Winkler)	Analytical	[34, 94]	[135]	[92]	[94]	[268]	[33]	[30]	Not applicable	
		Semi-analytical	[257]	[226]			[119]		[104]		
	Two-parameter (Pasternak)	Analytical	[177, 26, 9]	Chapter 2	[9, 170]	[121]	[223, 83]	[132, 239]	[249]	Not applicable	
							Chapter 2				
		Semi-analytical	[170]	[61]	[259]	[184]	[134]	[223]	[110, 75]		
	Multi-parameter	Analytical	Does not exist							Not applicable	
		Semi-analytical	[128]	[125, 149]	[15]	[13]	[23]	[114]	[152]		
Continuum	ModifiedVlasov's	Analytical		[236]	[242]	Does not exist		[240]	Does not exist		
		Semi-analytical		[16, 236]	[116, 236]	[173]	[12]	[179, 153, 219]	[102] (static)	[179] (Linear)	Chapter 7
					Chapter 3	Chapter 4	Chapter 4		Chapter 5	Chapter 6	
	Elastic half-space	Analytical	[222]	[7]	[228]	Does not exist		[?]	Not applicable	[207]	Does not exist
		Semi-analytical	[115, 258, 6]	[3, 22, ?]	[235, 22]	[48, 137]		[?]			

Note:SSD :Steady state (dynamic), TDD: Time-dependent (dynamic)

1.3.1 The Elastic Half-Space Model

One way, the soil is modeled is based on the concept of elastic half space, in which the soil is assumed to be an elastic isotropic and homogeneous solid/continuum extending to infinity in all directions except the upward vertical direction. The initial idea for the elastic half-space continuum model is attributed to Boussinesq (1885) [44], which was refined by Biot (1937) [34] and improved by Protsenko and Rvachev (1976) [183]. However, Reissner (1936) [190] was the first to apply the theory to dynamic analysis of beams on elastic foundation after which many approximate solutions have been developed by several authors [22, 6, 51, 7, 49]. Although, approximate solutions have been developed in the literature using this approach, many practical limitations were reported because of the mathematical complexity associated with the solutions using this method. In most practical situations, the deformable soil layer, under consideration, is bounded by a rigid base at a specified depth. This is not strictly considered in the half-space theory. Moreover, the half-space approach does not account for soil nonlinearity and damping effect. An assumed contact pressure distribution is necessary in the formulation of the governing equations and shear strain energy of soil is neglected, which are limitations [252, 73, 206, 263].

For dynamic analysis, the problem of beam resting on an elastic half space is complicated as it usually requires solving both the equation of motion of beam subjected to dynamic loads, as described by Equation 1.5, and an equation of Rayleigh wave propagating in layered elastic media, as proposed by Kausel and Roesset (1981) [123] and described by Equation 1.6. Equations 1.5 and 1.6 are coupled with the condition that the vertical displacement of the beam axis $w(x,t)$, and the surface displacement u_z of the half-space under it should be identical

$$E_b I_b \frac{\partial^4 w(x,t)}{\partial x^4} + \rho_b \frac{\partial^2 w(x,t)}{\partial t^2} - p(x,t) = 0 \tag{1.5}$$

$$\mu \Delta u_i + (\lambda + \mu) \nabla div(u_i) - \rho_s \frac{\partial^2 u_i}{\partial t^2} = 0 \tag{1.6}$$

where ρ_b is the mass density of the beam, u_z is the transverse beam displacement or the vertical surface soil displacement, $p(x,t)$ is the applied dynamic load, μ and λ are lame's constants, ρ_s is the mass density of the soil, and u_i is the soil displacement vector of the half space such that $u_i = (u_x, u_y, u_z)$.

1.3.2 Vlasov's Model

Unlike the pervious models proposed by several researchers who attempted to improve the Winkler model, the simplified continuum model by Vlasov and Leont'ev (1966) [247] developed using variational calculus method gave a precise representation of soil parameters k_s and t_s in Equation 1.3 in terms of the soil geometry and its properties (soil modulus of elasticity E_s, and Poisson ratio υ_s). The parameters in Vlasov's model account for the effect of the shear-strain energy in soil, and demonstrated the importance of the shear forces on the edges that come from the surrounding soil which was neglected in the elastic half-space model. Vlasov and Leont'ev (1966) [247] proposed a trial parameter γ that characterizes the vertical deformation profile within the soil continuum. This parameter is related to the a priori assumed vertical displacement decay function $\phi(z)$ as

$$\phi(z) = \frac{sinh\gamma(1 - \frac{z}{H})}{sinh\gamma} \tag{1.7}$$

Mathematically, the model is analysed by solving Equations 1.2, 1.3, and 1.7. However, the soil parameters k_s and t_s are related mechanistically to the soil properties through Equations 1.8 and 1.9, although the reliability of the model is still questionable because of its dependency on the trial parameter γ.

$$k_s = \frac{E_s b\gamma(1 - \upsilon_s)}{2(1 + \upsilon_s)(1 - 2\upsilon_s)} \tag{1.8}$$

$$t_s = \frac{E_s b}{8\gamma(1 + \upsilon_s)} \tag{1.9}$$

where b is the beam width and h is the thickness of the soil layer.

1.3.3 Modified Vlasov's Model

Vallabhan & Das 1991 [242] improved the model of Vlasov and Leont'ev (1966) [247] by introducing an iterative procedure of determining the vertical displacement decay function $\phi(z)$ without a priori assumption. According to Vallabhan & Das 1991 [242], the soil parameters k_s and t_s are given by

$$k_s = b \int_0^H E_s \left(\frac{d\phi}{dz}\right)^2 dz \tag{1.10}$$

$$t_s = \frac{b}{2}\int_0^H G_s \phi^2 dz \tag{1.11}$$

where E_s and G_s are the Young's modulus and the shear modulus of the soil.

1.4 Studies on Analysis of BOF Problems

1.4.1 Studies Based on Spring-Based Mechanical Soil Models

Spring-based mechanical soil models have been extensively used for the analysis of BOF problems. Akoz and Ergun 2012 [9], Daloglu and Vallabhan 2000 [68], Avramidis and Morfidis 2006 [15], Coskun et. Al 2008 [174], Chiwanga and Valsangkar 1988 [61], and others adapted the spring-based mechanical soil models for static analysis. In many cases, however, the beam-foundation system is subjected to dynamic loads in which the vibration (inertia) effects amplify the deformations in the system [184]. Such dynamic loads may arise from oscillatory or moving loads. Often because of high design speed associated with modern transportation projects, recent research outcomes have characterized the dynamic-resonance phenomena as the main deriving force for structural damages in railway track and pavement structures [132].The dynamic response of beams on two-parameter soil has also been the subject of many studies in the literature; Timoshenko et al. (1974) [227], Saito & Terasawa (1980) [196], Zhaohua & Cook (1983) [267], Ono & Yamada (1989) [171], Trochanis et al. (1987) [231], Chiwanga & Valsangkar (1988) [61], Lin & Trethewey, (1990) [151], Fryba et al. (1993) [94], Thambiratnam & Zhuge, (1996) [223], Sun & Luo (2008) [218], Teodoru & Musat (2010) [219], Raftoyiannis et al. (2012) [184], Uzzal et al. (2012) [239], Akoz & Ergun (2012) [9], Worku (2012) [257], Omolofe (2013) [170], Basu & Kameswara, (2013) [26], Kumari et al. (2012) [132], Patil et al. (2013) [178], Sapountzakis & Kampitsis (2013) [202], Limkatanyu et al. (2013) [149], and Jorge et al. (2015) [118]. In most of these studies, the effect of the velocity of the moving load, the stiffness of the foundation, and the damping of the system on the deflection dynamic amplification factor are studied for both steady state and time dependent problems. However, the reliability of the results is questionable because the model parameters k_s and t_s are determined empirically. Additionally, most of these studies were considered beams with infinite length which simulate the study state response.

1.4.2 Studies Based on Half-Space Model

The Elastic Half-Space model has been proposed for the modeling of BOF dynamic problems with infinite/semi-infinite soil depths. In order to simplify this type of model, researchers presented different idealization with respect to the soil continuum [21, 103, 59, 74, 6, 52, 51, 7, 49]. In these models, the foundation is assumed as linear isotropic elastic continuum, linear anisotropic elastic continuum, and linear inhomogeneous elastic continuum. Beams and plates have been assumed as the structural parts. But these simplified models are still complicated to be used. In a recent study by Chahour et al. (2017) [56], the problem of train moving on multilayered poroviscoelastic soil deposit was analysed by introducing a semi-analytical modular model. The proposed model consisted of two sub models. The first sub model is a mechanical discrete (sandwich model) model, which was first introduced by Sheng et al. (1999) [210] to calculate the loads induced by the train axles. These induced loads are then used to analyse a multilayered poro-viscoealstic half space sub model by solving the equations of wave propagation through the soil media. He et al. (2014) [106] developed an approximate solution for the interaction between an infinite beam subjected to harmonic moving load and a poroelastic half space. The method of integral transformation was implemented to solve the differential equations for the both the beam and the elastic half space. Lefeuve-Mesgouez and Mesgouez (2012) [137], also studied the steady state response of an infinite beam resting on multilayered poroelastic half space based on Helmholtz decompositions, Fourier transforms and a matrix formulation technique in terms of incident and reflected waves for the layers.

1.4.3 Studies Based on Modified Vlasov Model

Some researchers adopted the modified Vlasov model for static analysis of beam on elastic foundation. Vallabhan & Das (1991) [242] implemented the modified Vlasov model in the axisymmetric analysis of circular tank foundations resting on a single elastic soil layer. A consistent finite element model to study the static behaviour of rectangular plates resting on layered soil deposit was also presented by Vallabhan & Daloglu (1999) [241]. Within the framework of modified Vlasov model, the steady state response of pavement-subgrade system under traffic was studied by Liang & Zhu (1995) [147] although their analysis has some errors. One main limitation in this study is the introduction of the time variable in the mode displacement function, which invalidates the analysis. Ayvaz & Ogzgan (2002) [16] applied the modified Vlasov model in study of the free vibration response of beams on elastic foundations problem. The study showed that the depth of soil contributing to the vibration has a major effect on the natural frequencies of the system, which also affect the

deformation of the beam.

The reliability of the modified Vlasov model in the analysis of beam on elastic foundation was studied comprehensively by Teodor & Muşat (2010) [219]. The results from the modified Vlasov model were found to be in a good agreement with those form the 2D finite element model, but slightly conservative results were obtained using the modified Vlasov model. Liu & Ma (2013) [153] extended the modified Vlasov model by incorporating both vertical and horizontal soil displacements and analyzed beams subjected to both horizontal and vertical static loads. The modified Vlasov foundation is adopted to model the layered soil continuum in this thesis. A brief review of the recent studies from the literature regarding continuum-based analysis of BOF problems is given in Table 1.1.

1.5 Incorporation of Soil Nonlinearity in BOF Analysis

Soil is known to behave as a highly nonlinear material. Therefore, idealizing soil as a linear material could lead to considerable error in the analysis. Few researchers have incorporated soil nonlinearity in the BOF problem. Beaufait & Hoadley 1980 [30] have introduced nonlinearity in Winkler's discrete model by approximating Winkler's parameter k with soil displacement w using a bilinear curve, and the differential equation was solved using the midpoint-difference method together with weighted averaging approach. Tsiatas (2010) [233] proposed a new nonlinear parameter to be added to the differential equation of the Pasternak foundation. The added parameter, however, accounts only for the nonlinearity in the compressive resistance of the soil, whereas the shear interaction parameter was considered to act linearly. Following Tsiatas's assumption, Jorge et al. (2015) [117] developed a finite element analysis framework for beams resting on discrete nonlinear foundation of Winkler-type subjected to moving loads. The outcomes of this study revealed that soil nonlinearity affects the critical velocity of the system. The limitation of these studies, however, is that the nonlinearity in Winkler's parameter k has been taken into account artificially without recourse to the fundamental nonlinear stress-strain response of soil. In real soil, the stress-strain response is nonlinear and that should be translated to the nonlinearity of k_s using proper mechanics. Haldar & Basu (2016) [102] developed a new analytical technique for the static analysis of beams resting on heterogeneous nonlinear layered soil deposit, based on the Modified Valsov model. The principle of Virtual work was used to derive the governing differential equations of the system and an iterative finite element procedure were developed to solve the nonlinear differential equations. The soil nonlinearity was incorporated by considering nonlinear-elastic constitutive law and secant

shear modulus to account for the reduction in the soil modulus. The accuracy of the results were verified using sophisticated finite element results. Additional literature review on the topic of incorporating soil nonlinearity in the analysis of BOF problems is given in Table 1.1 and in Chapter 5.

1.6 Incorporation Poromechanics in BOF Analysis

Soil being a porous material, poromechanics should be ideally used instead of classical continuum mechanics to represent the soil beneath beams and other foundation elements. The elastodynamic theory for fluid-filled elastic porous solids was first introduced by Biot (1962) [39]. Thereafter, the theory has been widely adapted by researchers in the field of geomechanics and geotechnical engineering. Nevertheless, the applications of the theory in analysing beams on foundations (soils) are limited. The fundamentals of the problem of beams resting on a half space poroelastic soil layer were investigated by Selvadurai & Shi (2015) [207]. The study also presented a basic analytical solution of the dynamic equation by combining Fourier and Laplace transforms, and the results were validated using a multi-physics software. Jin (2004) [115] proposed a Fourier transform-based solution for the Biot's problem of beam resting on poroelastic half space and subjected to a periodic oscillating moving loads of constant velocity. In this study, the effect of moving velocity and frequency of the moving load on the response was demonstrated using numerical examples. The Fourier transform method was also adopted by Xu et al. (2007) [258] to solve the dynamic problem of Timoshenko beam vibrating on a poroelastic half space. Cai et al. (2008) [49] applied the dynamic theory of Biot to the analysis of the problem of railway track system on poroelastic half space and subjected to a moving train load. In this study, the train-track system is considered as a separate mechanical discrete model and solved using the Green functions concept, and the track-soil model was considered as a beam an elastic half space, and the dynamic equations were solved using the Fourier transform technique.

Direct application of the finite element method for the analysis of the poroelastic BOF problem has been done by some authors. Xu et al. (2007) [258], for example, established a two dimensional (2-D) finite element model for dynamic analysis of poroelastic soil layer subjected to wave loading. In a recent study by Ai & Hu (2016) [3], a finite element based solution for a beam resting on a soil deposit that have anisotropic permeability and saturated with compressible fluid is proposed. Other recent studies on the subject are given in Table 1.1 and in Chapters 6 and 7.

1.7 Research motivation

The competition between railways/vehicle manufacturers has led to the need for faster and more efficient transportation systems [138, 120]. However, this has also increased the need to understand the behavior of the track/road subgrades and their supporting soils under dynamic loads, as excessive vibrations generated by axle loads can lead to serviceability or ultimate limit state related problems [191, 90]. Geotechnical engineers play a critical role in developing this understanding to ensure that transportation systems can perform at their optimal levels without causing significant damage to the track/road subgrades and supporting soils [46, 67].

By gaining a better understanding of the behavior of the subgrades and supporting soils, geotechnical engineers can also help to reduce the higher maintenance costs associated with transportation systems. This is because by designing and constructing transportation systems that are better suited to their environment, engineers can minimize the amount of maintenance needed to keep the systems functioning properly. Ultimately, this leads to cost savings for both transportation system operators and end-users [155, 195, 214].

The technical problems associated with High-Speed Rail (HSR) track systems are mainly related to the dynamic interaction between the trains and the track, which can result in excessive stress, deformations, and other issues. Some of the specific technical problems include [138, 238, 205, 141]:

- Repeated dynamic loading: High-speed trains generate significant dynamic loads that are repeatedly applied to the track and subgrade. These loads can cause progressive shear failure and excessive plastic deformation.
- Heavy traffic loads: High Speed Railway (HSR) systems typically have a high frequency of service, with many trains running at high speeds. This puts significant pressure on the track and subgrade, resulting in problems such as ballast migration and track settlement at shallow depths.
- Fine-grained and soft subsoil: In areas with fine-grained and soft subsoil, the track and subgrade can experience problems such as differential settlement and subgrade attrition with mud pumping at shallow depths.
- Excessive moisture content: When the subgrade is saturated with water, it can lead to problems such as progressive shear failure and excessive plastic deformation.

- Environmental factors: Environmental factors such as temperature changes, frost heave, and seismic activity can also affect the track and subgrade, leading to surface to shallow depth problems such as track buckling and rail distortion.

To address these technical problems, it is important to have a detailed understanding of the behavior of the track/road system and subgrade, as well as the impact of dynamic loading on these components [146]. Accurate mathematical modeling and numerical solutions can help in this regard, as can field measurements and experience gained from past HSR projects. These technical problems can eventually lead to partial or complete failure in the subgrade or the supporting soil. It was found that the mechanism of failure lies in the form of one or a combination of the following types of failures [142, 194]:

- Progressive Shear Failure: A plastic flow of soil caused by overstressing at the subgrade by repeated loading in the existence of fine-grained soils (clays) and water [141, 142] see Figure 1.3a.
- Subgrade attrition with mud pumping: a result of effect combination of soil, water, and dynamic load [194, 262], Figure 1.3b.
- Excessive Plastic Deformation: It includes both the vertical component of deformation from progressive shear failure and the components from the compaction and consolidation under repeated loads [139] Figure 1.3c.

Evidently, any proposed analytical/numerical method for the analysis of railway tracks and subgrade interaction need to be linked to the associated failure mechanisms [243]. The model should consider the pores in the in both the subgrade and the underlaying soils by simulating the soil as a multi-phase material to account for excess pore-water pressure dissipation and long-term deformations. The model should also consider the effect cyclic dynamic loads generated by loading/unloading conditions, by adopting a time-dependent dynamic framework. The model should involve a failure criterion to accommodate the progressive shear failure of soil by employing a softening soil model. The model should account for cumulative plastic deformations due to repeated loading scenarios by implementing a nonlinear soil model with a plastic flow criterion.

1.8 Gaps in the Literature

There are several limitations that are inherent in the available mathematical models concerning dynamic analysis of BOF problems. The most prominent gaps are:

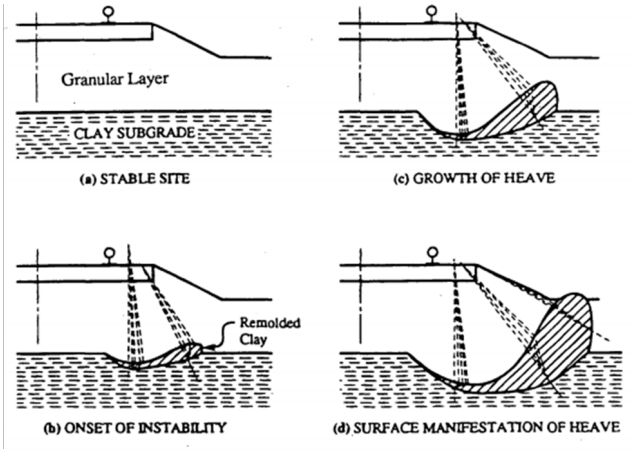

(a)

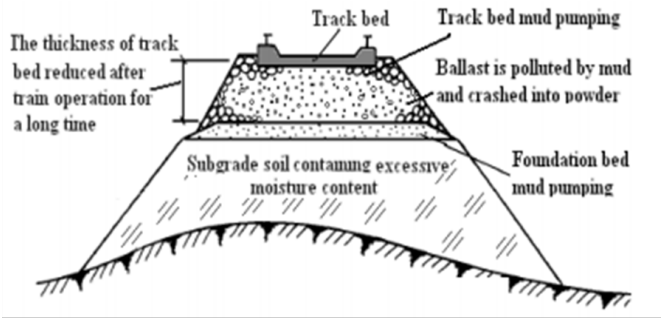

(b)

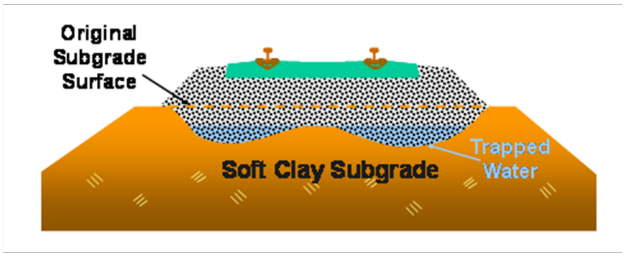

(c)

Figure 1.3: Failure mechanisms of railway subgrades: (a) Progressive shear failure in railway foundation[141, 142], (b) Subgrade attrition with mud pumping [194, 262], and (c) Excessive Plastic Deformation [139]

- The computational effort associated with three dimensional (3D) dynamic analysis using finite elements is quite high compared to spring-based analytical approaches. On the other hand, the discrete spring-type analytical models do not represent the soil behavior properly and are not reliable because of the need to predefine the parameters of the model done based on empirical relations. Therefore, continuum-based models are essential in the analysis.

- Only a few mathematical studies consider soil nonlinearity in the dynamic analysis of BOF problems because of the complexities associated with simulating the stress-strain nonlinearity. The existing nonlinear models empirical spring-based nonlinearity that does not represent the true nonlinear soil behavior. This necessitates the need for a simplified but reliable nonlinear dynamic analysis framework that accounts soil stress-strain nonlinearity.

- Only a few studies consider the soil as a multi-phase material (porous material) in the dynamic analysis of BOF. Continuum based models that are mathematically tractable are rather few.

- The majority of the mathematical models assume linear elastic homogenous continuum materials in dynamic analysis of BOF moving load problems. Soil nonlinearity is largely not considered in these moving load problems.

- The coupling between soil nonlinearity and poroelasticity in the dynamic analysis, and specifically in dynamic load problems does not exist in the literature on analytical continuum-based models, and it's computationally very expensive to perform using standard finite element software.

- There is a need to develop analytical solutions for dynamic analysis of beams with finite length resting on two parameters foundation and subjected to moving loads.

- No study based on the improved continuum model of Vlasov and Leont'ev (1966) [247] that comprehensively considers both the free and forced vibration of beams resting on soils with explicit multiple layering exists.

- No single study considers the soil nonlinearity in the Modified Vlasov's model within a dynamic framework.

- The coupling between soil nonlinearity and poroelasticity in the dynamic analysis using the modified Vlasov's model does not exist in the literature.

1.9 Research Objective and Tasks

The objective of this research study is to develop analytical and semi-analytical models for nonlinear dynamic interaction of beams with underlying soils with particular focus on moving loads. The soil should be represented by its stress-strain nonlinearity and the time-dependent consolidation response of soil under applied loads should be captured. These models should be computationally efficient and accurate, and act as alternatives to conventional 2-D and 3-D numerical models such as finite element models that are computationally expensive and require specialized user skills (on meshing and use of the software) for modeling. In this study, the continuum-based modified Vlasov foundation model is adopted for such model development. The completed research tasks can be summarized as follows:

- Response of finite Euler-Bernoulli beams resting on two-parameter spring foundation subjected to moving loads are studied.
- The range of applicability of the Euler-Bernoulli and Timoshenko beam theories is established for soil-structure interaction problems. Further, reliable equations of the parameters ks and ts representing multi-layer deposits are developed for use with both the beam theories.
- The response of the BOF problem is investigated in which the soil is assumed to be a linear elastic simplified continuum that follows the modified Vlasov model.
- The elastodynamic modified Vlasov continuum model is enhanced by implementing heterogeneity and soil stress-strain nonlinearity and nonlinear dynamic BOF problems are investigated.
- The modified Vlasov continuum model is improved to take into account the poromechanics-based consolidation of soil following Biot's consolidation theory. Thus, beams consolidating on layered soil are studied.
- Subsequently, the poromechanics-based consolidation model is used to study the inertia based vibration of beams on consolidating soil.

Published Journal papers:

- Elhuni, H., & Basu, D. (2019). Dynamic soil structure interaction model for beams on viscoelastic foundations subjected to oscillatory and moving loads. Computers and Geotechnics, 115, 103157.

- Elhuni, H., & Basu, D. (2021). Novel nonlinear dynamic beam–foundation interaction model. Journal of Engineering Mechanics, 147(4), 04021012.
- Elhuni, H., & Basu, D. (2022). Interaction of Beams with Consolidating Nonlinear Poroelastic Layered Soil. Journal of Engineering Mechanics, 148(3), 04021167.
- Elhuni, H., & Basu, D. (2022). Dynamic Analysis of Beams Vibrating on Nonlinear Poroelastic Multi-layered Continuum. International Journal for Numerical and Analytical Methods in Geomechanics.DOI: 10.1002/nag.3479.
- Elhuni, H., Gupta, B., & Basu, D. (2023). Analysis of circular tank foundation on multi-layered soil subject to combined vertical and lateral loads. Journal of Geomechanics and Engineering, Volume 32, Number 6, March 25 202, pages 553-566.

Submitted Journal papers:

- Interaction of Timoshenko beam with Multi-layered Continuum (second round review by the International Journal of Geotechnical Engineering).

1.10 Verification and validation of the results from the proposed model

Although the soil-structure interaction model, which is developed as part of this study can be used to simulate vehicle–track subgrade interaction response dynamics and moving loads, a proper validation with measured results from field test is not provided in this thesis because of the limited vehicle-track subgrade field data available in the literature. Alternatively, the PLAXIS software package has been used to verify the results from the proposed model. PLAXIS is a software package for geotechnical analysis and finite element modeling. It is developed and distributed by Bentley Systems to provide solutions for geotechnical infrastructure design, construction, and operation. PLAXIS is selected as a verification tool in this study for the following reasons:

- PLAXIS is widely used in the industry and academic research for geotechnical engineering applications to simulate soil-structure interaction behaviour under various loading conditions [264, 124, 17].

- PLAXIS has already been verified and validated by experimental and field results. The software developers have conducted extensive testing and benchmarking to ensure the accuracy and reliability of the software. In addition, many researchers and practitioners have compared simulation results obtained from PLAXIS with experimental and field measurements, and the results have been found to be in good agreement [162, 246, 164, 11].

- PLAXIS offers advanced features for modeling complex soil-structure interaction and geotechnical problems under various types of dynamic loads, and it includes a wide range of material models to simulate the behaviour of the soils including modeling water flow. Additionally, the software has a user-friendly interface with various options for visualization and data analysis. It allows users to import data from various sources and export simulation results to different formats [160].

1.11 Justification of the selected inputs for simulation

The selection of material and the geometric properties for simulations in this study is based on several factors, including the availability of data from laboratory testing of soil samples, the actual behaviour of these materials under the expected loading conditions, the nature of the problem being modeled, and the level of accuracy required. The material properties include, but are not limited to, soil elastic modulus, soil Poisson's' ratio, soil layering, constitutive law, and soil permeability. The geometric properties on the other hand may include soil thickness, soil depth, and foundation length and depth. The loading conditions (such as loading values and loading nature) are also chosen to be consistent with the nature of the problems and according to the actual data provided in the literature [168, 126, 109, 176, 45, 203, 188, 70, 197].

1.12 Limitations of the proposed study

Transparency about the limitations of a proposed model is essential for ensuring that the results are not overinterpreted or misused. This can help users of the model to better understand the strengths and weaknesses of the model, and to make more informed decisions based on the model's outputs. Additionally, being transparent about limitations can help to guide future research and development efforts, as it can highlight areas where improvements are needed [148, 166]. In addition to the potential sources of uncertainty and error

associated with the proposed model, there are several potential limitations of the proposed model arising from simplified assumptions of the theories of mechanics implemented in the proposed research. These limitations are summarized in Table 1.2. These limitations will be formulated into recommendations for future research in Chapter 8.

Table 1.2: Limitations associated with the proposed model

Aspect of limitation	Description
Full contact is assumed between the structural part (beam) and the subgrade (soil)	Separation is not allowed at all times. The assumption is often applied in scenarios where the load transfer mechanism relies on the friction and bearing capacity of the soil-structure interface. It is commonly used in the analysis of shallow foundations, slab-on-grade structures, and certain types of retaining walls.
Only vertical deformation is allowed within the soil body.	The assumption is typically applied in problems involving vertical loading on soils, such as the settlement analysis of shallow foundations or vertical retaining walls. In these cases, the primary concern is the vertical deformation and settlement of the soil, and the horizontal displacements are assumed to be minimal.
The water flow through soil is assumed to happen only in the vertical direction.	Water flow through soil only occurs in the vertical direction and is a common simplifying assumption used in many geotechnical and hydrological models. In reality, water flow through soil can occur in multiple directions, including horizontal flow, depending on factors such as the soil's permeability, hydraulic gradients, and boundary conditions.
Plane strain conditions with geometrical and loading symmetry is assumed	The assumption of plane strain condition implies that the soil and structural elements behave as if they are infinitely wide in the out-of-plane direction, allowing the analysis to focus on the behavior within a 2D plane.
Nonlinearity is considered for soil material.	Other sources of nonlinearity, such as geometric nonlinearity and damping nonlinearity, are not explicitly considered in the analysis. This is to simplify the analysis and focus on the primary nonlinearity associated with the soil response [96].
Fully saturated soil condition is assumed for consolidation analysis.	The soil in reality may not be fully saturated, and the presence of air or gas in the soil voids can affect the consolidation behavior. However, assuming fully saturated conditions ensures that the worst-case scenario is considered, as the presence of air or gas can potentially cause additional consolidation settlement [57].
Only low-to-medium range of frequencies is considered in the dynamic simulation (10-120 Hz)	Considering a wide-range of frequencies (10-300 Hz) for analysis of railway-track and machine foundations is important for the assessment of potential resonance, excessive vibrations, settlements, and structural damage of the foundations/tracks [168, 176].
Rayleigh damping concept is used in dynamic soil-structure interaction analysis to simulate the damping effects in this study.	This concept provides a convenient and effective approach to incorporate damping in numerical analysis. Rayleigh damping, however, assumes a constant damping ratio for the entire soil-structural system, regardless of the level of soil strains. This assumption may not accurately represent the behavior of soils, as damping in soils can vary with the level of deformation. In fact, soil damping can change as the soil undergoes increasing strains. This is known as strain-dependent damping. As the strains increase, the soil particles may undergo rearrangement or densification, leading to changes in the energy dissipation and damping characteristics of the soil [250, 175].
The soil nonlinearity is represented by small strain hyperbolic elastic constitutive model	Small strain material models are typically used to represent the nonlinear behavior of soils within their small strain range, where the soil stiffness changes as a function of strain. However, for larger strains, such as those that occur during earthquakes or other dynamic loading events, the material behavior of soil can become highly nonlinear and more complex models may be needed to accurately capture this behavior [31].

1.13 Structure of the Thesis

The chapters of the thesis are described shortly as below:

In **Chapter 1**, a literature review of the research related to BOF problems are presented, the development of the theory of the BOF is summarized and the most common analytical and semi-analytical models, related to the subject are also evaluated and their limitations are highlighted. The chapter concludes with identification of research gaps, objectives, and tasks.

In **Chapter 2**, elasto-dynamic analysis of finite beams resting on two-parameter soil springs are performed along with a broad parametric study.

In **Chapter 3**, the applicability of the Timoshenko and Euler-Bernoulli beam theories for multi-layered soil-structure interaction problems is investigated. The effect of beam and soil bending stiffness on the soil-structure interaction aspect of the problem is investigated. The effect of the presence of two and three foundation layers on the beam response is also studied.

In **Chapter 4**, the elasto-dynamic continuum-based linear analysis of the BOF problem using the modified Vlasov's continuum foundation is presented. The model is used to investigate the steady state response of infinitely long beams. A few problems are analyzed that illustrate the novel features of the dynamic foundation model.

In **Chapter 5**, the elasto-dynamic continuum linear model developed in **Chapter 4** is improved to account for the stress-strain nonlinearity of the soil in the analysis, in which the shear modulus and damping ratio of soil are assumed to be functions of soil strains.

In **Chapter 6**, the quasi-static long-term response of the BOF problem is investigated after extending the modified Vlasov's continuum model to incorporate poroelasticity. A semi-analytical framework for obtaining the consolidation settlement of flexible foundations such as beams and strip footings resting on nonlinear, saturated, poroelastic, and layered continuum (soil) is developed. The Biot's consolidation theory is used in the analysis, and the differential equations governing the displacements and excess pore pressure dissipation of the beam-soil system are developed using the variational principles of mechanics in which the soil is modeled as a simplified continuum.

In **Chapter 7**, the quasistatic analysis method presented in **Chapter 6** is improved to account for inertia based vibration of beams under dynamic loads. The novelty of the framework is that it rigorously takes into account the nonlinear poroelastic soil-structure interaction within a dynamic time-integration framework with minimal computational re-

sources. The characteristics of the developed nonlinear poroelastic foundation dynamic model are illustrated through examples.

In **Chapter** 8, the conclusions derived from the research study are presented, and recommendations are provided.

Chapter 2

Dynamic Analysis for Beams on Visco-elastic Two-Parameter Spring Foundation

2.1 Overview

The dynamic response of beam on elastic foundation under moving load is of interest in many fields of engineering. In most studies, the foundation is modeled as discrete linear Winkler springs and simplest model considered was a beam supported by a Winkler-type foundation that act in response only to local deflections and ignore the shear interaction between the foundation spring elements. In this paper, the dynamic response of beam supported by two parameters visco-elastic foundation and subjected to a moving load is, investigated analytically. It is assumed that the load moves with constant velocity. The Integral Transformation method is used to develop the analytical solution of the problems; the solution is given in closed form expressions. The reliability of the proposed solution was verified with other solutions from the literature. The effects of some important parameters such the foundation stiffness, the travelling speed, the span length of the beam, the damping of the system, and the mass density of the system were addressed through numerical examples. By analysing wide range of responses "span lengths and moving velocities": Normalized Speed-Span diagrams "NSS"; that describe the translation of behaviour from a relatively short beam to infinitely long beam; are introduced for both Winkler-type and Pasternak-type foundations. The dynamic amplifications curves are used as a criterion to illustrate the variation in behaviour trend as the span length/ and or moving velocity

change; within different regions in the NSS diagrams. As far as the concern of the application of the theory of beam on elastic foundation, the deflection dynamic implication carves can be used for the design purpose.

2.2 Introduction

The problem of beam on elastic foundation has applications in many engineering disciplines such as pavement engineering, railway engineering, marine engineering, bio-mechanics, structural engineering, and geotechnical engineering [24]. In geotechnical, pavement, and railway engineering, the beam usually represents foundation elements such as strip footings or grade beams, pavements, and railway tracks, and the foundation beneath is usually the soil mass. Pavement and railway track are often modeled as Euler-Bernoulli beams and the soil is most often modeled as a bed of springs. The soil spring model proposed by Winkler (1867) [255] is based on the assumption that the springs compress (or extend) independent of the adjacent springs. Because the springs are not influenced by the adjacent springs, no displacement occurs beyond the loaded region, which is a limitation of the model. The Winkler springs are characterized by the spring constant k_s, which is often related to the modulus of subgrade reaction of soil [220]. The Winkler model is also known as one-parameter model because only one parameter k_s characterizes the model. Several authors have proposed two-parameter soil spring models, characterized by the parameters k_s and t_s, as an improvement to the Winkler model such that interactions exist between the adjacent soil springs. In the different two-parameter models, the interaction between the springs is interpreted differently [92, 107, 177, 267], but the governing differential equations for these models are the same. Because soil resists stresses through compression and shear, it is most reasonable to assume that the interaction between the soil springs arise from shear forces between the soil springs. Thus, in this study, the second parameter t_s is considered to be a shear parameter that quantifies the shear resistance of soil, while the first parameter k_s is the spring constant and quantifies the compressive resistance of the soil. However, irrespective of the interpretation of t_s, the mathematical formulation remains the same.

Dynamic response of beams on elastic foundations is an important topic and has many applications. Such inertia-based beam vibration arises when the applied load is time dependent, either oscillating with time (e.g., sinusoidal variation of load as in the case of machine foundations) or moving spatially (similar to a moving car or train) or both. In these studies, two general principles were used by researchers to derive the governing equations of the problem. Many researchers applied the Newton's third law together with the classical elastic theories of beam-bending to develop the differential equation for the system

[34, 267, 268, 212]. Others applied the energy methods accompanied by the calculus of variation to obtain the equilibrium differential equations [247, 261, 256, 184, 234, 149]. The ensuing governing fourth-order linear differential equation describing the beam vibration is usually solved using classical analytical and numerical methods with proper use of the associated boundary conditions [177, 95, 260, 218, 257, 259, 165, 153].

Analytical methods have been applied on a variety of dynamic beam on elastic foundation problems. The quasi-stationary (steady state) dynamic behavior of an infinite beam supported by a one-parameter spring foundation and subjected to moving point load was obtained by Raftoyiannis et al. (2012) [184] who obtained their solution based on the modal superposition technique. Modal analysis was also performed by Uzzal et al. (2012) [239] to evaluate the response of a free beam subjected to a moving mass and resting on a two-parameter foundation. Timoshenko et al. (1974) [227] used the modal analysis to capture the free vibration of a beam on one parameter elastic foundation with different boundary conditions.

Basu & Rao (2013) [26] and Kumari et al. (2012) [132] investigated the steady state response of an infinite Euler-Bernoulli beam resting on a visco-elastic two-parameter foundation and subjected to a concentrated load moving at a constant speed and obtained closed form solutions. Fryba (2013) [95], Saito & Terasawa (1980) [196], and Trochanis et al. (1987) [231] used the exponential Fourier transform technique to analyze the same problem but with one-parameter foundation. Ono and Yamada (1989) [171] used an alternative closed form solution for both free and forced vibration cases of finite beams on two-parameter foundation and subjected to concentrated forces. Sun & Luo (2008) [218] performed frequency domain analysis to investigate the vibration response of a free beam on two-parameter elastic foundation.

Analytical solutions often have limited applications, particularly with respect to the beam boundary conditions. Therefore, the finite element (FE) method has been widely used to analyze the dynamic response of beams on elastic foundations [151, 19, 223, 131, 265, 117]. However, finite element analysis usually requires a greater computational effort compared with analytical solutions and may have problems related to numerical stability and convergence. Therefore, analytical solutions are often preferred by researchers [196, 171, 231, 218, 184, 239, 26, 132].

Mourelatos and Parsons (1987) [167] presented a 3D Finite element formulation of the problem of free beams resting on one-parameter and two-parameter foundation and subjected to static and dynamic distributed loads. The energy concept is used to derive the displacement-based finite element equation for which the coupling between the shear and the axial stresses is considered. Rodrigues et al. (2018) [193] studied the response

of the free beam on elastic foundation subjected to a moving vibrating mass. Nonlinear one-parameter and two-parameter models were used to simulate the soil and the finite element method is used to formulate the solution. Adhikari et al. (2021) [1] proposed a finite element formulation of the dynamic stiffness, damping, and mass matrices of pinned-pinned nano-beams resting on one-parameter foundation and subjected to harmonic forces. The response of the system was investigated under different damping models and different beam-materials.

In most studies on beam on elastic foundation, the beam was represented by infinite length and hence closed form solutions for infinite beams on one-parameter and two-parameter soil models are meant to study the steady state response which is applied to many engineering applications such as railway track problems. Beams with hinged ends resting on elastic foundation, however, are also important to other engineering applications. Studies have shown that pipes with finite lengths embedded in soils may experience higher buckling loads and deformations [99, 71, 143]. To authors knowledge no closed form analytical solution is reported in the literature for the problem of simply supported beam on two-parameter elastic foundation.

In this chapter, the dynamic response of finite-sized, simply supported Euler-Bernoulli beams resting on two parameter visco-elastic spring foundations and subjected to a moving concentrated load with constant velocity is studied. The governing differential equation is transformed from the physical space-time domain using Fourier-sine and Laplace-Carlson transforms, respectively. The equation is solved in the transformed domain and subsequently inverse transformed back to the physical domain. A parametric study is conducted to investigate the effect of soil spring stiffness, traveling speed of load, beam span length, damping coefficient, and mass density of beam on the beam response. Numerical examples are provided for illustration. By analysing a wide range of responses comprising different span lengths and load velocities, normalized speed-span (NSS) diagrams that describe the gradual transition of beam behaviour as the beam span increases from a finite length to infinite length. The dynamic amplifications curves are used to illustrate the change of beam behaviour in the NSS diagrams. The NSS diagrams provides insights and the dynamic amplification curves may be used for quick calculations by the practicing engineers.

2.3 Description of the Problem

The differential equation governing the dynamic response of an Euler-Bernoulli beam with uniform cross section resting on on visco-elastic two-parameter spring foundation and subjected to a moving concentrated force is given by

$$EI\frac{\partial^4 w}{\partial x^4} - 2t_s\frac{\partial^2 w}{\partial x^2} + k_s w + \rho\frac{\partial^2 w}{\partial t^2} + c\frac{\partial w}{\partial t} = P\delta(x - Vt) \tag{2.1}$$

where w=$w(x,\ t)$ is the transverse deflection of beam (m), E_b is the Young's modulus of beam (N/m^2), I_b is the moment of inertia of beam (m^4), ρ is the mass per unit length of beam (kg/m), c is the coefficient of viscous damping of the system per unit beam length (N-sec/m^2), P is the applied moving concentrated force (N), δ is the Dirac delta function, v is the velocity of the moving load (m/sec), x is the horizontal distance (m), t is the time (sec), k_s is the Winkler soil spring constant quantifying compressive resistance (N/m^2), t_s is the shear deformation parameter of soil springs quantifying the shear resistance (N). Note that, in the two-parameter foundation, soil reaction q beneath the beam depends both on the compressive and shear resistances arising from the soil spring, and is given by [247]

$$q(x,t) = k_s w - 2t_s\frac{\partial^2 w}{\partial x^2} \tag{2.2}$$

In this study, simply supported beams are considered for which the boundary conditions are $w\ |_{x=0} = 0$, $w\ |_{x=l} = 0$, $\frac{\partial^2 w}{\partial x^2}\ |_{x=0} = 0$, and $\frac{\partial^2 w}{\partial x^2}\ |_{x=l} = 0$ for all t, where l is the beam length. The boundary conditions imply that the beam deflection and bending moment are zero at the two hinged ends of the beam at all times. The initial conditions are $w\ |_{t=0} = 0$ and $\frac{\partial w}{\partial x}\ |_{t=0} = 0$ for all x (i.e., the displacement and velocity are zero everywhere at the beginning).

2.4 The Proposed Analytical Solution

To obtain analytical solutions for the differential Equation 2.1, Fourier sine integral transform is used, which is given by

$$w(j,t) = \int_0^l w(x,t).sin\left(\frac{j\pi x}{l}\right)\partial x \quad j = 1, 2, 3, ... \tag{2.3a}$$

$$w(x,t) = \frac{2}{l}\sum_{j=1}^{\infty} w(j,t).sin\left(\frac{j\pi x}{l}\right) \tag{2.3b}$$

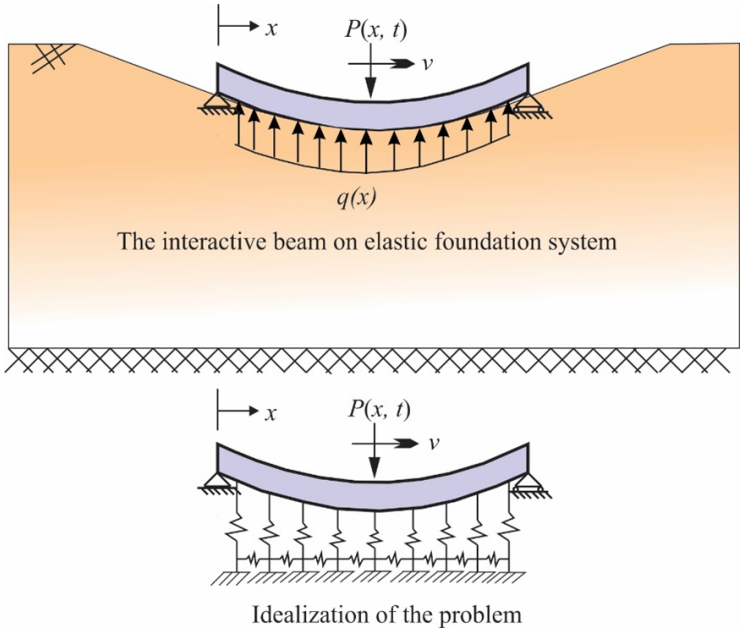

Figure 2.1: Beam-foundation interaction

Further, the solution procedure requires Laplace-Carson transform given by

$$w(j,p) = p\int_0^{\infty} w(j,t)e^{-pt}dt \tag{2.4a}$$

$$w(j,t) = \frac{1}{2\pi i}\int_{a_0-i\infty}^{a_0+i\infty} e^{pt}\frac{w(j,p)}{p}dp \tag{2.4b}$$

where a_0 is a real is valued constant, $i\infty$ is an imaginary axis, and p is the variable in the exponent.

Equation 2.3 can be rewritten as

$$EI\frac{\partial^4 w}{\partial x^4} - 2t_s\frac{\partial^2 w}{\partial x^2} + k_s w + \rho\frac{\partial^2 w}{\partial t^2} + 2\rho\omega_b\frac{\partial w}{\partial t} = P\delta(x - Vt) \tag{2.5}$$

where ω_b is the circular frequency of damping of the system. Applying Fourier sine integral transform to Equation 2.5, i.e. multiplying Equation 2.5 by $sin(j\pi x/l)$ and integrating with respect to x between 0 and l and rearranging, the following equation is obtained

$$\frac{j^4\pi^4}{l^4}EI\frac{\partial^4 w(j,t)}{\partial x^4} - 2t_s\frac{j^2\pi^2}{l^2}\frac{\partial^2 w(j,t)}{\partial x^2} + k_s w(j,t) + \rho\frac{\partial^2 w(j,t)}{\partial t^2} + 2\rho\omega_b\frac{\partial w(j,t)}{\partial t} = Psin\left(\frac{j\pi vt}{l}\right) \tag{2.6}$$

Assuming the square of circular frequency of the j^{th} mode of vibration to be

$$\omega_{(j)}^2 = \left[\frac{j^4\pi^4}{l^4}\frac{EI}{\rho} + \frac{k_s}{\rho} + 2t_s\frac{j^2\pi^2}{l^2\rho}\right] \tag{2.7}$$

The corresponding frequency is given by

$$f(j) = \frac{\omega_{(j)}}{2\pi} \tag{2.8}$$

Further, the circular frequency can be given by

$$\omega = \frac{\pi v}{l} \tag{2.9}$$

Substituting Equations 2.7, 2.8, and 2.9 into Equation 2.6 and rearranging the following equation is obtained

$$\frac{\partial^2 w(j,t)}{\partial t^2} + 2\omega_b\frac{\partial w(j,t)}{\partial t} + \omega_{(j)}^2 w(j,t) = \frac{p}{\rho}sin\left(\frac{j\pi vt}{l}\right) \tag{2.10}$$

Applying the Laplace-Carson transform to Equation 2.10, i.e., multiplying Equation 2.10 by pe^{-pt} , integrating with respect to t between 0 and ∞, and rearranging, the following equation is obtained

$$w(j,p) = \frac{P.j.\omega}{\rho}.\frac{p}{p^2 + j^2\omega^2}.\frac{1}{p^2 + 2\omega_b p + \omega_{(j)}^2} \tag{2.11}$$

A parameter α representing the effect of speed on the system is defined as

$$\alpha = \frac{\omega}{\omega_{(1)}} = \frac{v}{2f_{(1)}l} = \frac{v}{\left[\frac{\pi^2 EI}{\rho l^2} + \frac{k_s l^2}{\pi^2\rho} + \frac{2t_s}{\rho}\right]^{0.5}} = \frac{v}{v_{ch}} \tag{2.12}$$

where v_{ch} is given by

$$v_{ch} = \left[\frac{\pi^2 EI}{\rho l^2} + \frac{k_s l^2}{\pi^2 \rho} + \frac{2t_s}{\rho}\right]^{0.5} \tag{2.13}$$

The variable v_{ch} represents the characteristic velocity, which is the velocity at which a free wave may propagate in a finite beam. Further, a parameter β representing the effect of damping on the system is defined as

$$\beta = \frac{\omega_b}{\omega_{(1)}} = \omega_b \left[\frac{\pi^4 EI}{\rho l^4} + \frac{k_s}{\rho} + \frac{2t_s \pi^2}{\rho l^2}\right]^{-0.5} \tag{2.14}$$

Now, two cases can be identified with respect to the damping of the system: (a) light damping corresponding to $\beta \ll 1$ and (b) heavy damping corresponding to $\beta \gg 1$. For light damping, the frequency of the damped beam-foundation system $\omega'_{(j)}$ is given by

$$\omega'^2_{(j)} = \omega^2_{(j)} - \omega^2_b \tag{2.15}$$

On the other hand, for heavy damping, $\omega'_{(j)}$ is given by

$$\omega'^2_{(j)} = \omega^2_b - \omega^2_{(j)} \tag{2.16}$$

For the case of light damping case ($\beta \ll 1$), applying the inverse Laplace-Carson transform on Equation 2.11, the following equation is obtained

$$\begin{aligned} w(j,t) = \frac{P.j.\omega/\rho}{\left[(\omega_b^2 + \omega'^2_{(j)} - j^2\omega^2)^2 + 4\omega_b^2.j^2\omega^2\right]} \Bigg[& \frac{\omega_b^2 + \omega'^2_{(j)} - j^2\omega^2}{j.\omega} sin(j.\omega.t) \\ & - \frac{\omega'^2_{(j)} - \omega_b^2 - j^2\omega^2}{\omega'(j)} . e^{-\omega_b t} sin(\omega'_{(j)}.t) \\ & - 2\omega_b(cos(j.\omega.t) - e^{-\omega_b t}.cos(j.\omega.t)) \Bigg] \end{aligned} \tag{2.17}$$

Further, applying the inverse Fourier sine integral transform on Equation 2.17, the following equation is obtained

$$w(j,t) = \sum_{j=0}^{\infty} \frac{(2p/l\rho)sin(\frac{j\pi x}{l})}{\left[(\omega_{(j)}^2 - j^2\alpha^2\omega_{(1)}'^2)^2 + 4j^2\omega_{(1)}^4.\beta^2\alpha^2\right]} \Bigg[\omega_{(j)}^2 - j^2\alpha^2\omega_{(1)}^2.sin(j.\omega.t) - \frac{(j\alpha\omega_{(1)})[\omega_{(j)}'^2 - \beta^2\omega_{(1)}^2 - j^2\alpha^2\omega_{(1)}^2]}{\omega_{(j)}'} e^{-\omega_b t} sin(\omega_{(j)}' t) - 2\omega_{(1)}^2\alpha\beta j(cos(j\omega t) - e^{-\omega_b t}cos(\omega_{(j)}' t))\Bigg] \tag{2.18}$$

The static mid-span deflection can be produced from Equation 2.18 by substituting α = 0, j=1, and $\frac{x}{l} = 0.5$ as

$$w_{(\frac{x}{l}=0.5)} = \frac{2p}{\rho l}\left[\frac{\pi^4 EI}{l^4\rho} + \frac{k_s}{\rho} + \frac{2t_s\pi^2}{l^2\rho}\right]^{-1} \tag{2.19}$$

A few special cases in the category of light damping can be recognized. For example, the static deflection can be obtained from Equation 2.18 by setting $\alpha = 0$, and is given by

$$w(x) = \sum_{j=0}^{\infty} \frac{2p}{\rho l\omega_{(j)}^2} sin\left(\frac{j\pi x}{l}\right) \tag{2.20}$$

Further, the case with no damping can be obtained by setting $\beta = 0$. For $\alpha \neq$ j, Equation 2.18 becomes

$$w(j,t) \approx \frac{2p}{\rho l}\sum_{j=0}^{\infty} \frac{sin\left(\frac{j\pi x}{l}\right)}{(\omega_{(j)}^2 - j^2\alpha^2\omega_{(1)}^2)^2}\Bigg[\omega_{(j)}^2 - j^2\alpha^2\omega_{(1)}^2.sin(j.\omega.t) - (j\alpha\omega_{(1)})\left[\frac{\omega_{(j)}^2 - j^2\alpha^2\omega_{(1)}^2}{\omega_{(j)}}\right]sin(\omega_{(j)}t)\Bigg] \tag{2.21}$$

and, for $\alpha = n$, Equation 2.11 becomes

$$w(x,t) = \frac{2P}{\rho \cdot l \cdot \omega_{(n)} \left(n^2\omega^2 - \omega_{(n)}^2\right)} \left[n \cdot \omega \sin\left(\omega_{(n)} \cdot t\right) - \omega_{(n)} \cos(n \cdot \omega \cdot t)\right] \cdot \sin\left(\frac{n\pi \cdot x}{l}\right) +$$
$$\frac{2P}{\rho \cdot l} \sum_{j \neq n}^{\infty} \frac{\sin\left(\frac{j\pi \cdot x}{l}\right)}{\left(\omega_{(j)}^2 - j^2\alpha^2\omega_{(1)}^2\right)^2} \left[\left(j\alpha\omega_{(1)}\right) \cdot \left[\frac{\left(\omega_{(j)}^2 - j^2\alpha^2\omega_{(1)}^2\right) \cdot \sin(j \cdot \omega \cdot t) -}{\omega_{(j)}\alpha^2\omega_{(1)}^2}\right] \sin\left(\omega_{(j)} \cdot t\right)\right] \tag{2.22}$$

Note that, for the case of very light damping case ($\beta \ll 1$), Equation 2.18 can be used for all values of α.

For the case of critical damping ($\beta = \beta_{cr} = n^2 = \omega_{(n)}/\omega_{(1)}$), substituting in Equation 2.11 again for the case with $j = n$ and adding Equation 2.18 for $j < n$ and adding Equation 2.24 for $j > n$, the following equation is obtained

$$w(x,t) = \frac{2Pj\omega}{\rho l \left(n^2\omega^2 - \omega_{(n)}^2\right)^2} \left[\frac{\omega_{(n)}^2 - \omega^2 n^2}{n\omega} \sin(n\omega t) - 2\omega_{(n)} \cos(n\omega t)\right.$$
$$\left. + e^{-\omega.nt}\left\{\left(n^2\omega^2 + \omega_{(n)}^2\right) t + 2\omega n\right\}\right] \sin\left(\frac{n\pi x}{l}\right) + \text{ Equation 2.18 } |_{j<n} + \text{ Equation 2.24 } |_{j>n} \tag{2.23}$$

For the case of heavy damping ($\beta > \beta_{cr}$), Equation 2.14 is solved by using $\omega_{(j)}'^2 = \omega_b^2 - \omega_{(j)}^2$ and that gives

$$w(x,t) = \frac{2P}{\rho l} \sum_{j=1}^{n} \frac{\sin\left(\frac{j\pi x}{l}\right)}{\left[j^2\omega^2 + \left(\omega_b + \omega'_{(j)}\right)^2\right]\left[j^2\omega^2 + \left(\omega_b - \omega'_{(j)}\right)^2\right]} \left[\left(\omega_b^2 - \omega_{(j)}^2 - j^2\omega^2\right) \sin(j\omega t)\right.$$
$$\left. - j\omega\left(2\omega_b\right) \cos(j\omega t) + \frac{j\omega}{2\omega'_{(j)}} \left\{j^2\omega^2 + \left(\omega_b + \omega'_j\right)^2\right\} e^{-\left(\omega_b - \omega'_{(j)}\right)} - \frac{j\omega}{2\omega'_{(j)}} \left\{j^2\omega^2 + \left(\omega_b - \omega'_j\right)^2\right\} e^{-\left(\omega_b + \omega'_{(j)}\right)}\right]$$
$$+ \text{ Equation (2.18) } |_{j>n} \tag{2.24}$$

Figure 2.2 illustrates the solution flowchart for the governing equation (Equation 2.4) for the different cases of damping and velocities. The inputs for the analysis are the geometry of the beam, the material properties of both the beam and the foundation, the load velocity and magnitude, and the damping coefficient of the system.

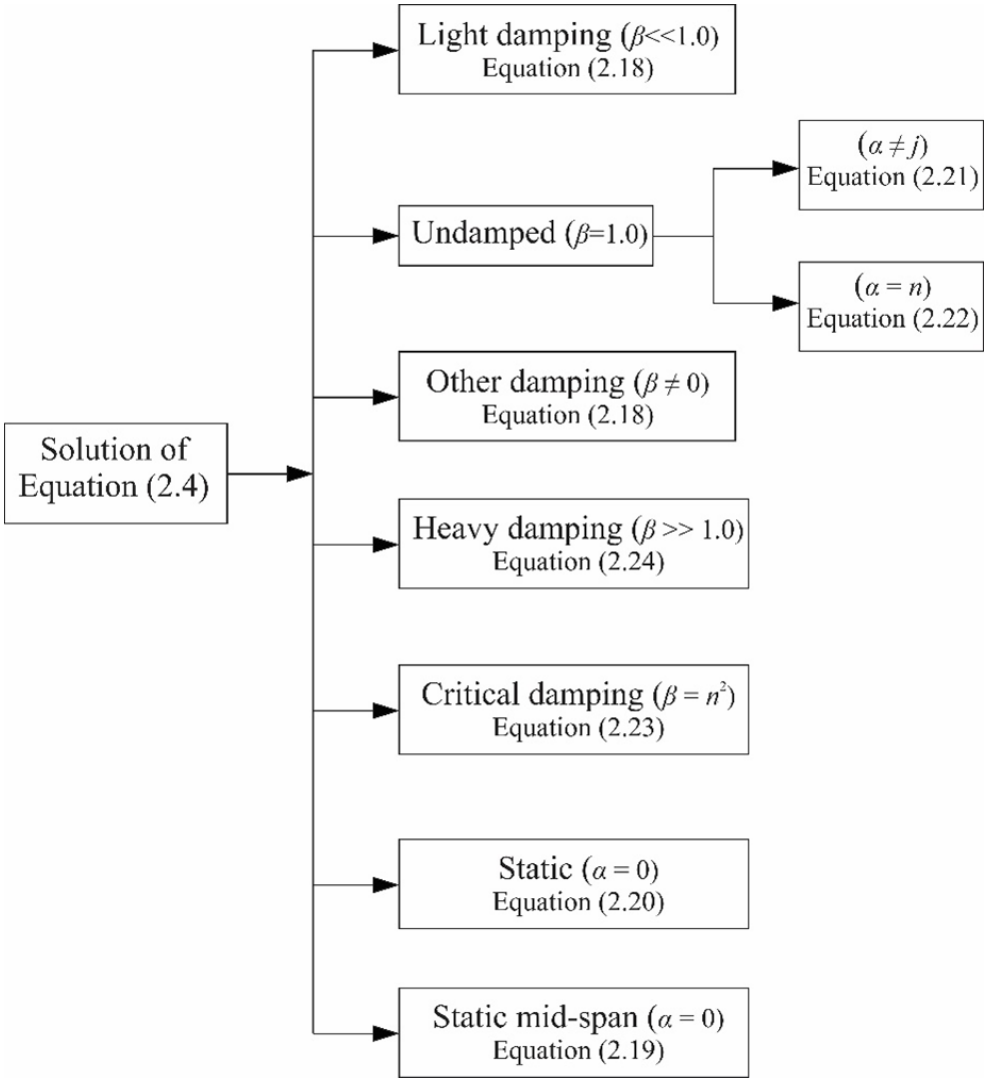

Figure 2.2: Solution flowchart

2.5 Finite Element Analysis

Finite element (FE) analyses of beams with moving loads were also performed, mostly for cross checking that the analytical solutions developed in the previous section produced correct results. The FE analysis was developed not only for finite-sized beams but also for infinite beams. Two-noded beam elements with cubic Hermitian shape functions were

used to represent the primary variables (beam deflection w and slope dw/dx). However, for analyzing infinite beams, infinite elements with three nodes were used at the two ends instead of the regular two-noded elements (Figure 2.3). If the input of the boundary condition type is bounded "e.g. hinged, fixed" the infinite elements are replaced with classical finite elements, and the end boundary (force, displacement or rotation) are enforced in the final assembled matrices using the direct imposition approach [28].

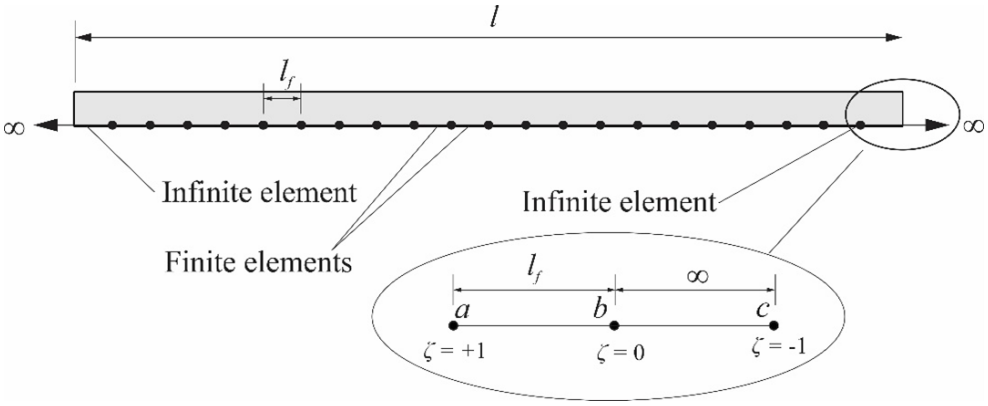

Figure 2.3: Beam-foundation system discretized with finite and infinite elements The shape functions of the three nodded infinite elements (Figure 2.3) are given by [265]

$$N(x) = \left\{ \begin{array}{l} (1/4)(4+3x)x^2(x-1)^2 \\ (1/4)(1+x)x^2(x-1)^2 \\ (1-4x)(x+1)^2(x-1)^2 \\ x(x+1)^2(x-1)^2 \\ (1/4)(4-3x)x^2(x+1)^2 \\ (1/4)(x-1)x^2(x+1)^2 \end{array} \right\} \tag{2.25a}$$

where the mapping function ζ is given by

$$\zeta = 1 - \frac{l_f}{x} \tag{2.25b}$$

Considering the displacement and the rotation of the far node c of the infinite element is zero, Equation 2.25(a) becomes

$$N(x) = \left\{ \begin{array}{l} (1/4)(4+3x)x^2(x-1)^2 \\ (1/4)(1+x)x^2(x-1)^2 \\ (1-4x)(x+1)^2(x-1)^2 \\ x(x+1)^2(x-1)^2 \end{array} \right\} \tag{2.25c}$$

The shape functions of the two nodded finite elements (Figure 2.3) are given by

$$N(x) = \left\{ \begin{array}{l} (1/4)(4+3x)x^2(x-1)^2 \\ (1/4)(1+x)x^2(x-1)^2 \\ (1-4x)(x+1)^2(x-1)^2 \\ x(x+1)^2(x-1)^2 \\ (1/4)(4-3x)x^2(x+1)^2 \\ (1/4)(x-1)x^2(x+1)^2 \end{array} \right\} \tag{2.26}$$

The weak form of Equation 2.1 is given by

$$\begin{aligned} &\left[\int_0^l \left(\frac{\partial^2 N}{\partial x^2} EI \frac{\partial^2 N}{\partial x^2} + N k_s N^T + \frac{\partial N}{\partial x} 2t_s \frac{\partial N}{\partial x}\right) dx\right] w \\ &+ \left[\int_0^l \left(N^T c N\right) dx\right] \dot{w} + \left[\int_0^l \left(N^T \rho N\right) dx\right] \ddot{w} - N \cdot P|_{x=vt} = 0 \end{aligned} \tag{2.27}$$

where N represents the shape function vector, and the dots ($\bullet$) and ($\bullet\bullet$) indicate the first and the second time derivative of the displacement, respectively. Discretizing the beam results in

$$[K]w + [C]\dot{w} + [M]\ddot{w} - \{F\} = 0 \tag{2.28}$$

where $[K], [C]$, and $[M]$ are the global stiffness, damping and mass matrices, respectively, and $\{F\}$ is the global force vector. These are obtained by assembling the corresponding elemental matrices. The implicit Wilson- Θ method is used for the direct time integration of the equation of motion (Equation 2.1).

The elemental mass, stiffness, and damping matrices, and force vector for the elements are given by

$$[m]^e_{4\times 4} = \int_{x_i}^{x_j} \left[\{N\}^T(\rho)\{N\}\right] dx \tag{2.29a}$$

$$[c]^e_{4\times 4} = \int_{x_i}^{x_j} \left[\{N\}^T c\{N\}\right] dx \tag{2.29b}$$

$$[k]^e_{4\times4} = \int_{x_i}^{x_j} \left[\left(\frac{d^2\{N\}}{dx^2} \right)^T E_b I_b \left(\frac{d^2\{N\}}{dx^2} \right) + \{N\}^T k_s \{N\} + \left(\frac{d\{N\}}{dx} \right)^T 2t_s \left(\frac{d\{N\}}{dx} \right) \right] dx \tag{2.29c}$$

$$\{f\}^e_{4\times1} = \int_{x_i}^{x_j} N^T P \Big|_{x=vt} dx \tag{2.29d}$$

The integrations in Equation 2.29 are evaluated numerically, and Loads are usually not put on the infinite elements; the algorithm is stopped before the load moves over an infinite element.

2.6 Results

2.6.1 Verification Studies

The developed analytical solutions are checked against the corresponding FE solutions to ensure that the obtained analytical equations are all correct. Examples of such verification studies are shown in Figure 2.4. The data used for this study are given in Table 2.1. Figure 2.4 shows comparisons of normalized mid-span beam deflections as a function of normalized distance along the length of the beam (or normalized time), obtained from analytical and FE solutions, for different damping and velocity ratios. The match between the analytical and FE results are quite good.

For the second set of verification, an infinite beam was considered. To simulate the response of an infinite beam, the analytical solutions for the simply supported beams was applied after making the length of the beam excessively large to nullify the effect of the boundary conditions near the central region of the beam. Steady-state beam responses were obtained near the mid-span of the beam (the response was found to be constant for multiple successive time steps). The steady-state responses were compared with those obtained from the analytical solutions of Basu and Kameswara (2013) [26] developed for infinite beams. Further, FE analysis results were obtained for the same problems and plotted. The data used for this set of verifications is given in Table 2.2.

Figures 2.5 and 2.6 show the steady-state beam deflection profiles for different load velocity ratios. The results obtained from the present analytical solutions match well with those from the analytical solutions of Basu and Kameswara (2013) [26] and the FE analysis with infinite elements for both one-parameter and two-parameter soil models.

Table 2.1: Data for the verification study of a simply supported beam on a two-parameter foundation

Parameter	**Value**
Beam length (l)	5 m
Beam Young's modulus (E)	2×10^8 kN/m^2
Beam moment of inertia (I)	3.06×10^{-5} m^4
Mass per unit length of the beam (ρ)	150 kg/m
Soil compression parameter (k_s)	0 and 1.6×10^4 kN/m^2
Soil shear parameter (t_s)	0 and 0.32×10^4 kN
Velocity ratio of the moving load (α)	0, 0.5, 1, and 2
Damping ratio of the system (β)	0, 0.1, 1, and 2

Table 2.2: Data for the infinite beam verification studies

Parameter	**Value/unit**
Beam length (l)	∞ m
Beam Young's modulus (E)	2×10^8 kN/m^2
Beam moment of inertia (I)	3.06×10^{-5} m^4
Mass per unit length of the beam (ρ)	150 kg/m
Soil compression parameter (k_s)	0 and 1.6×10^4 kN/m^2
Soil shear parameter (t_s)	0 and 0.32×10^4 kN
Velocity ratio of the moving load (α)	0.5, 1, and 2
Damping ratio of the system (β)	0.05

2.6.2 Effect of Foundation Stiffness on Dynamic Amplification Factor

The increase in the magnitude of beam deflection arising from the dynamic response of the simply supported beams (caused by moving loads) over and above the static beam deflection (if the load is stationary) is quantified in this study using the dynamic amplification factor ϕ_D defined as the ratio between the mid-span dynamic deflections to the maximum midspan static deflection substituted

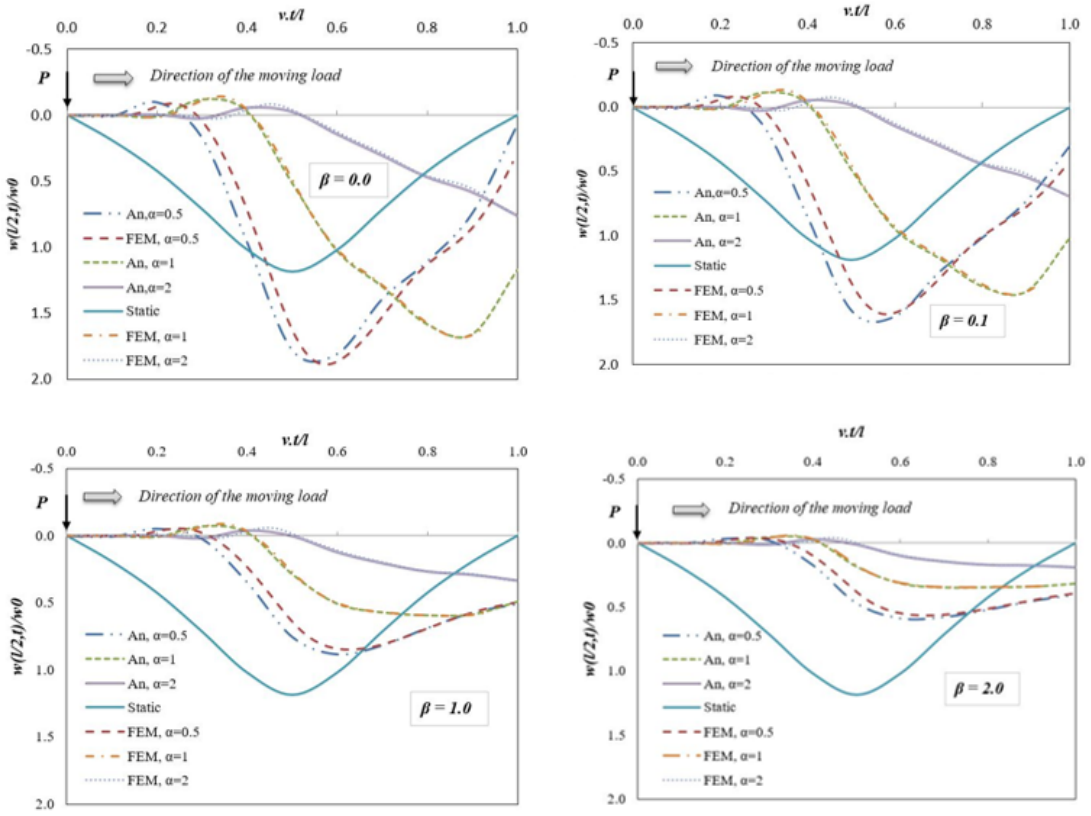

Figure 2.4: Mid span deflection of a simply supported beam on a two-parameter foundation with damping ratio $\beta = 0$, 0.1, 1, and 2 and subjected to a moving load with velocity ratio $\alpha = 0$, 0.5, 1, and 2

$$\varphi_D = \frac{w\left(\frac{x}{l} = 0.5, t\right) \text{ Substituted in Equation (2.18)}}{w\left(\frac{x}{l} = 0.5\right) \text{ Substituted in Equation (2.19)}} \tag{2.30}$$

The effect of foundation stiffness is studied by varying k_s and t_δ and the dynamic amplification factor ϕ_D is plotted as a function of vt/l in Figure 2.6 where t is the time after the load enters the beam form the left side. The foundation stiffness-parameters k_s and t_s are varied from 0 to 1.14×10^{11} N/m^2 and from 0 to 2.28×10^9 N respectively, in which t_s/k_s is kept constant as 0.2 m^2. The input data used is given in Table 2.3. Figure 2.6 shows that foundation stiffness has a significant impact on the beam response.

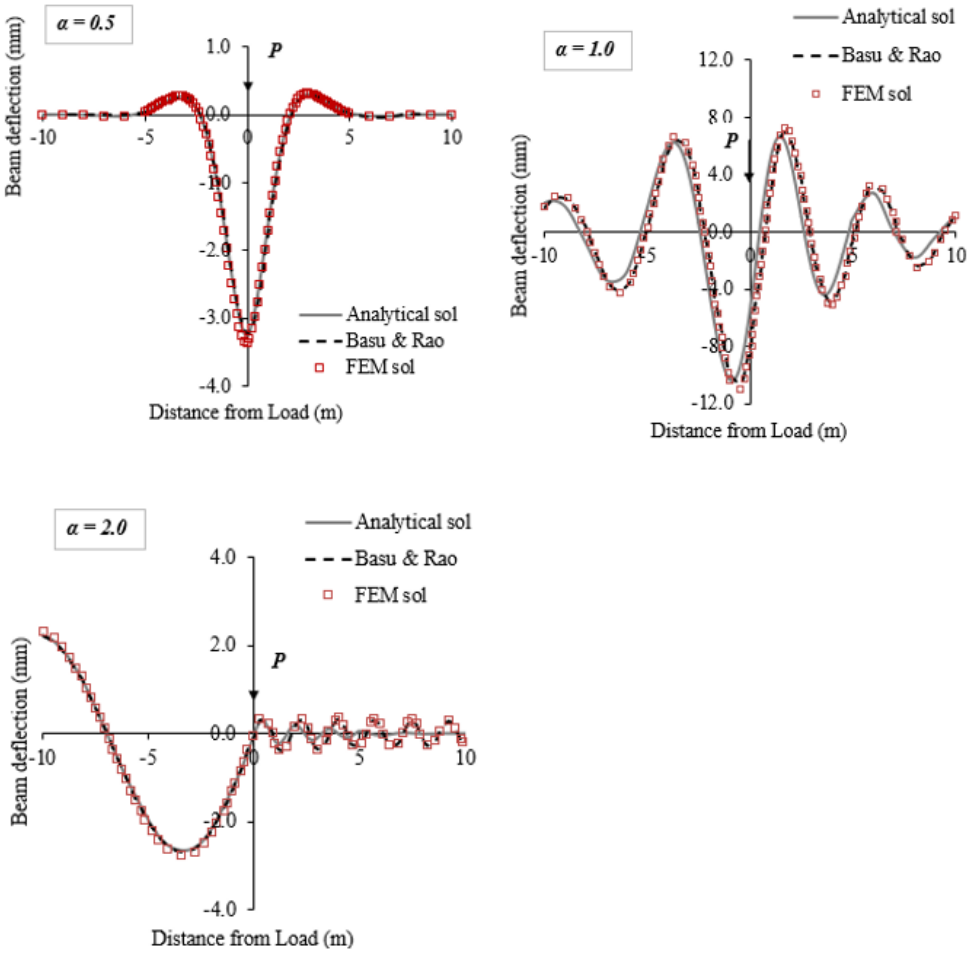

Figure 2.5: Steady state deflections of an infinite beam on a one-parameter foundation subjected to a point load moving with velocities corresponding to $\alpha = 0.5$, 1, and 2 when the damping ratio $\beta = 0.05$

2.6.3 Effect of Speed of Load on Dynamic Amplification Factor

Using the inputs given in Table 2.3 and maintaining k_s and t_s at 1.14×10^7 N/m^2 and 2.28×10^6 N, respectively, and $\beta = 0.05$, the mid-span dynamic amplification factor ϕ_D is plotted in Figure 2.8 as a function of vt/l for different speeds of load varying from 4.18 m/sec (15 km/h) to 82 m/sec(300 km/h). The results show that load speed has a significant influence on the beam response.

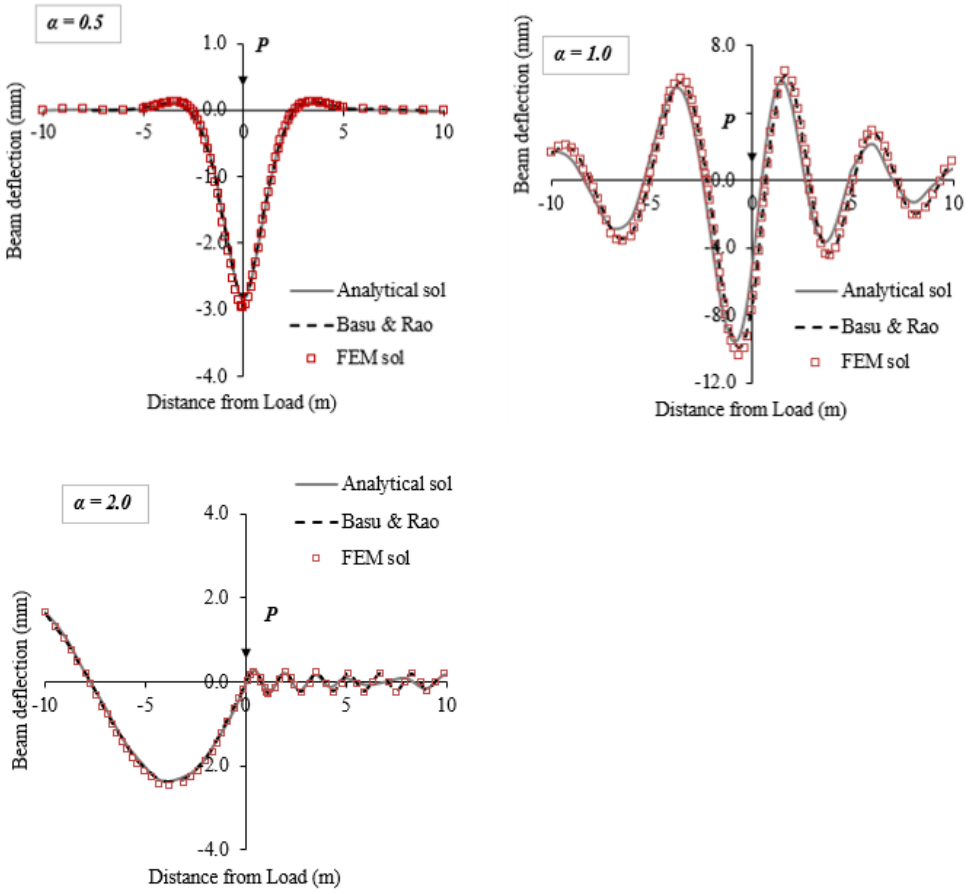

Figure 2.6: Steady state deflections of an infinite beam on a two-parameters foundation subjected to a load moving with velocities corresponding to $\alpha = 0.5$, 1, and 2 when the damping ratio $\beta = 0.05$

2.6.4 Effect of Beam Length on Dynamic Amplification Factor

The beam length is varied between 5 m to 45 m and ϕ_D is plotted in Figure 2.9 as a function of vt/l. The input data for this study is given in Table 2.4. The results show that the longer the span length, the higher the amplification factor.

Table 2.3: Input data to show the effect of the foundation stiffness of simply supported beam

Parameter	**Value/unit**
Beam length (l)	10 m
Beam models of elasticity (E)	2.05×10^8 kN/m^2
Beam moment of inertia (I)	1.84×10^{-4} m^4
Mass per unit length of the system (ρ)	150 kg/m
Soil compressive parameter (k_s)	0-1.14×10^{11} N/m^2
Soil shear parameter (t_s)	0-2.28×10^9 N
Velocity of the moving load (v)	16.7 m/sec
Damping coefficient (c)	0 kN-sec/m^2

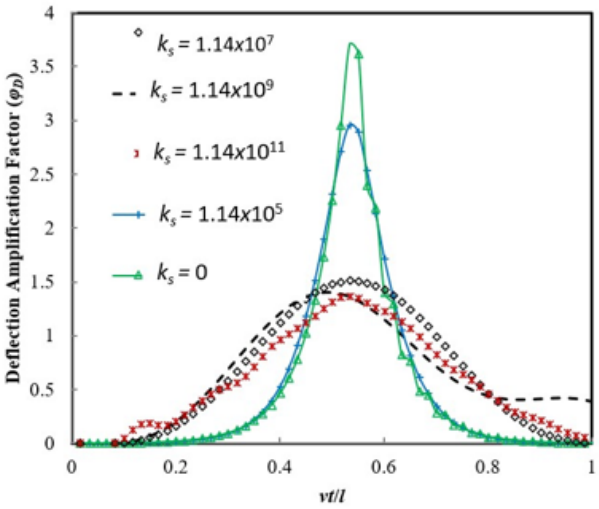

Figure 2.7: Effect of foundation stiffness-parameters on the mid-span response of simply supported beam on two-parameter foundation

2.6.5 Effect of Damping Ratio on Dynamic Amplification Factor

The damping ratio β is varied from 0.05 to 2 as detailed in Table 2.5, which contains the data used for this study, and ϕ_D is calculated and plotted as a function of vt/l in Figure 2.10. It is evident that the increase in damping ratio decreases the dynamic amplification factor.

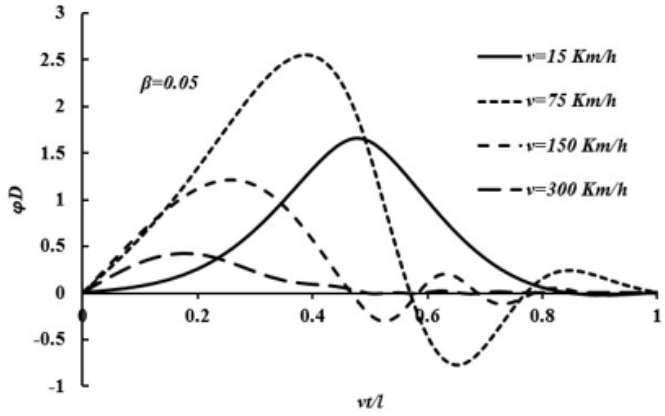

Figure 2.8: Effect of travelling speed on the mid-span dynamic amplification

Table 2.4: Input data to show the effect of the beam length of simply supported beam

Parameter	**Value/unit**
Beam length (l)	(5-45) m
Beam models of elasticity (E)	2.05×10^8 kN/m^2
Beam moment of inertia (I)	1.84×10^{-4} m^4
Mass per unit length of the system (ρ)	150 kg/m
Soil compressive parameter (k_s)	1.14×10^{11} N/m^2
Soil shear parameter (t_s)	2.28×10^9 N
Velocity ratio (α)	0.5
Damping ratio (β)	0.05

2.6.6 Effect of Beam Mass Density on Maximum Dynamic Amplification Factor

The beam mass density ρ is varied from 150 to 600 kg/m and maximum $\phi_D, \phi_{D\,\max}$, is calculated and plotted in Figure 2.11 as a function of vt/l in Figure 2.11. The data presented in Table 2.5 is used. For lower damping ratio, the amplification factor initially start with a value of 1.6; achieves its maximum value at a velocity equal to half of the characteristic velocity of the system; v_{ch}. And then decrease sharply to 0.5 as the velocity ratio increases to a value of about double of the critical velocity of the system, followed

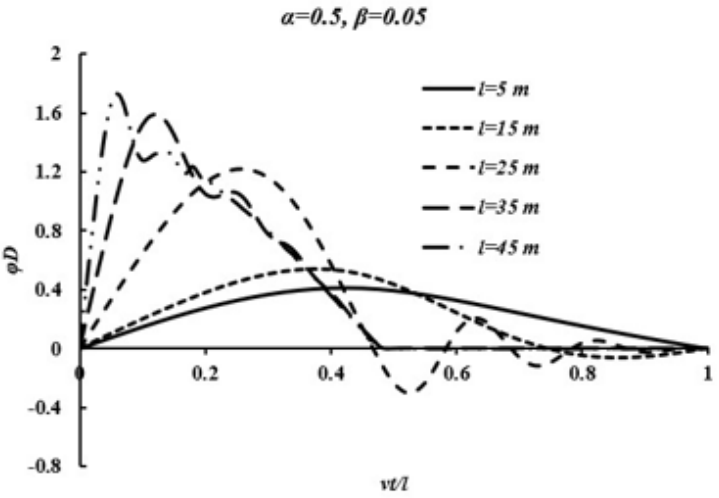

Figure 2.9: Effect of beam length on the mid-span amplification factor

Table 2.5: Input data to show the effect of the damping of simply supported beam

Parameter	**Value/unit**
Beam length (l)	10 m
Beam models of elasticity (E)	2.05×10^8 kN/m^2
Beam moment of inertia (I)	1.84×10^{-4} m^4
Mass per unit length of the system (ρ)	150 kg/m
Soil compressive parameter (k_s)	1.14×10^{11} N/m^2
Soil shear parameter (t_s)	2.28×10^9 N
Velocity ratio (α)	0.5
Damping ratio (β)	0.05-2

by a gentle increase as the velocity increase to a value of 3 times the characteristic velocity. However, for high and supper high damping ratio, the maximum amplification factor decreases softly with the increase in the velocity ratio.

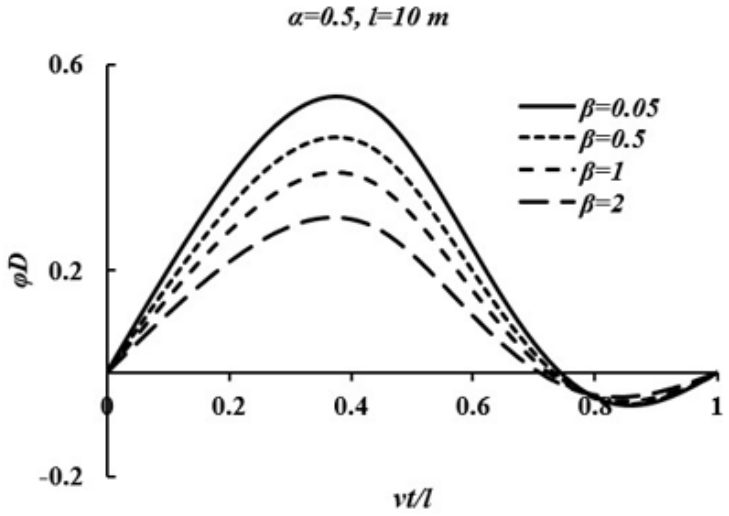

Figure 2.10: Effect of damping ratio on mid-span dynamic amplification

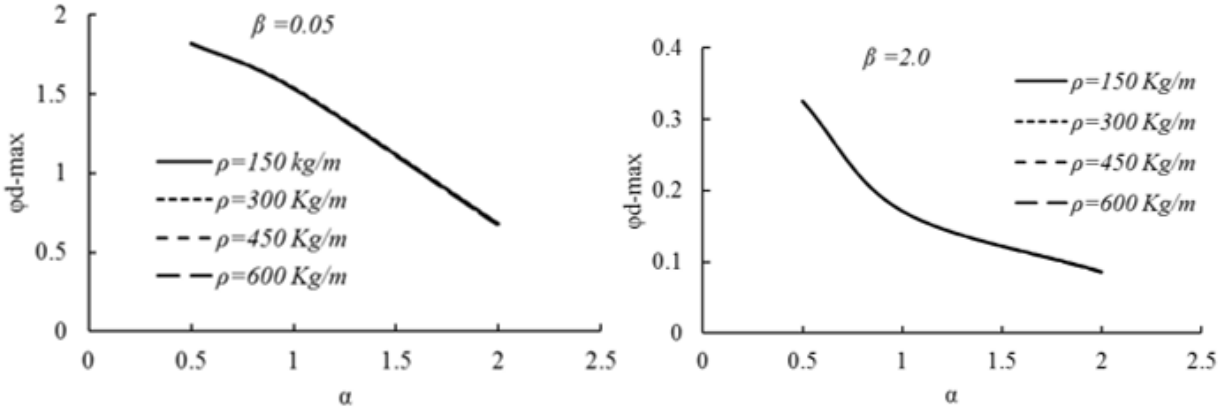

Figure 2.11: Effect of the mass density on the maximum amplification factor

2.6.7 Generalization of the Beam on Elastic Foundation Response: Normalized Speed-Span Diagram

Depending on the beam length and speed of load, the dynamic beam response changes, and this is categorized in this study by using a figure, which is named Normalized Speed-Span (NSS) diagram shown in Figure 2.12. This figure was generated after investigating the

beam response for a large set of input data. This NSS diagram is intended to describe the transition of the response of the beam-foundation system as the beam length increases and the load speed changes. The NSS diagram is constructed by plotting the velocity ratio α given by Equation 2.12 as a function of a dimensionless characteristic length η with a unit of (1/m) given by

$$\eta = \left[\frac{k_s}{4EI}\right]^{0.25} \tag{2.31}$$

The NSS diagram (Figure 2.12) is divided into twenty regions for which a single amplification curve is normalized to describe the behaviour of each region within a specified range of characteristic lengths and velocity ratios (Figures 2.13 and 2.14). Dynamic amplification curves are constructed by plotting the dynamic amplification factor ϕ_d as a function of relative load position vt/l along the span of the beam. The dynamic amplification curves for different regions of the NSS diagram are shown in Figures 2.13 and 2.14 for both one-parameter (Winkler) and two-parameter foundations, respectively.

The compacted form of the amplification curves shown in Figures 2.13 and 2.14 are built by assembling each five of the dynamic amplification curves given by these figures in a single extremum amplification chart (see Figures 2.15 and 2.16). The extremum amplification chart is constructed by plotting the velocity ratio α versus the maximum amplification factor $\phi_{d\,\max}$ for both one-parameter and two-parameter foundations, respectively.

It is important to state that the upper bound response of the beam shown in Figure 2.12 is well-thought-out as a simply supported beam with a finite length and a characteristic velocity v_{ch} given by Equation 2.13. However, the lower bound response is believed to be an infinitely long beam described by the steady state response and characterized by the critical velocity v_{cr} derived by Basu and Rao (2013) [26] (Equation 2.32). The two bounds are represented on the NSS diagram, by plotting the relative bound velocity ratio v_{cr}/v_{ch} versus the characteristic length ηl (Figure 2.12).

$$v_{cr} = \left[\left(\frac{4k_sEI}{\rho^2}\right)^{0.5} + \frac{2t_s}{\rho}\right]^{0.5} \tag{2.32}$$

2.7 Conclusions

An analytical solution for dynamic response of simply supported beams on two parameters elastic foundations subjected to a moving concentrated load with constant speed is devel-

oped. Linear integral transformers is used to solve the governing equilibrium equation of motion. The solutions are obtained in the closed form for different load speed and damping cases. An alternative finite element analysis-based solution is also developed and used to verify the analytical solutions. Verification studies are performed to show the accuracy of the developed analytical solutions. Parametric studies are performed to investigate the effect of different beam, foundation, and load parameters on the beam response in terms of dynamic amplification factor. Finally, a Normalized Speed-Span diagram is generated that can be used to demarcate the different beam responses as functions of beam length and load speed.

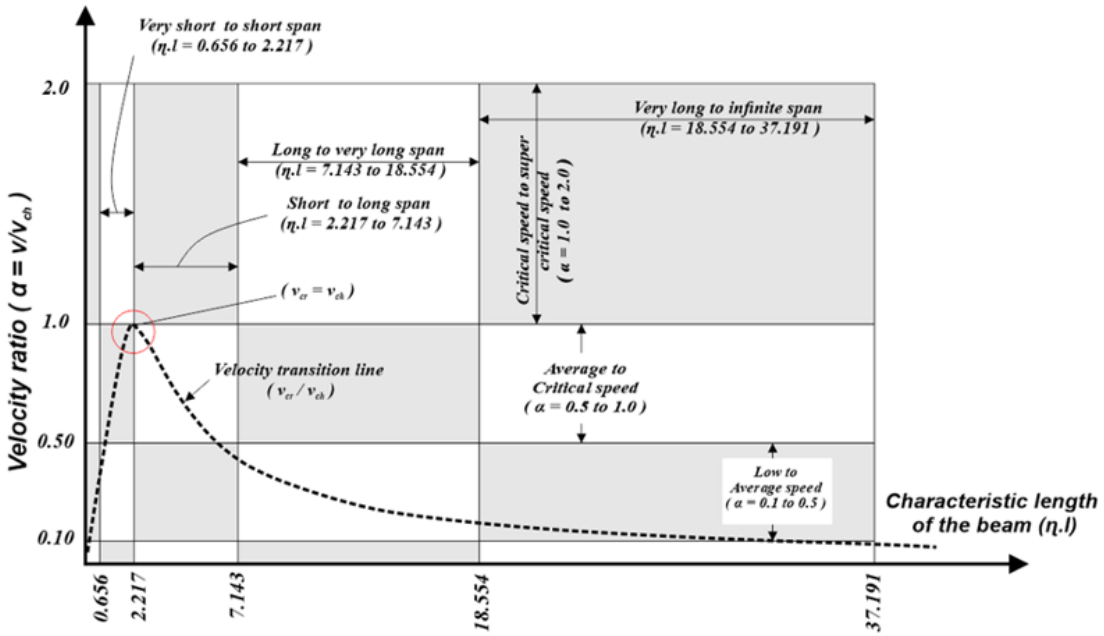

Figure 2.12: Normalized Speed-Span (NSS) diagram

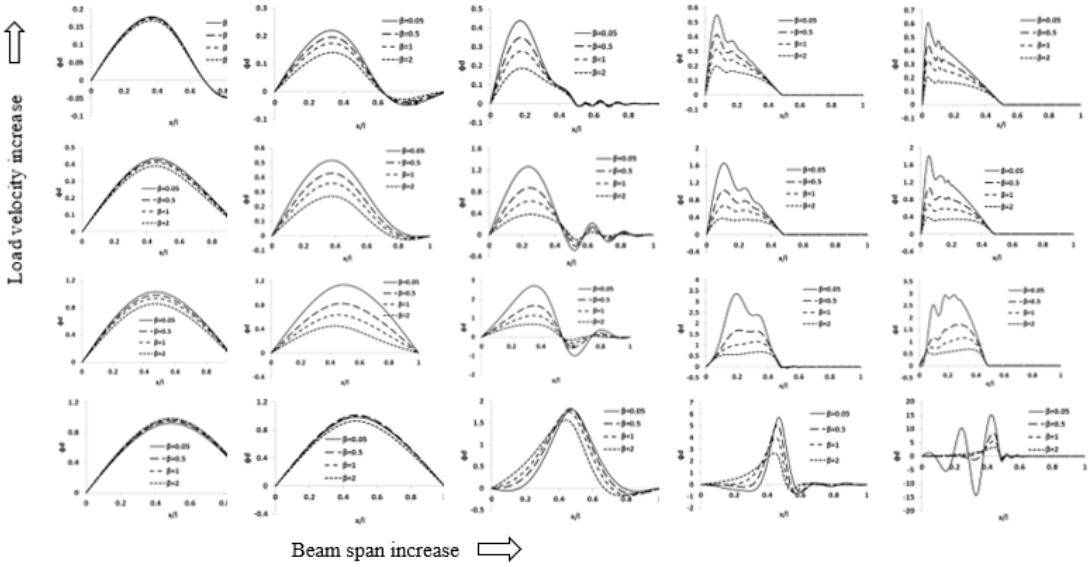

Figure 2.13: Dynamic amplification curves for Winkler foundation (used to construct the NSS diagram)

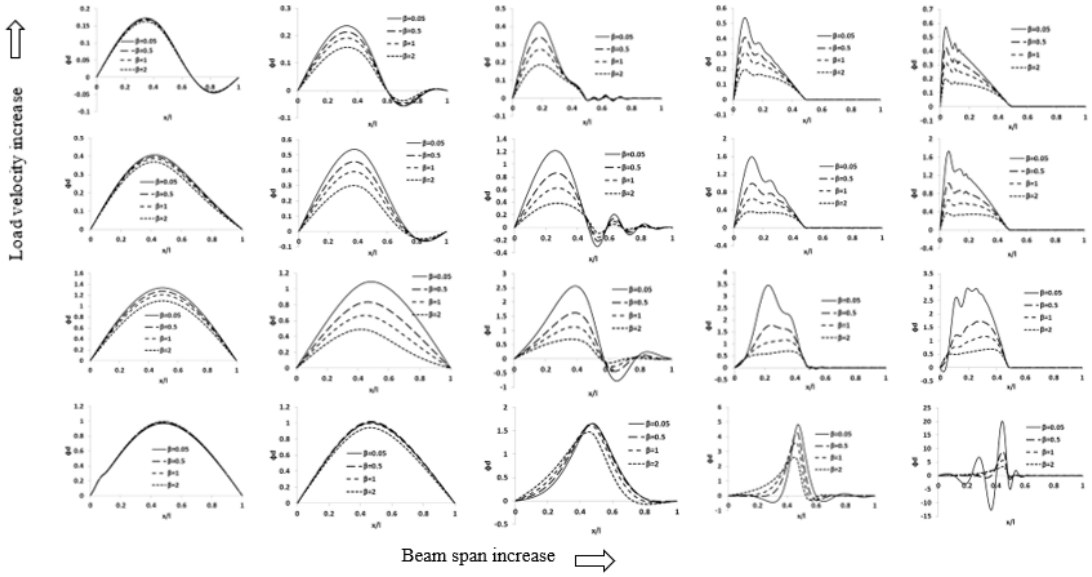

Figure 2.14: Dynamic amplification curves for Pasternak foundation (used to construct the NSS diagram)

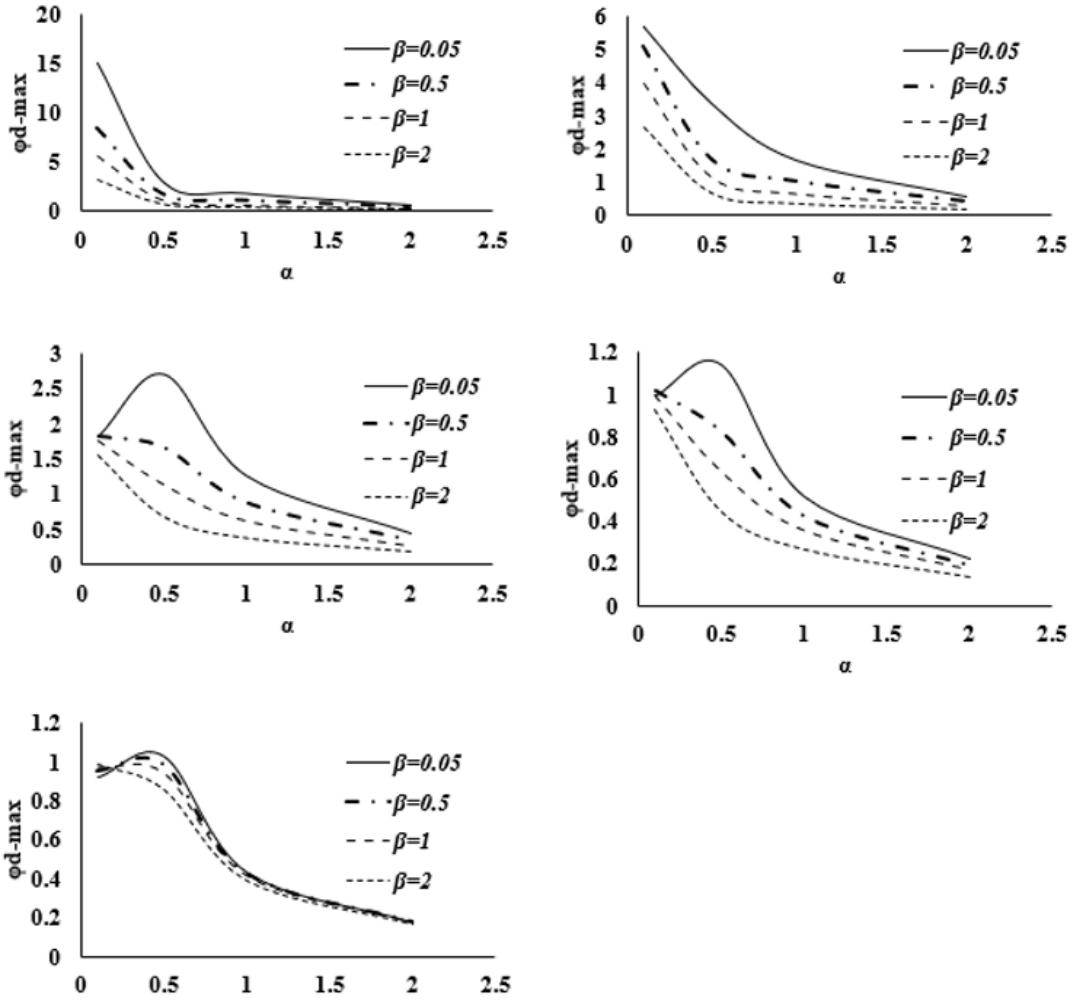

Figure 2.15: Extremum amplification curves for Winkler foundation (used to construct the NSS diagram)

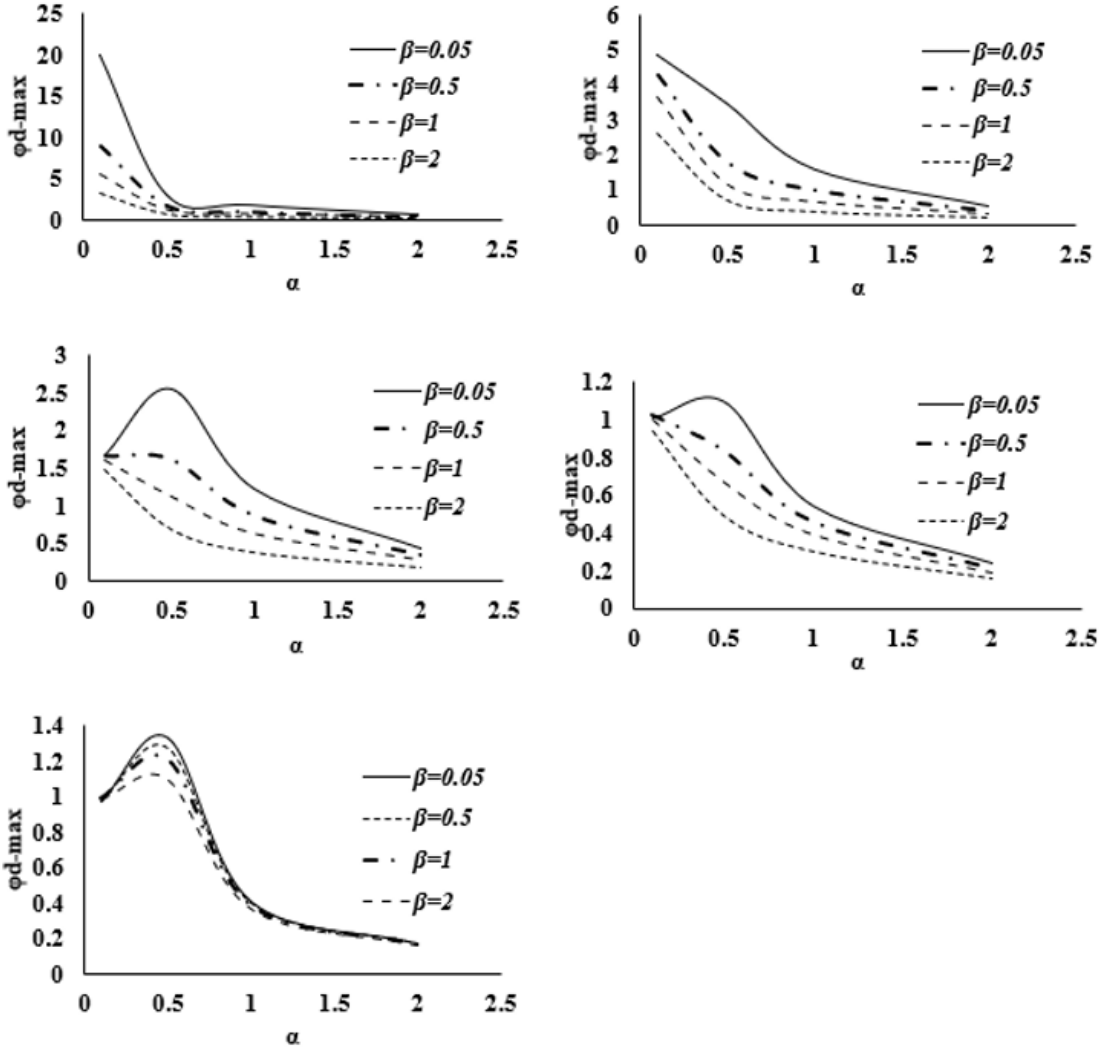

Figure 2.16: Extremum amplification curves for Pasternak foundation (used to construct the NSS diagram)

Chapter 3

Interaction of Timoshenko Beam with Multi-Layered Continuum

This chapter is submitted as a second revised Manuscript in the International Journal of Geotechnical Engineering, Ref.; IGE3195, 223173794.

3.1 Overview

An analysis of Timoshenko beam resting on multilayered continuum (soil) is presented. The variational principles of mechanics in conjunction with simplified assumptions on the displacement field in the continuum are used to obtain a set of coupled differential equations describing the beam deflection and soil displacements under equilibrium. Solutions of these equations are obtained analytically and numerically following an iterative algorithm. The resulting differential equation governing the beam deflection resembles that of a beam resting on two parameter foundation with the parameters k_s and t_s representing respectively the compressive and shear resistances of soil. The advantage of the present analysis is that the foundation parameters k_s and t_s are mechanistically related to the elastic constants (e.g., Young's modulus and Poisson's ratio) of the multi-layer foundation. Based on the study, algebraic equations of k_s and t_s have been developed for use by practitioners without recourse to the iterative algorithm presented in this paper. The effect of beam and soil bending and shear stiffnesses on the soil-structure interaction aspect of the problem is investigated. The range of applicability of Timoshenko beam theory on the beam on foundation problem is investigated.

3.2 Introduction and Related Literature

Beams on foundations are widely studied in several disciplines like civil, mechanical, bio- and nano-engineering, and have multiple applications especially in geotechnical engineering for analysis of strip foundations, laterally loaded pile foundations, pipelines, railroads, and pavements [47, 24, 180, 169]. The beam is a three-dimensional (3D) structural element with one of the dimensions (length) much greater than the other two dimensions (width and thickness/depth). Therefore, instead of analyzing it using the three- or two-dimensional elasticity theory, the beam theories are conveniently used that maintain simplicity and ensure accuracy and computational efficiency of the analysis [133]. The most used classical beam theory is the Euler-Bernoulli theory introduced in the 18th century in which it is assumed that plane sections in the beam remain plane after bending and remain orthogonal to the neutral axis (deflected elastic curve). The classical theory considers only flexural deformations and neglects shear deformations, which results in underestimation of the beam deformations. Thus, the Euler-Bernoulli theory works well only for long and slender beams [18]. A more accurate representation of beam mechanics that allows plane sections in the beam to rotate independently without being perpendicular to the slope of the deflected curve of the beam was proposed by Timoshenko (1921) [225]. The Timoshenko beam theory accounts for transverse shear deformations in the beam, and therefore, predicts the response of thick beams with low slenderness ratios better than the Euler-Bernoulli beam theory [224, 212].

Studies on beams resting on foundations (soils) have been performed with both Euler-Bernoulli and Timoshenko beam theories [34, 220, 80, 245, 68, 121]. However, which beam theory is most appropriate under what set of conditions (i.e., geometry and material properties of beam and foundation) is not properly established in the literature.

The studies on beams on foundations have mostly considered the foundation as a bed of disconnected linear springs as hypothesized by Winkler (1867) [255]. The Winkler-spring foundation model (also sometimes known as the one-parameter foundation model) considers the resistance of soil arising from compressive strains (captured by the spring constant k_s) and neglects the resistance arising from shear strains. Most foundations beneath beams are continuums (such as soil) and offer resistance against both the normal and shear strains because of which improvement to the Winkler model is necessary for obtaining realistic beam-foundation responses.

Many two-parameter spring-foundation models have been proposed by several authors (e.g., Filonenko-Borodich (1945) [92], Pasternak (1954) [177]) as improvements to the Winkler model. In the two-parameter models, mechanical interaction between adjacent springs

is considered (i.e., the springs are assumed to be mechanically connected, for example, by a stretched membrane or a plate element or a shear layer) and is captured by the second parameter t_s. Although the mechanical interaction between the foundation springs is interpreted in multiple ways, the interpretation of shear resistance seems most rational (because continuums like soil exhibit resistance against both normal and shear strains). Irrespective of the different interpretations of the second parameter t_s, the two parameter foundations proposed by different authors and characterized by the parameters k_s and t_s have the same governing differential equation [267, 219, 178, 9, 170].

Although Winkler and two-parameter foundation models have been developed several decades ago, their use in practical problems in geotechnical engineering has been rather limited because of the difficulty in obtaining the numerical values of the parameters k_s and t_s. This is not surprising because k_s and t_s are artificial parameters that are strictly not related to the continuum properties such as the Young's modulus E_s and Poisson's ratio υ_s of soil. Several empirical equations and procedures have been proposed to relate k_s to E_s, υ_s and the beam properties based on the Euler-Bernoulli theory [34, 245, 45, 64, 68, 256]. However, these equations and procedures have limited applicability (e.g., the equation proposed by Vesic (1961) [245] is applicable for very long beams) and their accuracy and reliability in real field applications are not well established. Such equations of k_s for Timoshenko beams are not available. Moreover, empirical equations of ts are not available for either Euler-Bernoulli or Timoshenko beams. At the same time, equations for k_s and t_s are not available or multi-layered soil deposits.

Simplified continuum models have also been proposed to represent the foundations underneath beams [247, 242, 190]. In this approach, the foundation (soil) underneath the beam is represented by a continuum with the stress or displacement field assumed a priori. The advantage of this approach is that stresses, strains, and displacements in the soil can be calculated as part of the solution, and the foundation parameters can be mathematically related to the elastic constants of the continuum (without recourse to empiricism) in a physically meaningful way. However, most simplified continuum-based studies consider only a single soil layer and Euler-Bernoulli beam. Recently, Haldar and Basu (2016) [102] and Elhuni and Basu (2019) [86] studied the interaction of Euler-Bernoulli beams with multi-layered continuums. But, studies on Timoshenko beams resting on multi-layered continuums are rather limited [2].

It is clear from the foregoing discussion that the range of applicability of the Euler-Bernoulli and Timoshenko beam theories is not established for soil-structure interaction problems. Further, reliable equations of k_s and t_s representing multi-layer deposits are not available for use with both the beam theories. In this study, a generalized analysis framework is developed following a simplified continuum approach in which both the Tim-

oshenko and Euler-Bernoulli beam theories are analyzed with multi-layered soil deposits. The analysis framework is based on the variational principles of mechanics using which the foundation parameters k_s and t_s are mathematically related to the elastic constants E_s and υ_s of soil without any empiricism. The developed framework is an improved and generalized version of the model developed by Vlasov and Leont'ev (1966) [247]. In the analysis, two sets of governing differential equations are obtained - one for the beam and the other for the foundation - which are solved numerically and analytically following an iterative algorithm. Systematic parametric studies are performed to determine the range of applicability of the different beam theories, and to develop fitted algebraic equations for k_s and t_s that can be readily used by practitioners without recourse to the iterative algorithm. The equations of k_s and t_s are developed separately for Timoshenko and Euler-Bernoulli beams. The effect of multiple soil layers on the beam responses is also investigated and fitted equations of k_s and t_s are developed for one-, two-, and three-layer deposits.

3.3 Analysis

3.3.1 Problem Definition

A beam lying on multi-layered foundation (soil) is considered as shown in Figure 3.1. The beam geometry (L = length, b = width, and d = depth or thickness, $Ab = bd$ = cross-sectional area, and $I_b = \frac{bd^3}{12}$ = second moment of area) and material properties (υ_b = beam Poisson's ratio and E_b = beam Young's modulus) are given as inputs. The material properties and layering of the soil deposit (for any soil layer i, E_{si} = Young's modulus, υ_{si} = Poisson's ratio, $T_i = H_i - H_{i-1}$ = thickness, H_i = depth of the bottom surface of the layer) are also given as inputs with the assumption that each layer is homogeneous, isotropic and linear elastic. The bottom layer n rests on a rigid substratum (like bed rock) and the total thickness of all the elastic layers is H_{total} $(= \sum_{i=1}^{n} T_i)$. Multiple static vertical loads act on the beam - these loads can be either a series of concentrated loads Q_j (j = 1, 2, ..., m) acting at different discrete points on the beam or a distributed load $q(x)$, or a combination thereof.

With the cartesian $x - z$ coordinate system assumed as shown in Figure 1, the domain in the x (horizontal) direction is generally assumed from x = - χL to x = L + χL ($\chi >$ 1 and chosen by trial and error) to capture the displacements in the continuum beyond the loaded beam. The domain in the z (vertical) direction is assumed to be from $z = 0$

to $z = \mathrm{H}_{total}$. Further, a strip of width b perpendicular to the $x - z$ plane is considered for analysis, similar to the plane-strain assumption made by Vlasov and Leont'ev (1966) [247].

3.3.2 Potential Energy Minimization of Beam-Foundation System

The horizontal displacement u_x in the continuum (soil) is neglected and the vertical displacement u_z is expressed as (Figure 3.1)

$$u_z = w(x)\phi(z) \tag{3.1}$$

where $w(x)$ = displacement of the top surface of the continuum = beam deflection for 0 $\leq x \leq$ L, and $\phi(z)$ = dimensionless displacement decay function. Assuming $\phi(0) = 1$ ensures contact between the beam and continuum at all times, and assuming $\phi(\mathrm{H}_{total}) = 0$ ensures a decrease in vertical displacement in the continuum with increase in depth, with the displacement vanishing at the interface with the rigid layer.

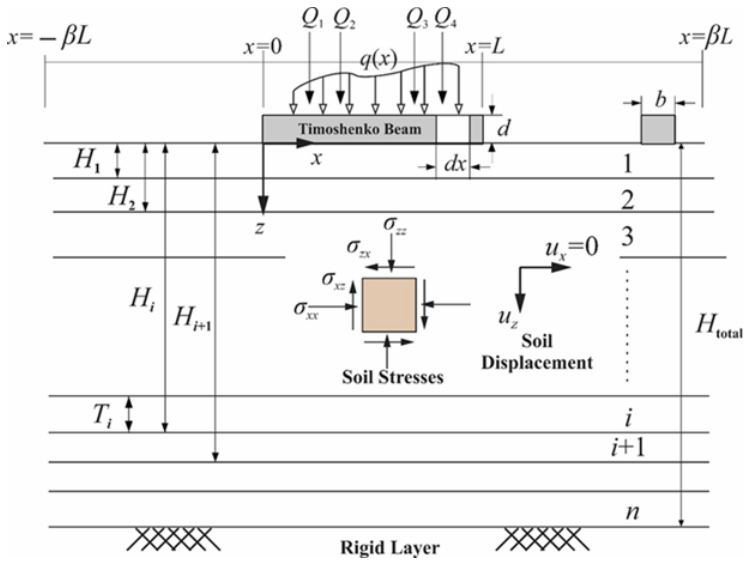

Figure 3.1: Timoshenko beam on multi-layered foundation

The strain tensor at any point in the continuum is given by

$$\varepsilon_{ij} = \begin{Bmatrix} \varepsilon_{xx} \\ \varepsilon_{zz} \\ \varepsilon_{xz} \end{Bmatrix} = \begin{Bmatrix} 0 \\ -w\frac{d\phi}{dz} \\ -\frac{1}{2}\frac{\partial w}{\partial x}\phi(z) \end{Bmatrix} \tag{3.2}$$

and the corresponding stress tensor is given by (Figure 3.1)

$$\sigma_{ij} = \begin{Bmatrix} \sigma_{xx} \\ \sigma_{zz} \\ \sigma_{xz} \end{Bmatrix} = \frac{E_s}{(1+\upsilon_s)(1-2\upsilon_s)} \begin{bmatrix} 1-\upsilon_s & \upsilon_s & 0 \\ \upsilon_s & 1-\upsilon_s & 0 \\ 0 & 0 & 0.5-\upsilon_s \end{bmatrix} \begin{Bmatrix} 0 \\ -w(x,t)\frac{d\phi(z)}{dz} \\ -0.5\frac{dw(x)}{dx}\phi(z) \end{Bmatrix} \tag{3.3}$$

Therefore, the strain energy density $\frac{1}{2}\sigma_{ij}\varepsilon_{ij}$ for any layer i is given by:

$$U_{D-continuum} = \frac{1}{2}\left[\bar{E_{si}} w^2 \left(\frac{d\phi_i}{dz}\right)^2 + G_{si}\phi_i^2 \left(\frac{dw}{dx}\right)^2\right] \tag{3.4}$$

where $\phi_i = \phi(z)$ within the ith layer, and $\bar{E_{si}}$ (constrained modulus) and G_{si} (shear modulus) are given by

$$\bar{E_{si}} = \frac{E_{si}(1-\upsilon_{si})}{(1+\upsilon_{si})(1-2\upsilon_{si})} \tag{3.5a}$$

$$G_{si} = \frac{E_{si}}{2(1+\upsilon_{si})} \tag{3.5b}$$

From Equation 3.4, the total potential energy of the continuum over a volume Ω is given by

$$\Pi_{continuum} = \int_\Omega U_{D-continuum} d\Omega_{continuum} = \sum_{i=1}^{n} \frac{b}{2} \int_{-\chi L}^{\chi L} \int_{H_{i-1}}^{H_i} \left[\bar{E_{si}} w^2 \left(\frac{d\phi_i}{dz}\right)^2 + G_{si}\phi_i^2 \left(\frac{dw}{dx}\right)^2\right] dz dx \tag{3.6}$$

In Timoshenko beam theory, plane sections within a beam remain plane after bending but the rotation of the section is not necessarily normal to the longitudinal axis (elastic curve) of the beam. Thus, the rotation of the plane is represented by $\psi(x)$ which includes the rotation of the beam axis dw/dx and the rotation caused by the shear strain γ_{xz} in the beam (Figure 3.2). In contrast, Euler-Bernoulli beam theory neglects the shear strains in the beam so that $\psi(x) = dw/dx$. Therefore, the axial and transverse displacements u_x and u_z within the Timoshenko beam is given by (Figure 3.2).

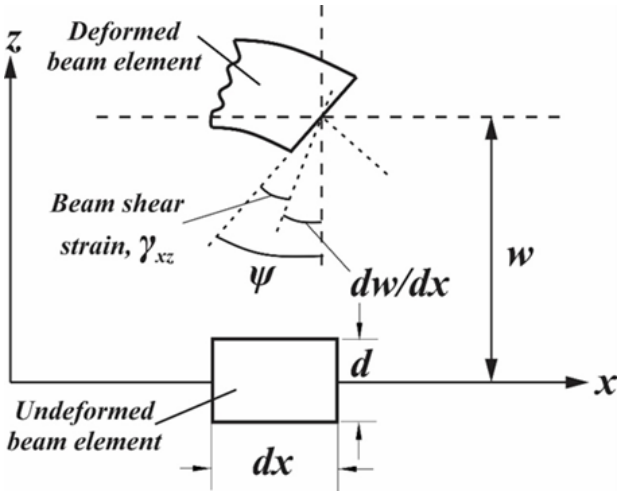

Figure 3.2: Kinematics of Timoshenko beam

$$u_x = z\psi(x) \tag{3.7a}$$

$$u_z = w(x) \tag{3.7b}$$

where $w(x)$ is the transverse vertical deflection of the beam axis. The corresponding strain and stress tensors in the beam are given by

$$\varepsilon_{ij} = \begin{Bmatrix} \varepsilon_{zz} \\ \varepsilon_{xx} \\ \gamma_{xz} \end{Bmatrix} = \begin{Bmatrix} 0 \\ z\dfrac{d\psi}{dx} \\ \psi(x) + \dfrac{dw(x)}{dx} \end{Bmatrix} \tag{3.8}$$

$$\sigma_{ij} = \begin{Bmatrix} \sigma_{xx} \\ \sigma_{zz} \\ \tau_{xz} \end{Bmatrix} = \begin{bmatrix} 0 & 0 & 0 \\ 0 & E_b & 0 \\ 0 & 0 & \kappa G_b \end{bmatrix} \begin{Bmatrix} 0 \\ z\dfrac{d\psi}{dx} \\ \psi(x) + \dfrac{dw(x)}{dx} \end{Bmatrix} \tag{3.9}$$

where κ is the shear correction factor, which is commonly defined as the ratio of the average shear strain over a beam cross section to the shear strain at the centroid of the cross section [227], and G_b is the beam shear modulus given by

$$G_b = \frac{E_b}{2(1+\upsilon_b)} \tag{3.10}$$

Table 3.1 can be used to determine the shear correction factor for beams with rectangular cross-sections for different beam Poisson's ratios and different beam depth to width (d/b) ratios [100].

Table 3.1: Shear correction factor for a Timoshenko beam with rectangular cross-section

Beam Poisson's	**Beam depth to width ratio** d/b			
ratio υ_b	**2**	**1**	**0.5**	**0.25**
0	0.8333	0.8333	0.8333	0.8333
0.25	0.8331	0.8295	0.7961	0.6308
0.5	0.8325	0.8228	0.7375	0.4404

Based on Equations 3.8-3.9, the strain energy density in the Timoshenko beam is given by

$$U_{D-beam} = \frac{1}{2}\sigma_{ij}\varepsilon_{ij} = \frac{1}{2}\left[E_b z^2 \left(\frac{d\psi}{dx}\right)^2 + \kappa G_b \phi_i^2 \left(\frac{\partial w}{\partial x} + \psi\right)^2\right] \tag{3.11}$$

and the corresponding potential energy for the beam is given by

$$\Pi_{beam} = \int\limits_{volume} U_{D-beam} dV_{beam} = \frac{1}{2} \int\limits_{-\chi L}^{\chi L} \int\limits_{H_{i-1}}^{H_i} \left[E_b z^2 \left(\frac{d\psi}{dx} \right)^2 + \kappa G_b \phi_i^2 \left(\frac{\partial w}{\partial x} + \psi \right)^2 \right] A_b dx$$

$$= \frac{1}{2} \int\limits_0^L \left[E_b I_b \left(\frac{d\psi}{dx} \right)^2 + \kappa G_b A_b \left(\frac{dw}{dx} \right)^2 + \kappa G_b A_b \psi^2 + 2\kappa G_b A_b \frac{dw}{dx} \psi \right] dx \tag{3.12}$$

The potential energy of the Euler-Bernoulli beam can be obtained from Equation 3.12 by setting $\psi = dw/dx$.

The potential lost by the external work done on the beam-foundation system is given by

$$\Pi_{load} = - \int\limits_0^L q(x) w dx - \sum_{j=1}^{m} Q_j w \mid_{x=x_j} \tag{3.13}$$

To obtain the differential equations of the beam-foundation system, the principle of minimum potential energy is used

$$\delta \Pi_{system} = \delta(\Pi_{continuum} + \Pi_{beam} + \Pi_{load}) = 0 \tag{3.14}$$

where δ is the variational operator. Substituting Equations 3.6, 3.12, and 3.13 in Equation 3.14 results in

$$\delta \sum_{i=1}^{n} \frac{b}{2} \int_{-\chi L}^{\chi L} \int_{H_{i-1}}^{H_i} \left[\bar{E_{si}} w^2 \left(\frac{d\phi_i}{dz} \right)^2 + G_{si} \phi_i^2 \left(\frac{dw}{dx} \right)^2 \right] dz dx +$$

$$\frac{1}{2} \delta \int\limits_0^L \left[E_b I_b \left(\frac{d\psi}{dx} \right)^2 + \kappa G_b A_b \left(\frac{dw}{dx} \right)^2 + \kappa G_b A_b \psi^2 + 2\kappa G_b A_b \left(\frac{dw}{dx} \right) \psi \right] dx + \tag{3.15}$$

$$- \delta \int\limits_0^L q(x) w dx - \delta \sum_{j=1}^{m} Q_j w \mid_{x=x_j} = 0$$

3.3.3 Differential Equations for Beam Displacements

Considering the variations of w and ψ in Equation 3.15 over $0 \leq x \leq$ L, the following differential equations of beam deflection and rotation for Timoshenko beams are obtained

$$\kappa A G_b \frac{d\psi}{dx} - (\kappa A G_b + 2t_s)\frac{d^2w}{dx^2} + k_s w - q(x) - \sum_{j=1}^{m} Q_j \mid_{x=x_j} = 0 \quad (0 \leq x \leq L) \tag{3.16a}$$

For Euler-Bernoulli beams, the corresponding differential equation of beam deflection over $0 \leq x \leq$ L is obtained from Equation 3.15 (with $\psi = dw/dx$) as

$$E_b I_b \frac{d^2\psi}{dx^2} - \kappa A G_b(\psi - \frac{dw}{dx}) = 0 \quad (0 \leq x \leq L) \tag{3.16b}$$

Considering the variation of w in Equation 3.15 over -χ L $\leq x \leq 0$ and L $\leq x \leq \chi$ L, the governing differential equation of surface displacement of the foundation (soil deposit) is obtained as

$$-2t_s \frac{d^2w}{dx^2} + k_s w = 0 \quad (-\chi L \leq x \leq 0) \; and \; (L \leq x \leq \chi L) \tag{3.16c}$$

For free-end beams, the displacements are spread on either side of beam. Therefore, the continuum and the beam have to be taken together and Equation 3.16(a,c) have to be solved simultaneously to obtain the beam response. For simply supported and fixed-end beams for which the displacements are zero at and beyond the beam ends, only differential Equations 3.16(a,b) for Timoshenko beam or Equation 3.16(c) for Euler-Bernoulli beam has to be solved.

Boundary conditions are required for solving the preceding differential equations. For free-free beams with domains -χ L $\leq x \leq 0$ and $0 \leq x \leq \chi$ L on either side of the beam, $\chi > 1$ is chosen by trial and error so that $w = 0$, and $\psi = 0$ or $dw/dx = 0$ at $x =$ -χ L and at $x = \chi$ L. The continuity of displacement, shear force, and bending moment across the free ends of the beam (at $x = 0$ and at $x =$ L) are maintained by the following conditions:

$$w_{Right} \mid_{x=0} = w_{Left} \mid_{x=0} \tag{3.17a}$$

$$w_{Left} \mid_{x=L} = w_{Right} \mid_{x=L} \tag{3.17b}$$

$$\left[-2t_s \tfrac{dw}{dx}\right]_{Left} \mid_{x=0} = \left[\kappa A_b G_b(\psi - \tfrac{dw}{dx}) - 2t_s \tfrac{dw}{dx}\right]_{Right} \mid_{x=0} \tag{3.17c}$$

$$\left[\kappa A_b G_b(\psi - \tfrac{dw}{dx}) - 2t_s \tfrac{dw}{dx}\right]_{Left} \mid_{x=L} \tag{3.17d}$$

$$E_b I_b \frac{d\psi}{dx} \mid_{x=0 \ \& \ x=L} = 0 \tag{3.17e}$$

For simply supported or fixed-end beams, the required boundary conditions are

$$w \mid_{x=0 \ \& \ x=L} = 0 \quad \text{(for hinged or fixed end)} \tag{3.17f}$$

$$\psi \mid_{x=0 \ \& \ x=L} = 0 \quad \text{(for fixed end)} \tag{3.17g}$$

$$E_b I_b \frac{d\psi}{dx} \mid_{x=0 \ \& \ x=L} = 0 \quad \text{(for hinged end)} \tag{3.17h}$$

$$\left[\kappa A_b G_b(\psi - \tfrac{dw}{dx}) - 2t_s \tfrac{dw}{dx}\right] \mid_{x=0 \ \& \ x=L} = 0 \quad \text{(for fixed or hinged end)} \tag{3.17i}$$

The assumption made in the foregoing boundary-condition equations is that no applied point load or moment acts at the beam ends. If such load(s) and/or moment(s) act on the beam, then these applied forces and moments have to be appropriately included in the corresponding boundary conditions. Note that Equation 3.17(a,b,f) are related to beam deflection; Equation 3.17(g) is related to beam slope (or rotation); Equation 3.17(c,d,i) are related to shear force; and Equations 3.17(e,h) are related to bending moment. Applied point loads and moments at the beam ends are associated with the shear force and bending moment boundary conditions, respectively, such that force and moment equilibria are satisfied. The above boundary-condition equations are applicable to Timoshenko beams, and the corresponding boundary conditions for Euler-Bernoulli beams can be obtained by setting $\psi = dw/dx$ in the above equations except the shear force boundary conditions given by Equation 3.17(c,d,i).

The foundation (soil) parameters used in the above equations are given by

$$k_s = b \sum_{i=1}^{n} \int_{H_{i-1}}^{H_i} \bar{E}_{si} \left(\frac{d\phi_i}{dz}\right)^2 dz \tag{3.18a}$$

$$t_s = \sum_{i=1}^{n} \frac{b}{2} \int_{H_{i-1}}^{H_i} G_{si} \phi_i^2 dz \tag{3.18b}$$

It is important to note that k_s represents the compressive/tensile resistance of the foundation (soil) and is a function of the foundation constrained modulus $\bar{E_{si}}$. The parameter t_s represents the shear resistance of the foundation (soil) and is a function of the foundation shear modulus G_s. Both k_s and t_s depend on the function $\phi(z)$, which takes into account the interaction of the beam with the foundation. Therefore, k_s and t_s are not mere foundation parameters but interaction parameters that depend on the interactive response of both the foundation and beam. Further, these parameters are related to the elastic constants of the foundation (soil) in addition to the beam geometry because of which empirical equations are not required to determine these parameters.

Another feature of the foundation model is that the shear force generated along any vertical section across the beam and foundation (soil) is a summation of the shear force present in the beam and the shear force present in the continuum. The beam shear force at any section is given by $[\kappa A_b G_b(\psi\text{-}dw/dx)]$ for Timoshenko beams and by $(E_b I_b d^3w/dx^3)$ for Euler-Bernoulli beams, and the shear force in the layered continuum (i.e., the soil shear force) at any vertical section is given by $(\text{-}2t_s\ dw/dx)$.

3.3.4 Differential Equations for Soil-Displacement Function

Considering the variation of the function ϕ in Equation 3.15 over $0 \leq z \leq H_{total}$, the differential equation of $\phi(z)$ within the i^{th} layer can be obtained as

$$\frac{d^2\phi_i}{dz^2} - \left(\frac{\bar{\gamma_i}}{T_i}\right)^2 \phi_i = 0 \tag{3.19a}$$

where

$$\left(\frac{\bar{\gamma_i}}{T_i}\right)^2 = \left(\frac{n_{si}}{m_{si}}\right) \tag{3.19b}$$

with

$$m_{si} = b \int_{-\chi L}^{\chi L} \bar{E_{si}} w^2 dx \tag{3.20a}$$

$$n_{si} = b \int_{-\chi L}^{\chi L} G_{si} \left(\frac{dw}{dx}\right)^2 dx \tag{3.20b}$$

such that the dimensionless parameter $\bar{\gamma}_i$ is given by

$$\left(\frac{\bar{\gamma}_i}{T_i}\right)^2 = \frac{G_{si} \int_{-\chi L}^{\chi L} \left(\frac{dw}{dx}\right)^2 dx}{\bar{E_{si}} \int_{-\chi L}^{\chi L} w^2 dx} \tag{3.20c}$$

The corresponding boundary conditions are $\phi(0) = 1$, $\phi(H_{total}) = 0$, and $\phi_i = \phi_{i+1}$ at z $= H_i$, and these conditions ensure perfect contact between the beam and the underlying foundation (soil), zero vertical displacement at the interface between the foundation (soil) and underlying rigid layer, and continuity of vertical displacement across foundation layer boundaries.

3.3.5 Solution of the Differential Equations

Solution of the differential Equations 3.16(a,b) for Timoshenko beam deflection w and rotation ψ is obtained by using the displacement-based finite element (FE) method. Considering the weak form of the differential equations in which the highest derivatives of w and ψ are dw/dx and $d\psi/dx$ it is apparent that linear Lagrangian shape functions are required to interpolate both w and ψ over the elements. However, using a linear interpolation polynomial for w and ψ leads to the shear locking phenomenon for Timoshenko beams, which causes numerical difficulties [82]. Shear locking is the incapability of the FE analysis to produce zero shear strains as the beam becomes very slender, thus underestimating the beam displacement significantly [93]. Considering the fact that the minimum admissible degree of interpolation function is linear such that $dw/dx \neq 0$ and $d\psi/dx \neq 0$ in the weak form and that $\psi = dw/dx$ for thin beams, a consistent interpolation for w and ψ are chosen such that ψ and dw/dx are polynomials of the same order [187]. Thus, a three-noded beam element is used such that there are only two degrees of freedom ψ_k and ψ_l for rotation ψ at the left and right nodes k and l, respectively, but there is no rotation degree of freedom at the middle node m; and there are three degrees of freedom w_k, w_m, and w_l for the nodes k, m, and l, respectively (Figure 3.3). Lagrangian shape functions with linear polynomials $\{N^{\psi}\}^{l}_{2\times 1}$ are used to interpolate ψ_k and ψ_l, and Lagrangian shape functions with quadratic polynomials $\{N^{w}\}^{Q}_{3\times 1}$ are used to interpolate w_k, w_m, and w_l (Figure 3.3). These shape functions are given by

$$\{N^{\psi}\}^{l}_{2\times 1} = \begin{bmatrix} 1 - \frac{\hat{x}}{h_e} & \frac{\hat{x}}{h_e} \end{bmatrix}^T = \begin{bmatrix} N^{\psi}_k & N^{\psi}_l \end{bmatrix}^T \tag{3.21}$$

$$\{N^{\psi}\}^{Q}_{3\times1} = \left[(1-\tfrac{\hat{x}}{h_e})(1-\tfrac{2\hat{x}}{h_e}) \quad (\tfrac{4\hat{x}}{h_e})(1-\tfrac{\hat{x}}{h_e}) \quad (\tfrac{-\hat{x}}{h_e})(1-\tfrac{2\hat{x}}{h_e})\right]^T = \left[N^w_k \quad N^w_m \quad N^w_l\right]^T \quad (3.22)$$

where h_e is the length of the element and $\hat{x}$ is the local coordinate within any element with its origin at the left (k^{th}) node of the element.

The use of $\{N^{\psi}\}^{l}_{2\times1}$ and $\{N^{w}\}^{Q}_{3\times1}$ leads to the following elemental equilibrium equation $[k]^e\ \{w\}^e = \{f\}^e$ for any beam element ($[k]^e$ is the elemental stiffness matrix for the beam element, $\{f\}^e$ is the elemental force vector for the beam element, and $\{w\}^e$ is the elemental degrees of freedom vector for the beam element), given by

$$\begin{bmatrix} 7\alpha+2\varsigma & -8\alpha+\varsigma & \alpha-0.5\varsigma & -5\gamma & -\gamma \\ -8\alpha+\varsigma & 16\alpha+8\varsigma & -8\alpha+\varsigma & 4\gamma & -4\gamma \\ \alpha-0.5\varsigma & -8\alpha+\varsigma & 7\alpha+2\varsigma & \gamma & 5\gamma \\ 5\gamma & 4\gamma & \gamma & \delta+\zeta & -\delta+0.5\zeta \\ -\gamma & 4\gamma & 5\gamma & -\delta+0.5\zeta & -\delta+\zeta \end{bmatrix} \begin{Bmatrix} w_k \\ w_m \\ w_l \\ \psi_k \\ psi_l \end{Bmatrix} = \frac{qh_e}{2} \begin{Bmatrix} 1/3 \\ 4/3 \\ 1/3 \\ 0 \\ 0 \end{Bmatrix} \quad (3.23)$$

in which a constant value of distributed load q is assumed within any element (which is a reasonable assumption for small elements), and $\alpha = (\kappa A_b G_b + 2t_s)/(3h_e)$, $\varsigma = k_s h_e/15$, $\gamma = \kappa A_b G_b/6$, $\delta = E_b I_b/h_e$, and $\zeta = \kappa A_b G_b h_e/3$.

Implementing Equation 3.23 in the assembly process leads to numerical difficulties [187] because of the difference in the number of degrees of freedom at the nodes (the middle node m has only one degree of freedom w_m while the end nodes k and l have two degrees of freedom each w_k and ψ_k, and w_l and ψ_l). As the middle node is not connected to other elements, the degree of freedom wm corresponding to this node can be eliminated from the system of algebraic Equation 3.23. The elimination is done by rewriting the second equation in 3.23 as $w_m = f(w_k, w_l, \psi_k, \psi_l)$ and then substituting the resulting wm in the remaining four equations. These algebraic operations change the system of equations in 3.23 to

$$\begin{bmatrix} \frac{-25\varsigma^2}{8(2\alpha+\varsigma)}+3\alpha+5\varsigma & \frac{-5\varsigma\gamma}{2(2\alpha+\varsigma)}-3\gamma & \frac{-25\varsigma^2}{8(2\alpha+\varsigma)}-3\alpha+\frac{5\varsigma}{2} & \frac{-5\varsigma\gamma}{2(2\alpha+\varsigma)}-3\gamma \\ \frac{-5\varsigma\gamma}{2(2\alpha+\varsigma)}-3\gamma & \delta+\zeta+\frac{2\gamma^2}{2\alpha+\varsigma} & \frac{-5\varsigma\gamma}{2(2\alpha+\varsigma)}+3\gamma & -\delta+\frac{\zeta}{2}-\frac{2\gamma^2}{2\alpha+\varsigma} \\ \frac{-25\varsigma^2}{8(2\alpha+\varsigma)}-3\alpha+\frac{5\varsigma}{2} & \frac{-5\varsigma\gamma}{2(2\alpha+\varsigma)}+3\gamma & \frac{-25\varsigma^2}{8(2\alpha+\varsigma)}+3\alpha+5\varsigma & \frac{5\varsigma\gamma}{2(2\alpha+\varsigma)}+3\gamma \\ \frac{5\varsigma\gamma}{2(2\alpha+\varsigma)}-3\gamma & -\delta+\frac{\zeta}{2}-\frac{2\gamma^2}{2\alpha+\varsigma} & \frac{5\varsigma\gamma}{2(2\alpha+\varsigma)}+3\gamma & \delta+\zeta+\frac{2\gamma^2}{2\alpha+\varsigma} \end{bmatrix} \begin{Bmatrix} w_k \\ \psi_k \\ w_l \\ \psi_l \end{Bmatrix} = qh_e \begin{Bmatrix} \frac{1}{2}-\frac{5\varsigma}{12(2\alpha+\varsigma)} \\ \frac{-\gamma}{3(2\alpha+\varsigma)} \\ \frac{1}{2}-\frac{5\varsigma}{12(2\alpha+\varsigma)} \\ \frac{\gamma}{3(2\alpha+\varsigma)} \end{Bmatrix} \tag{3.24}$$

and this form of the elemental equation $[k]^e\ \{w\}^e = \{f\}^e$ can be readily incorporated in the assembly process.

Solution of the differential Equation 3.16(c) for surface displacement w of the foundation (soil) is also obtained using FE analysis. As the maximum derivative of w in the weak form of Equation 3.16(c) is dw/dx, linear Lagrangian shape functions $\{N^w\}^l_{2\times1}$ are used to interpolate w within the two-noded rod (bar) elements (Figure 3.3) used to discretize the domains -χ L $\leq x \leq$ 0 and L $\leq x \leq \chi$ L. This leads to the elemental equilibrium equation $[k]^e\ \{w\}^e = \{f\}^e$ given by

$$\begin{bmatrix} \frac{k_s h_e}{3}+\frac{2t_s}{h_e} & \frac{k_s h_e}{3}-\frac{2t_s}{h_e} \\ \frac{k_s h_e}{3}-\frac{2t_s}{h_e} & \frac{k_s h_e}{3}+\frac{2t_s}{h_e} \end{bmatrix} \begin{Bmatrix} w_k \\ w_l \end{Bmatrix} = \begin{Bmatrix} 0 \\ 0 \end{Bmatrix} \tag{3.25}$$

Solution is obtained after assembling the elemental matrices and then solving for nodal displacements and rotations (rotation is applicable only for the beam). The assembly process is rather involved because of the different sizes of elemental matrices of the beam (Equation 3.24) and the adjacent foundation (Equation 3.25),

Solution of the differential Equation 3.19(a) of ϕ is obtained analytically, and is given by

$$\phi_i(z) = A^{(i)} e^{\sqrt{\frac{-n_{si}}{m_{si}}}z} + B^{(i)} e^{-\sqrt{\frac{-n_{si}}{m_{si}}}z} \tag{3.26a}$$

where the integration constants $A^{(i)}$ and $B^{(i)}$ for the i^{th} layer are obtained from the boundary conditions given previously. For a single layer ($i = 1$), $\phi(z)$ is given by

$$\phi_1(z) = \frac{sinh[\bar{\gamma_1}(1 - \frac{z}{T_1})]}{sinh(\bar{\gamma_1})} \tag{3.26b}$$

For the special case of a single soil layer of infinite thickness (i.e., $H_1 \to \infty$), $\phi(z)$ is given by

$$\phi_1(z) = e^{-\sqrt{\frac{-n_{s1}}{m_{s1}}}z} \tag{3.26c}$$

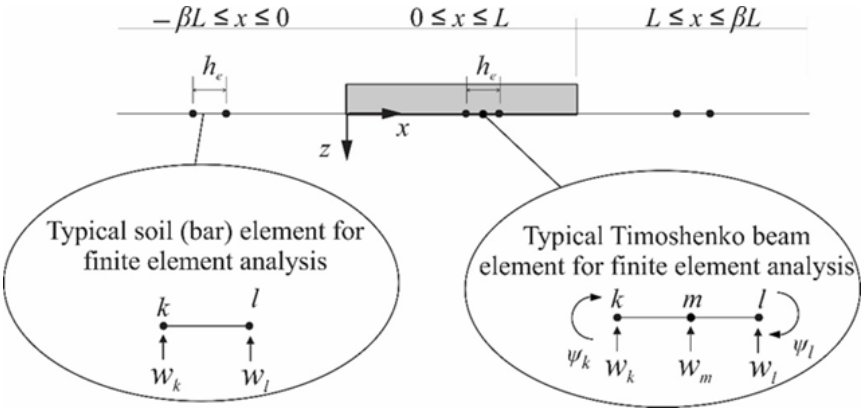

Figure 3.3: Finite element formulation and assembly

3.3.6 Solution Algorithm

Equations 3.16(a-c) and Equation 3.19(a) are inter-dependent and solved simultaneously following an iterative algorithm. A linear distribution of ϕ with depth, $\phi_{initial}$(z), is assumed as the initial guess with which k_s and t_s are calculated and used to obtain the w and ψ from Equations 3.16(a-c). The calculated w and ψ are used to determine m_{si} and n_{si}, which are then used to obtain a new ϕ(z). The newly calculated ϕ, $\phi_{calculated}$, is compared with the assumed $\phi_{initial}$ by calculating the difference and, if the difference is greater than a prescribed tolerance 10^{-5}, then the calculations are repeated with $\phi_{calculated}$ as the new guess $\phi_{initial}$. The iterative calculations are continued until the assumed and calculated ϕ values fall within a tolerable limit (see Figure 3.4 for the flow chart).

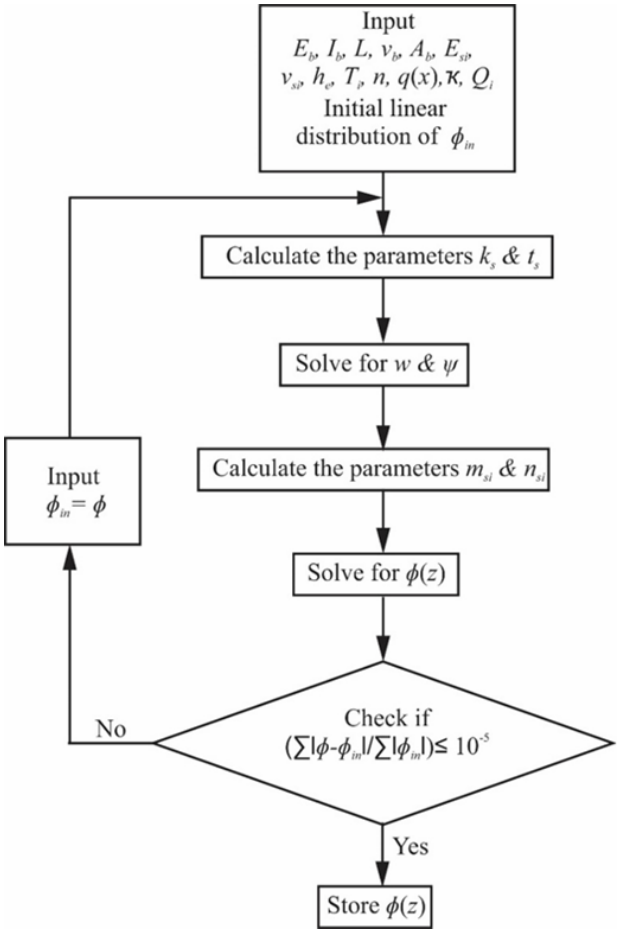

Figure 3.4: Solution algorithm

3.4 Results

3.4.1 Verification with Two-Dimensional FE Analysis

The accuracy of the proposed analysis is verified with the help of two example problems. The beam-soil responses obtained for the example problems using the present analysis are compared with those obtained from equivalent two-dimensional (2D) FE analysis performed using Plaxis 2D.

As the first verification problem, a beam with $L = 5$ m, $b = 1$ m, $d = 0.5$ m, $E_b = 200$ MPa, and $\upsilon_b = 0.25$ is considered. The beam rests on a three-layered soil deposit and the

beam ends are free to rotate and deflect. The beam is subjected to a uniform distributed vertical load of 50 kN/m acting over the entire length of the beam. The details of the properties of the beam-foundation system are given in Figure 3.5. Figure 3.5 also shows the deflection of the beam obtained from the present analysis (using both the Timoshenko and Euler-Bernoulli theories) and 2-D FE analysis using Plaxis. It is apparent that the present method is accurate - the difference in the maximum beam displacement at the beam centre is 3.5%.

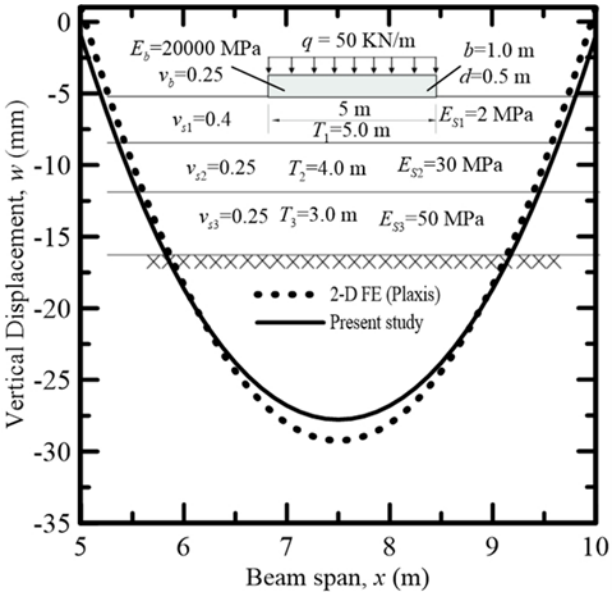

Figure 3.5: Displacement responses of a 5 m long free beam subjected to 50 kN/m uniformly distributed load obtained from present analysis and 2D FE analysis

For the second example, a 10 m long beam is considered with both ends fixed against deflection and rotation, lying on a two-layer deposit, and subjected to a 10 kN point acting at the mid-span (inputs to the analysis are given in Figure 3.6). The beam deflection profiles $w(x)$ obtained from the present analysis (using both the Timoshenko and Euler-Bernoulli theories) and 2-D FE analysis are shown in Figure 3.6. It is evident that the beam responses obtained from the present analysis and 2-D FE analysis are in good agreement with the maximum difference being 5%.

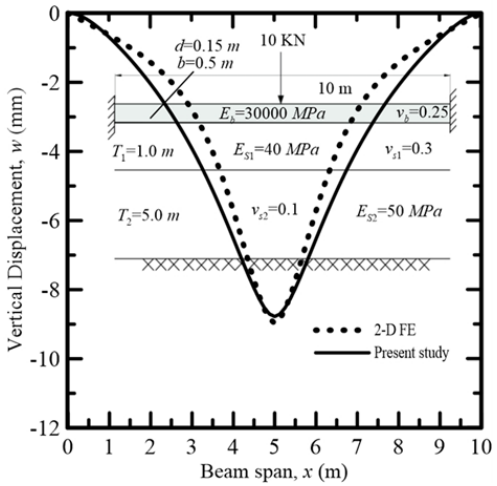

Figure 3.6: Displacement responses of a 10 m long fixed beam subjected to 10 kN point load obtained from present analysis and 2D FE analysis

3.4.2 Range of Applicability of Beam Theories for One-Layer Foundation

The beam-continuum system can be best investigated with respect to a flexibility index λ proposed by Vlasov and Leont'ev (1966) [247] and defined as

$$\lambda = \sqrt[3]{\frac{E_0 b L^3}{16 E_b J (1-\upsilon_0^2)}} \tag{3.27}$$

where $E_0 = E_s/(1\text{-}\upsilon_s^2)$, $J = bd^3/[12(1\text{-}\upsilon_b^2)]$, $\upsilon_0 = \upsilon_s/(1\text{-}\upsilon_s)$ This index, however, is most appropriate for a single-layer foundation.

Further, a dimensionless stiffness ratio is defined as

$$\eta_{bending} = \left[\frac{E_b I_b}{E_{si} T_{si}^3 b}\right] \tag{3.28}$$

The stiffness ratio focuses on the flexural aspects of the beam and is used to investigate the effect of the relative stiffness of beam and soil on the beam-soil interaction.

Figure 3.7(a)-(b) show the normalized mid-span beam deflections $w_{mid-span}/(E_b I_b/\text{qL}^4)$, and wmid-span/$(E_b I_b/\text{PL3})$ corresponding to a uniformly distributed load and a point load

at mid-span, respectively, as a function of λ [or beam aspect ratio a $(= L/d)$] for different values of $\eta_{bending}$. The study is performed for beams with free ends resting on a single-layer foundation with $T_1/L = 0.5$, (T_1 is the thickness of the single-layer continuum) and using both Timoshenko and Euler-Bernoulli beam theories. It is observed that the response of the Timoshenko and Euler-Bernoulli beams are the same for $\lambda \geq 0.86$ and $\lambda \geq 1.4$ for the cases of uniformly distributed load and point load, respectively. The values of $\lambda = 0.86$ and $\lambda = 1.4$ can therefore be thought of as the thresholds exceeding which Timoshenko and Euler-Bernoulli beams will produce identical beam response under distributed and central point loads, respectively. Simulations were also done for $T_1/L = 1$, and 2, and exactly the same threshold values of $\lambda = 0.86$ and $\lambda = 1.4$ are obtained for uniformly distributed load and point load, respectively. Thus, the ratio T_1/L has no impact on the threshold values of λ. Similar studies can be done for soil deposits with multiple layers.

The range of applicability of the beam theories is further investigated by calculating the ratios $k_s^{Timoshenko}/k_s^{Euler-Bernoulli}$ and $t_s^{Timoshenko}/t_s^{Euler-Bernoulli}$ of the foundation parameters k_s and t_s obtained using Timoshenko and Euler-Bernoulli beam theories, and plotting these ratios as functions of λ. It is clear from Figure 3.9(a)-(c), plotted for $T_1/L = 1.0$, the threshold values of λ obtained from Figure 3.7(a)-(d) and Figure 3.8(a)-(d) are correct. Although not plotted, the $k_s^{Timoshenko}/k_s^{Euler-Bernoulli}$ and $t_s^{Timoshenko}/t_s^{Euler-Bernoulli}$ versus λ plots were also obtained for $T_1/L = 0.5$ and 2.0, and no effect of T_1/L on the results was observed.

3.4.3 Mid-Span Beam Deflection in One-Layer Foundation

Fitted equations for mid-span beam deflection are developed based on the plots given in Figures 3.7 and 3.8 and are given by

$$w_{mid-span} = a_1 \lambda^{b_1} \frac{qL^4}{E_b I_b} \tag{3.29}$$

$$w_{mid-span} = a_2 \lambda^{b_2} \frac{QL^3}{E_b I_b} \tag{3.30}$$

where the fitting coefficients a_1, a_2, b_1, and b_2 are given in Tables 3.2 and 3.3. These equations are applicable for beams with free ends.

Characteristics of one-layer foundation parameters k_s and t_s

Although the interaction parameters k_s and t_s are rigorously related to the elastic constants of the soil continuum (Equations 3.18(a,b), the iterative algorithm described

earlier is required to obtain beam response. If the iterative approach is to be avoided, then algebraic equations of k_s and t_s in terms of the foundation (soil) elastic constants have to be known such that determination of the function ϕ can be avoided. This is done by performing a systematic parametric study described next.

Figure 3.10(a,b) show the normalized k_s and t_s, defined as $\bar{k_s} = k_s T_1/(E_{s1}\mathrm{b})$ and $\bar{t_s} = t_s/(T_1 G_{s1}\mathrm{b})$ for a free-end Timoshenko beam lying on single-layer continuum as a function of λ. The beam is subjected to two loading cases: uniformly distributed load and a mid-span point load. Similar plots are obtained for free-end Euler-Bernoulli beam as well, as shown in Figure 3.11(a,b). The normalized k_s and t_s are found to be mostly independent of T_1/L and λ for the case of uniformly distributed load. Based on these plots, fitted algebraic equations of k_s and t_s are proposed for beams with free ends and resting on a single-layer continuum (soil) and subjected to uniformly distributed load as

$$k_s = a_3 \frac{\bar{E_{s1}} b}{T_1} \tag{3.31a}$$

$$t_s = a_4 G_{s1} T_1 b \tag{3.31b}$$

where the fitting coefficients a_3, and a_4 are given in Table 3.4. For the case of mid-span point load, however, normalized k_s and t_s are mostly independent of λ but depend on T_1/L (Figure 3.10(a)-(b)). Therefore, multiple fitting analyses were performed to obtain equations of k_s and t_s, and are given by

$$k_s = a_5 \frac{\bar{E_{s1}} b}{T_1} \left(\frac{T_1}{L}\right)^{b_3} \tag{3.32a}$$

$$t_s = a_6 G_{s1} T_1 b \left(\frac{T_1}{L}\right)^{-b_4} \tag{3.32b}$$

where the fitting coefficients a_5, a_6, b_3, and b_4 are given in Table 3.5.

It is important to note that Equations 3.31 and 3.32 are applicable for beams with any end conditions (free or hinged or fixed) - Interestingly, it was found that Equations 3.31 and 3.32 work irrespective of the beam boundary conditions.

3.4.4 Mid-Span Beam Deflection in Two-Layer Foundation

The response of beams resting on two-layer foundation (soil) is investigated by varying the thickness of the two layers and by varying the elastic constants of both the layers. A

two-layer continuum is assumed with thicknesses T_1 and T_2, Young's moduli E_{s1} and E_{s2}, and Poisson's ratio υ_{s1} and υ_{s2} of the top (first) and second layer, respectively, such that $T_1 + T_2 = H_{total}$. A reference single-layer continuum system with thickness H_{total} is also assumed with elastic constants E_{s1} and υ_{s1} that are the same as those of the top layer of the two-layer continuum. For both the two-layer and reference (single layer) foundation systems, an identical beam with free ends and subjected to a uniformly distributed load is assumed.

Characteristics of one-layer foundation parameters k_s and t_s

For the two-layer system described in the previous section, Figure 3.12(a,b) show the ratios $k_s^{two-layers}/k_s^{single-layer}$ and $t_s^{two-layers}/t_s^{single-layer}$ of k_s and t_s for the two-layer system to those of the reference single-layer system as functions of λ_2/λ_1, respectively, where λ_2/λ_1 is defined based on Equation 3.27 as

$$\frac{\lambda_2}{\lambda_1} = \sqrt[3]{\frac{E_{02}}{E_{01}}\frac{1-\upsilon_{01}^2}{1-\upsilon_{02}^2}} \tag{3.33}$$

where E_{01} [$= E_{s1}/(1 - \upsilon_{s1}^2)$] and υ_{01} [$= \upsilon_{s1}/(1- \upsilon_{s1})$] are elastic constants for the top layer, andE_{02} [$= E_{s2}/(1 - \upsilon_{s2}^2)$] and υ_{02} [$= \upsilon_{s2}/(1- \upsilon_{s2})$] are elastic constants for the second (bottom) layer. If the top layer is stiffer than the bottom layer, then the values of k_s and t_s for the two-layer system is greater than the values of k_s and t_s for the two-layer system in which the top layer is weaker than the bottom layer. Based on these plots, fitted equation are developed as shown below such that k_s and t_s for two-layer system can be determined from k_s and t_s of the reference single-layer system.

$$k_s^{two-layers} = a_7 k_s^{single-layer} e^{b_5(\frac{\lambda_2}{\lambda_1})} \tag{3.34a}$$

$$t_s^{two-layers} = a_8 t_s^{single-layer} e^{b_6(\frac{\lambda_2}{\lambda_1})} \tag{3.34b}$$

where the fitting coefficients a_7, a_8, b_5, and b_6 are given in Table 3.6.

3.4.5 Mid-Span Beam Deflection in Three-Layer Foundation

In order to investigate the effect of the existence of a three-layer foundation on the response of the beam, a system of a free beam on three-layer foundation system is studied. The material and the geometric properties of the foundation layers are selected to vary in this study, whereas those of the beam are kept constant. Nine different problems are

analyzed such that three cases of soil modulus: E_{s1}, E_{s2}, and E_{s3} are selected, and for each soil modulus case, three different combinations of layer thickness: H_1, H_2, and H_3 are considered (see Figure 3.13). For the soil modulus cases, E_{s1}, E_{s2}, and E_{s3} of the three layers are chosen such that their values are different multiples of a single soil modulus E_s, so there average is always equal to that single modulus E_s. Details of the soil modulus cases are given in Table 3.7. For the layer thickness combinations, the values of the layer thickness are selected as a different multiples of a fixed total thickness of the system H_{total}. Details of the layer thickness combinations are given in Table 3.8.

Figure 3.13 shows the mid-span beam displacement caused by a mid-span concentrated load, normalized with respect to applied load for all nine problems described earlier in this section versus the aspect ratio of the beam. It is evident from the plots that both the soil modulus and thickness of each soil layer affect the beam response.

Table 3.2: Fitting parameters for mid-span displacement for free beam on single layer foundation and subjected to uniformly distributed load (Figure 3.7)

T1/L	η_b	**Beam Theory**	a_1	b_1
2	0.01	T	1.54	5.29
		EB	1.43	5
	0.1	T	102.22	5
		EB	96.36	5.22
	1	T	999.87	5
		EB	944.6	5.23
	10	T	4842.8	5
		EB	4395.9	5.31
1	0.01	T	1.68	5
		EB	1.61	5.19
	0.1	T	120.25	5
		EB	113.36	5.22
	1	T	1176.3	5
		EB	1111.3	5.23
	10	T	5697.5	5
		EB	5171.6	5.3
0.5	0.01	T	24.56	5
		EB	22.69	5.48
	0.1	T	71.89	5
		EB	67.62	5.28
	1	T	273.32	5
		EB	257.7	5.26
	10	T	1006.8	5
		EB	899.55	5.4

Table 3.3: Fitting parameters for mid-span displacement for free beam on single layer foundation and subjected to mid-span applied concentrated load (Figure 3.8)

T1/L	η_b	**Beam Theory**	a_1	b_1
2	0.01	T	0.74	4
		EB	0.63	4.38
	0.1	T	36.13	4
		EB	27.41	4.59
	1	T	259.73	4
		EB	227.81	4.26
	10	T	761.97	4
		EB	686.82	4.19
1	0.01	T	0.87	4
		EB	0.74	4.38
	0.1	T	42.51	4
		EB	32.25	4.58
	1	T	305.56	4
		EB	268.01	4.25
	10	T	896.44	4
		EB	808.02	4.17
0.5	0.01	T	14.19	4
		EB	12.05	4.35
	0.1	T	68.6	4
		EB	59.39	4.28
	1	T	157.83	4
		EB	135.13	4.27
	10	T	307.95	4
		EB	271.37	4.22

Table 3.4: Fitting parameters for k_s and t_s for free beam on single layer foundation and subjected to uniformly distributed load (Figure 3.10(a)-(b))

Beam theory	Timoshenko		Euler-Bernoulli	
Range of applicability	$\lambda < 0.86$	$\lambda > 0.86$	$\lambda < 0.86$	$\lambda > 0.86$
a_3	0.93	1.02	0.75	1.02
a_4	0.15	0.19	0.16	0.19

Table 3.5: Fitting parameters for k_s and t_s for free beam on single layer foundation and subjected to uniformly distributed load (Figure 3.10(a)-(b))

Beam theory	Timoshenko		Euler-Bernoulli	
Range of applicability	$\lambda < 1.4$	$\lambda > 1.4$	$\lambda < 1.4$	$\lambda > 1.4$
a_5	1.44	1.47	1.36	1.47
b_3	0.33	0.31	0.32	0.31
a_6	0.09	0.115	0.105	0.115
b_4	0.32	0.32	0.31	0.32

Table 3.6: Fitting parameters for k_s and t_s for free beam on two-layer foundation and subjected to uniformly distributed load (Figure 3.12(a)-(b))

T_1/H_{total}	a_7	b_5	a_8	b_6
1	1	0	1	0
0.8	0.6	0.73	1.72	−1.27
0.6	0.42	1.07	2.08	−1.62
0.4	0.29	1.35	2.63	−1.88
0.2	0.16	1.68	3.75	−2.15
0	0.001	3.07	4.30	−2.30

Table 3.7: Details of the soil modulus cases: E_1, E_2, and E_3 for the free beam on three-layer foundation system

	Soil modulus cases		
	E_1	E_2	E_3
E_{s1}	$0.23E_s$	$0.69E_s$	$2.08E_s$
E_{s2}	$0.69E_s$	$0.23E_s$	$0.69E_s$
E_{s3}	$2.08E_s$	$2.08E_s$	$0.23E_s$

Table 3.8: Details of the layer thicknesses combinations: H_1, H_2, and H_3 for the free beam on three-layer foundation system

	Layer thickness combinations		
	H_1	H_2	H_3
T_1	0.33 H_{Total}	0.17 H_{Total}	0.17 H_{Total}
T_2	0.33 H_{Total}	0.5 H_{Total}	0.83 H_{Total}
T_3	0.33 H_{Total}	0.33 H_{Total}	0 H_{Total}

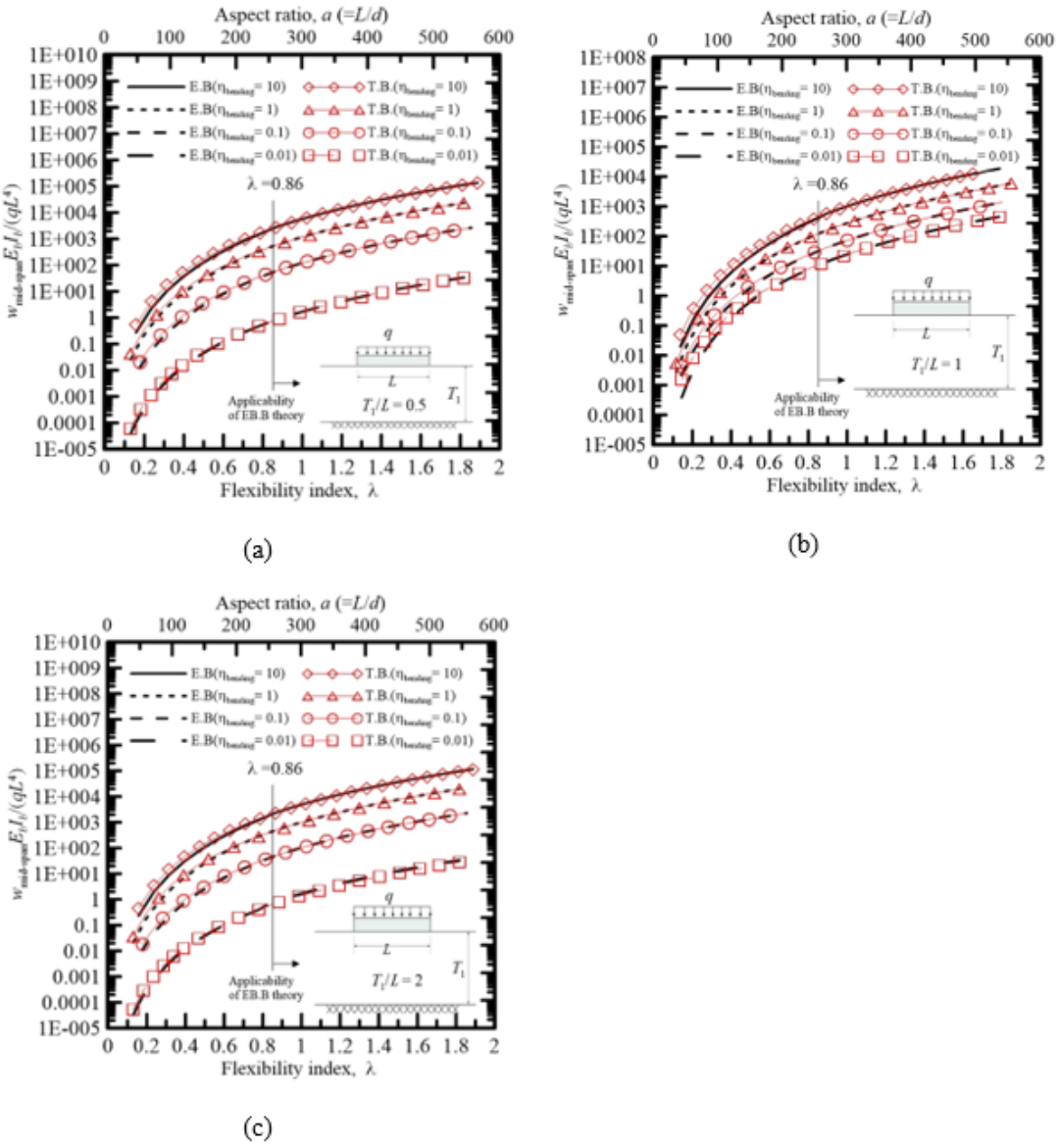

Figure 3.7: Normalized mid-span displacement versus λ for different values of η_b using Timoshenko and Euler-Bernoulli beam theories, for free beam resting on single layer foundation and subjected to uniformly distributed load: (a) T_1/L = 0.5, (b) T_1/L = 1 and (c) T_1/L = 2

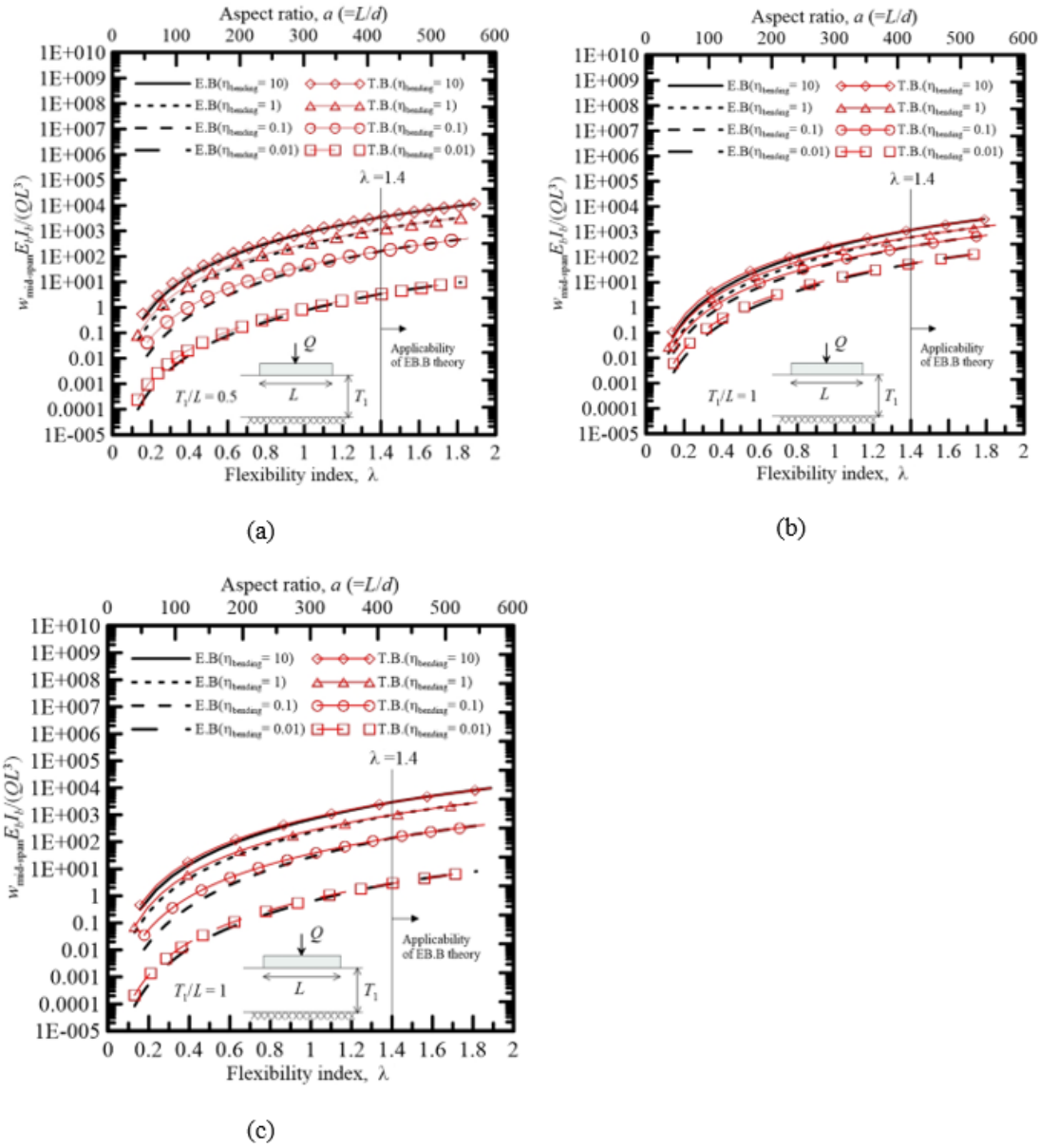

Figure 3.8: Normalized mid-span displacement versus λ for different values of η_b using Timoshenko and Euler-Bernoulli beam theories, for free beam resting on single layer foundation and subjected to mid-span concentrated load: (a) T_1/L = 0.5, (b) T_1/L = 1 and (c) T_1/L = 2

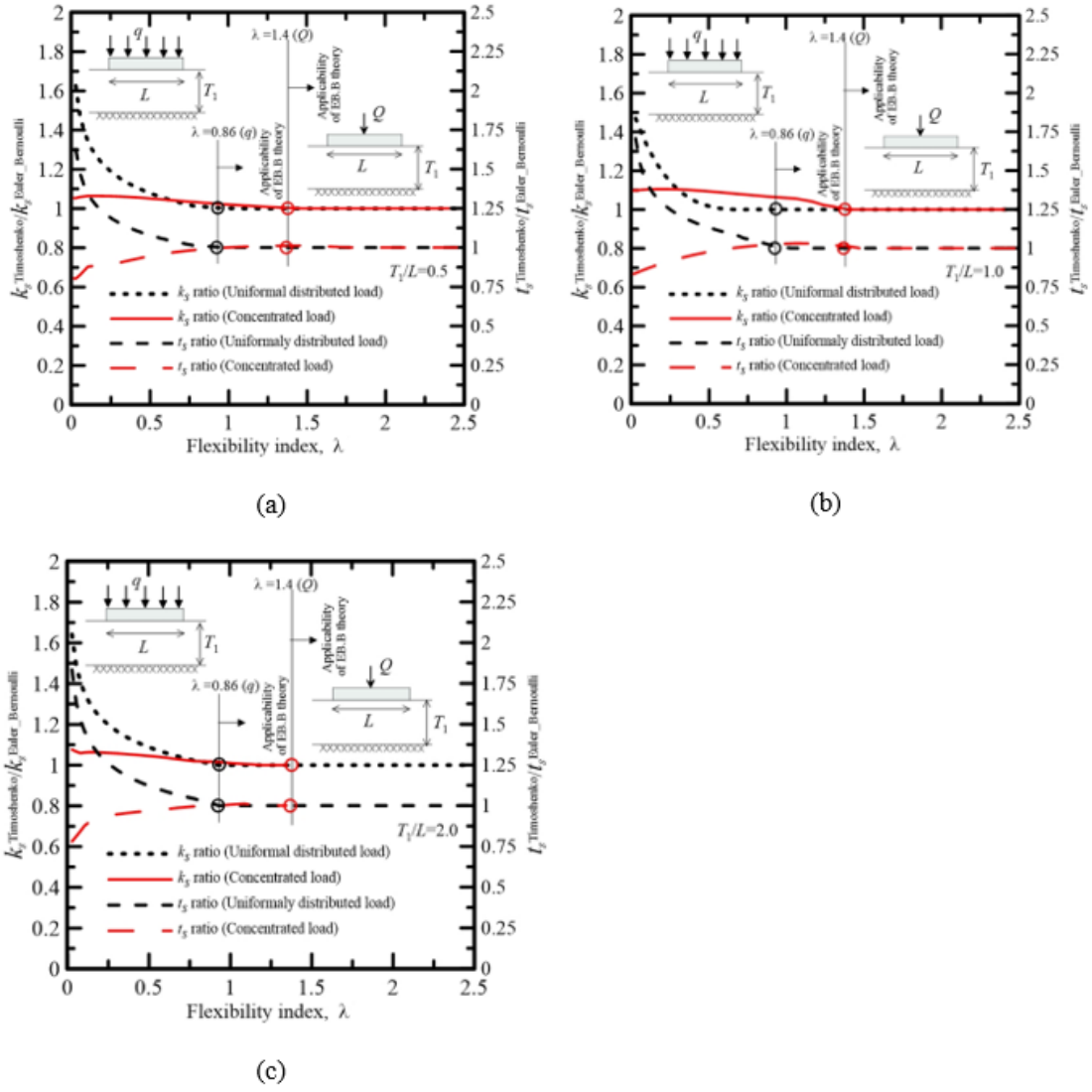

Figure 3.9: Range of applicability of Timoshenko and Euler-Bernoulli beam theories with respect to parameters k_s and t_s: (a) T_1/L = 0.5, (b) T_1/L = 1 and (c) T_1/L = 2

3.4.6 Design Examples Using the Fitted Equations

In this part, the use of the developed fitted equations for the calculation of the foundation parameters k_s and t_s, and the mid-span displacement $w_{mid-span}$ for beams on single-layer and two-layer foundations is illustrated by numerical examples.

Table 3.9: Comparison of the results from both the fitted equations and the iterative algorithm

	Results from fitted equations	Results from the iterative algorithm	Percentage of error (%)
k_s (GPa)	5.69	5.93	-4.05
t_s (N)	6905.14	7078.2	-2.44
$w_{mid-span}$ (mm)	9.523	9.011	5.68

As the first example, a Timoshenko free beam of $E_b = 20$ Gpa, $\upsilon_b = 0.25$, $d_p = 0.3$ m, and b = 1 m is assumed to rest on a 5 m thick single-layer foundation of $E_s = 25$ Mpa, and $\upsilon_s = 0.3$. The beam is assumed to be subjected to a 30 kN concentrated load acting vertically at the mid-span of the beam. Given these inputs, the flexibility index λ, and the bending stiffness ratio η_b are first calculated using Equations 3.27 and 3.28 , as 3.45 and 0.014, respectively. Using λ and η_b, the fitting coefficients of Equation 3.30 are determined with the aid Table 3.3 as $a_2 = 0.63$, and $b_2 = 4.38$. The mid-span beam displacement is then calculated as 9.523 mm. Similarly, the fitted coefficients of Equation 3.32 are determined with the aid of Table 3.5 as $a_5 = 1.47$, $a_6 = 0.32$, $b_3 = 0.31$, and $b_4 = 0.32$. Finally Equation 3.32 is used to calculate k_s , and t_s as 5.69 GPa and 6.905 kN, respectively. In order to verify the accuracy of the fitted equations, the earlier example is resolved using the iterative algorithm, and the results were compared to these from the fitted equations (Table 3.9). The comparison shows that the fitted equations underestimated the values of k_s and t_s, and hence overestimated the mid-span displacement. For the second example, the same beam from earlier example is assumed to rest on two-layer foundation of total thickness of 12 m. A mid-span concentrated load is assumed of 30 kN is assumed to act on the beam. A 5 m thick first layer is assumed to have an elastic modulus of 25 MPa, and a Poisson's ratio of 0.3. The first layer is underlying by a 7 m thick layer of elastic modulus of 30 MPa, and Poisson's ratio of 0.35. Equation 3.33 is used to calculate λ_2/λ_1 as 1.01, and k_s and t_s of the equivalent single-layer are determined using Equation 3.32 as 5.69 GPa and 6.905 kN (see the earlier example), respectively. With the aid of Table 3.6, the fitted parameters of Equation 3.34 are calculated as $a_7 = 0.29$, $a_8 = 2.63$, $b_5 = 1.35$, and $b_6 =$- 1.88. Finally, k_s and t_s for the two-layer foundation are determined as 6.365 GPa and 27.71 kN, respectively. It is important to mansion that k_s and t_s for the same two-layer foundation are calculated suing the iterative algorithm as 6.823 GPa and 30.83 kN, with an error of -6.71% and -10.12%, respectively.

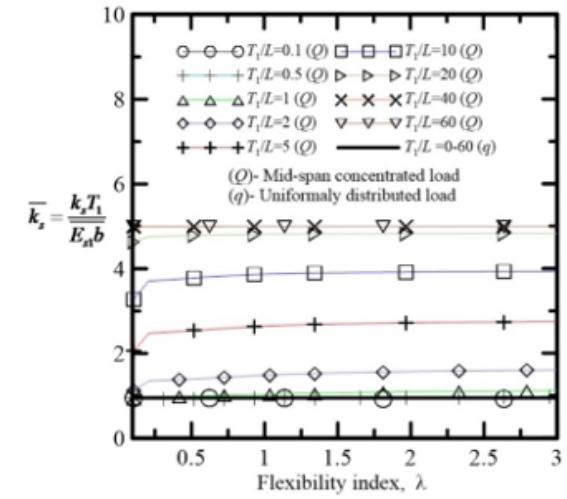

(a)

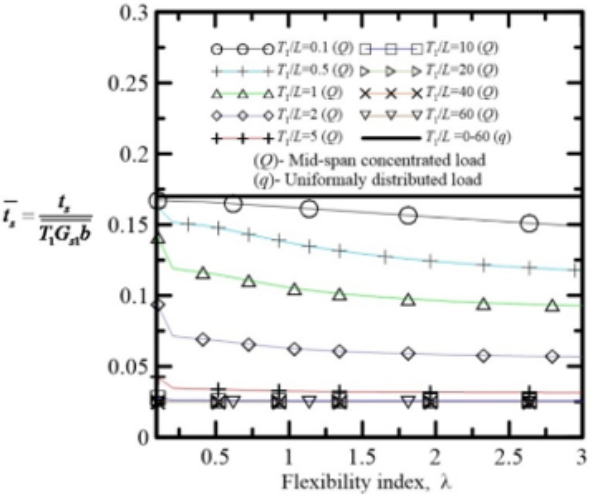

(b)

Figure 3.10: Soil subgrade parameters for Timoshenko free beam on Single-layer foundation: (a) variation of normalized k_s with λ for beams subjected to mid-span concentrated load and uniformly distributed load, (b) variation of normalized t_s with λ for beams subjected to mid-span concentrated load and uniformly distributed load

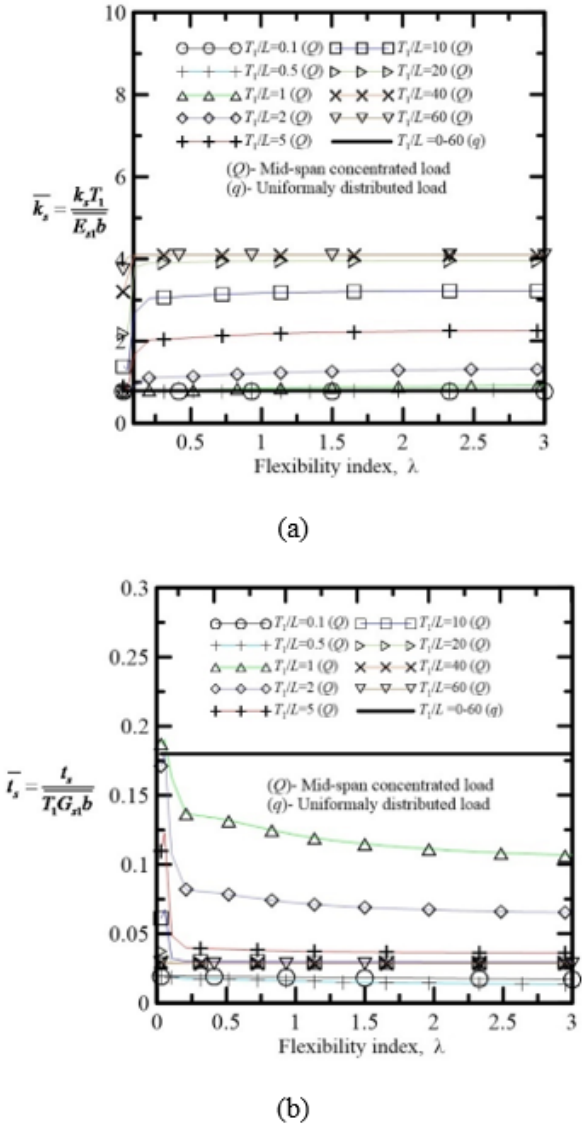

Figure 3.11: Soil subgrade parameters for Euler-Bernoulli beam on single-layer foundation: (a) variation of normalized k_s with λ for beams subjected to mid-span concentrated load and uniformly distributed load, (b) variation of normalized t_s with λ for beams subjected to mid-span concentrated load and uniformly distributed load

3.5 Conclusions

An analysis framework is presented for Timoshenko beams resting on multi-layer foundation (soil) in which the foundation is treated as a continuum. Simplified assumptions on the

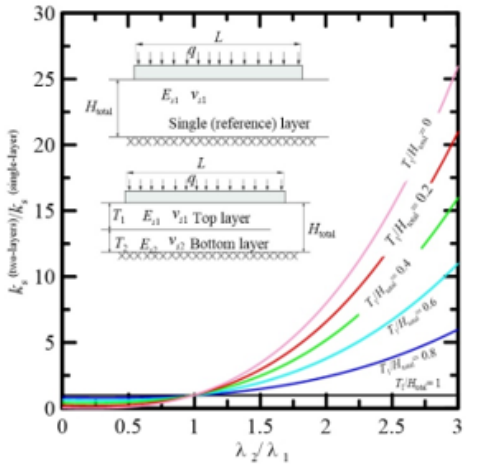

(a)

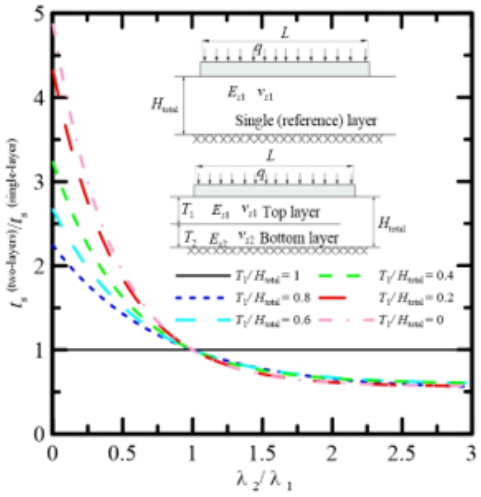

(b)

Figure 3.12: Soil subgrade parameters for Timoshenko beam on two-layer foundation a: (a) ratios of k_s for the two-layer system to those of the reference single-layer system for beams subjected to uniformly distributed load, (b) ratios of t_s for the two-layer system to those of the reference single-layer system for beams subjected to uniformly distributed load

displacement field within the continuum are made and the principle of minimum potential energy is applied to obtain the Euler-Lagrange equations describing the beam and soil dis-

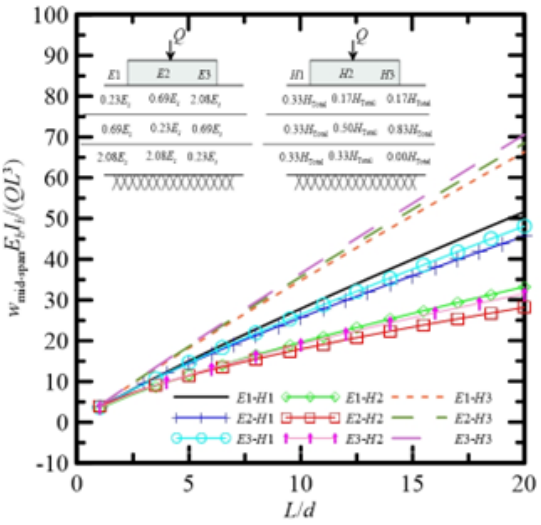

Figure 3.13: Normalized mid-span displacement versus the aspect ratio of free Timoshenko beam on three-layer foundation subjected to a mid-span concentrated load

placements. The differential equations describing the equilibrium of the beam-foundation system are solved analytically and using the one-dimensional finite element method. An iterative algorithm is used to solve the coupled differential equations. Modifications to the traditional finite element solution are made to avoid the shear locking phenomenon in the beam elements.

The resulting governing differential equation of beam deflection resembles that of beam resting on two-parameter foundation characterized with parameters k_s and t_s representing the compressive and shear resistances of soil. This is natural because the continuum-nature of the foundation assumed in the analysis naturally produces resistances arising from compression (or tension) and shear. The advantage of the present analysis is that closed form equations of k_s and t_s are obtained as part of the solution, and these parameters are rigorously related to the elastic constants of the multi-layered foundation (continuum). Thus, empiricism is not required in the estimation of the foundation parameters k_s and t_s.

Systematic parametric studies were performed based on the analysis to develop algebraic equations of k_s and t_s in terms of the elastic constants and beam and soil geometry for a single-layer foundation, which can be directly used by practitioners in their analysis of beams on foundations without the use of the iterative procedure described in this paper. Similar equations can be developed for beams resting on multiple layers as well. For a two-layer system, a stiffer top layer produces larger values of k_s and t_s.

The effect of relative bending and shear stiffnesses of beam and soil on the beam response is investigated by defining two stiffness ratios $\eta_{bending}$ and η_{shear} described above. As $\eta_{bending}$ and η_{shear} increases, the stiffnesses of the beam increases with respect to those of the foundation so that beam deflection decreases (for the same applied load). A flexibility index λ is defined in terms of the elastic constants and geometry of the beam-foundation system, and it is shown through a systematic parametric study that, for beams subjected to uniformly distributed load and resting on a single-layer foundation with the thickness T of the foundation layer equal to half the beam length L (i.e., $T/L = 0.5$), $\lambda \leq 0.5$ produces rigid beam behavior, $0.5 < \lambda \leq 0.86$ and $0.5 < \lambda \leq 1.4$ produce flexible beam behavior for which the Timoshenko beam theory is most appropriate (the limit of 0.86 is applicable for the case of uniformly distributed load and the limit of 1.4 is applicable for the case of mid-span concentrated load), and $\lambda > 0.86$ and $\lambda > 1.4$ produce flexible beam behavior for which both Timoshenko and Euler-Bernoulli beam theories are applicable. Similar studies demarcating the applicability of the different beam theories can be carried out for other values of T/L and for multiple soil layers.

Chapter 4

Dynamic Soil Structure Interaction Model for Beams on Viscoelastic Foundations Subjected to Oscillatory and Moving Loads

This chapter is published Manuscript in ELSVIER- Computers and Geotechnics, available online: https://doi.org/10.1016/j.compgeo.2019.103157, Elhuni, Hesham, and Dipanjan Basu. "Dynamic soil structure interaction model for beams on viscoelastic foundations subjected to oscillatory and moving loads." Computers and Geotechnics 115 (2019): 103157.

4.1 Overview

A new method for dynamic analysis of Euler-Bernoulli beams resting on multi-layered soil is presented. The governing differential equations for beam and soil displacements are obtained using the extended Hamilton's principle, and these equations are solved using one-dimensional finite element method and analytical solutions. An iterative solution algorithm is used in conjunction with an implicit time integration scheme to obtain beam and soil responses as functions of time. The developed model resembles the traditional two-parameter spring foundation model but the analysis shows that the traditional foundation spring parameters cannot be prescribed a priori but determined as part of the solution. The model produces accurate beam response as illustrated by comparisons with equivalent

two-dimensional finite element analysis. A few problems are analyzed that illustrate the novel features of the dynamic foundation model.

4.2 Introduction and Related Literature

The problem of beams on elastic or viscoelastic foundations is widely studied because of its wide range of applications in different fields of engineering [15]. In geotechnical engineering, the concept is widely used to analyze the behavior of flexible footings and structural elements, e.g., strip footings, grade beams, and concrete pavements, idealized as beams, resting on the underlying soil, termed as the foundation [24]. Different models with different degrees of idealization have been proposed to simulate the behavior of the foundation (soil). The simplest and oldest idealization is to represent the soil as a bed of closely spaced linear springs [255]. The Winkler model (also often termed as the one-parameter model) is characterized by the spring constant k_s, which represents the compressive resistance of soil against applied vertical loads and can be related to the modulus of subgrade reaction of soil. The main drawback of the Winkler model is that the vertical springs are assumed to work in isolation with respect to each other because of which the resistance of soil obtained through shear stresses are neglected. An improvement over the Winkler model was proposed by several researchers like Hetenyi (1946) [107], Filonenko-Borodich (1945) [92], Pasternak (1954) [177], and Terzaghi (1955) [220] by introducing a second parameter t_s, which essentially captures the shear interaction between adjacent Winkler springs (this model is often referred to as the two-parameter model).

Several studies on beams resting on Winkler and two-parameter foundations subjected to static and dynamic (vibrating and moving) loads have been performed [227, 94, 219, 239, 178]. In most of these studies, beam responses (e.g., deflection and bending moment) are investigated as functions of magnitude, frequency or velocity of applied loads, and the damping present in the system. The difficulty, however, in using the Winkler or two-parameter models is that the two foundation parameters k_s and t_s cannot be reliably obtained from measurable soil properties and are often inaccurately determined from ad hoc, empirical equations [45]. Further, for dynamic analysis, geometric damping cannot be explicitly considered using the one- or two-parameter models.

Improvements to the one- or two-parameter models have been proposed by some researchers in which the soil is idealized as an elastic continuum with simplified assumptions regarding its stress or displacement fields, and applied the simplified continuum approach to beam on foundation problems [34, 190, 125, 183, 247]. Ai and Ren (2017) [6] developed an analytical, steady state (time-independent) solution of an infinite Euler-Bernoulli beam

resting on isotropic multi-layered elastic half-space. The boundary element method (BEM) has also been used for solving beams on multi-layered foundations [20, 4]. However, these simplified continuum approaches depend on specifically assumed contact pressure distributions that may not be true for all possible cases of contact, are often mathematically complex, are applicable to linear elastic materials only, and do not take into account material damping in the system [102, 237, 215].

Out of the simplified continuum approaches, the one by Vlasov and Leont'ev (1966) [247] is distinct because it leads to the same simple differential equation as that of the two-parameter model (described earlier) but has the additional advantage that the parameters ks and ts in this model are rigorously related to the elastic constants of the soil without any empiricism involved. Because of its ability to capture the continuum nature of soil, the model by Vlasov and Leont'ev (1966) [247] has been widely used [9, 170, 257, 149]. Vallabhan and Das (1989) [240] improved the model of Vlasov and Leont'ev (1966) [247] for static beam problems, and Liang and Zhu (1995) [147] analyzed using the model the steady-state (time-independent) response of beams although with erroneous assumptions. Ayvaz and Ogzgan (2002) [16] used the model to obtain the natural frequency of vibration of beams resting on foundations. All these studies considered a single-layer soil (foundation) beneath the beam. As far as the authors know, there is no systematic time-dependent, dynamic study performed on beams resting on multi-layered elastic foundations following the modified simplified continuum approach by Vallabhan and Das (1989) [240], which is the focus of this paper.

In this chapter, a time-dependent, dynamic soil-structure interaction model is developed by extending the model of Vallabhan and Das (1989) [240] for dynamic analysis of beams resting on multi-layered soil. The analysis considers both the steady-state and transient vibrations of beams under both oscillatory and moving loads. A layered soil continuum under the beam is considered and the vertical soil displacement is expressed as a product of separable functions maintaining continuity and compatibility with the overlying beam. The differential equations describing the beam motion and soil displacement are obtained using Hamilton's principle and calculus of variations, and are solved following an iterative algorithm. The resulting differential equation for beam motion resembles that of a beam interacting dynamically with a two-parameter foundation with parameters k_s and t_s. These two parameters are mechanistically related to the soil Young's modulus and Poisson's ratio, and, interestingly, change with time even though the soil elastic constants remain constant – this is a novel development of the new model. The accuracy of the analysis is verified by comparing the results of the analysis with those of equivalent two-dimensional (2-D) finite element (FE) analysis performed using Plaxis. Examples illustrate the application of the method for different types of dynamic loads like oscillatory and moving loads. Para-

metric studies are performed to investigate the effect of soil properties, beam dimensions, frequency of oscillating load, speed of moving load, and number of soil layers on the beam response.

4.3 Analysis

4.3.1 Problem Definition

A uniform Euler-Bernoulli beam of length L, width b, and depth (thickness) d, mass density ρ_b, and Young's modulus E_b is assumed to be resting on a layered elastic continuum (Figure 4.1). A dynamic vertical load P(x, t) is assumed to act on the beam (t = time and x = space coordinate) which either moves from left to right with a velocity v (with or without acceleration) or oscillates in magnitude (with time) but remains stationary in space. In fact, the load P can both oscillate in magnitude and move with time. The beam is in full contact with the layered continuum at all times during the loading. The continuum (soil) beneath the beam is split into n layers with the bottom n^{th} layer resting on a rigid layer (e.g., bed rock). The i^{th} soil layer extends vertically downward to a depth H_i such that the thickness T_i of the i^{th} layer is $H_i - H_{i-1}$ ($H_0 = 0$). The total thickness of the soil deposit comprising of the n layers is H_{Total} ($= \sum_{i=1}^{n} T_i$). Each soil layer i is homogeneous and isotropic with mass density ρ_{si}, Young's modulus of E_{si}, and Poisson's ratio of υ_{si}.

A Cartesian x-z coordinate system is considered attached to the left end of the beam with x direction positive to the right and z direction positive vertically downward. For analysis, it is sometimes necessary to consider a domain extending beyond the two ends of the beam into the continuum in order to capture the displacements in the continuum (soil) that occurs beyond the loaded beam (Figure 4.1). The soil domains on both sides of the beam are required if the ends of the beam are free to deflect and/or rotate (i.e., free-end beams). Accordingly, the analysis domain is extended to a length βL (where $\beta \geq 1$) in positive and negative x directions, respectively, from the right and left ends of the beams to produce accurate beam response and soil displacement, and this eliminated any boundary effects (this was determined by trial and error). A continuum strip of width b beneath the beam is considered as the analysis domain perpendicular to the $x - z$ plane. This implies a plane-strain condition, similar to that assumed by Vlasov and Leont'ev (1966) [247] and Vallabhan and Das (1989) [240].

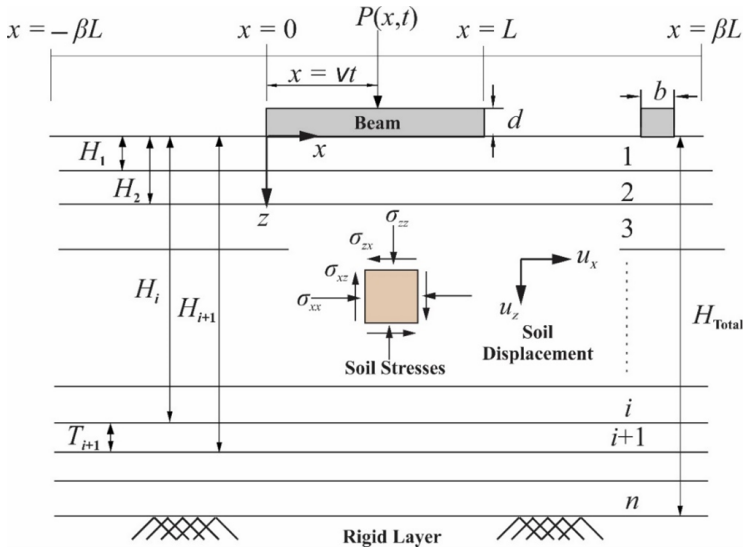

Figure 4.1: A beam resting on a multi-layered soil (foundation)

4.3.2 Soil Displacements, Strains, and Stresses

For the plane-strain problem considered, it is assumed that the soil displacement u_x in the horizontal x direction caused by the vertical forces are negligible (i.e., $u_x = 0$) and that the vertical soil displacement u_z (Figure 4.1) can be expressed as a product of separable functions

$$u_z = w(x,t)\phi(z) \tag{4.1}$$

where $w(x, t)$ is the displacement of the top surface of the continuum, which is the same as the beam displacement for $0 \leq x \leq$ L, and ϕ(z) is a dimensionless displacement function varying with depth. It is assumed in the analysis that $\phi(0) = 1$, which ensures perfect contact between the beam and the underlying continuum, and that $\phi(H_{total}) = 0$, which ensures that vertical displacement in the continuum arising from applied forces decreases with increase in depth and becomes zero at the interface with the rigid layer. Thus, the function ϕ takes into account the geometric damping of the beam-foundation system in the vertical direction.

For the assumed displacements in Equation 4.1, the strain tensor at any point in the continuum is given by

$$\varepsilon_{ij} = \begin{Bmatrix} \varepsilon_{xx} \\ \varepsilon_{zz} \\ \varepsilon_{xz} \end{Bmatrix} = \begin{Bmatrix} 0 \\ -w\frac{d\phi}{dz} \\ -\frac{1}{2}\frac{\partial w}{\partial x}\phi \end{Bmatrix} \tag{4.2}$$

The elastic constitutive relationship relates the strain tensor at any point within the continuum to the stress tensor (Figure 4.1)

$$\sigma_{ij} = \begin{Bmatrix} \sigma_{xx} \\ \sigma_{zz} \\ \sigma_{xz} \end{Bmatrix} = \frac{E_s}{(1+\upsilon_s)(1-2\upsilon_s)} \begin{bmatrix} 1-\upsilon_s & \upsilon_s & 0 \\ \upsilon_s & 1-\upsilon_s & 0 \\ 0 & 0 & 0.5-\upsilon_s \end{bmatrix} \begin{Bmatrix} 0 \\ -w(x,t)\frac{d\phi(z)}{dz} \\ -0.5\frac{\partial w(x)}{dx}\phi(z) \end{Bmatrix} \tag{4.3}$$

The stresses and strains can be used to calculate the strain energy density U_{D-soil} within each linear elastic soil layer i as

$$U_{D-soil} = \frac{1}{2}\sigma_{ij}\varepsilon_{ij} = \frac{1}{2}\left[\bar{E_{si}} w^2 \left(\frac{d\phi}{dz}\right)^2 + G_{si}\phi^2 \left(\frac{\partial w}{\partial x}\right)^2\right] \tag{4.4}$$

where $\bar{E_{si}}$ (constrained modulus) and G_{si} (shear modulus) are given by

$$\bar{E_{si}} = \frac{E_{si}(1-\upsilon_{si})}{(1+\upsilon_{si})(1-2\upsilon_{si})} \tag{4.5a}$$

$$G_{si} = \frac{E_{si}}{2(1+\upsilon_{si})} \tag{4.5b}$$

4.3.3 Extended Hamilton Principle

The extended Hamilton principle of least actions [40] is used to obtain the differential equations of motion of the beam and continuum under dynamic equilibrium

$$\delta \int_{t_1}^{t_2} (T - U + W_{nc}) dt = 0 \tag{4.6}$$

where T and U are the kinetic and strain energies of the beam-soil system participating in the vibration, W_{nc} is the work done by the non-conservative forces acting on the system, t_1 and t_2 are any arbitrary times at which the equilibrium configuration of the beam-soil system is known, and δ is the variational operator. For the present problem,

$$\begin{aligned} U &= \int_{volume} U_{D-beam} dV_{beam} + \int_{volume} U_{D-soil} dV_{soil} \\ &= \int_0^L \frac{E_b I_b}{2} \left(\frac{\partial^2 w}{\partial x^2} \right)^2 dx + \sum_{i=1}^{n} \frac{b}{2} \int_{-\beta L}^{\beta L} \int_{H_{i-1}}^{H_i} \left[E_{si} w^2 \left(\frac{d\phi_i}{dz} \right)^2 + G_{si} \phi_i^2 \left(\frac{\partial w}{\partial x} \right)^2 \right] dz dx \end{aligned} \tag{4.7a}$$

where U_{D-beam} is the strain energy density of the beam and is captured by the first term of the right hand side of Equation 4.7(a) in the second row; the second term on the right hand side of Equation 4.7(a) in the second row captures the strain energy of the continuum participating in the vibration; I_b ($=bd^3/12$) is the second moment of inertia of the beam section, and ϕ_i represents the function $\phi(z)$ within the i^{th} layer,

$$T = \int_0^L \frac{\rho_b A_b}{2} \left(\frac{\partial w}{\partial t} \right)^2 dx + \sum_{i=1}^{n} \int_{-\beta L}^{\beta L} \int_{H_{i-1}}^{H_i} \left[\frac{b}{2} \rho_{si} \left(\frac{\partial w}{\partial t} \right)^2 \phi_i^2 \right] dz dx \tag{4.7b}$$

in which the first and second terms on the right-hand side of Equation 4.7(b) represent the kinetic energies of the beam and the continuum participating in the vibration, respectively, and

$$W_{nc} = - \int_0^L P(t) \delta_d (x_0 - vt) w dx - \frac{1}{2} c \left(\frac{\partial w}{\partial t} \right)^2 \tag{4.7c}$$

where the first and second terms on the right hand side of Equation 4.7(c) represent the work done by the external force P and the damping force present in the system, respectively, δ_d is the Dirac delta function, c is the coefficient of material damping present in the beam-soil system, and x_0 is the initial position of the applied load. The force P can vary in magnitude with time and can also move with a velocity v.

Substituting Equation 4.7 in Equation 4.6 results in

$$\delta \int_{t_1}^{t_2} \left[\int_0^L \frac{\rho_b A_b}{2} (\frac{\partial w}{\partial t})^2 dx + \sum_{i=1}^{n} \int_{-\beta L}^{\beta L} \int_{H_{i-1}}^{H_i} \left[\frac{\rho_{si} b}{2} (\frac{\partial w}{\partial t})^2 \phi_i^2 \right] dz dx \right] dt -$$

$$\delta \int_{t_1}^{t_2} \left[\int_0^L \frac{E_b I_b}{2} (\frac{\partial^2 w}{\partial x^2})^2 dx + \sum_{i=1}^{n} \frac{b}{2} \int_{-\beta L}^{\beta L} \int_{H_{i-1}}^{H_i} \left(\bar{E_{si}} w^2 (\frac{d\phi_i}{dz})^2 + G_{si} \phi_i^2 (\frac{\partial w}{\partial x})^2 \right) dz dx - \int_0^L P \delta_d (x_0 - vt) w dx dt \right]$$

$$+ \delta \int_{t_1}^{t_2} \left[-\frac{1}{2} c (\frac{\partial w}{\partial t})^2 \right] dt \tag{4.8}$$

4.3.4 Differential Equations for Beam and Surface-Soil Displacements

Considering the variation of function w in Equation 4.8, the Euler-Lagrange equations of motion of beam and surface soil displacements can be obtained along with the corresponding boundary and initial conditions. For the domain $0 \leq x \leq$ L, i.e., for beam deflection, the governing differential equation (i.e., the Euler-Lagrange equation) is given by

$$E_b I_b \frac{\partial^4 w}{\partial x^4} - 2t_s \frac{\partial^2 w}{\partial x^2} + k_s w + c \frac{\partial w}{\partial t} + (\eta_s + \rho_b A_b) \frac{\partial^2 w}{\partial t^2} = P(t) \delta_d (x_0 - \nu t) (0 \leq x \leq L \tag{4.9a}$$

For the domains -βL $\leq x \leq$ 0 and L $\leq x \leq \beta$L (i.e., over the soil domains with no beam), the displacement of the top surface of the continuum (soil) is governed by the following differential equation

$$-2t_s \frac{\partial^2 w}{\partial x^2} + k_s w + c \frac{\partial w}{\partial t} + \eta_s \frac{\partial^2 w}{\partial t^2} = 0 \quad (-\beta L \leq x \leq 0) \ \& \ (L \leq x \leq \beta L) \tag{4.9b}$$

The initial conditions required to solve the set of differential Equation 4.9(a,b) are that the displacement and velocity are zero initially. Therefore, $w = 0$ and $\partial w / \partial t = 0$ at $t = 0$.

The boundary conditions required to solve the differential Equation 4.9(a,b) depends on the end conditions of the beam. For a beam with both ends free to deflect and rotate,

the adjacent soil deforms with deflection of beam, and the soil deformation has to be taken into account in order to get accurate beam response. Therefore, for free end beams, the soil domains on both sides of the beam are required in the analysis, and Equation 4.9(b) is required to be solved in conjunction with Equation 4.9(a). The domain of the problem (-$\beta L \leq x \leq \beta L$) is chosen to be sufficiently large such that the displacement at the outer soil boundaries are zero; i.e., $w = 0$ at x = -βL and at $x = \beta L$. At the beam ends (i.e., at $x = 0$ and x =L), continuity of displacement and shear force have to be maintained between the beam and the adjacent soil. Further, the bending moment at the beam ends is zero if no applied moment is acting at the ends. Therefore, the boundary conditions for free-end beams are

$$w_{Right} \mid_{x=0} = w_{Left} \mid_{x=0} \tag{4.10a}$$

$$w_{Left} \mid_{x=L} = w_{Right} \mid_{x=L} \tag{4.10b}$$

with no concentrated force acting

$$\left[-2t_s \frac{\partial w}{\partial x}\right]_{Left} \mid_{x=0} = \left[E_b I_b \frac{\partial^3 w}{\partial x^3} - 2t_s \frac{\partial w}{\partial x}\right]_{Right} \mid_{x=0} \tag{4.10c}$$

with no concentrated force acting

$$\left[E_b I_b \frac{\partial^3 w}{\partial x^3} - 2t_s \frac{\partial w}{\partial x}\right]_{Left} \mid_{x=L} = \left[-2t_s \frac{\partial w}{\partial x}\right]_{Right} \mid_{x=L} \tag{4.10d}$$

$$E_b I_b \frac{\partial^2 w}{\partial x^2} \mid_{x=0 \ \& \ x=L} = 0 \tag{4.10e}$$

For simply supported beams or fixed beams (i.e., when the beam ends are restrained against deflection or both deflection and rotation), the soil domain adjacent to the hinged or fixed end is not required in the analysis because deformations in the adjacent soil domain is zero and it does not influence the beam response. Consequently, Equation 4.9(b) is not required to be solved. The boundary conditions for simply supported or fixed beams are

$$w \mid_{x=0 \ \& \ x=L} = 0 \tag{4.10f}$$

for fixed end

$$\frac{\partial w}{\partial x} \mid_{x=0 \ \& \ x=L} = 0 \tag{4.10g}$$

for hinged end with no applied concentrated moment

$$E_b I_b \frac{\partial^2 w}{\partial x^2} \mid_{x=0 \ \& \ x=L} = 0 \tag{4.10h}$$

for hinged end with no applied concentrated force

$$\left[E_b I_b \frac{\partial^3 w}{\partial x^3} - 2t_s \frac{\partial w}{\partial x}\right] |_{x=0 \ \& \ x=L} = 0 \tag{4.10i}$$

The parameters in the above equations are given by

$$\eta_s = \sum_{i=1}^{n} \rho_{si} b \int_{H_{i-1}}^{H_i} \phi_i^2 dz \tag{4.11a}$$

$$k_s = \sum_{i=1}^{n} b \int_{H_{i-1}}^{H_i} \bar{E_{si}} \left(\frac{d\phi_i}{dt}\right)^2 dz \tag{4.11b}$$

$$t_s = \sum_{i=1}^{n} \frac{b}{2} \int_{H_{i-1}}^{H_i} G_{si} \phi_i^2 dz \tag{4.11c}$$

The parameter η_s represents the mass of soil per unit beam length participating in the vibration, the parameter k_s is analogous to the Winkler spring constant of soil and represents the compressive resistance of soil, and the parameter t_s represents the shear resistance of soil and can be interpreted as the shear force acting between adjacent soil springs that are compressed differently because of the applied load. It is important to note that these parameters depend on the properties of both the soil and the beam.

4.3.5 Differential Equations for Soil-Displacement Function

Considering the variation of the function ϕ in Equation 4.8, the Euler-Lagrange equation (i.e., the differential equation of $\phi(z)$ within the i^{th} layer) can be obtained as

$$\frac{d^2\phi_i}{dz^2} - \left(\frac{\bar{\gamma_i}}{T_i}\right)^2 \phi_i = 0 \tag{4.12a}$$

where the dimensionless parameter $\bar{\gamma_i}$, normalized with respect to the thickness of the i^{th} layer T_i, is given by

$$\left(\frac{\bar{\gamma_i}}{T_i}\right)^2 = \left(\frac{\zeta_{si} - n_{si}}{m_{si}}\right) \tag{4.12b}$$

with

$$m_{si} = b \int_{-\beta L}^{\beta L} \bar{E_{si}} w^2 dx \tag{4.13a}$$

$$n_{si} = b \int_{-\beta L}^{\beta L} G_{si} \left(\frac{\partial w}{\partial x} \right)^2 dx \tag{4.13b}$$

$$\zeta_{si} = b \int_{-\beta L}^{\beta L} \rho_{si} \left(\frac{\partial w}{\partial t} \right)^2 dx \tag{4.13c}$$

such that

$$\left(\frac{\bar{\gamma_i}}{T_i} \right)^2 = \frac{\rho_{si} \int_{-\beta L}^{\beta L} \left(\frac{\partial w}{\partial t} \right)^2 dx - G_{si} \int_{-\beta L}^{\beta L} \left(\frac{\partial w}{\partial x} \right)^2 dx}{\bar{E_{si}} \int_{-\beta L}^{\beta L} w^2 dx} \tag{4.13d}$$

For the boundary conditions of ϕ(z), it is assumed that $\phi(0) = 1$ to ensure perfect contact between the beam and the underlying soil and $\phi(H_{Total}) = 0$ to ensure that the displacements in soil decrease with depth and become zero at the boundary with the rigid layer. The continuity across the soil layers is also assured with the continuity condition that $\phi_i = \phi_{i+1}$ at z = H_i.

4.3.6 Solution of the Differential Equations

Solution of the differential Equation 4.9(a,b) of w is obtained by using the FE method. Two-noded rod (bar) elements with linear Lagrangian shape functions $\{N_L\}_{2\times1}$ are used to discretize the domains -$\beta L \leq x \leq 0$ and L $\leq x \leq \beta L$ (i.e., the domains in x direction with no beam) and two-noded beam elements with cubic Hermitian shape functions $\{N_H\}_{4\times1}$ are used to discretize the domain $0 \leq x \leq$ L (i.e., domain in x direction in which the beam is present) to obtain a set of algebraic equations of the form $\sum_e [m]^e \{\ddot{w}\} + \sum_e [c]^e \{\dot{w}\} + \sum_e [k]^e \{w\} = \sum_e \{f\}^e$ (Figure 4-2) where $[m]^e$, $[c]^e$ and $[k]^e$ are the elemental mass,

damping, and stiffness matrices, respectively, $\{f\}^e$ is the elemental force vector, $\{w\}$ is the global degrees of freedom vector (consisting of the unknown nodal displacements w for the entire domain and nodal slope $\partial w/\partial x$ for the portion of the domain within the beam), $\{\ddot{w}\}$ is the global acceleration vector, $\{\dot{w}\}$ is the global velocity vector, and $\sum_e$ represents assembly. Details of the assembly procedure to obtain the global matrices are provided in the Appendix. The time integration to obtain solutions is performed following the Wilson-θ method [28].

The elemental mass, damping, and stiffness matrices, and force vectors for $0 \leq x \leq \mathrm{L}$ are respectively given by

$$[m]^e_{4\times4} = \int_{x_i}^{x_j} \left[\{N_H\}^T (\rho_b A_b + \eta_s) \{N_H\} \right] dx$$

$$= (\rho_b A_b + \eta_s) \begin{bmatrix} \frac{13h_e}{35} & \frac{11h_e^2}{210} & \frac{9h_e}{70} & -\frac{13h_e^2}{420} \\ \frac{11h_e^2}{210} & \frac{h_e^3}{105} & \frac{13h_e^2}{420} & -\frac{h_e^3}{140} \\ \frac{9h_e}{70} & \frac{13h_e^2}{420} & \frac{13h_e}{35} & -\frac{11h_e^2}{210} \\ -\frac{13h_e^2}{420} & -\frac{h_e^3}{140} & -\frac{11h_e^2}{210} & \frac{h_e^3}{105} \end{bmatrix} \tag{4.14a}$$

$$[c]^e_{4\times 4} = \int_{x_i}^{x_j} \left[\{N_H\}^T c \{N_H\} \right] dx$$

$$= (\rho_b A_b + \eta_s) \begin{bmatrix} \frac{13h_e}{35} & \frac{11h_e^2}{210} & \frac{9h_e}{70} & \frac{13h_e^2}{420} \\ \frac{11h_e^2}{210} & \frac{h_e^3}{105} & \frac{13h_e^2}{420} & -\frac{h_e^3}{140} \\ \frac{9h_e}{70} & \frac{13h_e^2}{420} & \frac{13h_e}{35} & -\frac{11h_e^2}{210} \\ -\frac{13h_e^2}{420} & -\frac{h_e^3}{140} & -\frac{11h_e^2}{210} & \frac{h_e^3}{105} \end{bmatrix} \tag{4.14b}$$

$$[c]^e_{4\times4} = \int_{x_i}^{x_j} \left[\left(\frac{d^2\{N_H\}}{dx^2} \right)^T E_b I_b \left(\frac{d^2\{N_H\}}{dx^2} \right) + \{N_H\}^T k_s \{N_H\} + \left(\frac{d\{N_H\}}{dx} \right)^T 2t_s \left(\frac{d\{N_H\}}{dx} \right) \right] dx$$

$$= E_b I_b \begin{bmatrix} \frac{12}{h_e^3} & \frac{6}{h_e^2} & \frac{-12}{h_e^3} & \frac{6}{h_e^2} \\ \frac{6}{h_e^2} & \frac{4}{h_e} & \frac{-6}{h_e^2} & \frac{2}{h_e} \\ \frac{-12}{h_e^3} & \frac{-6}{h_e^2} & \frac{12}{h_e^3} & \frac{-6}{h_e^2} \\ \frac{6}{h_e^2} & \frac{2}{h_e} & \frac{-6}{h_e^2} & \frac{4}{h_e} \end{bmatrix} + k_s \begin{bmatrix} \frac{13h_e}{35} & \frac{11h_e^2}{210} & \frac{9h_e}{70} & -\frac{13h_e^2}{420} \\ \frac{11h_e^2}{210} & \frac{h_e^3}{105} & \frac{13h_e^2}{420} & -\frac{h_e^3}{140} \\ \frac{9h_e}{70} & \frac{13h_e^2}{420} & \frac{13h_e}{35} & -\frac{11h_e^2}{210} \\ -\frac{13h_e^2}{420} & -\frac{h_e^3}{140} & -\frac{11h_e^2}{210} & \frac{h_e^3}{105} \end{bmatrix}$$

$$+2t_s \begin{bmatrix} \frac{6}{5h_e} & \frac{1}{10} & \frac{-6}{5h_e} & \frac{1}{10} \\ \frac{1}{10} & \frac{2h_e}{15} & \frac{-1}{10} & \frac{-h_e}{30} \\ \frac{-6}{5h_e} & \frac{-1}{10} & \frac{6}{5h_e} & \frac{-1}{10} \\ \frac{1}{10} & \frac{-h_e}{30} & \frac{-1}{10} & \frac{2h_e}{15} \end{bmatrix} \tag{4.14c}$$

$$\{f\}^e_{4\times1} = \int_{x_i}^{x_j} N_H^T P \delta_d(x_0 - \nu t) dx \tag{4.15a}$$

where x_i and x_j are the coordinates of the first (or left) node and second (or right) node of the e^{th} element (rod or beam element), respectively, with the element length $h_e = x_j$ - x_i (Figure 4.2).

In the case of moving load where the magnitude of the applied vertical load remains constant at $\bar{P}$ but its spatial position changes, the elemental force vector is given by

$$\{f\}^e_{4\times1} = \bar{P} \begin{bmatrix} \frac{1}{2} & 0 & 0 & 0 \end{bmatrix}^T \; or \; \bar{P} \begin{bmatrix} 0 & 0 & \frac{1}{2} & 0 \end{bmatrix}^T \tag{4.15b}$$

for the load acting at the first (left) or the second (right) node of the element e, respectively. If the load is in between the two nodes at a distance of $\hat{x}$ from the second (right) node

$$\{f\}^e_{4\times1} = \bar{P}\left(\frac{h_e - \hat{x}}{h_e}\right)\begin{bmatrix}\frac{h_e}{2} & \frac{h_e^2}{12} & \frac{h_e}{2} & \frac{-h_e^2}{12}\end{bmatrix}^T \tag{4.15c}$$

In the case of oscillatory load where the magnitude of the load changes with time but its position remains constant, the elemental force vector is given by

$$\{f\}^e_{4\times1} = \bar{P}_t\begin{bmatrix}\frac{h_e}{2} & \frac{h_e^2}{12} & \frac{h_e}{2} & \frac{-h_e^2}{12}\end{bmatrix}^T \tag{4.15d}$$

where P_t is the magnitude of $P(x_0,t)$ at any time t and the position x_0 is such that the load lies on a node.

The corresponding stiffness, mass, and damping matrices for -$\beta L \leq x \leq 0$ and L $\leq x \leq \beta L$ are given by

$$\begin{aligned}\{k\}^e_{2\times2} &= \int_{x_i}^{x_j}\left[N_L^T k_s N_L + \left(\frac{dN_L}{dx}\right)^T 2t_s\left(\frac{dN_L}{dx}\right)\right]dx \\ &= \frac{k_s h_e}{6}\begin{bmatrix}2 & 1\\ 1 & 2\end{bmatrix} + \frac{2t_s}{h_e}\begin{bmatrix}+1 & -1\\ -1 & +1\end{bmatrix}\end{aligned} \tag{4.16a}$$

$$\{m\}^e_{2\times2} = \int_{x_i}^{x_j}\left[N_L^T \eta_s N_L\right]dx = \frac{\eta_s h_e}{6}\begin{bmatrix}2 & 1\\ 1 & 2\end{bmatrix} \tag{4.16b}$$

$$\{m\}^e_{2\times2} = \int_{x_i}^{x_j}\left[N_L^T c N_L\right]dx = \frac{c h_e}{6}\begin{bmatrix}2 & 1\\ 1 & 2\end{bmatrix} \tag{4.16c}$$

Solution of the differential Equation 4.12(a) for ϕ is obtained analytically, and is given by

$$\phi_i(z) = A^{(i)}e^{\sqrt{\frac{\zeta_{si} - n_{si}}{m_{si}}}z} + B^{(i)}e^{-\sqrt{\frac{\zeta_{si} - n_{si}}{m_{si}}}z} \tag{4.17a}$$

where the integration constants $A^{(i)}$ and $B^{(i)}$ are obtained from the boundary conditions of $\phi(z)$ described earlier. For a single layer (with $i = 1$), ϕ is given by

$$\phi_1(z) = \frac{sinh[\bar{\gamma_1}(1 - \frac{z}{T_1})]}{sinh(\bar{\gamma_1})} \tag{4.17b}$$

(4.17c)

For the special case of a single soil layer of infinite thickness (i.e., $H_1 \to \infty$), ϕ is given by

$$\phi_1(z) = e^{-\sqrt{\frac{\zeta_{si} - n_{s1}}{m_{s1}}}z} \tag{4.17d}$$

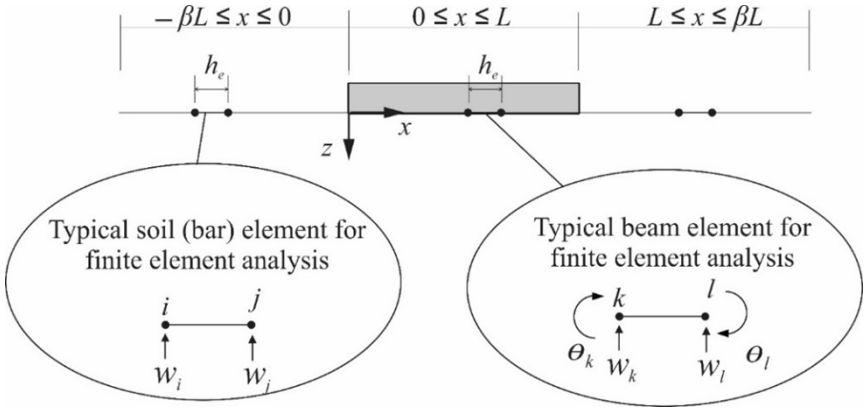

Figure 4.2: Finite element discretization in x-direction

4.3.7 Iterative Solution Algorithm

The parameters k_s, t_s, and η_s must be known in order to solve the differential equations for w (Equation 4.9(a,b)) and these parameters depend on ϕ. At the same time, the parameters m_{si}, n_{si} and ζ_i must be known in order to obtain ϕ (from Equations 4.12(a) or 4.17(a)) and these parameters depend on w. Therefore, the equations of w and ϕ are coupled, and are solved simultaneously following an iterative scheme.

To begin with, the function $\phi(z)$ is determined iteratively for static loading condition (ϕ_{static}) using the same magnitude of load as that of the dynamic load. In the case of oscillatory load, a static load that has the same amplitude of the dynamic load is used and

is placed at the same point on the beam where the dynamic load acts. In the case of moving load, a static load with the same magnitude as the moving load is placed at the mid-span of the beam. In order to obtain $\phi_{static}(z)$, an initial guess for the spatial distribution of ϕ is made by assuming a linear distribution of ϕ. With this assumed distribution, k_s and t_s are calculated (note that η_s is not required for static loading as inertia forces are negligible) using Equation 4.11(b,c), and these parameters are then used to calculate the displacement w and its spatial derivative $\partial w/\partial x$. Using the calculated w and $\partial w/\partial x$, parameters m_{si} and n_{si} are calculated from Equation 4.13(a,b) (note that ζ_{si} is zero under static loading). The parameters m_{si} and n_{si} are then used to obtain a new $\phi_{static}(z)$. The newly calculated $\phi_{static}(z)$ is compared with the assumed $\phi_{static}(z)$ and, if the difference is greater than a prescribed tolerance, the calculations are repeated with the calculated $\phi_{static}(z)$ as the new guess. The iterative calculations are continued until the assumed and calculated $\phi_{static}(z)$ values fall within a tolerance limit. The tolerance limit set for the iterations is 10^{-5} and is calculated as per the following equation

$$\frac{\sum_{j=1}^{m} \mid \phi_{Calculated}^{(j)} - \phi_{Initial}^{(j)} \mid}{\sum_{j=1}^{m} \mid \phi_{Initial}^{(j)} \mid} \leq \text{prescribed tolerance} = 10^{-5} \tag{4.18}$$

where $\phi^{(j)}$ is the value of ϕ at the discrete j_{th} point along z, the subscript "Calculated" represents $\phi^{(j)}$ calculated in the current iteration, the subscript "Initial" represents $\phi^{(j)}$ calculated during the previous iteration, and m is the number of discrete points at which $\phi^{(j)}$ values are calculated.

For the dynamic time integration scheme (following the Wilson-θ method), iterations similar to that described in the previous paragraph are performed within each time increment Δt. For the first time step, the initial position x_0 of the applied load, geometry, material properties, and $\phi_{static}(z)$ are given as inputs, and the parameters k_s, t_s, and η_s are calculated. These calculated parameters are used to obtain the beam and soil displacement w, spatial derivative $\partial w/\partial x$ (which is the slope for the beam), velocity $\partial w/\partial t$, and acceleration $\partial^2 w/\partial t^2$. These quantities are used to calculate m_{si}, n_{si} and ζ_{si}, which are used to calculate the distribution $\phi_{dynamic}(z)$ of the function ϕ. The newly obtained $\phi_{dynamic}$ is checked against the previous ϕ (which is ϕ_{static} for the first iteration of the first time increment), and iterations are continued until the difference between two consecutive distributions of $\phi_{dynamic}$(z) are within tolerable limit of 10^{-5} (following Equation 4.18). At this point, the calculated w, $\partial w/\partial x$, $\partial w/\partial t$, and $\partial^2 w/\partial t^2$ are the final values for the given time step, and the next increment of time is then applied and the whole iterative process

is repeated for each subsequent time steps until the final time increment is complete to reach the final time t_{final}. A detailed solution algorithm is given in Figure 4.3.

4.4 Results

4.4.1 Verification

In order to verify the accuracy of the present analysis, a comparison of the beam response obtained from the present analysis is performed with that of equivalent two-dimensional (2-D) FE analysis using linear elastic constitutive relationship. The nature and type of load, geometry of the problem, end conditions of the beam, and the material constants are selected differently in multiple verification problems to ensure that the present analysis works for all possible cases. In the 2-D FE analysis (performed using PLAXIS 2-D), the beam is modeled using 1-D beam (plate) elements whereas the soil layers are modeled using 2-D triangular elements. PLAXIS automatically generates an interface between the beam (structural) layer and/or soil layers to ensure no slippage or separation such that full contact is ensured during loading - this is the same assumption made in the analysis developed in this paper. Appropriate boundary conditions are prescribed at the soil boundaries of the 2-D FE model - all components of displacements are assumed to be zero along the bottom horizontal boundary and the horizontal displacement is assumed to be zero along the vertical sides of the FE domain. Additional boundary conditions are prescribed at the end points of the beams to simulate different types of end conditions (i.e., fixed, free, and hinged supports). Because of a lack of any built-in function for moving loads in PLAXIS 2D, the moving load is simulated by means of a series of single-load envelopes at different points and different time intervals along the span of the beam. The response is determined by applying the first single-load envelope to the beam element at the specified position and time interval. Then the process is repeated for each subsequent single-load envelope, progressively moving along the span of the beam by updating the load position and time interval.

Figure 4.4(a,b) show the response of a free-free beam resting on a three-layer soil subjected to a concentrated step load of 50 KN amplitude acting at the mid-span of the beam over a duration of 1 sec. Figure 4.4(a) shows the displacement profile $w(x, t_{final})$ at the end of 1 sec, and Figure 4.4(b) show the time history $w(L/2, t)$ of beam deflection at the mid-span. The details of the beam and soil properties are given in the figure itself. The analysis is performed following the developed method and 2-D FE analysis using PLAXIS.

The difference between the calculated mid-span beam deflection at tfinal obtained from the present analysis and 2-D FE analysis is 6.3%.

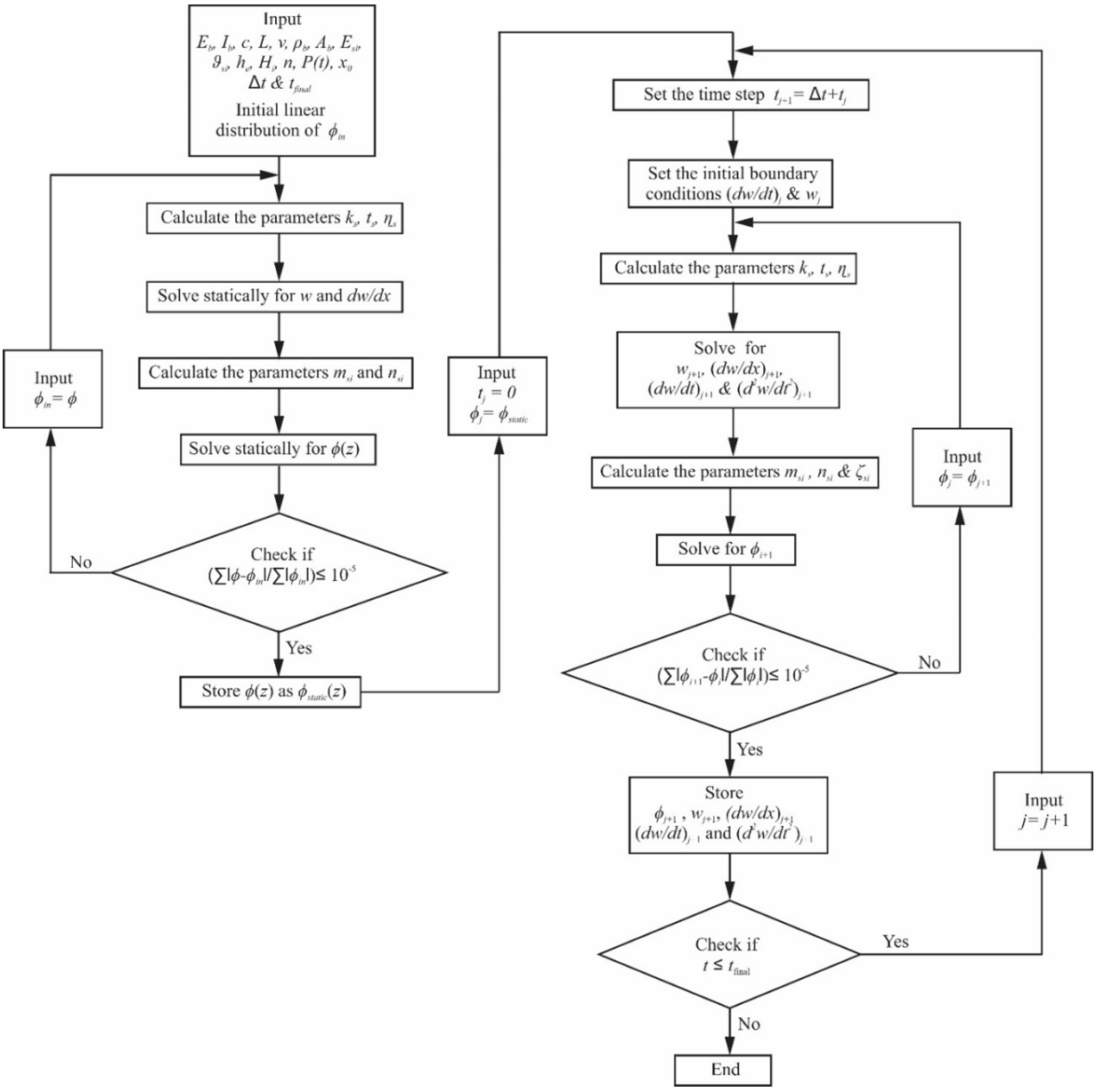

Figure 4.3: Solution algorithm

Figure 4.5 shows the beam response for an applied concentrated sinusoidal load of 10

kN amplitude, 10 Hz frequency, and 0.5 sec duration acting at the mid-span of a 5 m long freely supported beam, resting on a single layer soil deposit of 2 m thickness (details of inputs are given in the figure). The time-history $w(L/2, t)$ of mid-span deflection is shown in Figure 4.5 and the maximum difference between the results of the present analysis and 2-D FE analysis is 5.1%.

A comparison of the beam responses obtained by the present analysis and 2-D FE analysis for a concentrated load moving over a 6 m long free-free beam at a constant velocity of 10 m/sec is shown in Figure 4.6 (other inputs are shown in the figure). The beam deflection profiles obtained when the load is at the mid span and when it is at the right end of the beam are shown in the figure. It is evident that the beam responses obtained from the present analysis and 2-D FE analysis are in good agreement with the maximum difference being 4.3%.

Figure 4.7 shows the comparison of beam deflection profiles $w(x, t_{final})$ at the end of 0.5 sec obtained from the present analysis and 2-D FE analysis for two concentrated step loads of 15 kN acting over a duration of 0.5 sec applied at 2.5 m from both ends of a beam. The beam is 12.5 m long with full restraint against deflection and rotation at both the ends (fixed ends), and rests on a 6 m thick soil homogeneous layer. The maximum difference at the mid-span beam deflection is 4.1%. It is evident that the results obtained from the present analysis are sufficiently accurate.

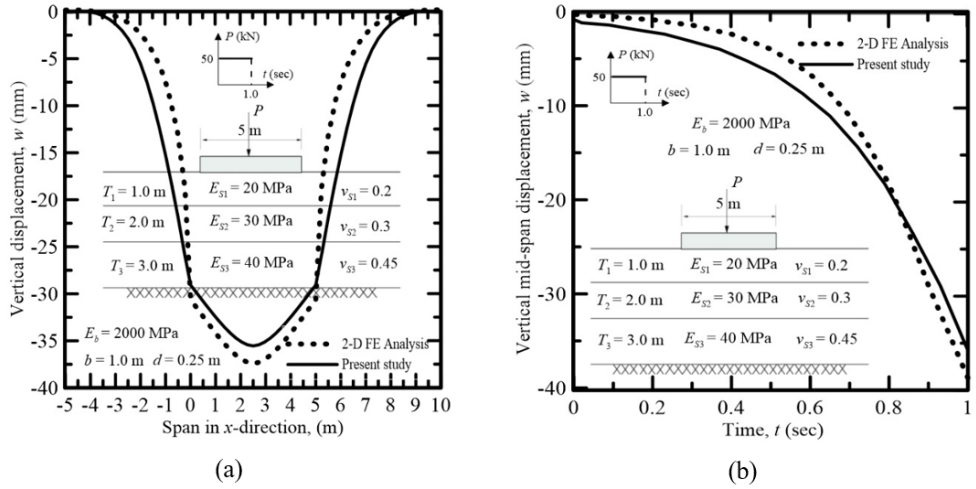

Figure 4.4: Time dependent response of a 5 m long free beam resting on a three-layer soil deposit and subjected to 50 kN concentrated step load: (a) displacement along the span at time $t = 0.5$ sec, and (b) time history of mid-span displacement

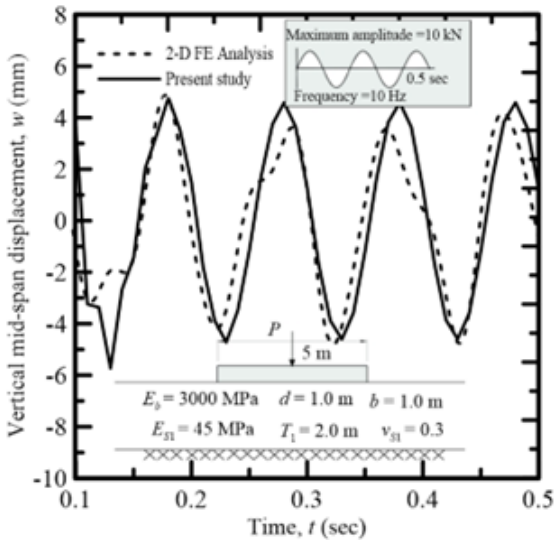

Figure 4.5: Time history of mid-span displacement of a 5 m long free beam resting on a 2 m thick homogeneous soil deposit and subjected to a sinusoidal load with a maximum amplitude of 10 kN

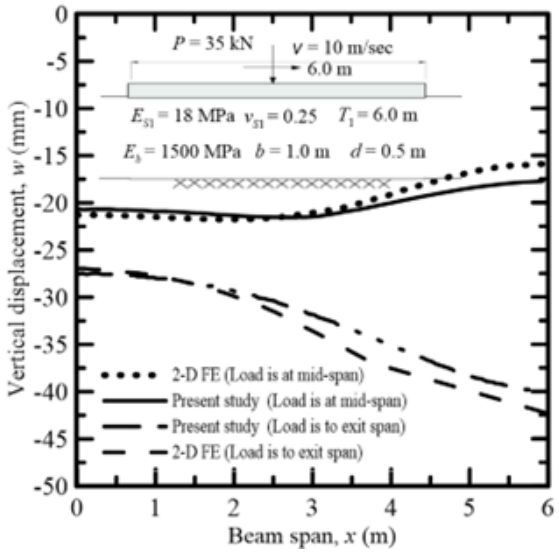

Figure 4.6: Displacement response of a 6 m long free-free beam resting on a homogeneous (one-layer) soil and subjected to a 35 kN point load moving with a constant velocity of 10 m/sec

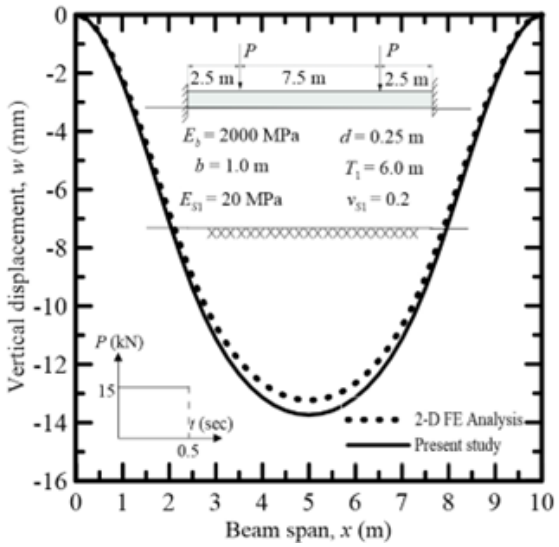

Figure 4.7: Displacement response of a 10 m long fixed beam resting on a 6 m thick homogeneous soil and subjected to two 15 kN point-step loads at time $t = 0.5$ sec

4.4.2 Dynamic Characteristics of the Foundation

Six example problems are studied to illustrate the characteristics of the dynamic two-parameter foundation model developed in this study. The time dependent response of beams on multi-layered soil deposits is illustrated by Figures 4.8(a)-(d) and 4.9(a)-(d). The details of the beam-soil inputs are given in the figures themselves. The beams are considered to be free to displace and rotate at both ends (free ends). A concentrated ramp load with a maximum amplitude of 25 kN and duration of 1 sec is assumed to act at the mid-span of the beam in Figure 4.8, and a concentrated step load with 40 kN amplitude and 3 sec duration is assumed to act at the mid-span of the beam in Figure 4.9. The time histories of the mid-span displacements, the parameters k_s and t_s, and the vibrating soil masses η_s are plotted in Figures 4.8(a)-(c) and 4.9(a)-(c), and the soil displacement functions $\phi(z)$ is plotted at selected times in Figures 4.8(d) and 4.9(d). The parameters k_s and t_s tend to be constant at the beginning of the dynamic analysis when contribution of the vibrating soil mass η_s is small. As η_s starts contributing to the vibrating system over time, the parameters k_s and t_s starts to change as functions of time. This is in stark contrast with the discrete two parameter model in which k_s and t_s are kept constants and η_s is neglected.

Figure 4.10(a)-(d) show the parameters k_s, t_s, and η_s, and the soil displacement func-

tion $\phi(z)$ for a beam-soil system (properties of the beam-soil system are shown within the figures) in response to a sinusoidal load with a frequency f and with a maximum amplitude of 15 kN acting over a duration of 0.5 sec at the mid-span of a simply supported beam. Different load frequencies, f = 5-45 Hz, are considered, and how the different parameters vary with load frequency is investigated. It is clear that k_s, t_s, and η_s and $\phi(z)$ are functions of frequency of the applied load. The effect on the vibrating soil mass η_s of the load frequency, however, is rather marginal.

Figure 4.11(a)-(d) show the time histories of k_s, t_s, and η_s, and $\phi(z)$ at different times for a simply supported beam resting on a homogeneous soil layer and subjected to a load of 40 kN moving with a constant velocity from the left to the right of the beam starting from an initial position x_0 = 0.1 m (from the left end of the beam). Different load velocities, 10-25 m/sec, are considered to investigate the effect of load velocity on the different parameters. The properties of the beam-soil system are shown within the figures. It is obvious that k_s, t_s, and η_s, and $\phi(z)$ are functions of load velocity.

The response of very long beam (which is similar to an infinite beam) resting on a homogeneous (single layer) soil and subjected to a point load of 10 kN traveling at a speed of 106 m/sec is shown in Figure 4.12(a)-(d). The properties of the beam-foundation system are shown in the figure. As the beam is very long, the steady-state response is independent of a fixed coordinate system and can be best captured by a moving coordinate system in the x direction with the origin attached to the moving load. Figure 4.12(a) shows the steady state response for the beam displacement $w(x, t)$. Figure 4.12(b)-(c) show the time histories of k_s, t_s, and η_s. It is evident that k_s, t_s, and η_s change initially with time and finally attain constant values under steady-state vibration of the beam. Similarly, $\phi(z)$ changes with time during transient vibration and attains a final profile at the steady state.

4.5 Conclusions

A new model for dynamic soil structure interaction is developed using the variational principles of mechanics. The model is applied to the analysis of beams resting on multi-layered visco-elastic soil subjected to oscillatory and moving loads. A continuum approach is adopted in which simplifying assumptions regarding the displacement field in the multi-layered soil are made. The extended Hamilton's principle is applied to obtain the Euler-Lagrange equations of motion describing the dynamic equilibrium of the beam-soil system. Solutions are obtained analytically and numerically using an iterative algorithm along with a numerical time integration scheme. The inputs required are the magnitude and frequency or velocity of applied loads; beam geometry, Young's modulus, and density; and

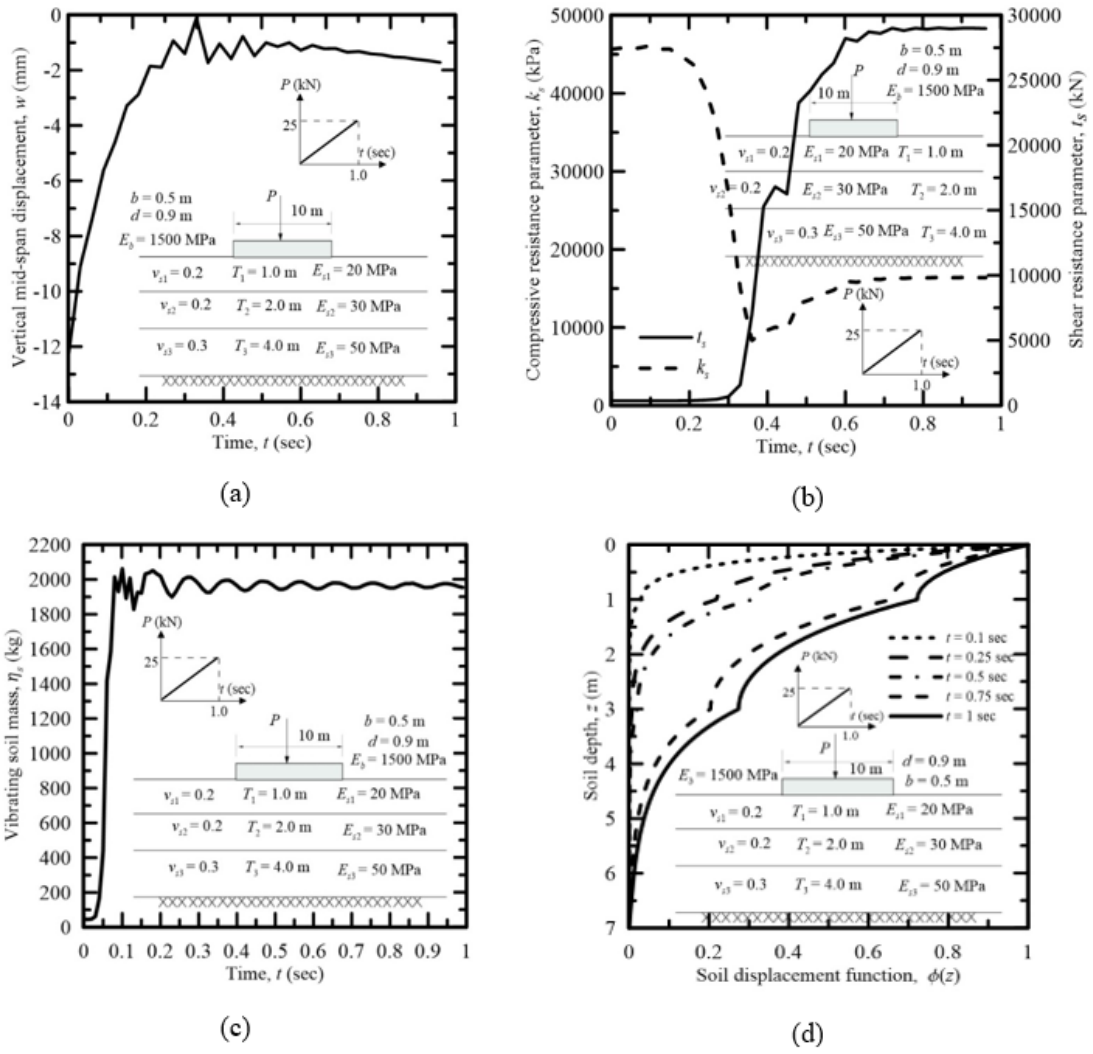

Figure 4.8: Time dependent response of a 10 m long beam resting on a three-layered soil deposit and subjected to a ramp point load with maximum amplitude of 25 kN: (a) time history of mid-span displacement, (b) time history of k_s and t_s, (c) time history of η_s, and (d) soil displacement function $\phi(z)$ at different times

soil geometry, density, and elastic constants. Accuracy of the model in producing reliable beam response is verified through comparisons with equivalent 2-D finite element analysis.

One of the advantages of the developed model is that it leads to equations similar to beams resting on bed of springs (i.e., the soil is represented by springs, which is commonly

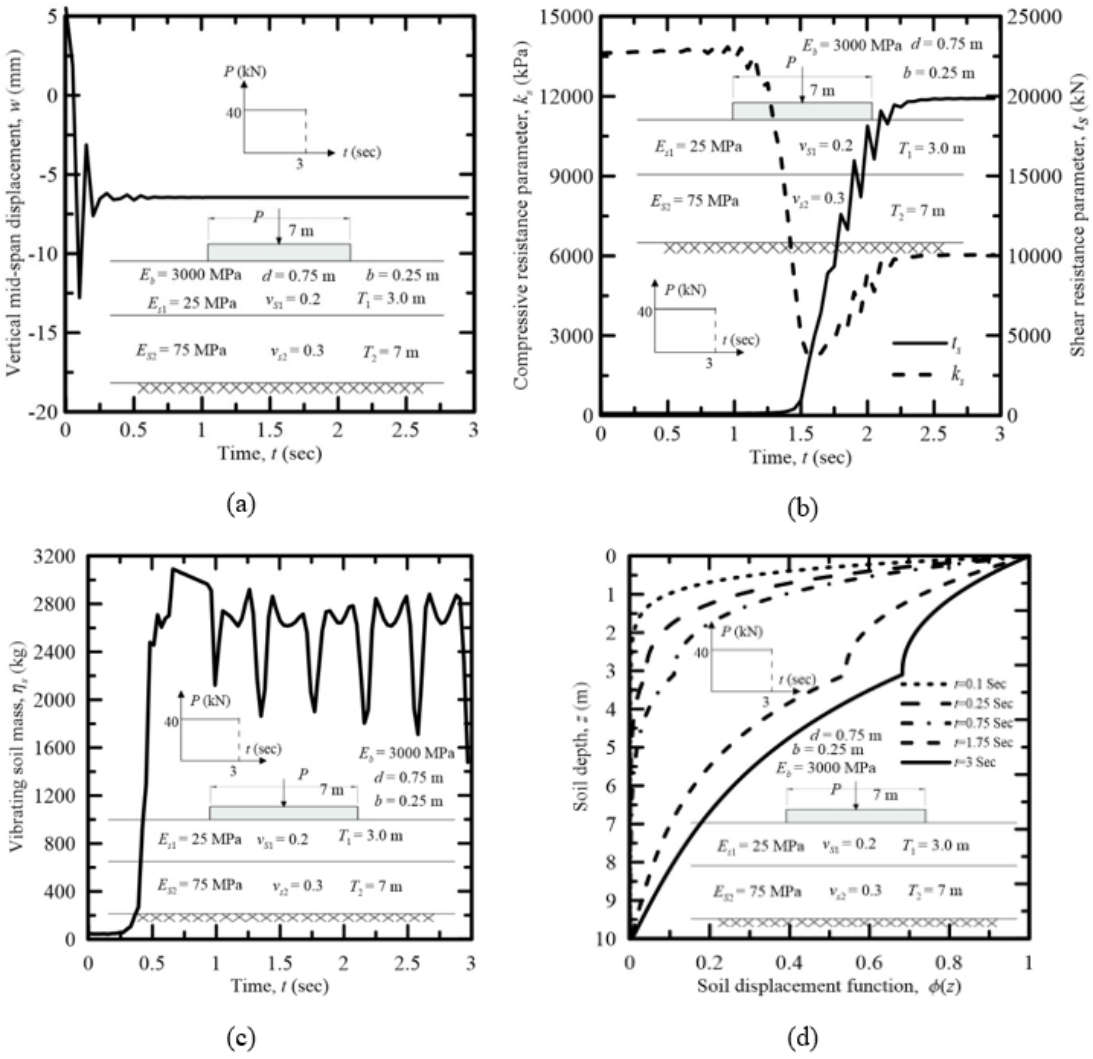

Figure 4.9: Time dependent response of a 7 m long beam resting on two-layered soil deposit and subjected to a 40 kN ramp step load: (a) time history of mid-span displacement (b) time history of k_s and t_s, (c) time history of η_s, and (d) time history of soil displacement function $\phi(z)$

termed as the foundation on which the beam rests) characterized by two parameters k_s and t_s representing the compressive and shear resistances of the foundation. It is shown in this analysis that, unlike the traditional approach, k_s and t_s are not foundation constants but depend on the beam-foundation interaction and, therefore, are functions of time – this

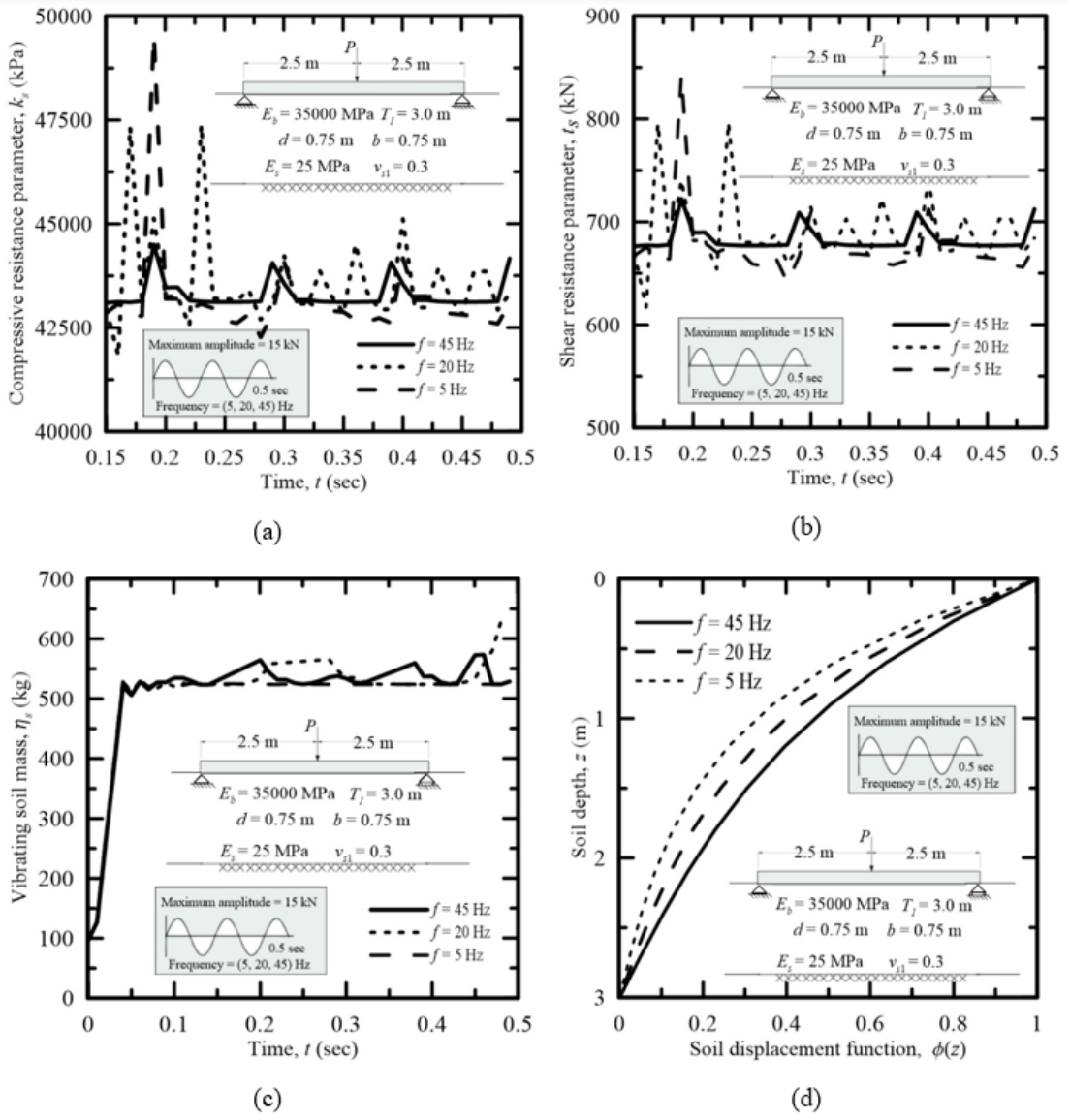

Figure 4.10: Frequency dependent response of a 5 m long beam subjected to a sinusoidal load with maximum amplitude of 15 kN: (a) time history of k_s , (b) time history of t_s, (c) time history of η_s, and (d) soil displacement functions $\phi(z)$ at $t = 0.5$ sec

is a novel finding and a significantly different approach for problems related to dynamic interaction of beams with underlying foundations. Another advantage of the present model is that the inertial resistance of soil (i.e., the foundation) is explicitly taken into account

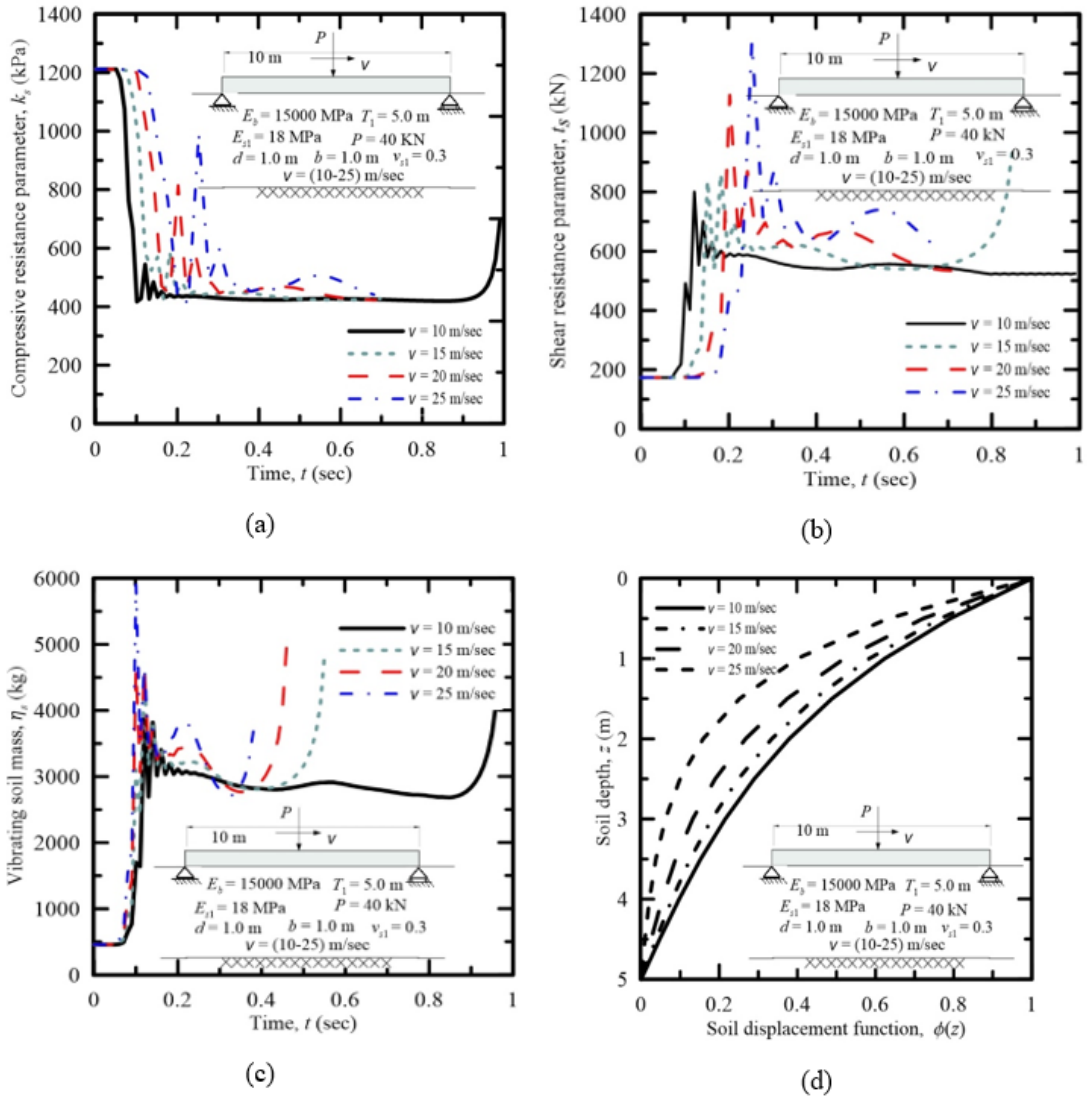

Figure 4.11: Velocity dependent response of a 10 m long beam subjected to a moving point load: (a) time history of k_s, (b) time history of t_s, (c) time history of η_s, and (d) soil displacement function $\phi(z)$ at time $t = 0.25$ sec

by a parameter η_s, which is also a function of time (inertia of foundations are not taken into account for traditional spring-based foundation models). Thus, the parameters k_s, t_s and η_s are interaction parameters and change with load frequency and velocity. Further,

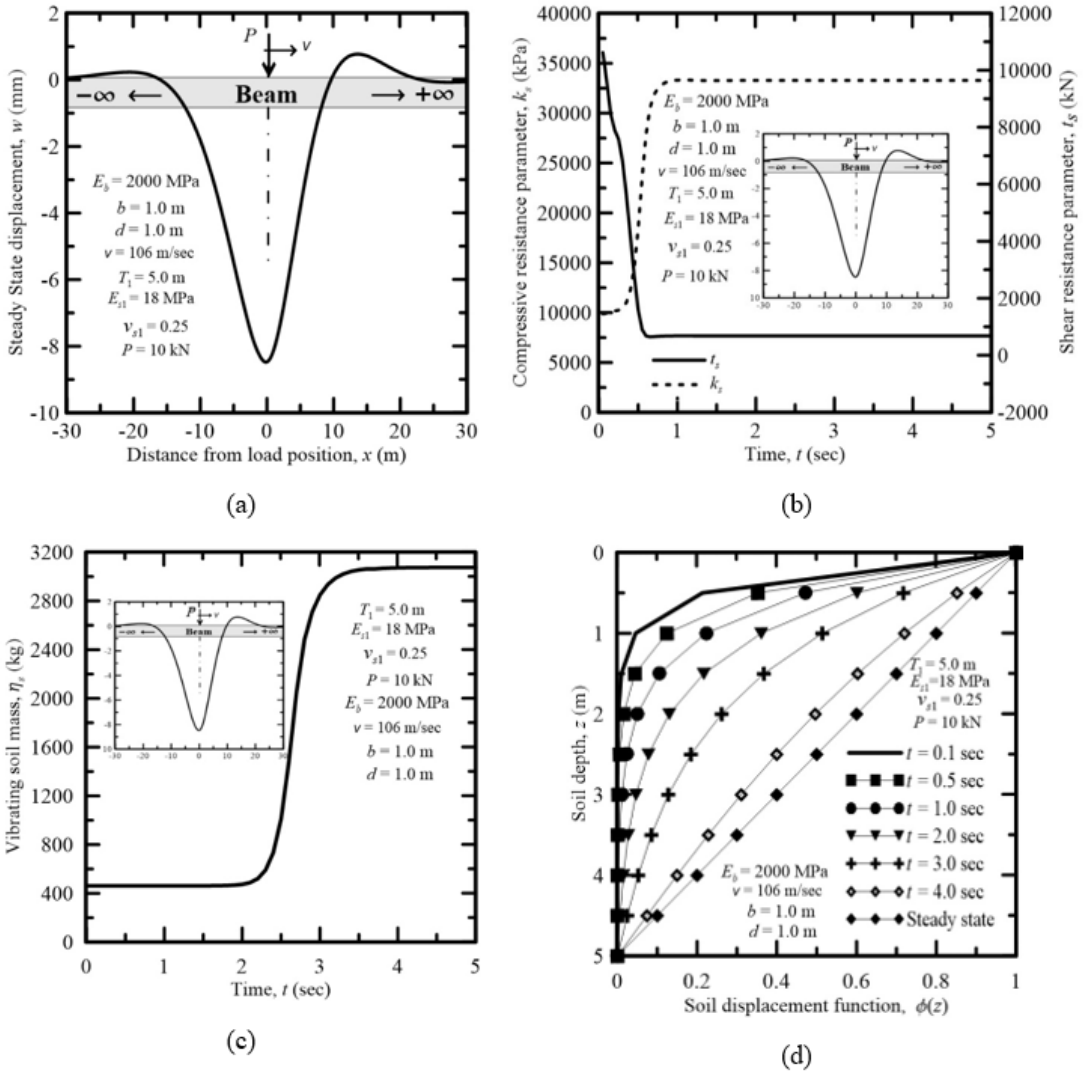

Figure 4.12: Response of an infinite long beam subjected to a 40 kN point load moving with a constant speed of 106 m/sec: (a) beam deflection profile under steady state, (b) time history of k_s and t_s, (c) time history of η_s, and (d) $\phi(z)$ at different times

geometric damping is also taken into account in this model through a function ϕ, which is typically not available in traditional spring-based soil-structure interaction models. Several example problems are analyzed to illustrate these characteristics of the foundation model.

Chapter 5

Novel Nonlinear Dynamic Beam-Foundation Interaction Model

This chapter is published Manuscript in ASCE- Journal of Engineering Mechanics, available online: https://doi.org/10.1061/(ASCE)EM.1943-7889.0001915, Elhuni, Hesham, and Dipanjan Basu. Elhuni, H., & Basu, D. (2021). Novel nonlinear dynamic beam–foundation interaction model. Journal of Engineering Mechanics, 147(4), 04021012.

5.1 Overview

A nonlinear dynamic framework for analysis of beam-foundation interaction is developed. The extended Hamilton's principle is used to analyze the response of Euler-Bernoulli beams vibrating on nonlinear continuums (e.g., soils) and subjected to vibrating and moving loads. The continuum beneath the beam is characterized by a nonlinear-elastic constitutive relationship that connects the secant shear modulus to the induced strain. The novel feature of the analysis is that the nonlinear compression and shear parameters k_s and t_s of the continuum (i.e., foundation) do not have to be assumed a priori, as is required in conventional beam on foundation analysis, and are obtained as part of the solution. In fact, it is shown that these parameters are not constants but change with time and depend on the beam-foundation interaction. Another novel feature of the analysis is that the mass of the foundation participating in the vibration is obtained as part of the solution and does not have to be assumed a priori. Thus, the analysis rigorously takes into account the nonlinear beam-foundation (soil-structure) interaction within a dynamic time-integration

framework. The developed framework is as accurate as and about 50% faster than conventional nonlinear dynamic finite element analysis. Inputs to the analysis can be given in the form of a text file without any requirement of numerical mesh generation, which makes the approach rather user friendly. The characteristics of the developed nonlinear dynamic foundation model are illustrated through examples of moving and vibrating loads.

5.2 Introduction and Related Literature

The theory of beams on foundations has been extensively used in civil engineering for modeling soil-structure interaction problems related to shallow strip footings, pavements, and railroads under static and dynamic loads [14]. The 'beam' typically represents the flexible shallow foundations, pavements, and railroads, and the soil underneath is referred to as 'foundation', which is traditionally modeled as a bed of springs [255]. Numerous research studies have been performed considering these discrete Winkler spring approach for both static and dynamic loads [200, 163, 144, 157]. In the Winkler model, there is no mechanical interaction between the adjacent springs because of which only compression in soil can be modeled by using the spring constant k_s and distortion is neglected. Therefore, several researchers introduced a two-parameter spring model to represent the soil in which the compressive and shear strains or stresses can be captured by using two parameters, k_s and t_s, in which k_s is the compression parameter (spring constant) and t_s is the shear parameter [92, 177]. Several studies using the two-parameter models exist involving both static and dynamic analysis of beams [178, 145]. However, the spring-based models cannot completely capture the continuum nature of soil. In fact, the soil spring is an artificial construct because of which the spring parameters k_s and t_s cannot be determined without additional assumptions (either using empirical equations or tests that have limited applicability) thus making the reliability of the spring-based approach questionable.

Representing the soil beneath foundations, pavements, and railroads as a continuum is conceptually superior but requires the use of two- or three-dimensional numerical methods like the finite element (FE), finite difference (FD), and boundary element (BE) methods that are computationally intensive [8, 233, 178, 4, 5]. Alternatively, the soil is assumed to be an elastic half-space, and several analytical and semi-analytical methods have been developed for beams on foundations problems with the half-space assumption [217]. However, this approach is mathematically complex and involves over-simplified assumptions (e.g., only linear elastic material with no material damping can be modeled) that may not be applicable to real field problems [102]. A simplified continuum approach exists in which the soil beneath the beam is treated as a continuum with simplified assumptions regarding

the stress or displacement field [190, 125, 247, 20]. This approach is conceptually robust and computationally less expensive than the two- or three-dimensional numerical methods. In fact, the simplified continuum approach by Vlasov and Leont'ev (1966) [247] results in the same differential equation of beam deflection as that obtained from the two-parameter spring model because of which it is computationally efficient and provides important insights into the beam on foundation problem from a soil-continuum perspective. Vallabhan and Das (1991) [242] improved the model by eliminating an assumption regarding the variation of soil displacements thereby making the model even more robust. Studies on static and dynamic responses of beams resting on elastic foundations using the model of Vlasov and Leont'ev (1966) [247] or its improved version show that the model produces accurate results and is computationally efficient [242, 147, 257, 149, 153, 86].

Soil nonlinearity plays an important role in soil-structure interaction and must be taken into account in problems on beams on foundations. The discrete spring models can take into account the soil nonlinearity by expressing the parameters k_s and t_s as nonlinear functions of beam displacements [122, 117]. Studies on beams on nonlinear foundations have been performed using the discrete nonlinear spring approach [201, 157]. However, these studies do not take into account the stress-strain nonlinearity of soil, which can only be taken into account in a soil continuum-based analysis using a nonlinear elastic or elasto-plastic soil constitutive model. For that purpose, the two- or three-dimensional numerical methods have been used requiring significant computational resources and specialized expertise [192]. Haldar and Basu (2016) [102] introduced the stress-strain nonlinearity of soil in the improved simplified continuum model of Vlasov and Leont'ev (1966) [247] and obtained the nonlinear response of beams under static loads. However, such semi-analytical approach has not been applied to dynamic problems.

This chapter presents a newly developed nonlinear dynamic beam-foundation (or beam-soil) interaction model by introducing the stress-strain nonlinearity of soil in the analysis. An elastic Euler-Bernoulli beam resting on a nonlinear layered continuum (soil) subjected to dynamic loads is analyzed in which the shear modulus and damping ratio of soil are assumed to be functions of soil strains. The vertical soil displacement beneath the beam is assumed to be a product of separable variables and the extended Hamilton's principle of least action is applied to obtain the differential equations governing the motions of the beam and soil. The one-dimensional FE method is used to solve these differential equations following an iterative algorithm. The implicit Wilson-θ time integration scheme is used to obtain the time history of beam and soil responses. The accuracy and computational efficiency of the present analysis are established by comparing the results obtained from the present analysis with those obtained from equivalent two-dimensional (2D) nonlinear elastic FE analysis performed using the software Plaxis 2D in which the same nonlinear

constitutive relationship of soil is used. The results show that the present analysis can generate accurate beam response and is at least 50% faster than equivalent 2D FE analysis.

5.3 Characterization of Soil Nonlinearity

Experimental investigations have shown that soils exhibit nonlinear stress-strain response in which a decrease in soil stiffness occurs with an increase in soil strain beyond very small strains of about 10^{-6} [31]. It is also observed in dynamic soil tests that the damping ratio increases with an increase in the soil strain [248]. In dynamic analysis of soil-structure interaction problems, the soil stiffness is often expressed in terms of secant shear modulus that reduces with an increase in strain [154]. Such modulus reduction/degradation curves have been developed by several researchers for different types of soils [79, 105, 91, 69, 244], which are commonly expressed in terms of the ratio G_s/G_{s0} (G_s = secant shear modulus of soil and G_{s0} = initial shear modulus of soil at small strains) that changes with the engineering shear strain γ of soil following a hyperbolic relationship. The widely used modulus reduction relationship proposed by Hardin and Drnevich (1972) [105] is used in this study, and is given by

$$\frac{G_s}{G_{s0}} = 1/\left[1 + |\frac{\gamma}{\gamma_{ref}}|\right] \tag{5.1}$$

where γ_{ref} is a reference shear strain in soil corresponding to the failure stress τ_{max} ($\gamma_{ref} = \tau_{max}/G_{s0}$). For the purpose of practical calculations, Ishibashi and Zhang (1993) [113] defined γ_{ref} as the shear strain at which the shear modulus G_s is reduced to 70% of its initial value, and Dobry et al. (1982) [77] proposed γ_{ref} to be taken as 10^{-4} for sands and 10^{-3} for clays. For the present two-dimensional problem in $x-z$ coordinate system, it is meaningful to use γ as the octahedral engineering shear strain of soil given by

$$\gamma_{oct} = \frac{2}{3}\left[\varepsilon_{xx}^2 + (\varepsilon_{xx} - \varepsilon_{zz})^2 + \varepsilon_{zz}^2 + 6\varepsilon_{xz}^2\right]^{\frac{1}{2}} \tag{5.2}$$

Note that the other elastic constant (e.g., Poisson's ratio) is assumed to remain constant with soil strain although this assumption is strictly not necessary for the development of the analysis.

Two fundamentally different damping phenomena are associated with dynamic soil behavior, namely, radiation damping and material damping. Radiation damping is caused

by waves traveling away from the region of interest, which is implicitly incorporated into the present analysis by introducing a displacement decay function $\phi(z)$ (z is the depth below the ground surface), as described later. Material damping is caused by internal energy dissipation that arises from a complex molecular interaction within the material. The internal energy dissipation in soil is characterized by a hysteretic mode, which is largely dependent on the shear strain level [105].

The material damping can be taken into account in the analysis by multiple procedures. One way to account for the strain-compatible damping is by adapting the principle of Rayleigh damping [186]. According to Rayleigh, the damping matrix [C] is in part composed of the mass matrix [M] and in part of the stiffness matrix [K], and the contributions of the mass and stiffness matrices are governed by the Rayleigh coefficients α_1 and α_2 as

$$[C] = \alpha_1[M] + \alpha_2[K] \tag{5.3}$$

where α_1 and α_2 are scalars with units of 1/sec and sec, respectively [62]. These coefficients are given as inputs in the analysis.

5.4 Analytical Framework

5.4.1 Problem Statement

The geometry of the Euler-Bernoulli beam considered in this study is described by its length L, width b, and depth (thickness) d. Further, the beam is characterized by its Young's modulus E_b and mass density ρ_b. The beam rests on a layered continuum (Figure 1) with no slip or separation, and acted upon by a dynamic vertical load $P(x, t)$ (t = time and x = horizontal space coordinate). The force may move from left to right at a constant or variable velocity V and may vibrate while moving or may vibrate being stationary at a given location.

The soil continuum consists of n horizontal layers such that the n^{th} layer seats on a rigid bed rock. The thickness of the i^{th} soil layer is T_i (= H_i - H_{i-1}) such that the depth to the top and bottom of the layer is H_{i-1} and H_i, respectively (H_0 = 0 m). The total thickness of all the n layers is H_{Total} (= $\sum_{i=1}^{n} T_i$).Within the i^{th} layer, the soil properties Young's modulus E_{si}, Poisson's ratio υ_{si}, and mass density ρ_{si} are assumed to be spatially varying, i.e., $E_{si} = E_{si}(x, z)$, $\upsilon_{si} = \upsilon_{si}$ (x, z) and $\rho_{si} = \rho_{si}$ (x, z).

The coordinate axes are pinned at the left end of the beam with the x axis pointing to the right and the z axis pointing downward (Figure 5.1). As the soil is treated as a continuum, displacements in soil may spread beyond the two ends of the beam. Therefore, the analysis domain requires to be extended beyond the beam ends. The horizontal extent (in the x direction) of the soil is taken as βL (where $\beta \geq 1$) on both sides of the beam and the value of β is determined by trial and error. This extra soil domain is required if the beam ends are not completely restrained against deflection and rotation. The plane-strain condition (in $x - z$ plane) with a soil strip of width b is considered in the analysis, as is commonly done [247, 242].

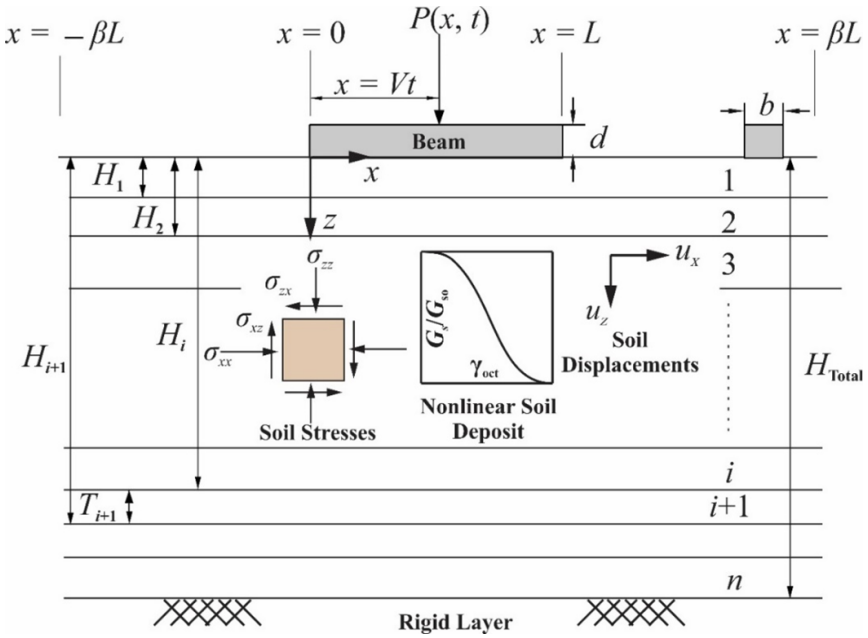

Figure 5.1: Beam resting on multi-layered nonlinear viscoelastic soil

5.4.2 Soil Strain Energy

The horizontal soil displacement u_x is assumed negligible (i.e., $u_x = 0$) and the soil displacement u_z in the vertical direction (Figure 5.1) is expressed as

$$u_z = w(x,t)\phi(z) \tag{5.4}$$

where $w(x,\ t)$ is the beam deflection for $0 \leq x \leq \mathrm{L}$ and the vertical displacement of the free surface for $\beta\mathrm{L} \leq x < 0$ and $0 < x \leq \beta\mathrm{L}$, and $\phi(z)$ is a displacement decay function. To ensure perfect beam-soil contact $\phi(0)$ is assumed to be one, and to ensure soil displacement becomes zero at the rigid rock boundary $\phi(H_{total})$ is assumed to be zero.

The soil strain tensor is given by

$$\varepsilon_{ij} = \begin{Bmatrix} \varepsilon_{xx} \\ \varepsilon_{zz} \\ \varepsilon_{xz} \end{Bmatrix} = \begin{Bmatrix} 0 \\ -w\frac{d\phi}{dz} \\ -\frac{1}{2}\frac{\partial w}{\partial x}\phi \end{Bmatrix} \tag{5.5}$$

which is related to the stress tensor as (Figure 4.1)

$$\sigma_{ij} = \begin{Bmatrix} \sigma_{xx} \\ \sigma_{zz} \\ \sigma_{xz} \end{Bmatrix} = \frac{E_s}{(1+\upsilon_{si})(1-2\upsilon_{si})} \begin{bmatrix} 1-\upsilon_s & \upsilon_s & 0 \\ \upsilon_s & 1-\upsilon_s & 0 \\ 0 & 0 & 0.5-\upsilon_s \end{bmatrix} \begin{Bmatrix} 0 \\ -w(x,t)\frac{d\phi(z)}{dz} \\ -\frac{1}{2}\frac{\partial w(x,t)}{\partial x}\phi(z) \end{Bmatrix} \tag{5.6}$$

As the soil follows nonlinear elasticity, E_s in Equation 5.6 is the secant Young's modulus.

The strain energy density of soil U_{D-soil} $(= \sigma_{ij}\varepsilon_{ij}/2)$ is obtained from Equations 5.4, 5.5, and 5.6 and expressed in terms of soil constrained modulus $\bar{E_{si}}$ (x,z) and shear modulus G_{si} (x,z) as

$$U_{D-soil} = \frac{1}{2}\left[\bar{E_{si}} w^2 \left(\frac{d\phi_i}{dz}\right)^2 + G_{si}\phi_i^2 \left(\frac{\partial w}{\partial x}\right)^2\right] \tag{5.7}$$

where

$$\bar{E_{si}} = \frac{E_{si}(1-\upsilon_{si})}{(1+\upsilon_{si})(1-2\upsilon_{si})} \tag{5.8a}$$

$$G_{si} = \frac{E_{si}}{2(1+\upsilon_{si})} \tag{5.8b}$$

5.4.3 Extended Hamilton's Principle

The governing differential equations for the beam-foundation system are obtained using the extended Hamilton's principle of least actions [40], given by

$$\delta \int_{t_1}^{t_2} (-U + T + W_{nc}) dt = 0 \tag{5.9}$$

where U and T are the potential and kinetic energies of the system, W_{nc} is the work done by the non-conservative forces, t_1 and t_2 are arbitrary times at which the equilibrium configuration of the system is known, and δ is the variational operator.

The potential energy U is given by

$$\begin{aligned} U &= \int_{V_{beam}} U_{D-beam} dV_{beam} + \int_{v_{soil}} U_{D-soil} dV_{soil} \\ &= \int_0^L \frac{E_b I_b}{2} \left(\frac{\partial^2 w}{\partial x^2} \right)^2 dx + \sum_{i=1}^{n} \frac{b}{2} \int_{-\beta L}^{\beta L} \int_{H_{i-1}}^{H_i} \left[\bar{E_{si}} w^2 \left(\frac{d\phi_i}{dz} \right)^2 + G_{si} \phi_i^2 \left(\frac{\partial w}{\partial x} \right)^2 \right] dz dx \end{aligned} \tag{5.10a}$$

where V_{beam} and V_{soil} are respectively the volumes (domains) of the beam and soil participating in the vibration, U_{D-beam} is the beam strain energy density; I_b $(= bd^3/12)$ is the second moment of inertia of the beam section, and ϕ_i is $\phi(z)$ in the i^{th} layer.

The kinetic energy T is given by

$$T = \int_0^L \frac{\rho_b A_b}{2} \left(\frac{\partial w}{\partial t} \right)^2 dx + \sum_{i=1}^{n} \int_{-\beta L}^{\beta L} \int_{H_{i-1}}^{H_i} \left[\frac{b}{2} \rho_{si} \left(\frac{\partial w}{\partial t} \right)^2 \phi_i^2 \right] dz dx \tag{5.10b}$$

where A_b $(= bd)$ is the cross-section area of beam.

The nonconservative force consists of applied and damping forces

$$W_{nc} = - \int_0^L P(t) \delta_d (x_0 - Vt) w dx - \frac{1}{2} c \left(\frac{\partial w}{\partial t} \right)^2 \tag{5.10c}$$

where δ_d is the Dirac delta function, c is the damping coefficient of the system, and x_0 is the initial (or stationary) position of the applied force.

Substituting Equation 5.10(a,c) in Equation 5.9 results in

$$\begin{aligned}\delta \int_{t_1}^{t_2} \Bigg[\int_0^L \frac{\rho_b A_b}{2} \left(\frac{\partial w}{\partial t}\right)^2 dx + \sum_{i=1}^{n} \int_{-\beta L}^{\beta L} \int_{H_{i-1}}^{H_i} \left[\frac{\rho_{si} b}{2} \left(\frac{\partial w}{\partial t}\right)^2 \phi_i^2\right] dz dx \Bigg] dt - \\ \delta \int_{t_1}^{t_2} \Bigg[\int_0^L \frac{E_b I_b}{2} \left(\frac{\partial^2 w}{\partial x^2}\right)^2 dx + \sum_{i=1}^{n} \frac{1}{2} \int_{-\beta L}^{\beta L} \int_{H_{i-1}}^{H_i} \Bigg[\bar{E_{si}} w^2 \left(\frac{d\phi_i}{dz}\right)^2 + \\ 2G_{si}\phi_i^2 \left(\frac{\partial w}{\partial x}\right)^2 \Bigg] dz dx - \int_0^L P \delta_d(x_0 - Vt) w dx dt \Bigg] \\ + \delta \int_{t_1}^{t_2} \left[-\frac{1}{2} c \left(\frac{\partial w}{\partial t}\right)^2 \right] dt\end{aligned} \tag{5.11}$$

The differential equations of $w(x,\ t)$ and $\phi(z)$ (Euler-Lagrange equations), and their associated boundary conditions are obtained next. The assumption of soil heterogeneity within each layer makes $\bar{E_{si}}$ and G_{si} spatially variable, which is necessary for capturing the soil nonlinearity in the analytical framework because strains in soil degrade (reduce) the soil modulus differently at different points and makes the soil heterogeneous (even for an inherently homogeneous soil).

5.4.4 Differential Equations of w

For the domain $0 \leq x \leq$ L, the differential equation governing beam deflection is obtained as

$$\begin{aligned}E_b I_b \frac{\partial^4 w}{\partial x^4} - 2t_s \frac{\partial^2 w}{\partial x^2} - 2\frac{\partial t_s}{\partial x}\frac{\partial w}{\partial x} + k_s w + c\frac{\partial w}{\partial t} + (\eta_s + \rho_b A_b)\frac{\partial^2 w}{\partial t^2} \\ = P(t)\delta_d(x_0 - Vt) \quad (0 \leq x \leq L\end{aligned} \tag{5.12a}$$

For the domains -$\beta L \leq x \leq 0$ and $L \leq x \leq \beta L$, the differential equation governing the soil surface displacement is obtained as

$$-2t_s\frac{\partial^2 w}{\partial x^2} - 2\frac{\partial t_s}{\partial x}\frac{\partial w}{\partial x} + k_s w + c\frac{\partial w}{\partial t} + \eta_s\frac{\partial^2 w}{\partial t^2} = 0 \quad (-\beta L \leq x \leq 0)\ \&\ (L \leq x \leq \beta L) \tag{5.12b}$$

The initial conditions for Equation 5.12(a,b) are $w = 0$ and $\partial w/\partial t = 0$ at $t = 0$. The boundary conditions for Equation 5.12(a,b) for free beams are

$$w\ |_{x=-\beta L} = w\ |_{x=\beta L} = 0 \tag{5.13a}$$

$$w_{Right}\ |_{x=0} = w_{Left}\ |_{x=0} \tag{5.13b}$$

$$w_{Left}\ |_{x=L} = w_{Right}\ |_{x=L} \tag{5.13c}$$

$$\left[-2t_s\tfrac{\partial w}{\partial x}\right]_{Left}\ |_{x=0} = \left[E_b I_b\tfrac{\partial^3 w}{\partial x^3} - 2t_s\tfrac{\partial w}{\partial x}\right]_{Right}\ |_{x=0} \tag{5.13d}$$

$$\left[E_b I_b\tfrac{\partial^3 w}{\partial x^3} - 2t_s\tfrac{\partial w}{\partial x}\right]_{Left}\ |_{x=L} = \left[-2t_s\tfrac{\partial w}{\partial x}\right]_{Right}\ |_{x=L} \tag{5.13e}$$

$$E_b I_b\frac{\partial^2 w}{\partial x^2}\ |_{x=0\ \&\ x=L} = 0 \tag{5.13f}$$

For simply-supported beams or fixed beams, Equation 5.12(b) is not required to be solved, and the boundary conditions for Equation 5.12(a) are

$$w\ |_{x=0\ \&\ x=L} = 0 \text{ (for fixed end)} \tag{5.13g}$$

$$\frac{\partial w}{\partial x}\ |_{x=0\ \&\ x=L} = 0 \text{ (for fixed end)} \tag{5.13h}$$

$$E_b I_b\frac{\partial^2 w}{\partial x^2}\ |_{x=0\ \&\ x=L} = 0 \text{ (for hinged end with no applied moment)} \tag{5.13i}$$

$$\left[E_b I_b\tfrac{\partial^3 w}{\partial x^3} - 2t_s\tfrac{\partial w}{\partial x}\right]\ |_{x=0\ \&\ x=L} = 0 \text{ (for hinged end with no applied force)} \tag{5.13j}$$

Note that, for vertical sections where the beam is present (i.e., for $0 \leq x \leq L$), the total shear force is the summation of beam shear force $E_b I_b(d^3w/dx^3)$ and soil shear force -$2t_s(dw/dx)$, and, where no beam is present, the total shear force at a vertical section is only the soil shear force -$2t_s(dw/dx)$. The parameters in the above equations are given by

$$\eta_s = b \sum_{i=1}^{n} \rho_{si} \int_{H_{i-1}}^{H_i} \phi_i^2 dz \tag{5.14a}$$

$$k_s = b \sum_{i=1}^{n} \int_{H_{i-1}}^{H_i} \bar{E}_{si}(x,z) \left(\frac{d\phi_i(z)}{dt} \right)^2 dz \tag{5.14b}$$

$$t_s = \frac{b}{2} \sum_{i=1}^{n} \int_{H_{i-1}}^{H_i} G_{si}(x,z) \phi_i^2(z) dz \tag{5.14c}$$

The parameter η_s represents the mass of continuum (soil) per unit length in the horizontal direction participating in the vibration (soil mass parameter), k_s is similar to the soil spring constant (soil compression parameter), and t_s is the shear resistance parameter of soil. The parameters k_s and t_s vary spatially in the x direction, and depend on the properties of both the continuum and beam. In Equation 5.14(a) the mass density of soil ρ_{si} is considered spatially constant within any layer (which is a reasonable assumption as density of soil does not vary much spatially). Therefore, the parameter η_s, when determined following Equation 5.14(a), is spatially constant. Note that ρ_{si} was assumed to be spatially varying at the beginning of the analysis (which makes η_s spatially varying as well), and such spatial variations can be taken into account in the analysis should a need arises.

5.4.5 Differential Equation of ϕ

The Euler-Lagrange equation of ϕ(z) for the i^{th} layer is obtained as

$$m_{si} \frac{d^2\phi_i}{dz^2} + \frac{dm_{si}}{dz} \frac{d\phi_i}{dz} + (\zeta_{si} - n_{si})\phi_i = 0 \tag{5.15}$$

with boundary conditions $\phi = 1$ at z = 0, $\phi_i = \phi_{i+1}$ at $z = H_i$ and $\phi = 0$ at $z = H_{Total}$. The parameters in Equation 5.15 are given by

$$m_{si}(z) = b \int_{-\beta L}^{\beta L} \bar{E}_{si}(x,z) w^2 dx \tag{5.16a}$$

$$n_{si}(z) = b \int_{-\beta L}^{\beta L} G_{si}(x,z) \left(\frac{\partial w}{\partial x}\right)^2 dx \tag{5.16b}$$

$$\zeta_{si} = b\rho_{si} \int_{-\beta L}^{\beta L} \left(\frac{\partial w}{\partial t}\right)^2 dx \tag{5.16c}$$

The parameters m_{si} and n_{si} vary spatially in the z direction (i.e., $m_{si} = m_{si}(z)$, $n_{si} = n_{si}(z)$) because of the heterogeneity of soil properties. However, in the case of multi-layered soil deposit with spatially constant $\bar{E}_{si}$ and G_{si} within each layer, m_{si} and n_{si} become constants.

5.4.6 Solution of Differential Equations

Because of the time-dependent nature of the problem and the spatial variation of $\bar{E}_{si}$ and G_{si} within each soil layer, the differential equations of w and ϕ cannot be solved analytically. Instead, the one-dimensional (1D) FE method is used to obtain the solutions of the differential Equations 5.12(a,b) and 5.15.

In order to obtain solutions using the FE method, the problem domain is discretized into horizontal and vertical strips of thickness Δz and Δx, respectively (Figure 5.2). A total of N equally spaced nodes in the z-direction (denoted generically by g) are used to discretize the soil domain into N–1 horizontal strips, such that HTotal = $(N–1)\Delta z$. A total of M_3 equally spaced nodes in the x-direction (denoted generically by f) are used to discretize the soil domain into M_3 –1 vertical strips, such that $(1 + 2\beta)L = (M_3 – 1)\Delta x$. Thus, the entire soil domain is divided into a grid of $(M_3 – 1)$ $(N–1)$ rectangular cells, each with dimensions $\Delta z \times \Delta x$. The discretization step Δz was so chosen such that each horizontal strip lies within a particular soil layer and does not overlap adjacent soil layers. The x-coordinate of the centerline of any vertical strip v is x_v, whereas the z-coordinate of the centerline of any horizontal strip h is z_h. The v^{th} vertical strip and the h^{th} horizontal strip intersect to form the cell (v, h), with the coordinates of its centroid given by (x_v, z_h). Two-noded beam and bar elements of length Δx are respectively used to discretize

Equation 5.12(a,b) in the x direction such that these elements seat on top of the vertical strips with the nodes placed on top of the vertical interfaces of the adjacent strips (i.e., v^{th} element with nodes f and $f+1$ seats exactly on top of the v^{th} vertical strip). Similarly, two-noded bar elements of length Δz are used to discretize Equation 5.15 such that the elements fit in between the horizontal strips with the nodes lying on the interfaces of the adjacent horizontal strips (i.e., h^{th} element with nodes g and $g+1$ exactly fits the h^{th} horizontal strip).

Cubic Hermitian shape functions $\{N_H\}_{4\times1}$ are used to discretize the domain for Equation 5.12(a) and linear Lagrangian shape functions $\{N_L\}_{2\times1}$ are used to discretize the domain for Equation 5.12(b). For the Hermitian beam elements of Equation 5.12(a), the elemental mass, damping, and stiffness matrices, and force vectors are respectively given by

$$[m]^v_{4\times4} = \int_{x_f}^{x_{f+1}} \left[\{N_H\}^T(\rho_b A_b + \eta_s)\{N_H\}\right] dx$$

$$= (\rho_b A_b + \eta_s) \begin{bmatrix} \frac{13l_v}{35} & \frac{11l_v^2}{210} & \frac{9l_v}{70} & -\frac{13l_v^2}{420} \\ \frac{11l_v^2}{210} & \frac{l_v^3}{105} & \frac{13l_v^2}{420} & -\frac{l_v^3}{140} \\ \frac{9l_v}{70} & \frac{13l_v^2}{420} & \frac{13l_v}{35} & -\frac{11l_v^2}{210} \\ -\frac{13l_v^2}{420} & -\frac{l_v^3}{140} & -\frac{11l_v^2}{210} & \frac{l_v^3}{105} \end{bmatrix} \tag{5.17a}$$

$$[c]^e_{4\times4} = \int_{x_i}^{x_j} \Big[\{N_H\}^T c \{N_H\} \Big] dx$$

$$= (\rho_b A_b + \eta_s) \begin{bmatrix} \frac{13l_v}{35} & \frac{11l_v^2}{210} & \frac{9l_v}{70} & \frac{13l_v^2}{420} \\ \frac{11l_v^2}{210} & \frac{l_v^3}{105} & \frac{13l_v^2}{420} & -\frac{l_v^3}{140} \\ \frac{9l_v}{70} & \frac{13l_v^2}{420} & \frac{13l_v}{35} & -\frac{11l_v^2}{210} \\ -\frac{13l_v^2}{420} & -\frac{l_v^3}{140} & -\frac{11l_v^2}{210} & \frac{l_v^3}{105} \end{bmatrix} \tag{5.17b}$$

$$[c]^e_{4\times4} = \int_{x_f}^{x_{f+1}} \Bigg[\left(\frac{d^2\{N_H\}}{dx^2}\right)^T E_b I_b \left(\frac{d^2\{N_H\}}{dx^2}\right) + \{N_H\}^T k_s \{N_H\}$$

$$+ \left(\frac{d\{N_H\}}{dx}\right)^T 2t_s \left(\frac{d\{N_H\}}{dx}\right) \Bigg] dx = E_b I_b \begin{bmatrix} \frac{12}{l_v^3} & \frac{6}{l_v^2} & \frac{-12}{l_v^3} & \frac{6}{l_v^2} \\ \frac{6}{l_v^2} & \frac{4}{l_v} & \frac{-6}{l_v^2} & \frac{2}{l_v} \\ \frac{-12}{l_v^3} & \frac{-6}{l_v^2} & \frac{12}{l_v^3} & \frac{-6}{l_v^2} \\ \frac{6}{l_v^2} & \frac{2}{l_v} & \frac{-6}{l_v^2} & \frac{4}{l_v} \end{bmatrix}$$

$$+ k_s \begin{bmatrix} \frac{13l_v}{35} & \frac{11l_v^2}{210} & \frac{9l_v}{70} & -\frac{13l_v^2}{420} \\ \frac{11l_v^2}{210} & \frac{l_v^3}{105} & \frac{13l_v^2}{420} & -\frac{l_v^3}{140} \\ \frac{9l_v}{70} & \frac{13l_v^2}{420} & \frac{13l_v}{35} & -\frac{11l_v^2}{210} \\ -\frac{13l_v^2}{420} & -\frac{l_v^3}{140} & -\frac{11l_v^2}{210} & \frac{l_v^3}{105} \end{bmatrix} \tag{5.17c}$$

$$+ 2t_s \begin{bmatrix} \frac{6}{5l_v} & \frac{1}{10} & \frac{-6}{5l_v} & \frac{1}{10} \\ \frac{1}{10} & \frac{2l_v}{15} & \frac{-1}{10} & \frac{-l_v}{30} \\ \frac{-6}{5l_v} & \frac{-1}{10} & \frac{6}{5l_v} & \frac{-1}{10} \\ \frac{1}{10} & \frac{-l_v}{30} & \frac{-1}{10} & \frac{2l_v}{15} \end{bmatrix}$$

$$\{f\}^v_{4\times1} = \int_{x_f}^{x_{f+1}} N_H^T P \delta_d(x_0 - Vt)dx \tag{5.18a}$$

where x_f and x_{f+1} are the coordinates of the left and right nodes of the vth element, respectively, with element length $l_v = x_{f+1}$ - $x_f = \Delta x$ (Figure 5.2). In the case of moving load of magnitude $\bar{P}$, the elemental force vector is given by

$$\{f\}^v_{4\times1} = \bar{P}\begin{bmatrix}1 & 0 & 0 & 0\end{bmatrix}^T \; or \; \bar{P}\begin{bmatrix}0 & 0 & 1 & 0\end{bmatrix}^T \tag{5.18b}$$

for the load acting on the left or the right node of the element v, respectively, or by

$$\{f\}^v_{4\times1} = \bar{P}\left(\frac{\hat{x}(l_v-\hat{x})}{l_v}\right)\begin{bmatrix}\frac{\hat{x}(3l_v-\hat{x})}{l_v(l_v-\hat{x})} & -\hat{x} & \frac{(l_v-2\hat{x})(l_v-\hat{x})}{l_v} & -(l_v-\hat{x})\end{bmatrix}^T \tag{5.18c}$$

if the moving load lies within the element at a distance of $\hat{x}$ from the right node. For vibrating loads of magnitude P_t at any time t, the elemental force vector is given by

$$\{f\}^v_{4\times1} = P_t\left(\frac{\hat{x}(l_v-\hat{x})}{l_v}\right)\begin{bmatrix}\frac{\hat{x}(3l_v-\hat{x})}{l_v(l_v-\hat{x})} & -\hat{x} & \frac{(l_v-2\hat{x})(l_v-\hat{x})}{l_v} & -(l_v-\hat{x})\end{bmatrix}^T \tag{5.18d}$$

For the Lagrangian bar elements of Equation 5.12(b), the stiffness, mass, and damping matrices are respectively given by

$$\begin{aligned}[K]^v_{2\times2} &= \int_{x_f}^{x_{f+1}} \left[N_L^T k_s N_L + \left(\frac{dN_L}{dx}\right)^T 2t_s\left(\frac{dN_L}{dx}\right)\right]dx \\ &= \frac{k_s l_v}{6}\begin{bmatrix}2 & 1\\ 1 & 2\end{bmatrix} + \frac{2t_s}{l_v}\begin{bmatrix}1 & -1\\ -1 & 1\end{bmatrix}\end{aligned} \tag{5.19a}$$

$$[M]^v_{2\times2} = \int_{x_f}^{x_{f+1}} \left[N_L^T \eta_s N_L\right]dx = \frac{\eta_s l_v}{6}\begin{bmatrix}2 & 1\\ 1 & 2\end{bmatrix} \tag{5.19b}$$

$$[C]^v_{2\times2} = \int_{x_f}^{x_{f+1}} \left[N_L^T c N_L\right]dx = \frac{c l_v}{6}\begin{bmatrix}2 & 1\\ 1 & 2\end{bmatrix} \tag{5.19c}$$

It should be noted that, in this analysis, [C] is determined using Rayleigh damping coefficients, as described earlier. Therefore, in the analysis, Equations 5.17(b) and 5.19(c) are not used; instead the following equations are respectively used as the damping matrices of the beam and bar elements

$$
\begin{aligned}
[C]^{v}_{4\times4} = \alpha_1(\rho_b A_b + \eta_s)
&\begin{bmatrix}
\frac{13l_v}{35} & \frac{11l_v^2}{210} & \frac{9l_v}{70} & -\frac{13l_v^2}{420} \\
\frac{11l_v^2}{210} & \frac{l_v^3}{105} & \frac{13l_v^2}{420} & -\frac{l_v^3}{140} \\
\frac{9l_v}{70} & \frac{13l_v^2}{420} & \frac{13l_v}{35} & -\frac{11l_v^2}{210} \\
-\frac{13l_v^2}{420} & -\frac{l_v^3}{140} & -\frac{11l_v^2}{210} & \frac{l_v^3}{105}
\end{bmatrix} \\
+\alpha_2 E_b I_b
&\begin{bmatrix}
\frac{12}{l_v^3} & \frac{6}{l_v^2} & \frac{-12}{l_v^3} & \frac{6}{l_v^2} \\
\frac{6}{l_v^2} & \frac{4}{l_v} & \frac{-6}{l_v^2} & \frac{2}{l_v} \\
\frac{-12}{l_v^3} & \frac{-6}{l_v^2} & \frac{12}{l_v^3} & \frac{-6}{l_v^2} \\
\frac{6}{l_v^2} & \frac{2}{l_v} & \frac{-6}{l_v^2} & \frac{4}{l_v}
\end{bmatrix}
+ \alpha_2 k_s
\begin{bmatrix}
\frac{13l_v}{35} & \frac{11l_v^2}{210} & \frac{9l_v}{70} & -\frac{13l_v^2}{420} \\
\frac{11l_v^2}{210} & \frac{l_v^3}{105} & \frac{13l_v^2}{420} & -\frac{l_v^3}{140} \\
\frac{9l_v}{70} & \frac{13l_v^2}{420} & \frac{13l_v}{35} & -\frac{11l_v^2}{210} \\
-\frac{13l_v^2}{420} & -\frac{l_v^3}{140} & -\frac{11l_v^2}{210} & \frac{l_v^3}{105}
\end{bmatrix} \\
&+2\alpha_2 t_s
\begin{bmatrix}
\frac{6}{5l_v} & \frac{1}{10} & \frac{-6}{5l_v} & \frac{1}{10} \\
\frac{1}{10} & \frac{2l_v}{15} & \frac{-1}{10} & \frac{-l_v}{30} \\
\frac{-6}{5l_v} & \frac{-1}{10} & \frac{6}{5l_v} & \frac{-1}{10} \\
\frac{1}{10} & \frac{-l_v}{30} & \frac{-1}{10} & \frac{2l_v}{15}
\end{bmatrix}
\end{aligned}
\tag{5.20a}
$$

$$[C]^v_{2\times 2} = \alpha_1 \frac{\eta_s l_v}{6}\begin{bmatrix}2 & 1\\ 1 & 2\end{bmatrix} + \alpha_2 \frac{k_s l_v}{6}\begin{bmatrix}2 & 1\\ 1 & 2\end{bmatrix} + \alpha_2 \frac{2t_s}{l_v}\begin{bmatrix}1 & -1\\ -1 & 1\end{bmatrix} \tag{5.20b}$$

Linear Lagrangian shape functions $\{N_L\}_{2\times 1}$ are used to discretize the domain of Equation 5.15. The resulting set of algebraic equations is of the form $\sum_h [K_\phi]^h\{\phi\} = 0$ (Figure 5.2) where $[K_\phi]^h$ is the elemental stiffness matrix (for the h^{th} element), ϕ contains the unknown nodal values of $\phi(z)$, and $\sum_h$ represents assembly. The elemental stiffness matrix $[K_\phi]^h$ is given by

$$\begin{aligned}\{k\}^h_{2\times 2} &= \int_{z_g}^{z_{g+1}} \left[N_L^T(\zeta_{si} - n_{si})N_L + \left(\frac{dN_L}{dz}\right)^T m_{si}\left(\frac{dN_L}{dz}\right)\right] dz \\ &= (\zeta_{si} - n_{si})\frac{l_h}{3}\begin{bmatrix}1 & 1/2\\ 1/2 & 1\end{bmatrix} + \frac{m_{si}}{l_h}\begin{bmatrix}1 & -1\\ -1 & 1\end{bmatrix}\end{aligned} \tag{5.21}$$

where $l_h = z_{g+1}$ - $z_g = \Delta$z (Figure 5.2) with z_g and z_{g+1} being the coordinates of the top and bottom node of the h^{th} element in z direction, respectively.

5.4.7 Algorithm

Equation 5.12(a,b) of w and Equation 5.15 of ϕ are coupled, and are solved simultaneously following an iterative scheme. The unconditionally stable Wilson-θ method is used as the time integration method [28], and equations of w and ϕ are solved at each time step Δt within the time integration scheme. Further, the load $P(x, t)$ is applied incrementally (i.e., in increasing increments of ΔP such that the first load step $P^{(1)} = 2\Delta$P, the second load step $P^{(2)} = 2\Delta$P and so on until the total load P is applied in p steps such that $P^{(p)} =$ pΔP = P) within each time step Δt to capture the nonlinearity in the beam-soil system. It is also assumed that, as an initial trial, ϕ(z) vary linearly at the beginning of the algorithm (i.e., at $t = 0$) but satisfy the boundary conditions $\phi(0) = 1$ and $\phi(H_{Total}) = 0$.

For a given applied load increment within a time step, the displacement function ϕ(z) is used to calculate the parameters k_s, t_s, and η_s (Equations 5.14(a,c)) which are then used to solve for w. The functions $w(x)$ and ϕ(z) are used to compute the strain components ε_{ij} at the discretized nodes of the grid (Figure 5.2) using Equation 5.5. From the calculated strain components, the octahedral shear strains γ_{oct} at these nodes are calculated using

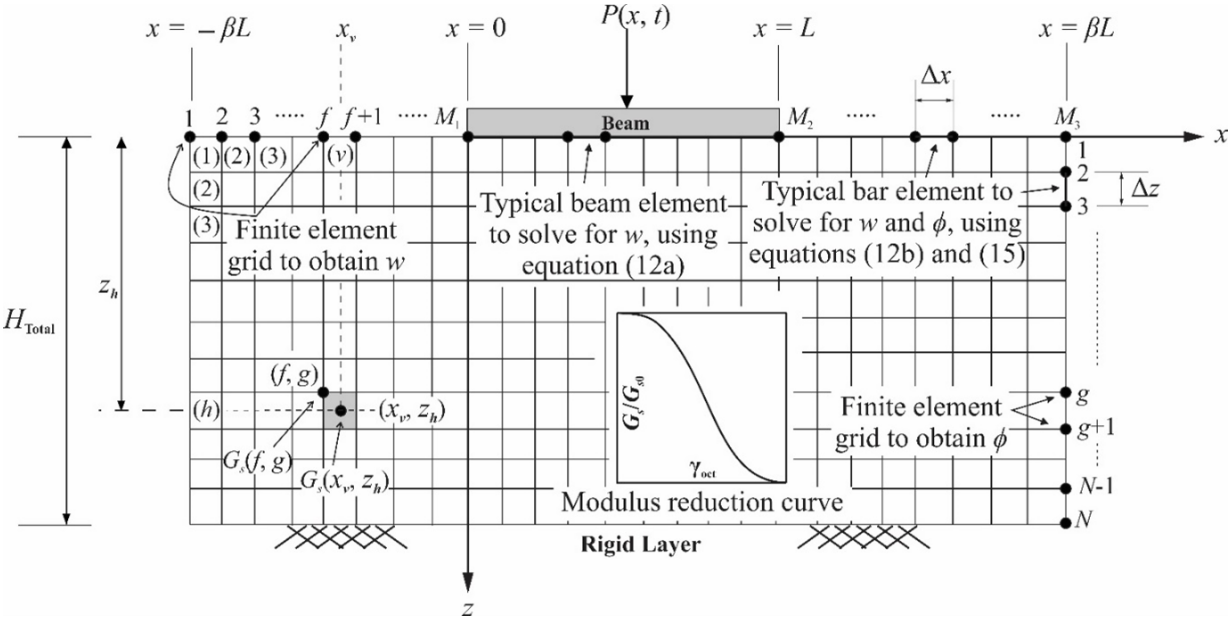

Figure 5.2: Discretization of beam-soil system

Equation 5.2. The octahedral strain values are then used to calculate the secant shear modulus $G_s(f, g)$ for any node (f, g) within the grid, using Equation 5.1. The parameters k_s, t_s, and η_s for each vertical soil strip are then recalculated by performing numerical integration following the trapezoidal rule:

$$k_s(x_v) = b\left\{\frac{1}{2}\bar{E}_s(x_v, z_1)\left(\frac{\phi_2 - \phi_1}{\Delta z}\right)^2 + \frac{1}{2}\bar{E}_s(x_v, z_{N-1})\left(\frac{\phi_N - \phi_{N-1}}{\Delta z}\right)^2 + \sum_{g=2,h=g}^{N-2}\left[\bar{E}_s(x_v, z_h)\left(\frac{\phi_{g+1} - \phi_g}{\Delta z}\right)^2\right]\right\}\Delta z \tag{5.22}$$

$$t_s(x_v) = \frac{b}{2}\left\{\frac{1}{2}\left[G_s(x_v, z_1)\phi_{(1)}^2 + G_s(x_v, z_{N-1})\phi_{(N-1)}^2\right] + \sum_{h=2}^{N-2}\left[G_s(x_v, z_h)\phi_{(h)}^2\right]\right\}\Delta z \tag{5.23}$$

$$\eta_s(x_v) = \rho_{si} b\left\{\frac{1}{2}\left[\phi_{(1)}^2 + \phi_{(N-1)}^2\right] + \sum_{h=2}^{N-2}\left[\phi_{(h)}^2\right]\right\}\Delta z \tag{5.24}$$

where ϕ_g is the value ϕ(z) at the g^{th} vertical node; and $\phi_{(h)}$ is the representative value of ϕ(z) for the h^{th} horizontal strip and is given by $\phi_{(h)} = (\phi_{g+1} + \phi_g)/2$ (Figure 5.2). Equations 5.22 and 5.24 are written for the v^{th} vertical strip with its centroidal x coordinate x_v. Thus, k_s, t_s, and η_s are obtained not as continuous functions but as discrete values for each vertical strip corresponding to each beam or bar element lying horizontally on top of the vertical strip.

The parameters k_s, t_s, and η_s are then used to calculate the displacement w, and its derivatives $\partial w/\partial x$ and $\partial w/\partial t$ (obtained directly from the Wilson-θ time integration scheme) by solving Equation 5.12(a,b). The parameters m_{si}, n_{si} and ζ_{si} are then calculated by numerical integrations following the trapezoidal rule along each horizontal strip

$$m_{si}(z_h) = b\left\{\frac{1}{2}\bar{E}_s(x_1, z_h)w^2_{(1)} + \frac{1}{2}\bar{E}_s(x_{M3-1}, z_h)w^2_{(M3-1)} + \sum_{v=2}^{M3-1}\left[\bar{E}_s(x_v, z_h)w^2_{(v)}\right]\right\}\Delta x \tag{5.25}$$

$$n_{si}(z_h) = b\left\{\frac{1}{2}G_s(x_1, z_h)\left[\frac{\partial w}{\partial x}\,|_{(1)}\right]^2 + \frac{1}{2}G_s(x_{(M3-1)}, z_h)\left[\frac{\partial w}{\partial x}\,|_{(M3-1)}\right]^2 + \sum_{v=2}^{M3-1} G_s(x_v, z_h)\left[\frac{\partial w}{\partial x}\,|_{(v)}\right]^2\right\}\Delta x \tag{5.26}$$

$$\zeta_{si}(z_h) = b\rho_{si}\left\{\frac{1}{2}\left[\frac{\partial w}{\partial t}\,|_{(1)}\right]^2 + \frac{1}{2}\left[\frac{\partial w}{\partial t}\,|_{(M3-1)}\right]^2 + \sum_{v=2}^{M3-1}\left[\frac{\partial w}{\partial t}\,|_{(v)}\right]^2\right\}\Delta x \tag{5.27}$$

where $w_{(v)}$ is the average displacement in the v^{th} element, $(\partial w/\partial x)|_{(v)}$ is the average slope in the v^{th} element, and $(\partial w/\partial t)|_{(v)}$ is the average velocity in the v^{th} element. The parameters m_{si}, n_{si} and ζ_{si} are then used to obtain a new $\phi(z)$. The newly calculated $\phi(z)$ is compared with the assumed $\phi(z)$ and, if the difference is greater than a prescribed tolerance, the calculations are repeated with the calculated ϕ as the new guess. A convergence tolerance limit of 10^{-5} is set

$$\frac{\sum_{g=1}^{N} |\ \phi_g^{Current} - \phi_g^{Previous}\ |}{\sum_{g=1}^{N} |\ \phi_g^{Previous}\ |} \leq \text{prescribed tolerance} = 10^{-5} \tag{5.28}$$

where the superscript "Current" represents ϕ_g calculated in the current iteration, and the superscript "Previous" represents ϕ_g calculated during the previous iteration. The iterations are continued until the convergence on ϕ is reached, and then w and ϕ are recorded as the final values for that load increment.

It is important to note that the secant shear modulus G_s used in the above Equations 5.22 and 5.27 is calculated first at the four corner nodes of any calculation cell (v, h), and then averaged to obtain the representative $G_s(x_v, z_h)$ at the centroid of the cell. The representative secant Young's modulus E_s is calculated from G_s using the relationship $E_s = 2G_s(1+\upsilon_s)$. In the algorithm, the Poisson's ratio υ_s is assumed to be spatially constant for each layer and independent of soil strains (although the spatial variation of υ_s and change in υ_s with soil strain can be accounted for in the analysis framework).

The iterative algorithm described above can be used for both linear and nonlinear dynamic analysis. For linear dynamic analysis, the load is applied at full magnitude $P(x, t)$ as an input for each time step Δt (with or without spatial variations of soil properties). For nonlinear dynamic analysis, however, the load is applied in increments: $P^{(1)}(t_q)$ (first load increment), $P^{(2)}(t_q)$ (second load increment),....., $P^{(p)}(t_q)$, where p is the number of load increments at (or right after) the q^{th} time step ($t_q + (\Delta t)_q = t_{q+1}$). The increments are usually selected as 5-10% of the total load magnitude (i.e., $\Delta P = (0.05\text{-}0.1)P$). For the first load increment $\Delta P^{(1)}(t_1)$ within the first time step $(\Delta t)_1$ (t_1 corresponds to the initial time $t = 0$ and $t_1 + (\Delta t)_1 = t_2$), the position x of the applied load, the geometry and material properties (including the initial shear modulus G_{s0}), the damping coefficients (α_1, α_2) and initial $\phi(z)$ are given as inputs. Using these inputs, the parameters k_s, t_s, and η_s are calculated using which w, ε_{ij} , γ_{oct} , and G_s are calculated at each point in the grid. Subsequently, the parameters k_s, t_s, and η_s are recalculated based on the new values of G_s. These calculated parameters are then used to obtain w, $\partial w/\partial x$, $\partial w/\partial t$, and $\partial^2 w/\partial t^2$. These quantities are subsequently used to calculate m_{si}, n_{si} and ζ_{si}, using which $\phi(z)$ is calculated. Before the convergence on $\phi(z)$ is checked, an additional set of iterations is done to ensure convergence on the secant modulus G_s (or E_s) at every node in the grid is achieved because these are not known a priori. This set of iterations ensures that the estimated secant modulus at each node in the grid corresponds to the induced octahedral shear strain at that node following the constitutive relationship given by Equation 5.1. After the convergence on G_s is checked and before the next load increment $\Delta P^{(2)}(t_1)$ is applied, the convergence on $\phi(z)$ is ensured. After convergence on $\phi(z)$ is reached, the calculated w, $\partial w/\partial x$, $\partial w/\partial t$, and $\partial^2 w/\partial t^2$ and the last updated ϕ are considered as the final values for the first load increment $\Delta P^{(1)}(t_1)$.

After convergence on the secant moduli and $\phi(z)$ are satisfied for load increment $\Delta P^{(1)}(t_1)$, the next load increment $\Delta P^{(2)}(t_1)$ is applied and the iterative process described

in the preceding paragraphs is repeated. Each subsequent load step is applied after convergences on the secant modulus and $\phi(z)$ are satisfied for the current load step, and this process is continued until the full load is applied, i.e., $P^{(p)}(t_1) = P(t_1)$. Subsequently, the next time increment Δt_2 is applied and the entire set of iterative calculations described so far is repeated. The calculations are continued until the final time t_{final} is reached. The algorithm is illustrated in Figure 5.3.

5.5 Results

5.5.1 Accuracy, Computational Efficiency, and Convergence

Verification of the accuracy of the present analysis is done by comparing results with two-dimensional (2-D) FE analysis performed using PLAXIS 2-D in which the same nonlinear constitutive equation is used. Damping is neglected in the verification problems. The convergence of the analysis method is also demonstrated. Further, how the analysis performs in terms of accuracy for different lengths of the beam (i.e., the scalability of the analysis) is investigated.

Figure 5.4 shows the linear and nonlinear responses of a beam with free ends on a three-layer continuum with a 50 KN step load acting at the mid-span for 1 sec. The beam and soil geometries and properties are given in the figure and in Table 5.1 (Problem 1). The input values of Young's modulus (given in Table 5.1) are the initial (small-strain) values (E_{s0}) from which the small-strain shear moduli are calculated using the input values of Poisson's ratio (see Equation 5.8(b)). Equation 5.1 is used to calculate the reduced shear moduli as functions of induced soil strains, for which $\gamma_{ref} = 0.002$ is assumed. For the linear response, the initial moduli are not reduced based on soil strains. The Poisson's ratio is kept constant at the prescribed values for both the linear and nonlinear beam responses. The plotted displacement profiles $w(x, t_{final})$ corresponding to $t = t_{final} = 1$ sec (i.e., the time corresponding to the end of applied load) match quite well showing that the present analysis produces results that are comparable with 2D FE analysis. The difference in the mid-span beam displacement is 6.7%. The CPU time taken to run the present nonlinear analysis is 61 sec using a computer with Intel CORE i7 3.6-GH$_z$ processor and 16GB DDR3 RAM while the time required to run the 2-D nonlinear FE analysis (in PLAXIS) using the same computer is 144 sec (i.e., 136% more).

Figure 5.5 shows the mid-span time history response of a beam with free ends resting on a homogeneous soil layer and acted upon by a sinusoidal force of 10 kN amplitude and

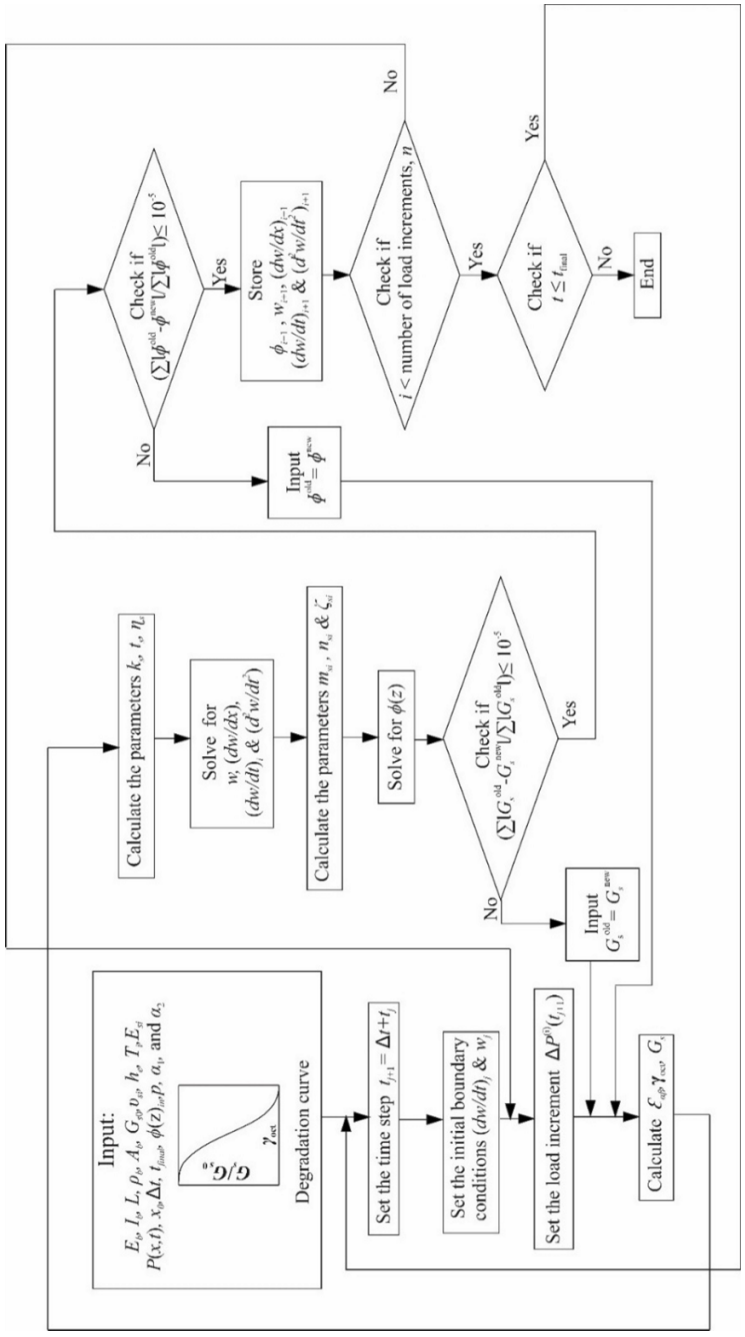

Figure 5.3: Solution algorithm

10 H_z frequency at the mid-span for 0.5 sec. The beam and soil geometries and the material properties are given in Table 5.1 (Problem 2). The time-history responses of mid-span deflection $w(L/2, t)$ obtained from both the proposed nonlinear analysis and equivalent 2-D nonlinear FE analysis match well. The corresponding linear responses are also presented to demonstrate the effect of soil nonlinearity. The maximum difference in the displacement between the present analysis and the 2-D FE analysis is 5.5%. The CPU time taken to run the present nonlinear analysis is 39 sec using the same computer while the time required to run the 2-D nonlinear FE analysis (in PLAXIS) is 83 sec (i.e., 112% more). Figure 5.6 shows the comparison of the displacement profiles of a beam of length 6 m with free ends and subjected to a moving load with velocity V = 10 m/sec (details of input are in Figure 4.6 and Table 5.1 corresponding to Problem 3). The deflections at the time when the load is at the midspan of the beam compare well with the maximum difference being 6.5%. The CPU run times required for obtaining the results (in the computer with Intel CORE i7 3.6-GH_z processor and 16GB DDR3 RAM) using the present nonlinear analysis is 33 sec and using 2-D nonlinear FE analysis is 62 sec (which is 88% more).

Figure 5.7 shows the deflection $w(x, t = 0.5)$ of a fixed beam subjected to a pair of step loads (see Figure 5.7 and Table 5.1 corresponding to Problem 4 for details). A maximum difference of 5.3% in the mid-span beam deflection is obtained. The CPU run time for the present nonlinear analysis is 28 sec (using the same computer) while the corresponding 2-D FE run time is 51 sec (82% more).

Figure 5.8 shows the deflection $w(x, t = 2.5)$ of a simply supported beam resting on a single soil layer with the initial Young's modulus E_{s0} varying spatially in the horizontal direction as $E_{s0} = 50 - 2.5x$ (where E_{s0} is in MPa and x is in meters measured from the left end of the beam), and subjected to a step load (see Figure 5.8 and Table 5.1 corresponding to Problem 5 for details). A maximum difference of 4.9% in the displacement is obtained. The CPU run time for the present nonlinear analysis is 21 sec (using the same computer) while the corresponding 2-D FE run time is 43 sec (104% more).

Figure 5.9 shows the deflection $w(x, t = 0.5)$ of a fixed beam resting on a single soil layer with the initial Young's modulus varying spatially with depth as $E_{s0} = 44 - 2.2z$ (where E_{s0} is in MPa and z is in meters measured from the ground surface), and subjected to a ramp load (see Figure 5.9 and Table 5.1 corresponding to Problem 6 for details). A maximum difference of 3.8% in the mid-span beam deflection is obtained. The CPU run time for the present nonlinear analysis is 25 sec (using the same computer) while the corresponding 2-D FE run time is 49 sec (i.e., 96% more).

In addition to the verification studies, a study is conducted to examine the scalability of the analysis with respect to 2-D FE analysis (performed using Plaxis). Three beams of

length L = 10 m, 20 m, and 50 m with free ends are considered resting on three single-layer soil deposits with thicknesses T_1 = 10 m, 20 m, and 50 m, respectively, and all the beams are subjected to a sinusoidal force with an amplitude of 25 kN and a frequency of 10 Hz acting at the mid-span for 2 sec (see Figure 5.10 and Table 5.1 corresponding to Problem 7 for details). The soil domain is extended horizontally beyond both the beam ends to a distance equal to the beam span. Figure 5.10 shows the maximum difference (obtained between the present analysis and corresponding 2-D FE analysis) in the mid-span displacement at $t = t_{final}$ = 2 sec of the three beams versus the normalized element size l_v/L. The maximum difference increases slightly with an increase in l_v/L but the difference lies within a reasonable limit (less than 10%).

A FE convergence study is conducted for the analysis to investigate how the element size and time step impact the results. The beams with L = 10 m and 20 m and with soil layer thicknesses T_1 = 10 m and 20 m, as described in Problem 7 of Table 5.1, are used for the study. The mid-span displacement at time $t = t_{final}$ = 2 sec is selected as the representative beam response for the convergence study. The total number of degrees of freedom $M_3 \times N$ (see Figure 5.2) is used to represent the element size for which the same element size is used in both x, and z directions. Figure 5.11 shows that the mid-span displacement for the 10 m long beam converged for $M_3 \times N$ = 30,401 corresponding to l_v/L = 0.01. The mid-span displacement for the 20 m long beam converged for $M_3 \times N$ = 120,801, which corresponds to l_v/L = 0.065. The effect of time step on the convergence of the mid-span displacement for both the 10 m and 20 m long beams is shown in Figure 5.12. The mid-span displacements converged at time step Δt = 0.01 sec and 0.075 sec for the 10 m and the 20 m long beams, respectively.

Clearly, the present analysis produces accurate and reliable results, and takes about 50% less time than 2D FE analysis. The comparisons described above do not include the additional time and expertise required for creating model geometry and meshing in 2D FE analysis. It is pertinent to note that the inputs of geometry and material properties for the present analysis are given in a text file (without requiring any numerical mesh generation), which makes the analysis rather user friendly.

5.5.2 Dynamic Characteristics of the Nonlinear Beam-Continuum System

The time-dependent linear and nonlinear responses of four different beams are shown in Figures 5.13- 5.16. For simulating the linear responses, the initial (small-strain) modulus is used in the calculations without any reduction with soil strain. Further, for these problems

Table 5.1: Details of the soil and beam geometries and properties corresponding to the problems analyzed

Problem Number	**Problem Type**	**Associated Figure(s)**	**Soil Properties**	**Layer 1**	**Layer 2**	**Layer 3**	**Beam Properties**	
1	Verification	4.4	E_s (MPa)	15	20	25	E_b (MPa)	2000
			υ_s	0.2	0.3	0.45	b (m)	1.0
			T_i (m)	1	2	3	d (m)	0.25
			$\gamma_{ref}^{(S)}$	0.002	0.002	0.002	L (m)	5
			a_1 (1/sec)	0	0	0		
			a_2 (1/sec)	0	0	0		
			ρ_{si} (kg/m^3)	1600	1800	1800		
2	Verification	4.5	E_s (MPa)	20			E_b (MPa)	3000
			υ_s	0.3			b (m)	1.0
			T_i (m)	2			d (m)	1.0
			$\gamma_{ref}^{(S)}$	0.002			L (m)	5
			a_1 (1/sec)	0				
			a_2 (1/sec)	0				
			ρ_{si} (kg/m^3)	1800				
3	Verification	4.6	E_s (MPa)	18			E_b (MPa)	1500
			υ_s	0.25			b (m)	1.0
			T_i (m)	6			d (m)	0.5
			$\gamma_{ref}^{(S)}$	0.0018			L (m)	6
			a_1 (1/sec)	0				
			a_2 (1/sec)	0				
			ρ_{si} (kg/m^3)	1700				
4	Verification	4.7	E_s (MPa)	20			E_b (MPa)	2000
			υ_s	0.2			b (m)	1.0
			T_i (m)	6			d (m)	0.25
			$\gamma_{ref}^{(S)}$	0.0018			L (m)	12.5
			a_1 (1/sec)	0				
			a_2 (1/sec)	0				
			ρ_{si} (kg/m^3)	1800				
5	Verification	4.8	E_s (MPa)	50-2.5x			E_b (MPa)	2000
			υ_s	0.25			b (m)	1.0
			T_i (m)	10			d (m)	0.5
			$\gamma_{ref}^{(S)}$	0.002			L (m)	10
			a_1 (1/sec)	0				
			a_2 (1/sec)	0				
			ρ_{si} (kg/m^3)	1800				
6	Verification	4.9	E_s (MPa)	44-2.2x			E_b (MPa)	2000
			υ_s	0.2			b (m)	1.0
			T_i (m)	5			d (m)	0.5
			$\gamma_{ref}^{(S)}$	0.0018			L (m)	10
			a_1 (1/sec)	0				
			a_2 (1/sec)	0				
			ρ_{si} (kg/m^3)	1800				
7	Scalability and convergence	4.10-4.12	E_s (MPa)	25			E_b (MPa)	2000
			υ_s	0.2			b (m)	1.0
			T_i (m)	10, 20, and 50			d (m)	0.5
			$\gamma_{ref}^{(S)}$	0.002			L (m)	10, 20, and 50
			a_1 (1/sec)	0				
			a_2 (1/sec)	0				
			ρ_{si} (kg/m^3)	1800				

Table 5.2: Details of the soil and beam geometries and properties corresponding to the problems analyzed (Cont...)

Problem Number	Problem Type	Associated Figure(s)	Soil Properties	Layer 1	Layer 2	Layer 3	Beam Properties	
8	Illustration	4.13(a)-4.13(h)	E_s (MPa)	25	18		E_b (MPa)	2500
			υ_s	0.25	0.2		b (m)	1.0
			T_i (m)	5	5		d (m)	0.75
			$\gamma_{ref}^{(S)}$	0.002	0.002		L (m)	20
			a_1 (1/sec)	0.05	0.05			
			a_2 (1/sec)	0.05	0.05			
			ρ_{si} (kg/m^3)	1800	1800			
9	Illustration	4.14(a)-4.14(h)	E_s (MPa)	25	16	18	E_b (MPa)	1500
			υ_s	0.2	0.25	0.2	b (m)	1.0
			T_i (m)	4	3	3	d (m)	0.3
			$\gamma_{ref}^{(S)}$	0.0018	0.0018	0.0018	L (m)	10
			a_1 (1/sec)	0.1	0.1	0.1		
			a_2 (1/sec)	0.1	0.1	0.1		
			ρ_{si} (kg/m^3)	1800	1600	1700		
10	Illustration	4.15(a)-4.15(i)	E_s (MPa)	25			E_b (MPa)	3000
			υ_s	0.3			b (m)	1.0
			T_i (m)	5			d (m)	1.0
			$\gamma_{ref}^{(S)}$	0.002			L (m)	7
			a_1 (1/sec)	0.15				
			a_2 (1/sec)	0.15				
			ρ_{si} (kg/m^3)	1600				
11	Illustration	4.16(a)-4.16(e)	E_s (MPa)	20	25		E_b (MPa)	2000
			υ_s	0.25	0.25		b (m)	1.0
			T_i (m)	6	4		d (m)	1.0
			$\gamma_{ref}^{(S)}$	0.002	0.002		L (m)	∞
			a_1 (1/sec)	1.0	1.0			
			a_2 (1/sec)	1.0	1.0			
			ρ_{si} (kg/m^3)	1700	1700			

(see Table 5.1 for the inputs), the soil Poisson's ratio remains spatially constant for any soil layer, and is not a function of soil strains.

A beam of 20 m length with free ends resting on a two-layer continuum and subjected to a moving force of 40 kN is considered, as shown in Figure 5.13(a)-(h) (see Table 5.2 corresponding to Problem 8 and Figure 5.13(a) for the inputs to the problem). Two constant velocities $V = 2$ and 10 m/sec are considered for the moving load. The linear and nonlinear mid-span displacement time histories $w(L/2, t)$ are shown in Figure 5.13(a). It is clear that the lower moving velocity produces higher nonlinear displacements.

The linear and nonlinear time histories of the parameters k_s and t_s are plotted in Figure 5.13(b)-(c) for the vertical section along the mid-span of the beam. The parameters k_s and t_s are lower in magnitude for nonlinear soil than for the corresponding linear soil (this explains why displacements are more for nonlinear soil than for linear soil). Further, both k_s and t_s fluctuate initially and then tend towards more stable values as time increases -k_s is more affected by soil nonlinearity than t_s. At the same time, the load velocity affects both k_s and t_s. The linear and nonlinear time histories of the parameter η_s are plotted in Figure 5.13(d). The parameter η_s is much less affected by soil nonlinearity or load velocity, and quickly attains a stable value as the load starts moving.

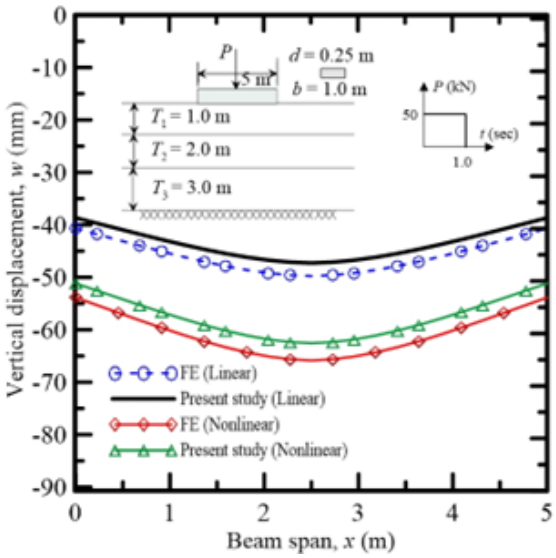

Figure 5.4: Linear and nonlinear displacement profiles at time $t = 1$ sec of a 5 m-long free beam resting on a three-layer soil deposit and subjected to 50 kN concentrated step load acting at the mid-span for a duration of 1 sec (Problem 1 of Table 5.1)

Figure 5.13(e) shows the variation of the normalized secant shear modulus G_s with depth for a vertical section along the mid-span of the beam when the load arrives at the mid-span of the beam. Interestingly, the depth up to which reduction of the modulus occurs depends on the velocity of the applied load (in other words, the zone over which soil nonlinearity is prevalent is dependent on the load velocity). The magnitude of modulus reduction/degradation is also higher for the lower load velocity. Figure 5.13(f) shows the nonlinear stress-strain response of a soil element just beneath the mid-span of the beam (at $z = 0$ m) for the two different load velocities. The stress strain-strain curve obtained directly from Equation 5.1 is also plotted for the similar range of strains produced by the lower moving velocity. The lower load velocity produces a higher strain level (21×10^{-4}) compared with that produced by the higher moving velocity (12×10^{-4}), which is consistent with the time-history of the mid-span displacements shown in Figure 5.8(a) and with the modulus reduction responses shown in Figure 5.13(e). It is also relevant to note that the nonlinear stress-strain responses in Figure 5.13(f) follow the "backbone curve" described by Equation 5.1, which indirectly corroborates that the nonlinear analysis has produced accurate and consistent results. Figure 5.13(g) shows how the stress-strain nonlinearity gets reflected in the nonlinearity of load-displacement relationships. The nonlinear load-displacement responses for multiple load positions are obtained at different times ($t = 0.1$,

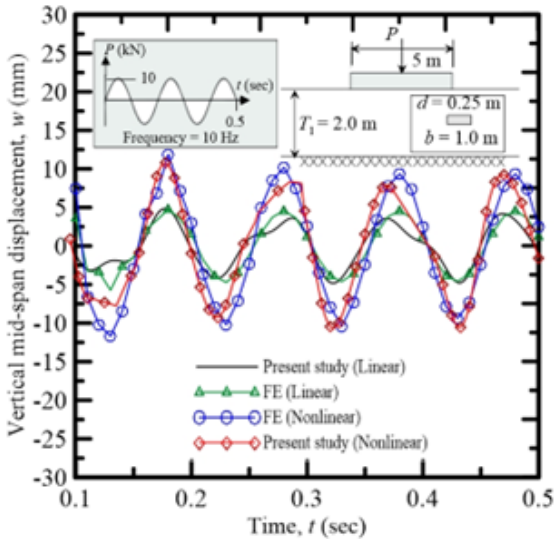

Figure 5.5: Nonlinear and linear time histories of mid-span displacement of a 5 m-long free beam resting on a 2 m thick soil deposit and subjected to a sinusoidal load with a maximum amplitude of 10 kN, frequency of 10 H_z and acting for a duration of 0.5 sec (Problem 2 of Table 5.1)

2, and 4 sec) for $V = 2$ m/sec. These times correspond to different load positions ($x = 0.2$, 4, and 8 m) measured from the left-hand side of the beam. It is important to note that the load-displacement responses measured at $t = 2$ and 5 sec do not start from the origin of the figure because of the accumulated displacements at these points corresponding to $t =$ 2 and 5 sec. The load-displacement response at $t = 0.1$ sec, however, starts from the origin with zero accumulated displacement. Finally, how the displacement function ϕ varies with depth is shown in Figure 5.13(h) for linear and nonlinear cases at different times $t = 4.95$ sec and 0.99 sec, corresponding to the two moving velocities $V = 2$ m/sec and 10 m/sec, respectively (at $t = 4.95$ sec and 0.99 sec, the load crosses the mid-span for $V = 2$ m/sec and 10 m/sec, respectively). It is clear that both the load velocity and soil nonlinearity affect ϕ but the effect of nonlinearity is more pronounced.

For the next example, a beam of length 10 m with free ends and subjected to a mid-span sinusoidal load of amplitude 15 kN and duration 2 sec with two frequencies $f_r =$ 2 and 10 Hz is considered. Table 5.2 corresponding to Problem 9 and Figure 5.14(a) give the details of the inputs. Figure 5.14(a) also shows the time histories of mid-span beam deflection $w(L/2, t)$ for the two loading frequencies. Greater load frequency results in greater displacements, and, as expected, the nonlinear displacement is greater than the

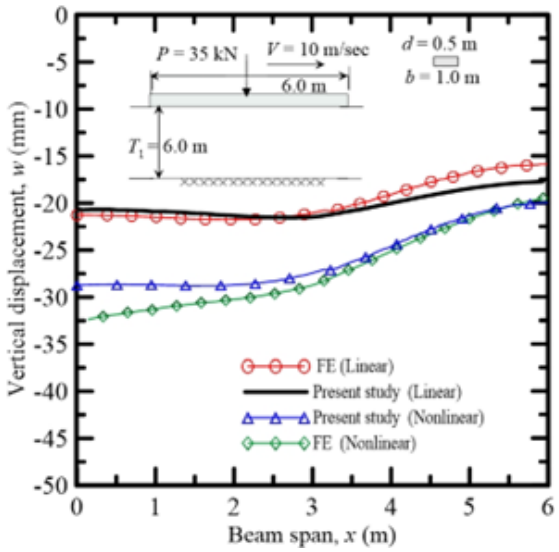

Figure 5.6: Nonlinear and linear displacement profiles of a 6 m-long free-free beam resting on a single-layer soil deposit and subjected to a 35 kN point load moving with a constant velocity of 10 m/sec when the load is at the mid span of the beam (Problem 3 of Table 5.1)

corresponding linear displacement. The parameters k_s and t_s are functions of the load frequency and nonlinearity, and these parameters oscillate initially and then attain stable values with increase in time (Figures 5.14(b)-(c)). The values of k_s and t_s for the nonlinear soil are lower than those of the linear soil, which explains why nonlinear displacements are greater than the corresponding linear displacement. The soil mass parameter η_s also attains stable values after initial oscillations but is much less affected by the nonlinearity and load frequency (Figure 5.14(d)).

Figure 5.14(e) shows the normalized secant shear modulus G_s/G_{s0} with depth along the vertical section through the mid-span of the beam at time t =1 sec. It is clear that the extent of nonlinear behavior depends on the load frequency. Figure 5.14(f) shows the modulus reduction curve as observed at a point in soil below the mid-span of the beam at a depth $z = 0.5$ m. Closely related to the modulus reduction curve is the nonlinear stress-strain curve of soil shown in Figure 5.14(g), which is obtained from the present analysis for a point in soil just beneath the mid-span of the beam. Also plotted in Figures 5.14(f)-(g) are the plots obtained directly from Equation 5.1 for this problem. These figures corroborate the fact that nonlinearity in soil is properly taken into account in the analysis. Figure 5.14(h) shows the variation of ϕ with depth at time $t = 1$ sec. Load frequency and

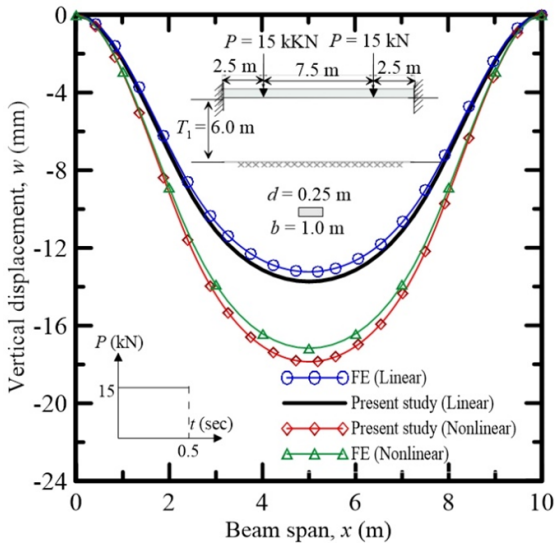

Figure 5.7: Nonlinear and linear beam displacement profiles at time $t = 0.5$ sec of a 10 m-long fixed beam resting on a 6 m thick soil layer and subjected to two 15 kN point-step loads acting for a duration of 0.5 sec (Problem 4 of Table 5.1)

nonlinearity affects ϕ(z), but the effect of nonlinearity on ϕ is more than the effect of load frequency.

For the third problem, a mid-span load ramping from 0 to 30 kN in 5 sec is considered to act on a 7 m-long simply-supported beam, as shown in Figure 5.15(a) (see Table 5.2 corresponding to Problem 10 for the remaining inputs). The nonlinear and linear beam displacement profiles are plotted in Figure 5.15(a) for $t = 2.5$ sec and 5 sec ($t = 5$ sec corresponds to the end of load application). As expected, the nonlinear displacement is greater than the linear displacement.

Figures 5.15(b)-(c) show the normalized profiles of soil compression parameter k_s, soil shear parameter t_s, and soil mass parameter η_s along the span of the beam at $t = 5$ sec. It is evident that soil nonlinearity influences the spatial distribution of k_s and t_s along the beam span, but η_s is much less affected by soil nonlinearity.

Vertical displacements and shear strains at depths of 2 m and 4 m are plotted along the beam span in Figures 5.15(d)-(e) for time $t = 5$ sec. Displacements and strains decrease with an increase in depth and the nonlinear responses are greater than the corresponding linear responses. Further, vertical displacements and shear strains along vertical sections are plotted for $x = 1.75$ m (at quarter of the beam-span distance from left end) and 3.5 m (mid-span) and for $t = 5$ sec (Figures 5.15(f)-(g)).

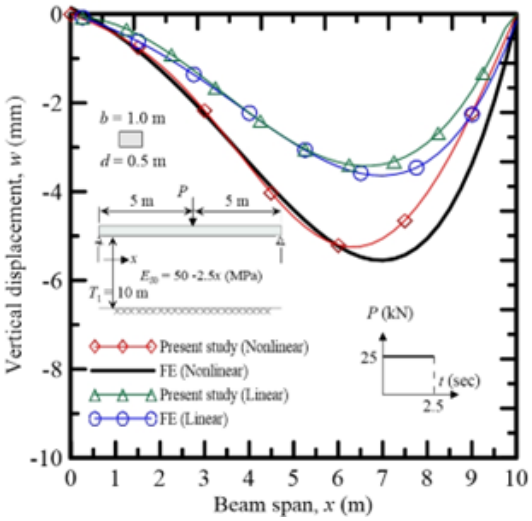

Figure 5.8: Nonlinear beam displacement profiles at time $t = 2.5$ sec of a 10 m-long simply supported beam resting on a 10 m thick soil layer with a horizontally varying initial Young's modulus and subjected to a 25 kN step point load acting at the mid-span for a period of 2.5 sec (Problem 5 of Table 5.1)

Figure 5.15(h) show the normalized secant modulus G_s/G_{s0} plotted along the beam span for two different depths of 2 m and 4 m and for time $t = 5$ sec. Figure 5.15(i) show the normalized secant modulus G_s/G_{s0} plotted along two vertical sections corresponding to $x = 1.75$ m and 3.5 m and $t = 2.5$ sec and 5 sec. These figures show that the secant modulus caused by induced soil strain varies spatially. Further, the modulus reduction does not occur along the vertical plane at the mid-span because the octahedral shear stress is zero there (because of the symmetry of the problem). This is consistent with the variations of the octahedral shear strain shown in Figures 5.15(e) and (g). Figure 5.15(j) shows the nonlinear stress-strain response of soil at a point just beneath the mid-span of the beam.

As the fourth example, an infinite (very long) beam with a 55 kN moving load travelling at 60 m/sec is considered (see Table 5.2 corresponding to Problem 11 for the inputs). The responses of the beam and soil displacements are shown in Figures 5.16(a)-(e). The steady-state response of the beam becomes invariant with time if the coordinate axis in the x-direction is attached to the moving load with the origin coinciding with the point at which the load acts. Figure 5.16(a) shows the steady state linear and nonlinear beam displacement profiles with respect to the moving axis. Figure 5.16(b) shows the time history of k_s and t_s for the vertical section at which the load acts. Figure 5.16(c) shows the time history of η_s for the same vertical section. Figure 5.16(d) shows the spatial

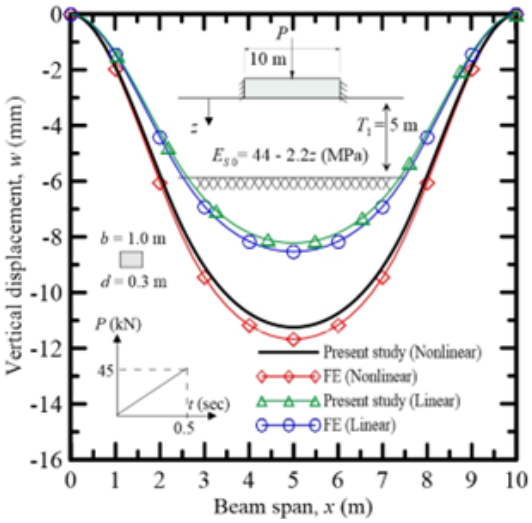

Figure 5.9: Nonlinear beam displacement profiles at time $t = 0.5$ sec of a 10 m-long fixed beam resting on a 5 m thick soil layer with a vertically varying initial Young's modulus and subjected to a ramp load with a 45 kN maximum force acting at the mid-span for a period of 0.5 sec (Problem 6 of Table 5.1)

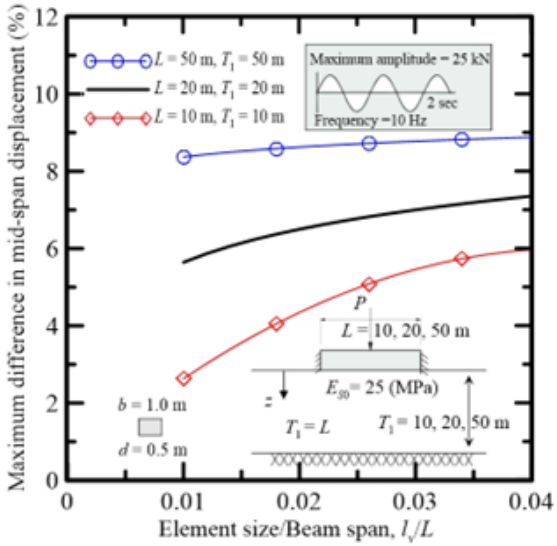

Figure 5.10: Effect of domain size on the accuracy of results (Problem 7 of Table 5.1)

variations of k_s and t_s with respect to the moving coordinate under steady state. The

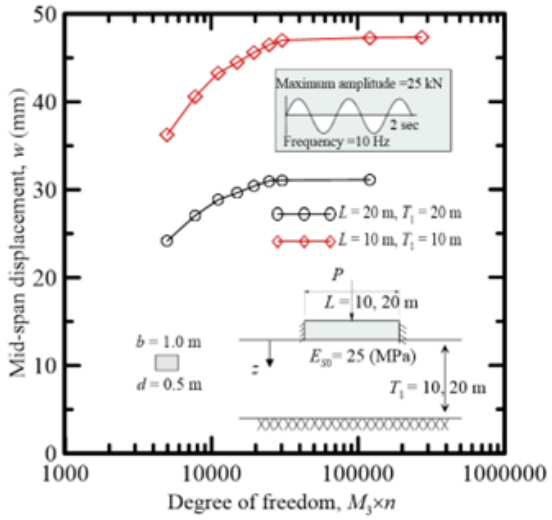

Figure 5.11: FE convergence study with respect to element size (Problem 7 of Table 5.1)

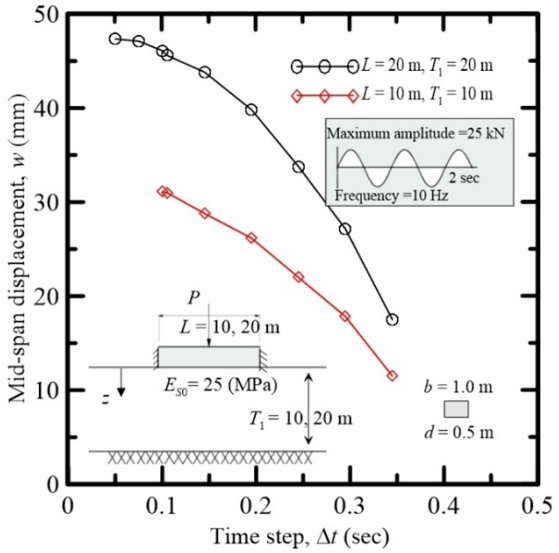

Figure 5.12: Convergence with respect to time step length (Problem 7 of Table 5.1)

values of k_s and t_s are greater for linear elastic soil than those for nonlinear soil. Further, under steady state, the linear and nonlinear k_s and t_s both remain spatially invariant. Figure 5.16(e) shows the nonlinear stress-strain response of the soil beneath the beam at when the load is at the mid-span of the beam.

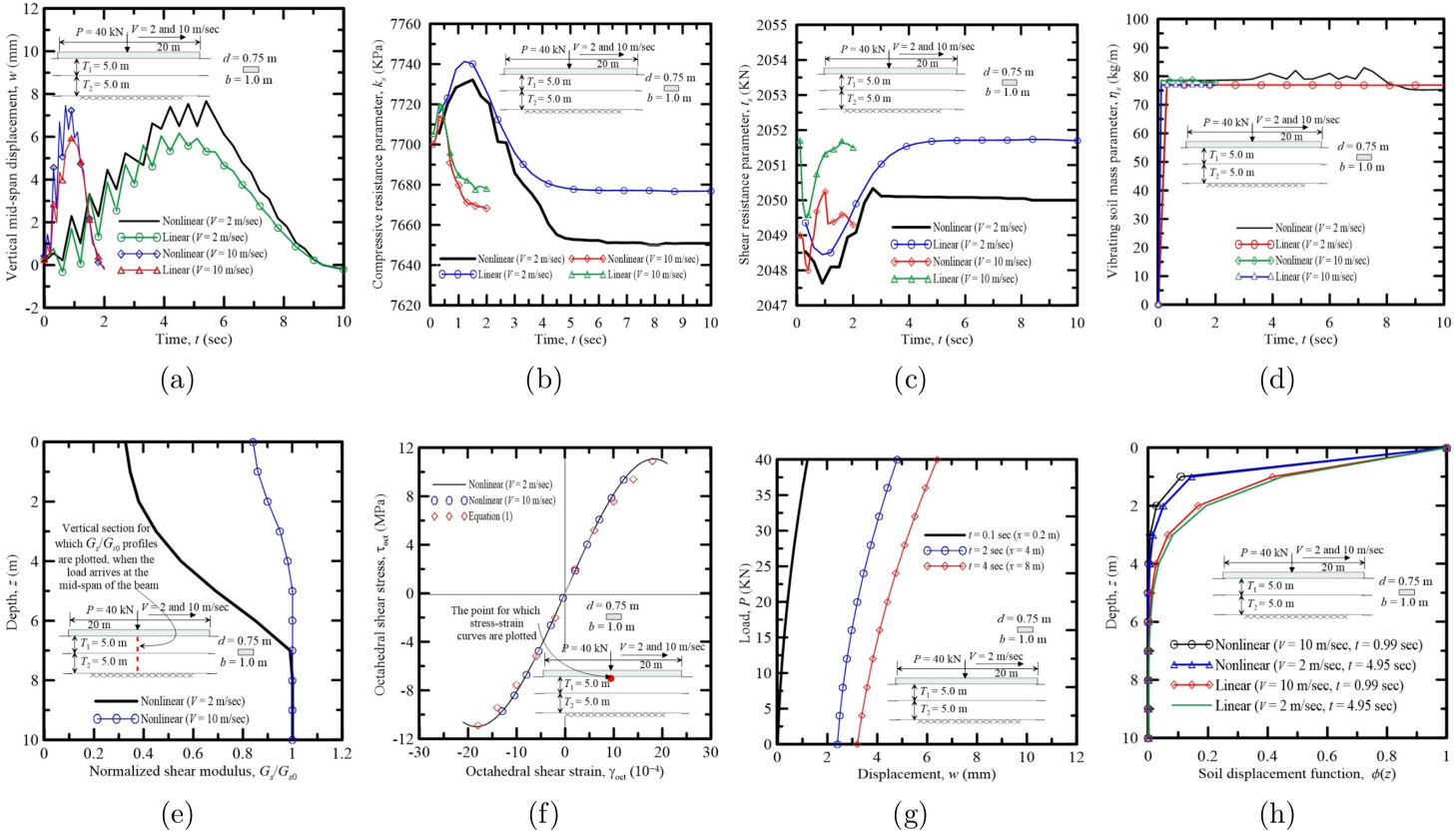

Figure 5.13: Nonlinear and linear time-dependent response of a 20 m-long free beam resting on a two layer soil deposit and subjected to a 10 kN point load moving with two different constant velocities of 2 m/sec and 10 m/sec (Problem 8 of Table 5.2): (a) time histories of mid-span displacement, (b) time histories of compression parameter k_s at the mid-span, (c) time histories of shear parameter t_s at the mid-span, (d) time histories of soil mass parameter η_s, (e) variations of G_s/G_0 with depth for the vertical section along the mid-span point of the beam when the load reaches the mid-span, (f) stress strain response of the point in soil just beneath the mid-span of the beam, (g) load-displacement responses for different load positions and at different times, and (h) soil displacement function $\phi(z)$ at different times when the load acts on the mid span

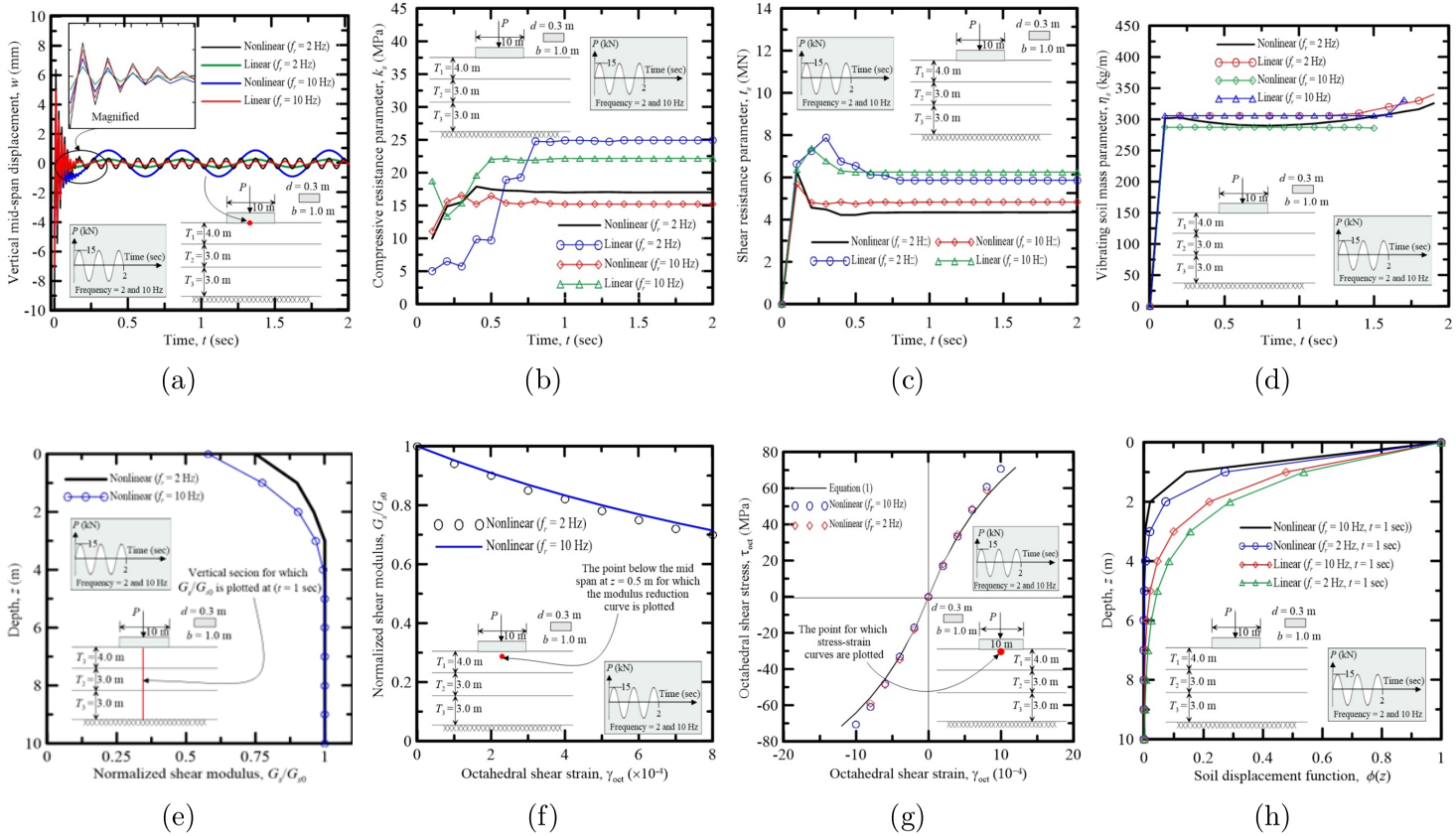

Figure 5.14: Nonlinear and linear time dependent responses of a 10 m long free beam resting on a three layer soil deposit and subjected to a sinusoidal load with a maximum amplitude of 15 kN and acting for a duration of 2 sec (Problem 9 of Table 5.2): (a) time histories of mid-span displacement, (b) time histories of ks at the mid-span, (c) time histories of t_s at the mid-span, (d) time histories of η_s, (e) variation of G_s/G_{s0} with depth along the vertical plane at the mid-span at time $t = 1$ sec, (f) modulus reduction curve recorded at a point in soil below the mid-span at a depth of 0.5 m, (g) stress-strain response of a point in soil just beneath the mid-span of the beam (at $z = 0$ m), and (h) soil displacement function ϕ with depth at $t = 1$ sec

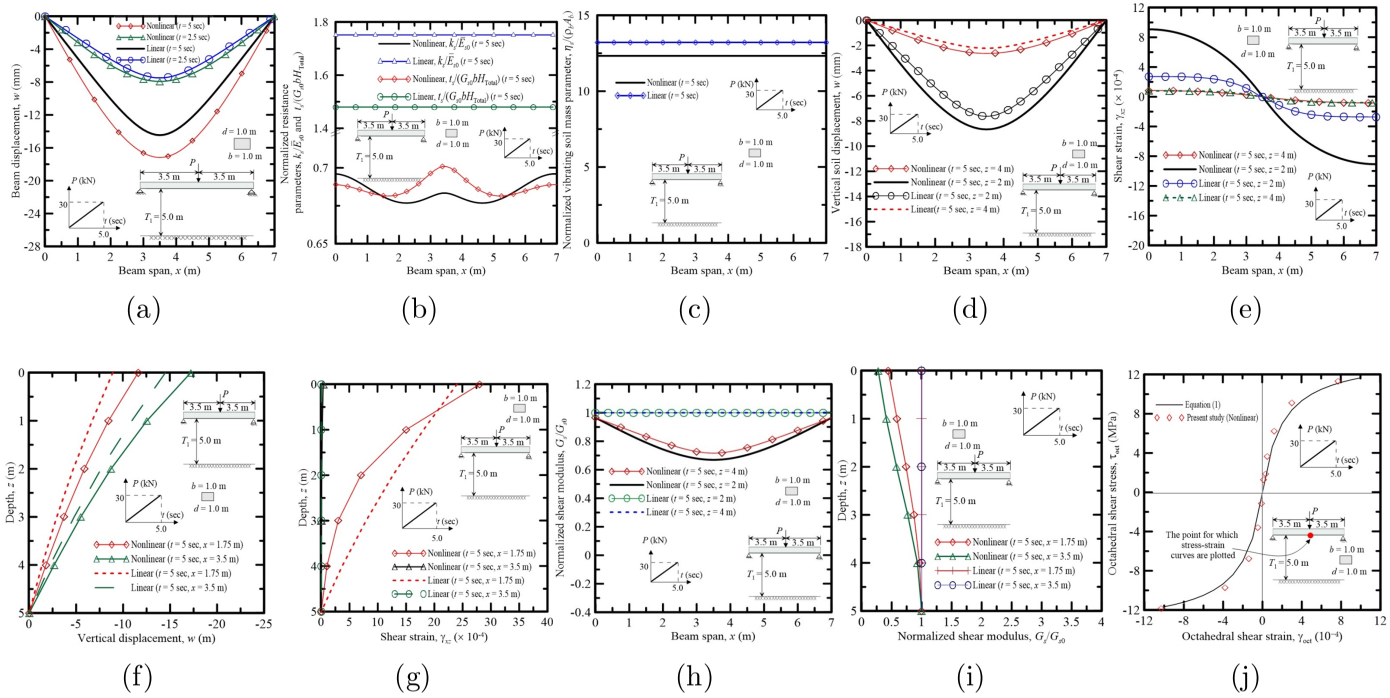

Figure 5.15: Nonlinear and linear time dependent responses of a 7 m-long simply-supported beam resting on a single layer soil deposit and subjected to a ramp point load with a maximum amplitude of 30 kN acting for a period of 5 sec (Problem 10 of Table 5.2): (a) beam displacement profiles at time $t = 2.5$ and 5 sec, (b) profiles of $k_s/\bar{E}_{s0}$ and $t_s/(G_{s0}bH_{Total})$ along the beam span at time $t = 5$ sec, (c) profiles of $\eta_s/(\rho_b A_b)$ along the beam span at time $t = 5$ sec, (d) soil displacement profiles along the span at time $t = 5$ sec and at depths of 2 m and 4 m, (e) octahedral shear strain profiles along span at time $t = 5$ sec and at depths of 2 m and 4 m, (f) vertical displacements along vertical sections at $x = 1.75$ m and 3.5 m and at $t = 5$ sec, (g) octahedral shear strains along vertical sections for $x = 1.75$ m and 3.5 m and at $t = 5$ sec, (h) normalized secant modulus G_s/G_{s0} profiles along the beam span for two different depths of 2 m and 4 m and for time $t = 5$ sec, (i) normalized secant modulus G_s/G_{s0} along two vertical sections corresponding to $x = 1.75$ m and 3.5 m and $t = 5$ sec, and (j) stress strain response of a point in soil just beneath the mid-span of the beam

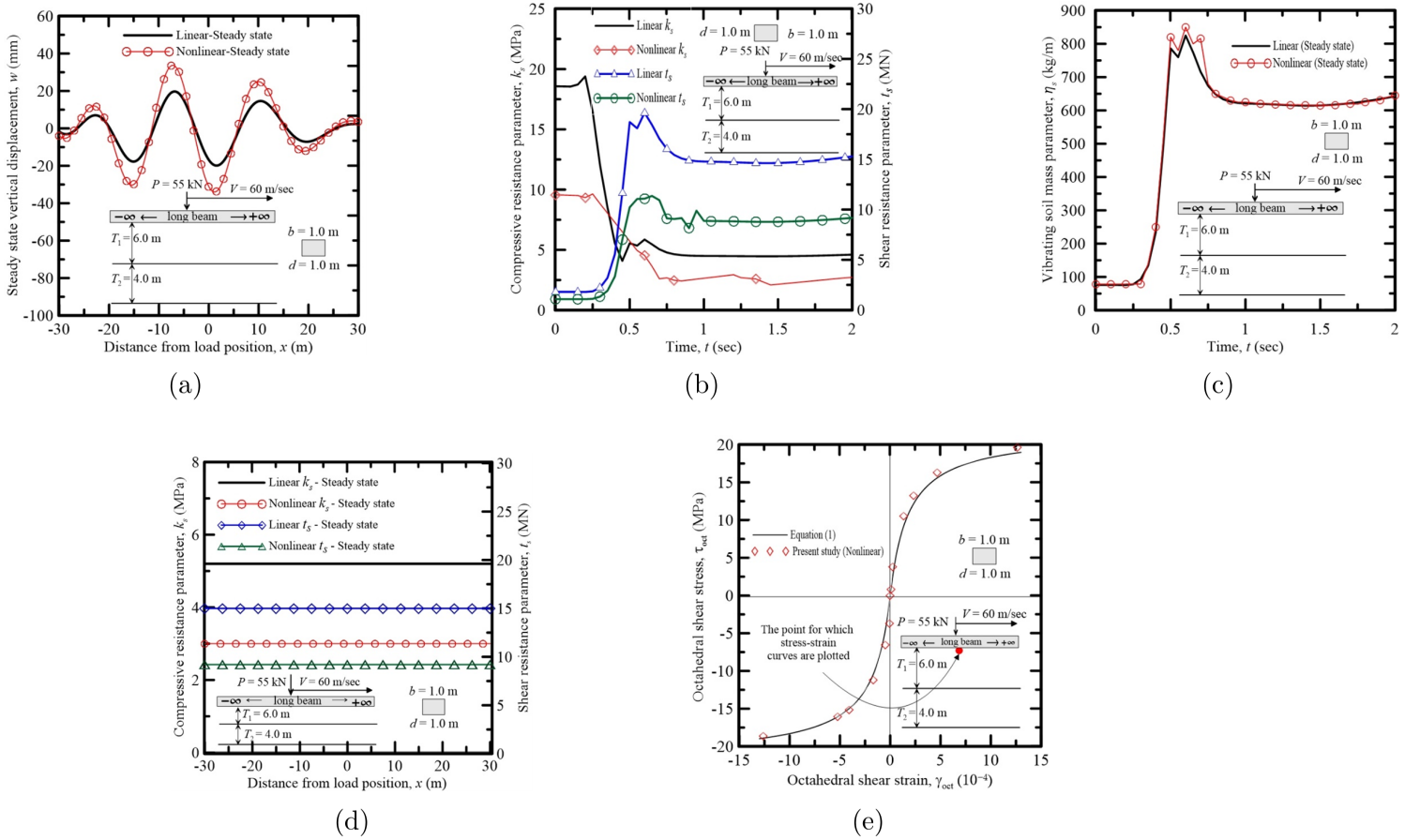

Figure 5.16: Nonlinear and linear time dependent responses of an infinitely long beam resting on two-layer soil and subjected to a 55 kN point load moving with a constant speed of 60 m/sec (Problem 11 of Table 5.2): (a) beam deflection profiles under steady state, (b) time histories of k_s and t_s, (c) time histories of η_s, (d) spatial variations of k_s and t_s, and (e) stress strain response of a point in soil just beneath the mid-span of the beam, when the load is at the mid-span of the beam

5.6 Conclusions

A new analysis is developed based on variational principles to obtain the time-dependent dynamic response of beams resting on multilayered nonlinear viscoelastic continuum/ foundation/soil and subjected to vibrating and moving loads. The displacement in the soil is assumed to be a product of separable functions and the extended Hamilton's principle is applied to obtain the differential equations of motion describing the dynamic equilibrium of the beam-continuum system. The equations are solved using the one-dimensional finite element analysis. As these equations are coupled, an iterative algorithm is used to obtain the solution. The implicit Wilson-θ time integration scheme is used to obtain the time history of the beam-soil system responses.

In the analysis, soil nonlinearity is taken into account by using a nonlinear-elastic soil constitutive model in which the stresses and strains are related following a hyperbolic law. In fact, in the constitutive model, the reduction of secant shear modulus is expressed as a function of the induced strain in soil. In order to capture the nonlinear response as a function of the loading history, the imposed dynamic loads are applied incrementally within each single dynamic time step.

The inputs required for the analysis (magnitude, duration, nature, and frequency or velocity of applied loads; geometry, Young's modulus, and mass density of beam; and layering, mass density, elastic constants and an appropriate modulus reduction rule for soil continuum) are conveniently given to the code through a text file. The accuracy of the analysis is verified with 2-D nonlinear dynamic finite element analysis (performed using PLAXIS). The results from the present analysis are obtained in about 50% of the time required for obtaining the results from PLAXIS analysis. The convergence and scalability of the present analysis method are also demonstrated. The present analysis is thus computationally efficient, user friendly, and accurate.

Four example problems are analyzed to demonstrate the use of the analysis and highlight the dynamic characteristics of the beam-foundation/soil system. An important feature of the analysis is that the soil "spring" parameters k_s and t_s are not constants as traditionally assumed but functions of the beam-foundation system (including the nonlinearity) and change with time. These parameters are not assumed a priori (as is conventionally done), but obtained as part of the solution. Thus, no recourse to empiricism is necessary for a priori determination of the parameters k_s and t_s. Further, the analysis automatically calculates the mass (inertial effect) of soil (continuum) participating in the vibration through the parameter η_s, which is generally not available for traditional, spring-based dynamic beam-foundation interaction problems. Thus, the analysis framework provides a rigorous,

easy-to-use, and quick methodology for analyzing beams resting on nonlinear viscoelastic continuums/foundations/soils subjected to dynamic loads.

Chapter 6

Interaction of Beams with Consolidating Nonlinear Poroelastic Layered Soil

This chapter is published Manuscript in ASCE- Journal of Engineering Mechanics, available online: https://doi.org/10.1061/(ASCE)EM.1943-7889.0002077, Elhuni, Hesham, and Dipanjan Basu. Elhuni, H., Basu, D. (2022). Interaction of Beams with Consolidating Nonlinear Poroelastic Layered Soil. Journal of Engineering Mechanics, 148(3), 04021167.

6.1 Overview

A semi-analytical framework for obtaining the consolidation settlement of flexible foundations such as beams and strip footings resting on nonlinear, saturated, poroelastic, and layered continuum (soil) is developed. The Biot's consolidation theory is used in the analysis, and the differential equations governing the displacements and excess pore pressure dissipation of the beam-soil system are developed using the variational principles of mechanics in which the soil is modeled as a simplified continuum. The coupled differential equations are solved iteratively using one-dimensional finite element analysis following a nonlinear, time-dependent algorithm. A distinct feature of the present framework is that the flexibility of the foundation is taken into account in the calculation of the consolidation settlement, which is generally not considered in the widely used Terzaghi's consolidation theory. In fact, it is observed that the beam dimensions, relative stiffness of the beam and

soil, and soil layering can significantly impact the foundation settlement and consolidation rate. The developed framework provides a computationally efficient, easy to use, and accurate method for estimating consolidation settlement of flexible shallow foundations.

6.2 Introduction and Related Literature

Problems in soil structure interaction and foundation engineering are often concerned with the deformation and settlement responses of foundations. The time-dependent consolidation settlement is of paramount importance in design of foundations in clayey soils. The diffusion theory of Terzaghi [221] is most widely used to model clay consolidation in which the coupled responses of the two phases, water and soil, are not explicitly considered and the soil deformation is modeled approximately using the coefficient of volume change mv that relates the applied effective stress increment in the soil to the corresponding strain increment. Terzaghi's consolidation theory has formed the basis for many consolidation studies on saturated clayey soils subjected to different types of surface loads [130].

Biot [35, 36, 38, 39] generalized Terzaghi's theory of consolidation and explicitly coupled the soil deformation with water flow in which the theory of elasticity is used to relate the soil stresses and strains and the generalized Darcy's law is used to quantify fluid/water flow [60]. Biot's theory treats clay consolidation more rigorously than Terzaghi's theory by accounting for the relative velocity between the solids and fluids [254]. In fact, Biot's theory has formed the basis of further developments on the theory of poroelasticity and has been applied in different soil-structure interaction problems [59].

Traditionally, in the studies on consolidation using Biot's theory, the foundations are assumed to be either perfectly rigid elements [150, 129] or perfectly flexible elements [35, 185] or elements of intermediate flexibility represented by beam or plate theories [207, 3]. In the consolidation studies considering perfect flexibility of foundations, the foundation loads are directly applied on the surface of the soil and this has been proven to underestimate the consolidation settlement [42]. In fact, applying the foundation load directly on the ground surface is widely practiced in clay consolidation studies using Terzaghi's theory. Usually, shallow foundations such as strip footings, grade beams, and rafts are of intermediate flexibility, and their responses to the applied loads depend on the relative stiffness of the foundation and the underlying soil [43]. A few Biot's theory-based consolidation studies considering the finite flexibility of foundations are available in which the foundation is modeled as an Euler-Bernoulli, Timoshenko or shear beam and the soil is modeled as a poroelastic solid or a saturated elastic half space with or without layering [207, 3].

Flexible shallow foundations (grade beams and strip footings), pavements, and railroads are usually modeled as beams resting on a bed of soil springs [255, 177]. The simplified continuum models developed for beam on foundation problems [247, 240, 86, 87], in which the soil is represented by a continuum with simplified assumptions on the stress or displacement fields, provide a better alternative for analysis of flexible foundations because these models are computationally more efficient and tractable than the traditional three-dimensional continuum-based analysis but are more accurate than the spring-based models [251]. Because of the treatment of soil as a continuum, the simplified continuum approach provides an alternative for consolidation analysis of flexible foundations using poroelastic theory [179].

Nonlinearity in the stress-strain response of soils plays an important role in real life soil-structure interaction problems and should be considered in the analysis [31]. In conventional consolidation studies on foundations, it is assumed that the stress-strain behavior of the soil is linear and elastic. In practice, many sources of nonlinearity affect the behaviour of clayey soils: the soil shear modulus reduces as the induced soil strains increase, the coefficient of compressibility changes nonlinearly with the logarithm of effective stress, and the compressibility increases rapidly as the effective stress exceeds the preconsolidation pressure [172]. These differences between the behavior of real clays and the linear stress-strain relationship assumed in conventional consolidation studies reduce the accuracy of estimated settlements [78]. Soil nonlinearity in consolidation analysis was approximately taken into account by assuming a proportionality between the decrease in soil permeability and the decrease in soil compressibility during consolidation [65]. However, these studies are either limited to the case where the interaction between the foundation and soil is neglected or the soil nonlinearity is not implemented through a proper stress-strain constitutive relationship. Two- or three-dimensional numerical methods requiring significant computational resources and specialized expertise are generally used for analysis of flexible foundations interacting with nonlinear, consolidating poroelastic soil [192]. However, the simplified continuum approach provides a computationally efficient and easy to use alternative of considering soil nonlinearity for foundation-soil interaction problems [102].

In this chapter, a simplified continuum-based analysis method is developed for flexible shallow foundations resting on nonlinear, consolidating soils subjected to static (sustained) loads. The soil is assumed to be a two-phase (soil and water) layered continuum that follows Biot's theory of poroelasticity, and the stress-strain nonlinearity in soil is implemented by varying the soil shear modulus as a function of the induced soil strain. The foundation is assumed to be an Euler-Bernoulli beam, and the vertical soil displacement and pore pressure are assumed to be products of separable functions. The potential energy functional for the beam-soil system is developed considering the time-dependent consolidation process.

The potential energy is minimized to obtain the system of coupled differential equations governing the behavior of the beam-poroelastic soil system. The one-dimensional (1D) finite element (FE) method is used to solve the differential equations following an iterative algorithm. The accuracy, computational efficiency, and applicability of the method are demonstrated through multiple numerical problems.

6.3 Problem Description

6.3.1 Beam-Poroelastic Foundation System

Assuming a plane-strain condition, as is typically done for beam on foundation problems [242], a beam or a strip footing of length L and uniform rectangular cross-sectional area A ($A = bd$, b = beam width, and d = beam depth or thickness) is assumed to be resting on a layered poroelastic continuum (soil), as shown in Figure 6.1. The flexural rigidity of the beam is E_bI_b where E_b = Young's modulus of beam and I_b = second moment of inertia of beam cross section = $bd^3/12$.

The layered continuum (clayey soil) beneath the beam comprises a two-phase medium with a solid (soil) skeleton with interconnected pores (voids) that are completely filled with an isotropic, viscous, and incompressible Newtonian fluid (which is water in the case of soil). The two-phase continuum (fully saturated soil) is considered to have the same width b as that of the beam and consists of n layers with the bottom n^{th} layer resting on a rigid substratum (e.g., bed rock or very dense sand). The i^{th} layer extends vertically downward to a depth H_i such that the thickness T_i of the i^{th} layer is $H_i - H_{i-1}$ ($H_0 = 0$). The total thickness of the continuum (soil deposit) is H_{Total} ($= \sum_{i=1}^{n} T_i$). Each poroelastic layer i is assumed to be isotropic and heterogeneous with spatially varying Young's modulus E_{si}, Poisson's ratio of υ_{si}, porosity f_i, and coefficient of permeability $\bar{k}_i$ (Figure 6.1), and it follows Biot's theory of poroelasticity [38]. The beam and poroelastic continuum (soil) are assumed to be in full contact at all times, and the interface friction is neglected. Further, the displacements in the beam and continuum occur only in the vertical direction (i.e., the horizontal displacements are assumed to be negligible).

A Cartesian $x - z$ coordinate system is considered attached to the left end of the beam with x direction positive to the right, and z direction positive vertically downward (Figure 6.1). In order to capture the accurate response of the beam-foundation (soil) system without any boundary effects, the analysis domain is assumed to extend beyond the two-ends of the beam (for beams with free ends) to a length βL (where $\beta \geq 1$ and its value

is determined through trial and error) in positive and negative x directions, respectively (Figure 6.1).

Fluid flow in the poroelastic continuum (soil) is assumed to occur only in the vertical direction. The fluid pressure in the pores (i.e., the pore pressure) becomes zero at the ground surface (i.e., at the interface of the beam and continuum where $z = 0$). The interface between the bottom (n^{th}) layer and the hard substratum (bed rock) at $z = H_{Total}$ may be permeable allowing free drainage (double-drainage condition) or may be completely impermeable (single drainage condition). Accordingly, the pore pressure at $z = H_{Total}$ may or may not become zero. The loads acting on the beam are static in nature or are applied slowly such that the quasi-static conditions is maintained. The applied loads are vertical and can be distributed spatially ($q(x)$) or concentrated at different discrete points x_j ($Q_j(x_j)$) (Figure 6.1).

6.3.2 Coupling of Porous Solid and Fluid

The coupling of the solid and fluid in the poroelastic medium (i.e., the soil-water coupling) is best explained by considering a two-dimensional (2D) small representative element (RE) of the two-phase medium that obey the plane-strain condition assumed in this problem (Figure 6.1). This element is chosen to be large enough compared to the size of the pores such that uniform water pressure can be assumed throughout the pores (the consolidation process is sufficiently slow such that the water pressure will redistribute between pores and the pressure difference vanishes within the RE). At the same time, the RE is chosen small enough compared to the scale of the soil continuum so that it may be considered infinitesimal in the mathematical sense. A stress state is assumed by means of the set of average stress components distributed uniformly on the faces of the RE, as shown in Figure 6.1.

According to Biot's theory, the stresses in a poroelastic solid (soil) RE are composed of two parts: an equivalent fluid stress $\sigma^{(F)}$ and the average stress in the soil skeleton $\sigma^{(S)}$. The equivalent fluid stress $\sigma^{(F)}$ is assumed to be proportional to the excess pore pressure θ (the actual pressure in the fluid occupying the pores) and are related through the volume fraction of the pores with respect to the bulk volume such that

$$\sigma^{(F)} = -\left(\frac{V_{pore}}{V_{bulk}}\right)\theta = -f\theta \tag{6.1}$$

where f = porosity of the porous medium (soil) = V_{pore}/V_{bulk}, V_{pore} is the volume of the pores (voids) and V_{bulk} = bulk volume of the porous medium (V_{pore} ¡¡ V_{bulk}), and the

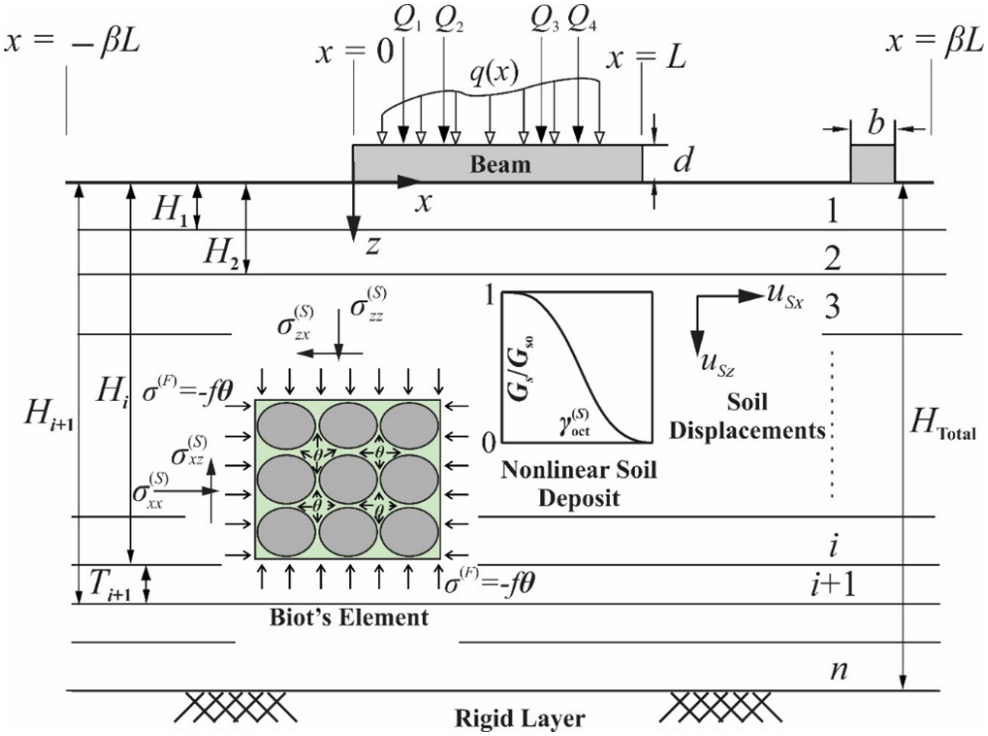

Figure 6.1: Beam resting on nonlinear, poroelastic and multi-layered soil (continuum)

negative sign indicates that $\sigma^{(F)}$ generates tension on the faces of the RE (Figure 6.1) [37]. The total stress in the RE is a summation of the skeleton stress $\sigma^{(S)}$ and the equivalent fluid stress $\sigma^{(F)}$ (stresses are carried partly by the fluid and partly by the porous solid). Thus, the total stress representative tensor for the RE considering the plane strain problem is given by

$$\sigma^{Total} = \begin{bmatrix} 0 & 0 & \sigma^{(S)}_{xz} \\ 0 & 0 & 0 \\ \sigma^{(S)}_{zx} & 0 & \sigma^{(S)}_{zz} + \sigma^{(F)}_{zz} \end{bmatrix} \tag{6.2}$$

To complete the description of mechanical coupling between the solid and fluid, Biot used the generalized Darcy's law to describe fluid flow through the pores during the consolidation process. The generalized form of Darcy's law for unidirectional vertical flow under plane-strain condition is given by

$$-\bar{k}\left(\frac{\partial\theta}{\partial z}+\frac{\partial\theta}{\partial x}\right)=\left(\frac{\partial u_{Fz}}{\partial t}-\frac{\partial u_{Sz}}{\partial t}\right) \tag{6.3}$$

where u_{Sz} = vertical displacement of the solid skeleton of the RE, u_{Fz} is the displacement of the fluid in the RE in the vertical direction, $\bar{k}$ is the hydraulic conductivity of the porous medium (soil), and t is the time. Equations 6.1-6.3 ensure force and momentum balance in the poroelastic continuum in the absence of body forces [35].

6.3.3 Stress-Strain Nonlinearity of Soil

In this chapter, the porous solid (soil) is assumed to be nonlinear elastic characterized by a pair of elastic constants such as E_s and υ_s or G_s and υ_s (E_s = Young's modulus, G_s = shear modulus, and υ_s = Poisson's ratio). It is common in geotechnical engineering to assume υ_s as a constant within an i^{th} soil layer (i.e., it is assumed that the nonlinearity has no significant impact on υ_s), and relate G_s with the shear strain to take into account the nonlinearity [213]. It is, in fact, well established that the shear stress-shear strain relationship of soil is nonlinear and effective stress dependent [204]. Several studies have experimentally established the nonlinearity in soil in terms of modulus reduction curves in which G_s is plotted as a function of the engineering shear strain γ in soil [112, 76]. Alternatively, the reduction of G_s with γ has been expressed as nonlinear elastic hyperbolic constitutive models [244].

In the present chapter, the nonlinear elastic model of Vardanega and Bolton (2013)[244] for clayey soils is adopted, which was developed based on the results of 67 laboratory tests performed on a variety of clayey soils

$$\frac{G_s}{G_{s0}}=\left[1+\left(\frac{\gamma^{(S)}}{\gamma^{(S)}_{ref}}\right)^{\alpha}\right]^{-1} \tag{6.4}$$

where G_s is the secant shear modulus in clayey soil, G_{s0} is the initial (small-strain) shear modulus in the clayey soil, $\gamma^{(S)}_{ref}$ is a reference shear strain in the soil, which is assumed to be equal to 0.002 in this study [244], α (= 0.736) is a parameter describing the curvature of the nonlinear stress-strain relationship, and $\gamma^{(S)}$ is the engineering shear strain in the soil. For the present plane strain problem, it is reasonable to represent $\gamma^{(S)}$ by the octahedral engineering shear strain of the solid (soil), given by

$$\gamma^{(S)}_{oct}=\frac{2}{3}\left[2\left(\varepsilon^{(S)}_{zz}\right)^2+6\left(\varepsilon^{(S)}_{xz}\right)^2\right]^{\frac{1}{2}} \tag{6.5}$$

6.4 Analytical Framework

6.4.1 Displacements, Strains, and Stresses in Two-Phase Medium

The poroelastic solid (soil) responds to both normal and shear stresses, but the Newtonian fluid (water) responds only to normal stresses. The horizontal displacement in the solid is assumed to be negligible and the horizontal displacement in the fluid is zero because the flow is assumed to occur only in the vertical direction. Denoting the vertical displacements in the solid and fluid respectively as u_{Sz} and u_{Fz}, and the strain tensors in the solid and fluid respectively as $\varepsilon^{(S)}$ and $\varepsilon^{(F)}$, the following strain displacement relationships can be obtained

$$\varepsilon^{(S)} = \begin{Bmatrix} \varepsilon_{xx}^{(S)} \\ \varepsilon_{zz}^{(S)} \\ \varepsilon_{xz}^{(S)} \end{Bmatrix} = \begin{Bmatrix} 0 \\ -\dfrac{\partial u_{Sz}}{\partial z} \\ -\dfrac{1}{2}\dfrac{\partial u_{Sz}}{\partial x} \end{Bmatrix} \tag{6.6a}$$

$$\varepsilon^{(F)} = \begin{Bmatrix} \varepsilon_{xx}^{(F)} \\ \varepsilon_{zz}^{(F)} \\ \varepsilon_{xz}^{(F)} \end{Bmatrix} = \begin{Bmatrix} 0 \\ -\dfrac{\partial u_{Fz}}{\partial z} \\ 0 \end{Bmatrix} \tag{6.6b}$$

The elastic constitutive relationship relates the strain tensor $\varepsilon^{(S)}$ at any point within the solid to the stress tensor $\sigma^{(S)}$ as (Figure 6.1)

$$\sigma^{(S)} = \begin{Bmatrix} \sigma_{xx}^{(S)} \\ \sigma_{zz}^{(S)} \\ \sigma_{xz}^{(S)} \end{Bmatrix} = \frac{E_s}{(1+\upsilon_s)(1-2\upsilon_s)} \begin{bmatrix} 1-\upsilon_s & \upsilon_s & 0 \\ \upsilon_s & 1-\upsilon_s & 0 \\ 0 & 0 & 0.5-\upsilon_s \end{bmatrix} \begin{Bmatrix} 0 \\ -\dfrac{\partial u_{Sz}}{\partial z} \\ -\dfrac{1}{2}\dfrac{\partial u_{Sz}}{\partial x} \end{Bmatrix} \tag{6.7}$$

where the Young's modulus E_s of the solid can be interpreted as the secant modulus for nonlinear elastic soil.

It is assumed that, at any given time t, the two state variables u_{Sz} (vertical soil displacement) and θ (excess pore pressure) can be decomposed into products of separable functions [179]

$$u_{Sz}(x, z, t) = w(x, t)\phi(z) \tag{6.8}$$

$$\theta(x, z, t) = p(z, t)\psi(x) \tag{6.9}$$

where $w(x,\, t)$ is the settlement (vertical displacement) of the top surface of the poroelastic continuum (soil), which is the same as the beam displacement for $0 \leq \mathrm{x} \leq \mathrm{L}$, $\phi(z)$ is a dimensionless displacement shape function varying with depth, $p(z,\, t)$ is the excess pore pressure at the beam center which varies with depth and time, and $\psi(x)$ is a dimensionless pore pressure shape function varying in the horizontal direction. It is assumed in the analysis that $\phi(0) = 1$, which ensures perfect contact between the beam and the underlying soil, and that $\phi(H_{total}) = 0$, which ensures that the vertical displacement in the continuum arising from applied forces decreases with depth and becomes zero at the interface with the rigid layer. It is also assumed that $\psi = 1$ at the point corresponding to the beam center (typically at the load center), and that $\psi = 0$ at the horizontal boundaries of the problem (away from the beam-ends).

Substituting Equation 6.8 into Equation 6.6(a) and substituting the result in Equation 6.7, the stress tensor in the soil can be expressed as

$$\sigma^{(S)} = \begin{Bmatrix} \sigma_{xx}^{(S)} \\ \sigma_{zz}^{(S)} \\ \sigma_{xz}^{(S)} \end{Bmatrix} = \frac{E_s}{(1+\upsilon_s)(1-2\upsilon_s)} \begin{bmatrix} 1-\upsilon_s & \upsilon_s & 0 \\ \upsilon_s & 1-\upsilon_s & 0 \\ 0 & 0 & 0.5-\upsilon_s \end{bmatrix} \begin{Bmatrix} 0 \\ -w(x,t)\frac{d\phi(z)}{dz} \\ -\frac{1}{2}\frac{\partial w(x,t)}{\partial x}\phi(z) \end{Bmatrix} \tag{6.10}$$

In order to express the relation between the solid displacement u and fluid displacement U in the algebraic form, Equation 6.3 is convoluted with the aid of the convolution product rule [216]. Thus, multiplying both sides of Equation 6.3 by a unit step function gr and integrating with respect to time results in

$$-\int_0^t \left[\bar{k}\left(\frac{\partial\theta}{\partial z}+\frac{\partial\theta}{\partial x}\right)g_r(\tau-t)\right]dt=\int_0^t\left[\left(\frac{\partial u_{Fz}}{\partial t}-\frac{\partial u_{Sz}}{\partial t}\right)g_r(\tau-t)\right]dt \tag{6.11}$$

Applying the convolution product rule given by

$$\int_0^t f_r(t)g_r(\tau-t)dt=f_r*g_r \tag{6.12}$$

to Equation 5.11 for an arbitrary function f_r (τ is a dummy variable and '*' refers to the convolution product), integrating both sides by parts, and rearranging results in

$$u_{Fz}=u_{Sz}-g_r*\bar{k}\left(\frac{\partial\theta}{\partial z}+\frac{\partial\theta}{\partial x}\right) \tag{6.13}$$

Substituting Equations 6.9, 6.8, and 6.13 into Equation 6.6(b) results in

$$\varepsilon^{(F)}=\begin{Bmatrix}\varepsilon_{xx}^{(F)}\\ \varepsilon_{zz}^{(F)}\\ \varepsilon_{xz}^{(F)}\end{Bmatrix}=\begin{Bmatrix}0\\ w(x,t)\dfrac{d\phi(z)}{dz}-g_r*\bar{k}\dfrac{\partial^2 p(z,t)}{\partial z^2}\psi(x)-g_r*\bar{k}\dfrac{\partial p(z,t)}{\partial z}\dfrac{d\psi(x)}{dx}\\ 0\end{Bmatrix} \tag{6.14}$$

6.4.2 Principle of Minimum Potential Energy

The strain energy density $\Pi_{D-continuum}$ of the poroelastic soil is given by [36]

$$\Pi_{D-continuum}=\frac{1}{2}\left(\sigma_{zz}^{(S)}\varepsilon_{zz}^{(S)}+\sigma_{xz}^{(S)}\varepsilon_{xz}^{(S)}+\sigma_{zz}^{(F)}\varepsilon_{zz}^{(F)}\right) \tag{6.15}$$

Substituting Equations 6.6(a), 6.1, 6.9, 6.6, and 6.10 into Equation 6.15, and considering any soil layer i, the strain energy density is given by

$$\begin{aligned}\Pi_{D-continuum,i} = \frac{1}{2}\left[\bar{E_{si}} w^2 \left(\frac{d\phi_i}{dz}\right)^2 + G_{si}\phi_i^2\left(\frac{\partial w}{\partial x}\right)^2\right] \\ + \frac{1}{2} f_i \left[p_i \psi w \frac{d\phi_i}{dz} - p_i \psi \bar{k_i}\left(p_i \frac{\partial^2 p_i}{\partial z^2} + \psi \frac{d^2\psi}{dx^2}\right) * g_r\right]\end{aligned} \tag{6.16}$$

where ϕ_i and p_i are respectively the functions ϕ(z) and $p(z,\ t)$ in the i^{th} layer; and $\bar{E_{si}} = \bar{E_{si}}(x, z)$ and $G_{si} = G_{si}(x, z)$ are respectively the constrained and shear moduli in the i^{th} layer given by

$$\bar{E_{si}} = \frac{E_{si}(1-\upsilon_{si})}{(1+\upsilon_{si})(1-2\upsilon_{si})} \tag{6.17a}$$

$$G_{si} = \frac{E_{si}}{2(1+\upsilon_{si})} \tag{6.17b}$$

Note that $\bar{E_{si}}$ and G_{si} are functions of x and z (i.e., $\bar{E_{si}} = \bar{E_{si}}(x, z)$ and $G_{si} = G_{si}(x, z)$) because each layer i is assumed to be heterogeneous with spatially varying E_{si}. The constrained modulus $\bar{E}_s$ is the reciprocal of the coefficient of volume change m_v ($\bar{E}_s = 1/m_v$). Further note that f_i and $\bar{k_i}$ are assumed to vary both in the horizontal and vertical directions (i.e., $f_i = f_i(x,\ z)$ and $\bar{k_i} = \bar{k_i}(x,z)$).

Considering the volumes V_{beam} and $V_{continuum,i}$ of the beam and the i^{th} soil (continuum) layer, respectively, the total potential energy of the beam-soil system (considering all the n layers) is given by

$$\begin{aligned}\Pi_{total} &= \int_{V_{beam}} \Pi_{D-beam} dV_{beam} + \sum_{i=1}^{n} \int_{V_{continuum,i}} \Pi_{continuum,i} dV_{continuum,i} + \Pi_{load} \\ &= \int_0^L \frac{E_b I_b}{2}\left(\frac{\partial^2 w}{\partial x^2}\right)^2 dx + \sum_{i=1}^{n} \frac{b}{2} \int_{-\beta L}^{\beta L} \int_{H_{i-1}}^{H_i} \left[\left\{E_{si} w^2 \left(\frac{d\phi_i}{dz}\right)^2 + G_{si}\phi_i^2\left(\frac{\partial w}{\partial x}\right)^2\right\} + \right. \\ &\qquad \left. f_i\left\{p_i \psi w \frac{d\phi_i}{dz} - p_i \psi \bar{k_i}\left(p_i \frac{\partial^2 p_i}{\partial z^2} + \psi \frac{d^2\psi}{dx^2}\right) * g_r\right\}\right] dz dx \\ &\qquad - \int_0^L Q_j \delta_d(x - x_j) w dx - \int_0^L q w dx\end{aligned} \tag{6.18}$$

where δ_d is the Dirac delta function, Π_{D-beam} $\left[= 0.5E_bI_b(\partial^2 w/\partial x^2)\right]$ is the strain energy density of the beam, and Π_{load} is the external potential energy caused by the applied loads. The first term on the right-hand side of Equation 6.18 in the second row captures the internal potential energy of the beam, the second term captures the internal potential energy of the poroelastic continuum (soil), and the third term captures the external potential energy.

Applying the principle of minimum potential energy $\delta(\Pi_{total})$ =0 where δ is the variational operator, and considering separately the variations of the functions w, p, ψ, and ϕ, the corresponding Euler-Lagrange equations (i.e., the governing differential equations and associated boundary conditions of $w(x,\ t)$, $p(z,\ t)$, $\psi(x)$, and $\phi(z)$) are obtained. These differential equations satisfy the principle of minimum potential energy and therefore maintain the equilibrium of the system.

In obtaining the differential equations it is assumed that the poroelastic soil is heterogeneous within each layer with spatially varying $\bar{E}_{si}$ and G_{si}, which is necessary to incorporate the effect of soil nonlinearity in the analytical framework because different strains are generated at different points in the soil because of beam displacement, and this results in different reductions of soil modulus at these points rendering the soil heterogeneous (even if the soil is homogeneous prior to loading).

6.4.3 Differential Equations for Beam Deflection and Surface Displacement of Poroelastic Soil

The differential equations of beam and surface soil displacements are obtained along with the corresponding boundary conditions. For the domain $0 \leq x \leq L$ over which the beam is present, the differential equation governing the beam deflection is obtained as

$$E_bI_b\frac{\partial^4 w}{\partial x^4} - 2t_s\frac{\partial^2 w}{\partial x^2} - 2\frac{\partial t_s}{\partial x}\frac{\partial w}{\partial x} + k_s w + r^{(w)}\psi = q + Q_j\delta_d(x - x_j) \quad (0 \leq x \leq L) \tag{6.19a}$$

For the domains -$\beta L \leq x \leq 0$ and $L \leq x \leq \beta L$ (i.e., over the soil domains with no beam), the differential equation governing the displacement of the top surface of the continuum (soil) is obtained as

$$-2t_s\frac{\partial^2 w}{\partial x^2} + k_s w - 2\frac{\partial t_s}{\partial x}\frac{\partial w}{\partial x} + r^{(w)}\psi = 0 \quad (-\beta L \leq x \leq 0)\ \&\ (L \leq x \leq \beta L) \tag{6.19b}$$

The boundary conditions for free-end beams are

$$w\ |_{x=-\beta L} = w\ |_{x=\beta L} = 0 \tag{6.20a}$$

$$w_{Right}\ |_{x=0} = w_{Left}\ |_{x=0} \tag{6.20b}$$

$$\left[-2t_s \frac{\partial w}{\partial x}\right]_{Left} |_{x=0} = \left[E_b I_b \frac{\partial^3 w}{\partial x^3} - 2t_s \frac{\partial w}{\partial x}\right]_{Right} |_{x=0} \quad \text{(with no concentrated force acting)} \tag{6.20c}$$

$$\left[E_b I_b \frac{\partial^3 w}{\partial x^3} - 2t_s \frac{\partial w}{\partial x}\right]_{Left} |_{x=L} = \left[-2t_s \frac{\partial w}{\partial x}\right]_{Right} |_{x=L} \quad \text{(with no concentrated force acting)} \tag{6.20d}$$

$$E_b I_b \frac{\partial^2 w}{\partial x^2}\ |_{x=0\ \&\ x=L} = 0 \text{(with no concentrated moment acting)} \tag{6.20e}$$

For simply supported beams or fixed beams (i.e., when the beam ends are restrained against deflection or both deflection and rotation), Equation 6.19(b) is not required to be solved and the boundary conditions are

$$w\ |_{x=0\ \&\ x=L} = 0 \tag{6.20f}$$

$$\frac{\partial w}{\partial x}\ |_{x=0\ \&\ x=L} = 0 \text{ (for fixed end)} \tag{6.20g}$$

$$E_b I_b \frac{\partial^2 w}{\partial x^2}\ |_{x=0\ \&\ x=L} = 0 \text{ (for hinged end with no applied concentrated moment)} \tag{6.20h}$$

$$\left[E_b I_b \frac{\partial^3 w}{\partial x^3} - 2t_s \frac{\partial w}{\partial x}\right]\ |_{x=0\ \&\ x=L} = 0 \text{ (for hinged end with no applied concentrated force)} \tag{6.20i}$$

The parameters in the above equations are given by

$$k_s(x) = \sum_{i=1}^{n} b \int_{H_{i-1}}^{H_i} \bar{E}_{si}(x,z) \left(\frac{d\phi_i}{dz} \right)^2 dz \tag{6.21a}$$

$$t_s(x) = \sum_{i=1}^{n} \frac{b}{2} \int_{H_{i-1}}^{H_i} G_{si}(x,z) \phi_i^2 dz \tag{6.21b}$$

$$r^{(w)}(x,t) = \sum_{i=1}^{n} \frac{1}{2} \int_{H_{i-1}}^{H_i} f_i p_i(z,t) \frac{d\phi_i}{dz} dz \tag{6.21c}$$

Note that the parameter k_s is analogous to the Winkler spring constant of soil and represents the compressive resistance of soil, and the parameter t_s represents the shear resistance of soil and can be interpreted as the shear force acting between adjacent soil springs that are compressed differently because of the applied load. It is important to note that k_s and t_s vary spatially in the x direction and depend on the properties of both the solid (soil) and beam. The parameter $r^{(w)}$ depends on porosity and fluid pressure (pore pressure), and varies horizontally and with time. It is important to note that the beam and continuum (soil) displacements are time dependent, and this time dependency is taken into account through the parameter $r^{(w)}$. Further, the beam displacement and surface soil displacement function w is coupled with both the vertical pore pressure distribution function p and the soil displacement shape function ϕ by means of the parameters k_s, t_s, and $r^{(w)}$. The function w is also coupled with the pore pressure shape function ψ through the last term $r^{(w)}\psi$ on the left-hand side of Equation 6.19(a,b).

6.4.4 Differential Equation for Horizontal Variation of Pore Pressure in Poroelastic Soil

The differential equation of $\psi(x)$ is obtained as

$$g_r * r_1^{(\psi)} \frac{d^2\psi}{dx^2} + g_r * \frac{\partial r_1^{(\psi)}}{\partial x} \frac{d\psi}{dx} - g_r * r_2^{(\psi)} \psi + r^{(w)} w = 0 \tag{6.22}$$

with the boundary conditions $\psi = 0$ and $d\psi/dx$ at both $x =$ - βL and $x = \beta L$, where

$$r_1^{(w)}(x,t) = \sum_{i=1}^{n} \int_{H_{i-1}}^{H_i} \bar{k}_i f_i p_i^2 dz \tag{6.23a}$$

$$r_2^{(w)}(x,t) = \sum_{i=1}^{n} \int_{H_{i-1}}^{H_i} \bar{k}_i f_i p_i \frac{\partial^2 p_i}{\partial z^2} dz \tag{6.23b}$$

Differentiating Equation 6.22 with respect to time and applying the inverse of the unit convolution integral rule (given by Equation 6.12) to the first three terms on the left hand side results in

$$r_1^{(\psi)} \frac{d^2\psi}{dx^2} + \frac{\partial r_1^{(\psi)}}{\partial x} \frac{d\psi}{dx} - r_2^{(\psi)} \psi + \frac{\partial}{\partial t}(r^{(w)} w) = 0 \tag{6.24}$$

The parameters $r_1^{(\psi)}$ and $r_2^{(\psi)}$ vary horizontally and are functions of time. Thus, the time dependency of the excess pore pressure in Equation 6.24 is partly captured by the parameters $r_1^{(\psi)}$ and $r_2^{(\psi)}$, and partly through the last term $\partial\left(r^{(w)}w\right)/\partial t$ on the left-hand side containing the time derivative. The last term also ensures coupling between the functions ψ and w. The function ψ is coupled with the function p through the parameters $r_1^{(\psi)}$ and $r_2^{(\psi)}$.

6.4.5 Differential Equation for Vertical Variation of Displacement in Poroelastic Soil

The differential equation of $\phi(z)$ within the i^{th} layer is obtained as

$$m_{si} \frac{d^2\phi_i}{dz^2} + \frac{dm_{si}}{dz} \frac{d\phi_i}{dz} - n_{si}\phi_i + r_i^{(\phi)} \frac{\partial p_i}{\partial z} = 0 \tag{6.25}$$

with the boundary conditions are $\phi(0) = 1$ (at the beam-soil interface), $\phi(H_{Total}) = 0$ (at the interface with the bedrock), and $\phi_i(H_i) = \phi_{i+1}(H_i)$ (at the interface of the adjacent layers), where

$$m_{si}(z) = b \int_{-\beta L}^{\beta L} \bar{E}_{si}(x,z) w^2 dx \tag{6.26a}$$

$$n_{si}(z) = b \int_{-\beta L}^{\beta L} G_{si}(x,z) \left(\frac{\partial w}{\partial x}\right)^2 dx \tag{6.26b}$$

$$r_i^{(\phi)}(z,t) = \frac{1}{2} \int_{-\beta L}^{\beta L} f_i \Big[\psi(x) w(x,t)\Big] dx \tag{6.26c}$$

The function ϕ is coupled with the function w through the parameters m_s and n_s, and is coupled with the function ψ through the parameter $r_i^{(\phi)}$. Note that m_s and n_s vary with depth, while $r_i^{(\phi)}$ varies with both depth and time and partly takes into account the time dependency of the soil displacements. The function ϕ is coupled with the function p through the last term $r_i^{(\phi)} \partial p / \partial z$ on the left-hand side of Equation 6.25.

6.4.6 Differential Equation for Vertical Variation of Pore Pressure in Poroelastic Soil

The differential equation of $p(z)$ within the i^{th} layer is obtained as

$$g_r * r_{2,i}^{(p)} \frac{\partial^2 \psi}{\partial z^2} + g_r * \frac{dr_{2,i}^{(p)}}{\partial z} \frac{\partial p_i}{\partial z} - g_r * r_{1,i}^{(p)} p_i + r_i^{(\phi)} \frac{d\phi_i}{dz} = 0 \tag{6.27}$$

with the boundary conditions $p = 0$ at $z = 0$ (at the surface) and $dp/dx = 0$ at $z = H_{total}$ (at the interface of the bedrock) for the single-drainage condition, and $p = 0$ at $z = 0$ and $z = H_{total}$ for the double-drainage condition; and $p_i = p_{i+1}$ at $z = H_i$ (at the interface of adjacent layers), where

$$r_{1,i}^{(p)}(z) = \int_{-\beta L}^{\beta L} \bar{k}_i f_i \psi \frac{d^2\psi}{dx^2} dx \tag{6.28a}$$

$$r_{2,i}^{(p)}(z) = \int_{-\beta L}^{\beta L} \bar{k}_i f_i \psi^2 dx \tag{6.28b}$$

Differentiating Equation 6.27 with respect to time and applying the inverse of the unit convolution integral rule to the first three terms on the left hand side results in

$$r_{2,i}^{(p)} \frac{\partial^2 p_i}{\partial z^2} + \frac{dr_{2,i}^{(p)}}{\partial z} \frac{\partial p_i}{\partial z} - r_{1,i}^{(p)} p_i + \frac{\partial}{\partial t}\left(r_i^{(\phi)} \frac{d\phi_i}{dz} \right) = 0 \tag{6.29}$$

The parameters $r_1^{(p)}$ and $r_2^{(p)}$ vary with depth and couple the functions p and ψ. The last term $r^{(\phi)} d\phi/dz$ on the left-hand side of Equation 6.29 capture the coupling between the functions ϕ and p.

6.5 Inputs, Solution Methodology, and Algorithm

The purpose of the developed model is to compute the long-term, time-dependent consolidation settlement of beams (foundations) by solving the differential Equations 6.19(a,b), 6.24, 6.25, and 6.29 of the functions w, ϕ, p, and ψ. The displacements and pore pressures are functions of time because of which the computations of w, ϕ, p, and ψ are performed with small time increments until the end of the consolidation. Before the calculation of the time dependent consolidation settlement, the model is designed to estimate the initial elastic settlement, which requires the solution of Equations 6.19(a,b), and 6.25 after dropping all the poroelasticity terms associated with p and ψ, and only considering the elastic terms. The total settlement is considered to be the summation of the elastic (immediate) and the consolidation (long-term) settlements.

The geometric inputs required for the analysis are the beam dimensions b, d, and L, and the thicknesses T_i of the different soil layers. The material inputs include the beam Young's modulus E_b, the soil elastic constants E_{si} and υ_{si} of each layer, the reference shear strain $\gamma_{ref}^{(S)}$ of each soil layer, and the coefficient of permeability $\bar{k}_i$ and porosity f_i of each layer. The inputs used for the different problems analyzed in this paper are given in Table 6.1.

6.5.1 1D Finite Element Analysis

In order to obtain solutions using the FE method, the problem domain is discretized into horizontal and vertical strips of thickness Δz and Δx, respectively, as shown in Figure 6.2. The entire soil domain is divided into a grid of $(M_3 - 1) \times (N - 1)$ rectangular cells, each with dimensions $\Delta z \times \Delta x$. The discretization step Δz was chosen such that each horizontal strip lies within a particular soil layer and does not overlap adjacent soil layers. The x-coordinate of the centerline of any vertical strip v is x_v, while the z-coordinate of the centerline of any horizontal strip h is z_h. The v^{th} vertical strip and the h^{th} horizontal strip intersect to form the cell $(v,\ h)$, with the coordinates of its centroid given by $(x_v,\ z_h)$. Two-noded beam and bar elements of length Δx with linear Lagrangian and cubic Hermitian shape functions, respectively, are used to discretize Equations 6.19(a,b) in the x direction such that these elements seat on top of the vertical strips with the nodes placed on top of the vertical interfaces of the adjacent strips. Equation 6.24 is similarly discretized in the x direction using two-noded bar element of length Δx (with linear Lagrangian shape functions). The v^{th} bar or beam element of length Δx seating on top of the v^{th} vertical strip Δx has the ς^{th} and $(\varsigma + 1)^{th}$ nodes as the first (left) and second (right) nodes, respectively. Equations 6.25 and 6.29 are also discretized with two-noded bar elements (with linear Lagrangian shape functions) such that the elements with length Δz fit in with the horizontal strips and the nodes lie on the interfaces of the adjacent horizontal strips (Figure 6.2). The h^{th} bar element of length Δz fitting into the h^{th} horizontal strip has the g^{th} and $(g + 1)^{th}$ nodes as the first (top) and second (bottom) nodes, respectively (Figure 6.2).

6.5.2 Solution Algorithm

The differential Equations 6.19(a,b), 6.24, 6.25, and 6.29 are coupled and solved simultaneously following an iterative algorithm (Figure 6.3). The iterative solution consists of two main interior loops (loops 1 and 2) and one exterior loop (loop 3), in addition to one starting loop (loop 0). The first interior loop (loop 1) is used to obtain the excess pore pressure function p and its companion shape function ψ, described by Equations 6.29 and 6.24, respectively, for predetermined sets of values of w and ϕ. The second interior loop (loop 2) is used to obtain beam-soil displacement w and its companion shape function ϕ, described by Equations 6.19(a,b), and 6.25, respectively, for predetermined values of p and ψ. The two interior loops are performed sequentially with iterations between the loops within the exterior loop (loop 3) until convergence on the values of p, ψ, w, and ϕ are obtained.

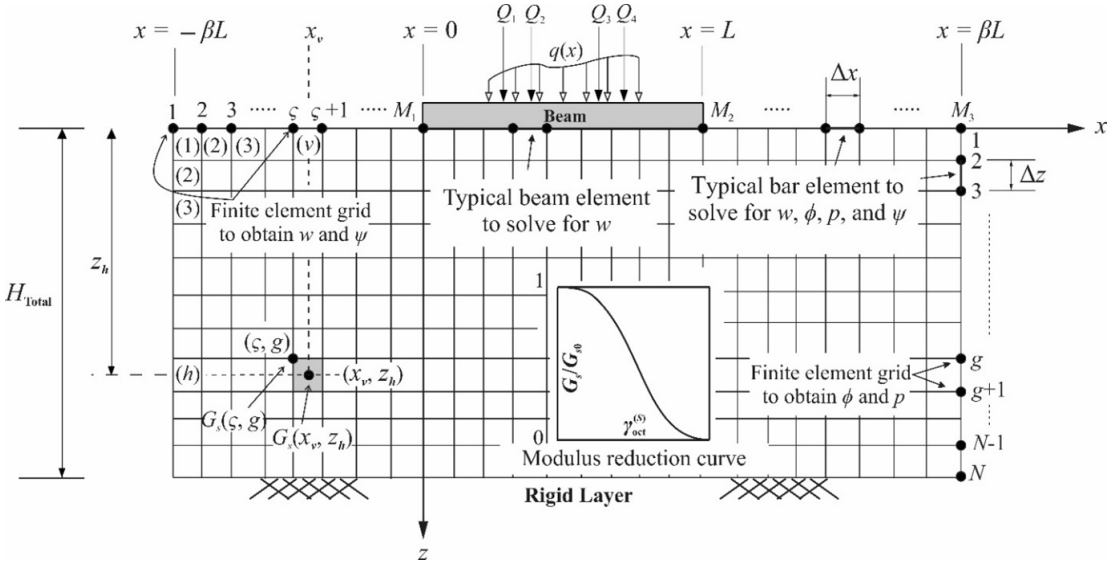

Figure 6.2: Discretization of beam-continuum (soil) system

Because consolidation is a time-dependent process, the calculations are performed at each time step within a specified tolerance for accuracy and convergence. An implicit time integration scheme is used to calculate the consolidation settlement and excess pore pressure dissipation with time. The load is applied incrementally within each time step to capture the nonlinearity of the poroelastic continuum (soil). For each load increment, the displacement functions w and ϕ are used to calculate the soil strain components at the discretized nodes of the grid (Figure 6.2) using Equation 6.6(a). From the calculated strain components, the octahedral shear strains $\gamma_{oct}^{(S)}$ at these nodes are calculated using Equation 6.5. The octahedral strain values are then used in Equation 6.4 to calculate the secant shear modulus $G_s(\varsigma, g)$ for any node (ς, g), which is subsequently used to calculate the reduced soil resistances k_s and t_s (Equations 6.21(a,b)) of nonlinear soil.

For computing the immediate (elastic) settlement, loop 0 is used at the initial stage of the algorithm for time $t = 0$ to solve for w and ϕ only described by Equations 6.19(a,b), and 6.25, respectively, after dropping all the terms and coefficients associated with p and ψ.

6.6 Results

6.6.1 Verification

Three problems are presented in this paper to verify the accuracy of the present analysis. The results from the present analysis are compared with both the results available from other existing analytical and semi-analytical methods and the results obtained from equivalent two-dimensional (2-D) FE analysis. To ensure that the present analysis works for all aspects of the problem, the type of load, the geometry of the problem, the constitutive relation of the soil (linear or nonlinear), the nature of the soil medium (solid or porous), the flexural rigidity of the beam, and the material parameters are varied throughout the verification problems.

In the first verification problem (Problem 1 in Table 6.1), the accuracy in simulating the consolidation process by the present analysis is checked against the one-dimensional consolidation theory by Terzaghi for linear elastic soils. A distributed load $q = 10$ kN/m is applied directedly on the surface of a 5 m thick saturated clay layer (with no beam on top), which is a classical Terzaghi's consolidation problem. Single drainage is assumed such that water flows only upward in the negative z-direction. Figure 6-4 shows the variation of the normalized excess pore pressure θ/p_0 ($p_0 = q$ = initial excess pore pressure in soil) as a function of the normalized depth z/H_{total} for different values of time factor T_v ($T_v = c_v t/H_d^2$ where c_v = coefficient of consolidation = $\bar{k}\bar{E}_s/\gamma_w$ and H_d = maximum drainage path = H_{total} for this problem) obtained from both the analytical solution by Terzaghi and the present analysis. The details of the soil properties and geometries are given in Figure 6.4 and Table 6.1 (corresponding to Problem 1). The maximum difference in the calculated excess porewater pressure obtained from the present analysis and Terzaghi's theory is 6.7%. It is evident that the present analysis can simulate the consolidation process quite accurately.

The second verification problem (Problem 2 in Table 6.1) is used to check the accuracy of the linear poroelastic model. The response of a 30 m long free-free beam resting on a 7.3 m thick saturated clay layer and subjected to a distributed load $q = 48.6$ kN/m is obtained from the present analysis and compared with that obtained by Pe (1995) [179] using a coupled field theory-based method. The double drainage condition was assumed by Pe (1995) [179] for the problem and is maintained the same in the present analysis. The details of the beam and soil properties and geometries are given in Figure 6.5 and Table 6.1 (Problem 2). Figure 6.5 also shows the total settlement (i.e., elastic plus consolidation settlement) profiles $w(x, t)$ along beam half-span obtained from both the present analysis and by Pe (1995) [179] for $t = 40$ days and 80 days. The maximum difference in total

Table 6.1: Details of geometry and properties for the poroelastic continuum (soil) and the beam for the different problems analyzed in this study

Problem Number	**Problem Type**	**Associated Figure(s)**	**Soil Properties**	**Layer 1**	**Layer 2**	**Layer 3**	**Beam Properties**	
1	Verification	5.4	E_s (MPa)	20			E_b (MPa)	
			υ_s	0.15			b (m)	
			T_i (m)	5			d (m)	
			$\gamma_{ref}^{(S)}$	–			L (m)	
			$\bar{k}$ (m/day)	0.0015				
			f	0.49				
2	Verification	5.5	E_s (MPa)	21.5			E_b (MPa)	2068
			υ_s	0.4			b (m)	0.91
			T_i (m)	7.3			d (m)	0.3
			$\gamma_{ref}^{(S)}$	–			L (m)	30
			$\bar{k}$ (m/day)	0.0086				
			f	0.51				
3	Verification	5.6	E_s (MPa)	15	18	20	E_b (MPa)	2000
			υ_s	0.3	0.3	0.4	b (m)	1.0
			T_i (m)	2.0	3.0	3.0	d (m)	0.2
			$\gamma_{ref}^{(S)}$	0.002	0.002	0.002	L (m)	7
			$\bar{k}$ (m/day)	–	–	–		
			f	–	–	–		
4 and 5	Illustration	5.7 and 5.8	E_s (MPa)	25			E_b (MPa)	2300
			υ_s	0.4			b (m)	1.0
			T_i (m)	5			d (m)	Vary
			$\gamma_{ref}^{(S)}$	0.002			L (m)	Vary
			$\bar{k}$ (m/day)	0.0007				
			f	0.5				
6	Illustration	5.9	E_s (MPa)	18	27	36	E_b (MPa)	2000
			υ_s	0.41	0.41	0.41	b (m)	1.0
			T_i (m)	3.0	3.0	4.0	d (m)	0.5
			$\gamma_{ref}^{(S)}$	0.002	0.002	0.002	L (m)	10
			$\bar{k}$ (m/day)	0.0005	0.00038	0.00025		
			f	0.59	0.55	0.51		

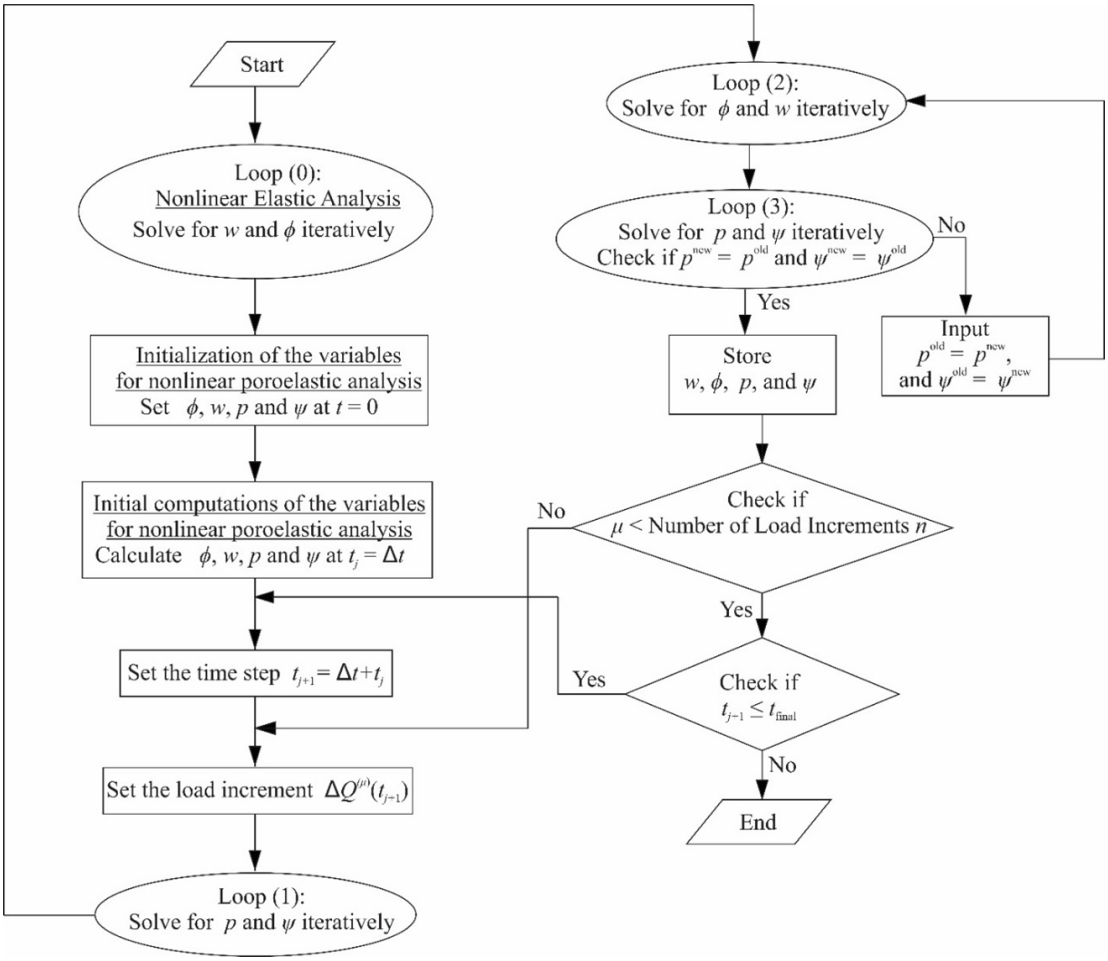

Figure 6.3: Solution algorithm

displacement between that obtained from the present analysis and by Pe (1995) [179] is 4.3% occurring at $t = 80$ days. Thus, the present analysis produces accurate beam response in linear poroelastic continuum.

The third verification example (Problem 3 in Table 6.1) is used to check the accuracy of the model in simulating the nonlinear behavior of the beam-soil system. A comparison of beam responses obtained from the present analysis is made with those obtained from equivalent two-dimensional (2-D) FE analysis (performed using PLAXIS 2-D) in which the same nonlinear elastic soil constitutive relationship is used. Figure 6.6 shows the linear and nonlinear responses of a beam with free ends resting on a three-layer continuum with

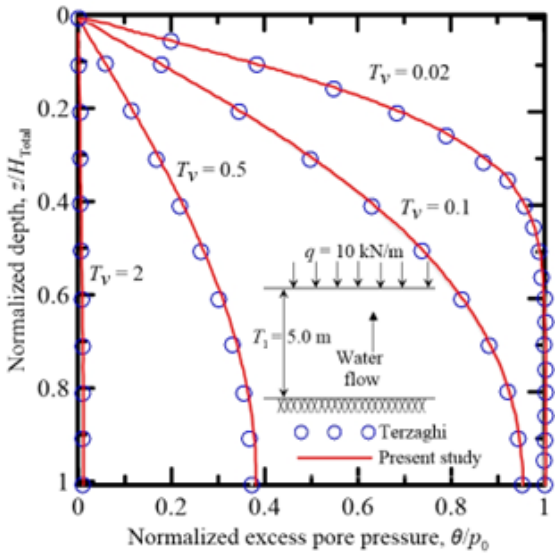

Figure 6.4: Normalized excess pore pressure θ/p_0 versus normalized depth z/H_{total} for different values of time factor T_v obtained from the present analysis and from Terzaghi's theory (Problem 1 of Table 6.1)

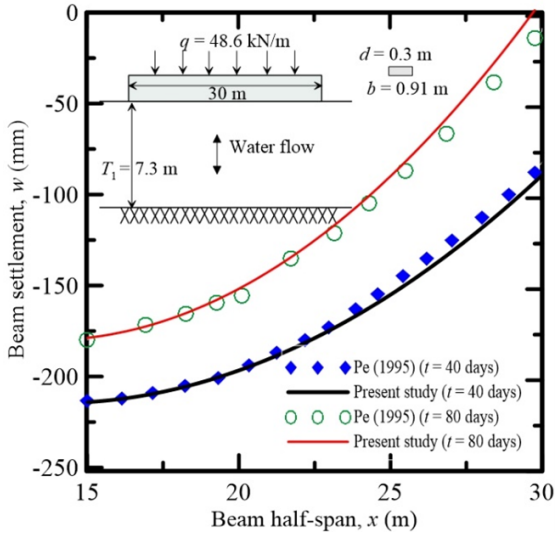

Figure 6.5: Comparison of displacement profiles of a 30 m long beam free at both ends and resting on a linear poroelastic continuum (clay deposit) at time $t = 40$ days and $t = 80$ days (Problem 2 of Table 6.1)

a 40 kN concentrated load acting at the mid-span. The beam and continuum geometries and properties are given in the figure and in Table 6.1 (Problem 3). The input values of Young's modulus (given in Table 6.11) are the initial (small-strain) values (E_{s0}) from which the small-strain shear moduli are calculated using the input values of Poisson's ratio (see Equation 6.17(b)). Equation 6.4 is used to calculate the reduced shear moduli as functions of induced soil strains. For the linear response, the initial moduli are not reduced based on soil strains. The Poisson's ratio is kept constant at the prescribed values for both the linear and nonlinear beam responses. The plotted linear and nonlinear displacement profiles $w(x)$ obtained from both the present analysis and equivalent 2-D FE analysis match well. The difference in the mid-span beam displacements are 5.1% and 6.3% for the linear and nonlinear cases, respectively. The CPU time taken to run the present nonlinear analysis is 28 sec using a computer with Intel CORE i7 3.6-GHz processor and 16GB DDR3 RAM while the time required to run the 2-D nonlinear FE analysis (in PLAXIS) using the same computer is 479 sec (i.e., 17 times greater).

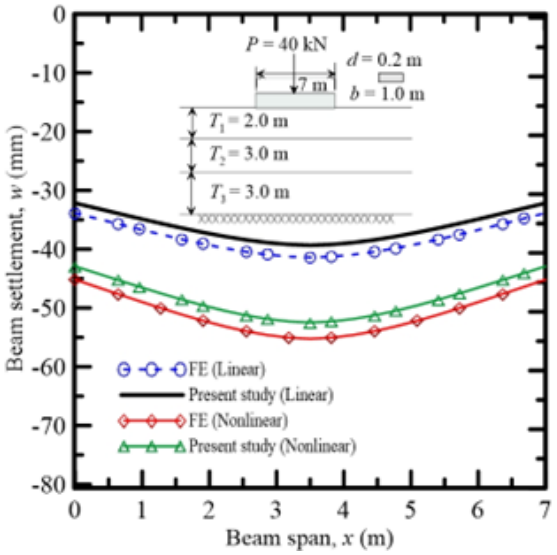

Figure 6.6: Nonlinear and linear elastic displacement profiles of a 7 m-long free beam resting on a three-layer continuum and subjected to a 40 kN point load acting at the mid-span of the beam (Problem 3 of Table 6.1)

6.6.2 Effect of Beam Flexibility on Consolidation Settlement

Two example problems (Figures 6.7-6.8) are analyzed to illustrate the influence of the foundation (beam) flexibility (or flexural rigidity) on the linear and nonlinear consolidation of the beam-soil system. Beams with different lengths and depths are considered for this purpose, as described below.

Free-end beams of lengths L = 2.5 m, 5 m, and 10 m, with a constant depth d = 0.4 m and width b = 1 m and resting on a 5 m thick saturated clay layer are considered, and these beams are subjected to a uniformly distributed sustained load of 50 kN/m acting along their spans (Figures 6.7(a)-(e)). Table 6.1. corresponding to Problem 4 and Figure 6.7 provide the inputs of the problem. Double drainage condition is assumed with the hydraulic conductivity $\bar{k} = 70 \times 10^{-5}$ m/day [45]. The immediate (elastic) settlement profiles wI(x) and the linear/nonlinear final consolidation settlement profiles $w(x, t \to \infty)$ are plotted in Figures 6.7(a,b), respectively. It is evident that for a typical beam-soil geometry and material properties, an increase in the beam span increases both the elastic settlement and final consolidation settlement for linear and nonlinear analysis. Soil nonlinearity also results in an increased beam settlement, as expected. Further, the nature of the deflected shape changes as the flexibility (or rigidity) of the beam changes. For shorter spans, a rigid response is observed while the response resembles that of a flexible beam as the length increases. The difference in the mid-span deflection between the 2.5 m long beam and 10 m long beam is 46.3% and 19.8% for the nonlinear immediate settlement and nonlinear consolidation settlement, respectively. Figures 6.7(a,b) show that the consolidation settlement depends on the flexibility of the foundation, which is completely ignored in Terzaghi's theory.

Figure 6.7(c) shows the linear and nonlinear mid-span consolidation settlement $w(L/2, t)$ as a function of time t and time factor T_v for the different beam lengths. The time factor is defined, following Terzaghi's theory, as $T_v = \bar{k}\bar{E_{s0}}/(\gamma_w H_d^2)$ in this paper, and this definition is applicable to only linear elastic soil. For nonlinear soil, the constrained modulus E_s changes with the progression of consolidation because of which a constant, dimensionless time factor cannot be defined. It is observed that a longer beam produces a greater final consolidation settlement. The time required to attain a particular settlement increases as the beam span increases. Soil nonlinearity reduces the time required to attain a particular (e.g., final) consolidation settlement when compared with the beam response in linear elastic soil.

The profiles of excess pore pressure p with depth z along the vertical section at the mid-span of the beam ($x = 0.5L$) are plotted in Figure 6.7(d) for the different beam lengths at t = 466 days (corresponding to $T_v = 0.1$ for linear elastic soil) and t = 2253

days (corresponding to $T_v = 0.5$ for linear elastic soil). It is clear that the beams with longer spans (i.e., with greater flexibility) dissipate less pore pressure with time resulting in slower consolidation rate compared with that of beams with shorter spans. This is consistent with the results of Figure 6.7(c). The excess pore pressure profiles with depth z along two vertical sections corresponding to $x = 0.5L$ and $x = 0.75L$ are plotted Figure 6.7(e) for the 10 m long beam at time t = 466 ($T_v = 0.1$ for linear soil). The figure shows that the excess pore pressure and its dissipation vary along the beam span and impact the consolidation rate.

Figure 6.8(a)-(c) show the response of free-free beams with a length $L = 10$ m and depths $d = 0.3$ m, 0.75 m and 1.5 m subjected to a uniformly distributed sustained load of 50 kN/m acting along the span of the beam. The beams rest on a 5 m thick single-layer saturated clayey soil with double drainage condition, as shown in Figure 6.8(a)-(c). Table 6.1 corresponding to Problem 5 and Figure 6.8 provides the inputs of this problem (same inputs as those of Problem 4 described in Figures 6.7(a)-(e)).

The linear and nonlinear final consolidation settlement profiles $w(x,\ t \rightarrow \infty)$ of the beams are plotted in Figure 6.8(a). The deflected shapes clearly indicate the influence of the beam flexural rigidity. A greater beam depth resulting in a greater second moment of inertia I_b makes a beam behave more like a rigid element. Figure 6.8(b) shows the mid-span consolidation settlement $w(L/2,\ t)$ versus time, which indicates that beam flexural rigidity has a strong influence on the rate and magnitude of consolidation settlement. The profiles of excess pore pressure p with depth z along the beam mid-span ($x = 0.5L$) are plotted in Figure 6.8(c) for $t = 375$ days (corresponding to $T_v = 0.1$ for linear soil) and $t = 1875$ days (corresponding to $T_v = 0.5$ for linear soil). Beams with greater flexural rigidities dissipate excess pore pressure at a faster rate.

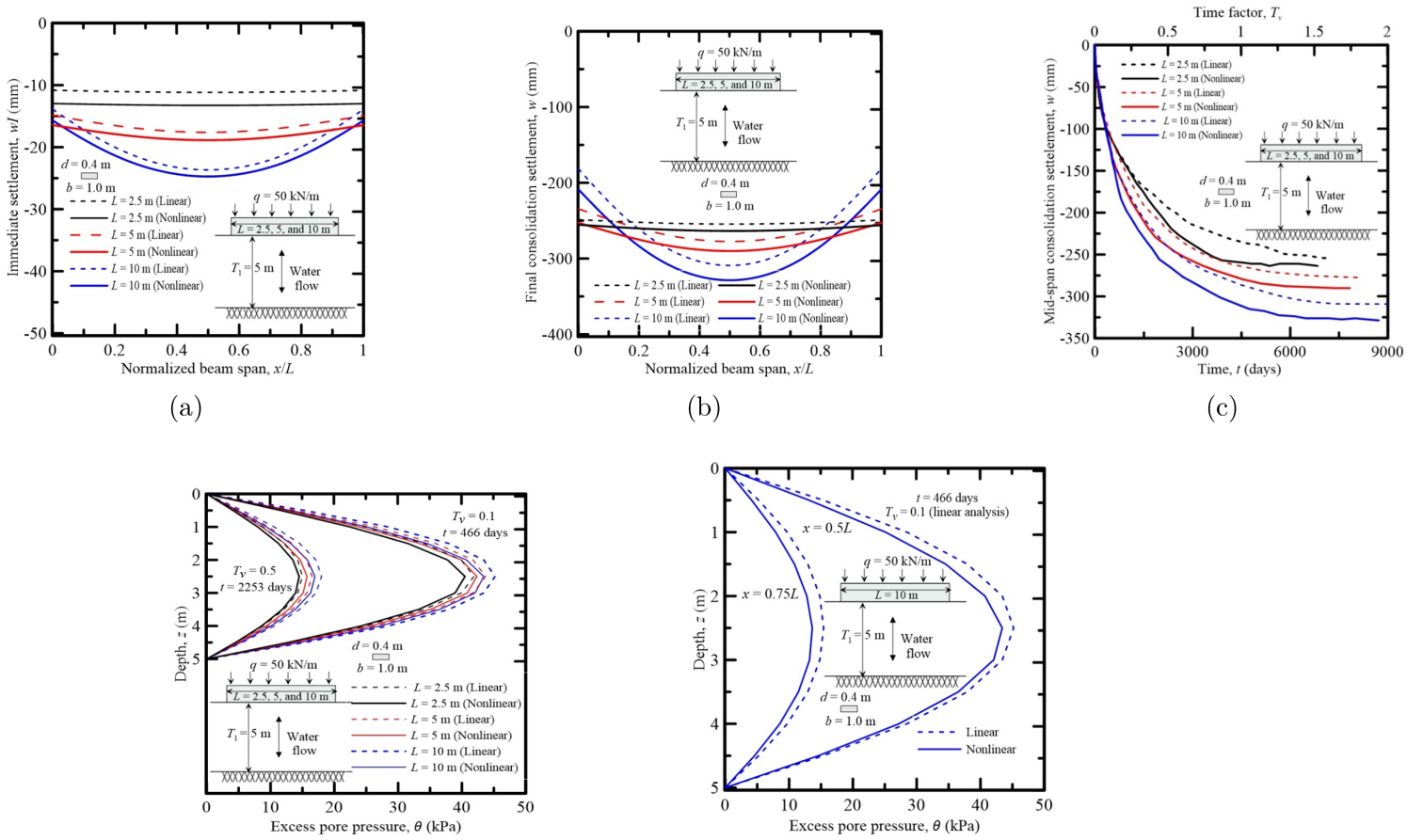

Figure 6.7: Linear and nonlinear poroelastic responses of free-end beams of different lengths resting on a 5 m thick saturated clayey deposit with double drainage and subjected to a uniformly distributed load of 50 kN/m (Problem 4 of Table 6.1): (a) immediate settlement profiles of the beams; (b) settlement profiles of the beams at the end of the consolidation; (c) mid-span settlement of beams with time as consolidation progresses; (d) excess pore pressure profiles with depth at the mid-span ($x = 0.5$L) of the beam for $t = 466$ and $t = 2253$ days; (e) excess pore pressure profiles with depth at two vertical sections corresponding to $x = 0.5$L and $x = 0.75$L for time $t = 466$ days (Note: In the different figures, T_v is applicable only for linear elastic soils)

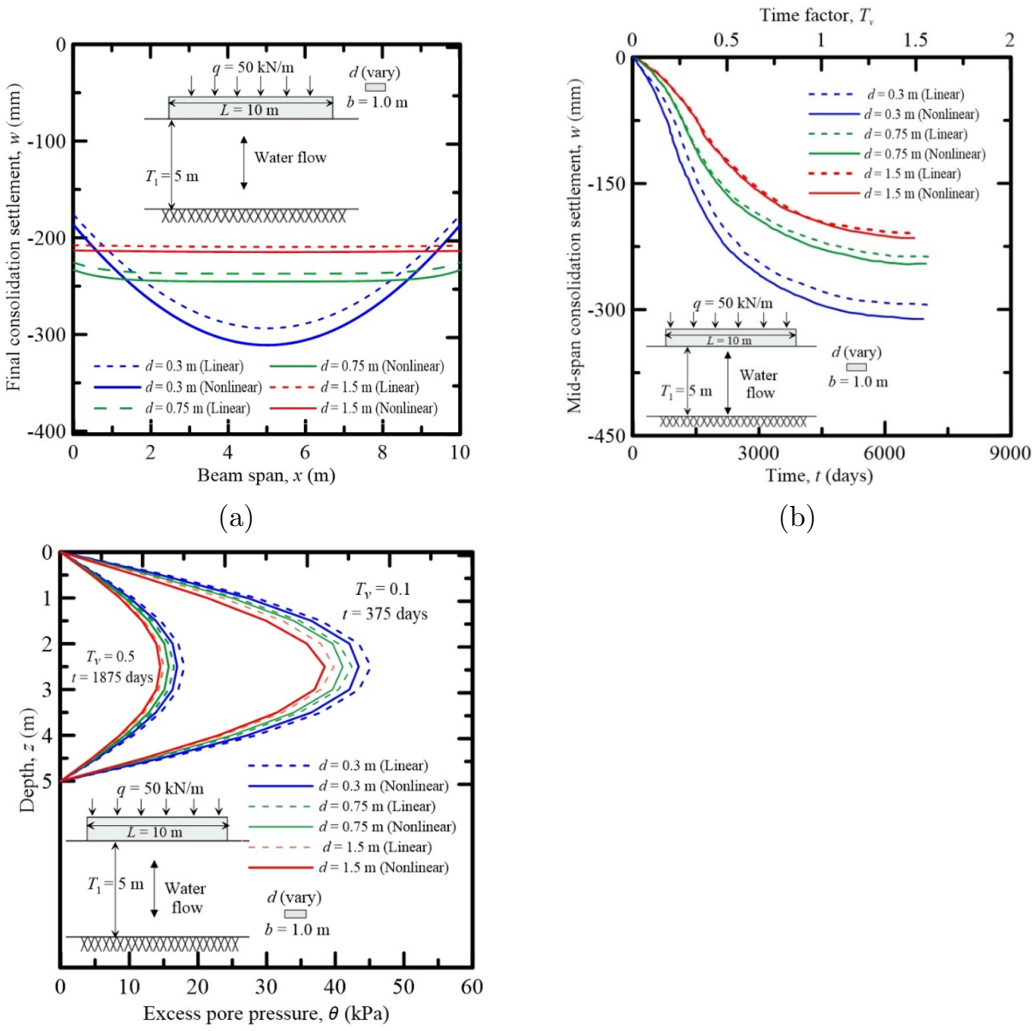

le 6.1): (a) settlement profiles of the b

Figure 6.8: Linear and nonlinear poroelastic response of 10 m-long free-free beams with different depths d resting on a 5 m thick saturated clayey deposit with double drainage and subjected to a uniformly distributed load of 50 kN/m (Problem 5 of Tabeams at the end of the consolidation; (b) mid-span settlement of beams with time as consolidation progresses; and (c) excess pore pressure profiles with depth at the mid-span (x = 0.5L) of the beam at t = 375 days and t =1875 days (Note: T_v is applicable only for linear elastic soils)

6.6.3 Characteristics of the Nonlinear Poroelastic Beam-Soil System

The nonlinear characteristics of the beam-poroelastic continuum (soil) system is illustrated through a problem described in Figures 6.9(a)-(e) (Problem 6 of Table 6.1). A 10 m long beam rests on a three-layered saturated clayey deposit with a single drainage condition and with different coefficients of hydraulic conductivity $\bar{k}_i$ in different layers. The beam is subjected to a sustained point load of 60 kN acting at the mid-span, as shown in Figure 6.9. Table 6.1 corresponding to Problem 6 and Figure 6.9(a) give the details of the inputs.

Figure 6.9(a) shows the normalized excess pore pressure θ/p_0 profiles over normalized depth z/H_{Total} at the mid-span for t = 0.91, 5.2, and 9.8 years (which corresponds to T_v = 0.1, 0.5, and 1.0 for linear elastic soil). The normalization is done with respect to the initial excess pore pressure p_0 at the beam-soil interface, which is the same as the contact stress at $t = 0$ and is given by

$$p_0 = -2t_s \frac{\partial^2 w}{\partial x^2} + k_s w - 2\frac{dt_s}{dx}\frac{\partial w}{\partial x} \tag{6.30}$$

The effect of soil layering (with different values of $\bar{k}$ and E_{s0} in different layers) is clear in the pore pressure profile plots. Further, soil nonlinearity accelerates the excess pore pressure dissipation, as evident from Figure 6.9(a), and therefore, impacts the rate of consolidation settlement, which is evident from Figure 6.9(b). The final consolidation settlement increased by 13.6% because of nonlinearity in the soil, as is evident from the linear and nonlinear mid-span consolidation settlement $w(L/2,\ t)$ plots shown in Figure 6.9(b).

The normalized profiles of secant shear modulus G_s/G_{s0} with depth z along the vertical section through the mid-span of the beam are shown in Figure 6.9(c) at time t = 0.91, 5.2, and 9.8 years, corresponding to T_v = 0.1, 0.5, and 1.0 for the linear elastic soil. The secant shear modulus decreases with time as the strains (and displacements) in soil increase with the progression of consolidation. Further, the depth over which nonlinear straining occurs increases as the consolidation progresses.

The variation of the soil parameters k_s and t_s with time are plotted in Figures 6.9(d)-(e) for the vertical section along the mid-span of the beam. Note that, for nonlinear soils, k_s and t_s are different at different vertical sections along the span (i.e., these parameters vary spatially along the span of the beam). These k_s and t_s are lower in magnitudes for nonlinear soil than for the corresponding linear soil, as expected (this explains why displacements are more for nonlinear soil than for linear soil). The time-dependent 'viscous' behavior of

the porous soil (continuum) because of the dissipation of excess pore pressure with time gets reflected in the asymptotic time dependent decrease of k_s and t_s, as shown in Figures 6.9(d)-(e).

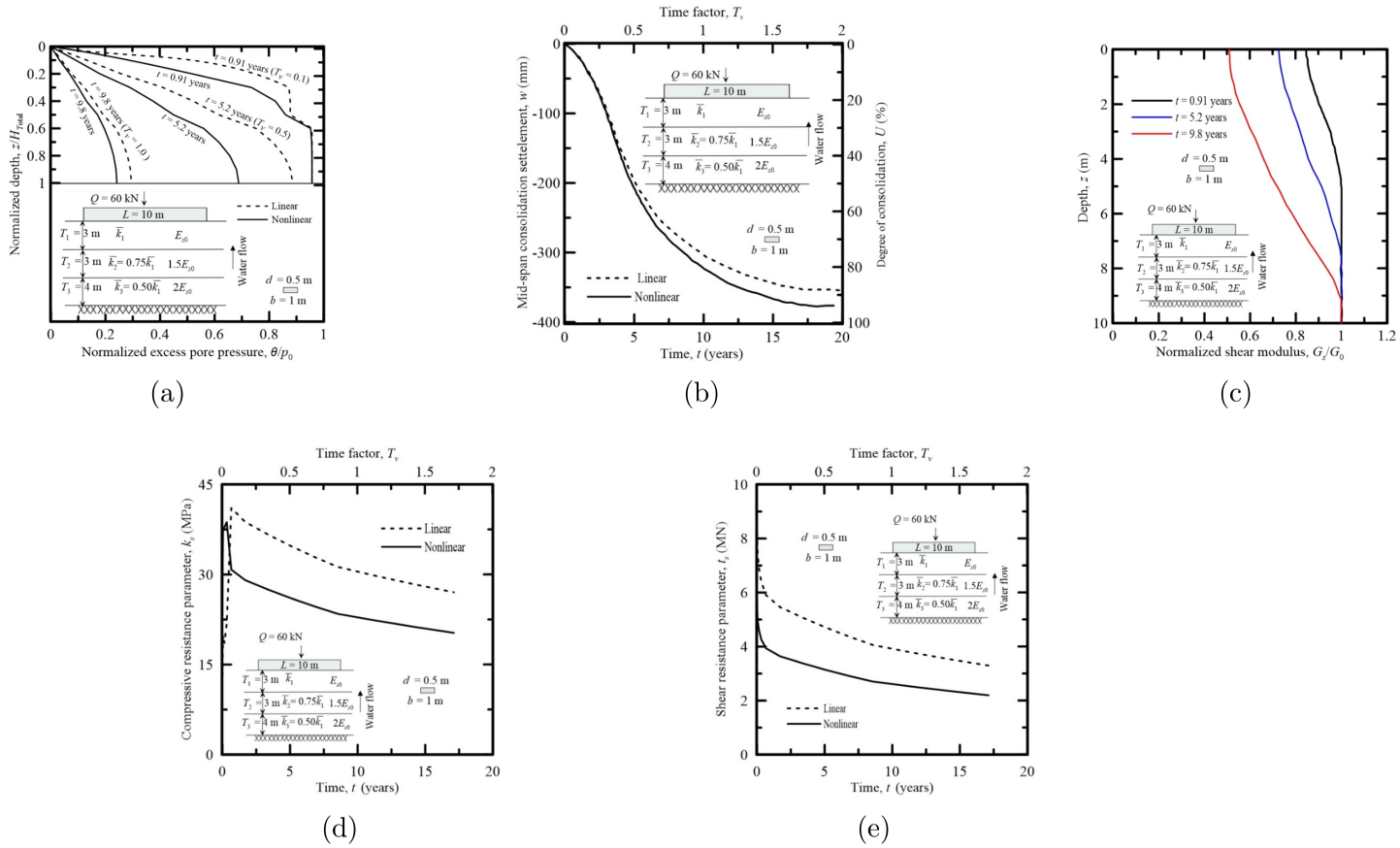

Figure 6.9: Nonlinear characteristics of a 3-layer poroelastic clayey deposit with single drainage beneath a 10 m-long free-free beam subjected to a 60 kN point at the mid-span (Problem 6 of Table 6.1): (a) normalized excess pore pressure profiles θ/p_0 with normalized depth z/H_{Total} along a vertical section at the mid-span (x = 0.5L) of the beam for time t = 0.91, t = 5.2, and t = 9.8 years (corresponding to T_v = 0.1, 0.5, and 1.0); (b) mid-span beam settlement and degree of consolidation with time; (c) variation of normalized shear modulus G_s/G_{s0} of soil with depth along the vertical plane at the mid-span of the beam for different times t = 0.91, t = 5.2, and t = 9.8 years; (d) time-dependent response of soil compression parameter k_s at the beam mid-span (x = 0.5L); and (e) time-dependent response of soil shear parameter t_s at the beam mid-span (x = 0.5L) (Note: T_v is applicable only for linear elastic soils)

6.7 Conclusions

A new analysis method is developed for calculating the consolidation settlement of flexible beams (foundations) resting on nonlinear, multilayered poroelastic continuums (soils). A simplified continuum model is assumed to represent the poroelastic soil in which the displacements and pore pressures are expressed as products of separable functions. The poroelastic soil is assumed to follow Biot's consolidation theory. The variational principles of mechanics is used in the analysis in which a total energy functional is developed and minimized to obtain the four Euler-Lagrange differential equations governing the time-dependent displacement and excess pore pressure in the beam-soil system. The differential equations are solved using one-dimensional finite element analysis. As these differential equations are coupled, they are solved simultaneously following an iterative algorithm. An implicit time-integration scheme is used to obtain the displacements and excess pore pressure as functions of time.

In the analysis, soil nonlinearity is considered by using a nonlinear-elastic soil constitutive model in which the stresses and strains are related through a hyperbolic constitutive equation developed for clayey soils. In the constitutive model, the reduction of the secant shear modulus is expressed as a function of the induced strain in soil, which is considered to be the octahedral shear strain in this analysis. The poroelastic soil domain is discretized into a two-dimensional grid such that the degraded shear modulus is calculated at the grid points and incorporated into the finite element discretized forms of the differential equations to obtain the nonlinear beam response. To capture the nonlinear response as a function of the loading history, the imposed sustained loads are applied incrementally within each time step.

The inputs required for the analysis are the magnitude and type of applied loads; geometry and Young's modulus of beam; and layering, initial elastic constants, permeability, porosity, drainage condition, and an appropriate modulus reduction equation (constitutive model) of soil. These inputs can be conveniently given to the code through a text file without any requirement for generation of the analysis domain and numerical mesh (as is required in finite element analysis). Thus, no specialized knowledge of numerical methods is required for performing the analysis. Further, the results from this analysis are obtained within minutes in a computer with Intel CORE i7 3.6-GHz processor and 16GB DDR3 RAM. The accuracy of the analysis is verified with both the results obtained from existing analytical sand emi-analytical methods, and with 2-D nonlinear finite element analysis (performed using PLAXIS). Thus, the analysis framework provides a rigorous, easy-to-use, and quick methodology for analyzing beams and similar flexible foundations (such as strip foundation) resting on nonlinear poroelastic soils subjected to sustained loads.

Three example problems are analyzed to demonstrate the use of the analysis and highlight the nonlinear poroelastic characteristics of the beam- soil system. The numerical results presented in the paper indicate that the interaction between the linear or nonlinear soil and the beam depends on the beam slenderness (aspect) ratio and the relative stiffness of the beam and soil. The magnitude of beam (foundation) settlement, the rate of consolidation settlement, and the rate of dissipation of the excess pore pressure depend on the flexibility (or rigidity) of the beam. This aspect is not taken into account in the widely used Terzaghi's consolidation theory.

Soil nonlinearity accelerates the consolidation process and produces larger consolidation settlements than linear elastic soils. The soil modulus degrades gradually over time in nonlinear elastic soils as the consolidation process progresses. The presence of soil layering with different values of soil permeability and modulus in different layers impact the dissipation of excess pore pressure and the consolidation rate. The soil compression and shear parameters, k_s and t_s, are affected by the poroelasticity and nonlinearity of soil. These parameters have lower values in nonlinear soils than in linear soils, and decrease with time in an asymptotic manner as the consolidation progresses.

Chapter 7

Dynamic Analysis of Beams Vibrating on Nonlinear Poroelastic Multi-layered Continuum

This chapter is published Manuscript in the International Journal for Numerical and Analytical Methods in Geomechanics, available online: https:// http://doi.org/10.1002/nag.3479, Elhuni, Hesham, and Dipanjan Basu. Elhuni, H., Basu, D. (2022). Dynamic analysis of beams vibrating on nonlinear poroelastic multi-layered continuum. International Journal for Numerical and Analytical Methods in Geomechanics.

7.1 Overview

The paper presents a framework for analysis of beams interacting with nonlinear-poroelastic, layered continuums (e.g., clayey soils) when subjected to time-dependent loads. The poroelastic layered continuum is characterized by a nonlinear-elastic constitutive relationship that relates the secant shear modulus to the induced shear strain. The Biot's theory of consolidation is combined with a dynamic beam-continuum interaction model to develop the analysis. The vertical consolidation settlement of the beam and the excess pore pressure in the porous continuum are assumed to be products of separable functions, and the extended Hamilton's principle of least action is applied to obtain the differential equations governing the inertial consolidation motion of the beam-continuum system and the dissipation of excess pore pressure. An iterative numerical algorithm is used to solve these coupled

differential equations following one-dimensional finite element analysis in which the implicit Wilson-θ time integration scheme is used to obtain the time history of beam and continuum responses. The novelty of the framework is that it rigorously takes into account the nonlinear poroelastic soil-structure interaction within a dynamic time-integration framework with minimal computational resources. The characteristics of this newly developed model are illustrated through examples.

7.2 Introduction and Related Literature

Poroelastic media usually comprise a porous elastic solid skeleton phase and a Newtonian viscous fluid phase that completely fills up the pores of the solid [208]. Such two-phase systems are characterized by time-dependent deformations when subjected to applied loads [60]. Because of the applied loads, a hydraulic gradient is generated, and the fluid migrates out of the pores of the solid over a finite period of time as the solid skeleton reduces in volume [111]. The theory of poroelasticity rigorously captures the coupled fluid flow and mechanical deformation of saturated porous solids and is applicable to clay consolidation problems [60]. Biot (1956) [38] developed the coupled consolidation theory by connecting soil deformation, modeled using the theory of elasticity, with fluid/water flow through soil, modeled using the generalized Darcy's law. In Biot's theory, the fluid pressure is assumed to generate volumetric strains in the poroelastic media so that it behaves as an isotropic deformable solid and reduces in volume when all the excess fluid pressure dissipates [182]. Thus, two sets of equations, one set governing the elasticity-based force equilibrium and the other set governing Darcy's law-based fluid flow, are used to model the stress coupling and velocity coupling between solids and fluids [60].

Biot's theory has been extensively used for obtaining solutions to different soil-structure interaction problems in the field of engineering and physics. However, only a limited number of studies are available in which the dynamic soil-structure interaction with inertia effects are considered [32]. For example, Lu et al. (2018) [156] calculated the dynamic cumulative undrained strains and pore pressures induced in a saturated poroelastic soil underlying an embankment track subjected to traffic-induced vibrations modeled as a discrete multi degree of freedom system. Senjuntichai et al. (2020) [209] analyzed the dynamic response of a buried circular footing interacting with poroelastic clayey soil using Mindlin's solution, integral transformation method and FE analysis. Santana et al. (2016) [199] investigated the dynamic and seismic responses of buildings resting on saturated poroelastic and viscoelastic soils using Biot's theory. Different simplified poroelastic continuum models have also been used to represent the soil underneath beams and the dynamic responses

have been obtained. For example, Xu et al. (2007) [258] and Sun et al. (2018) [217] analyzed infinite beams resting on linear poroelastic half-spaces and subjected to moving point loads using different integral transform methods. Di et al. (2018) [74] studied the interaction between a vehicle-track mass-spring model and a poroelastic half-space using finite elements and Green's functions. Shi and Selvadurai (2016) [211] analyzed using Fourier transform the interaction problem of a vehicle moving on a track supported by a saturated poroelastic soil subgrade. Cao and Cai (2013) [52] also used the Fourier transform method to analyze the interaction of an elastic soil embankment subjected to traffic loads with a linear poroelastic saturated half-space. Cao and Boström (2013) [51] analyzed using Fast-Fourier transforms and Fresnel integrals the problem of a railway-track system interacting with a linear poroelastic half-space and subjected to a time-history excitation. A few dynamic interaction studies have focused particularly on the consolidation settlement of foundations. Todorovska and Rjoub (2006) [229] analyzed consolidation settlement of shear beams on poroelastic soil using Fourier series. Ma et al. (2009) [159] and Lin et al. (2013) [150] analyzed the consolidation settlement of rigid footings on poroelastic soil using the boundary element method and the Precise Integration method, respectively. Han et al. (2019) [103] treated footings on poroelastic soil as multi-degree of freedom systems and obtained their consolidation settlement using the boundary element method.

The studies described in the preceding paragraph do not take into account the stress-strain nonlinearity of soil. Soil is highly nonlinear and accounting for the nonlinearity in foundation settlement is important. Settlement calculations for beams and shallow flexible foundations are usually done using the Winkler soil spring approach in which the soil is represented as a bed of springs characterized by a spring constant ks that is related to soil subgrade modulus [220] . Nonlinearity is approximately taken into account by representing ks as a nonlinear function of beam displacement. However, the nonlinear spring approach cannot properly take into account the stress-strain nonlinearity and, more importantly, cannot model the consolidation settlement of a poroelastic continuum. Stress-strain nonlinearity in a poroelastic continuum can be modeled using two-dimensional (2D) or three-dimensional (3D) numerical methods like the finite element (FE) and finite difference (FD) methods. However, these methods are computationally expensive and require specialized expertise for their use. The simplified continuum models, such as those of Reissner (1936) [189] and Vlasov and Leont'ev (1966) [247]in which the beam rests on a continuum (soil) with simplified stress or displacement fields, provide an opportunity to explicitly take into the stress-strain nonlinearity [102], soil consolidation [179], and dynamic interaction [87] with much less computational resources. However, no studies are available in which the inertia-based dynamic response of a beam or shallow foundation resting on a poroelastic simplified continuum with stress-strain nonlinearity is investigated.

In this chapter, a semi-analytical simplified continuum-based analysis framework is developed for beams and flexible shallow foundations resting on nonlinear poroelastic solids (soil) subjected to time-dependent loads. The soil is treated as a two-phase (soil solid and water) continuum following Biot's theory of poroelasticity, and the stress-strain nonlinearity in soil is implemented by varying the soil shear modulus and damping ratio as functions of the induced soil strain. The beam is assumed to follow the Euler-Bernoulli theory, and the vertical soil displacement and pore pressure are assumed to be products of separable functions. The potential and kinetic energy functionals for the beam-soil system is developed considering the dynamic-time-dependent consolidation process. The energy functionals are then minimized using Hamilton's principle of least action to obtain a system of coupled differential equations governing the dynamic behaviour of the beam-poroelastic soil system. The one-dimensional FE method is used to solve the differential equations using an iterative algorithm. The accuracy, computational efficiency, and applicability of the method are demonstrated through multiple numerical examples. The effect of soil nonlinearity on the beam and soil responses are demonstrated through the examples.

7.3 Model Description

7.3.1 Beam-Poroelastic Continuum System

The plane strain foundation-soil interaction model used in this analysis is shown in Figure 7.1. The flexible shallow foundation is composed of a homogeneous, isotropic and elastic solid represented as an Euler-Bernoulli beam of length L and uniform rectangular cross-sectional area A_b ($= bd$) with width b and depth (thickness) d. The flexural rigidity of the beam is E_bI_b where E_b = Young's modulus of beam and I_b = second moment of inertia of beam cross section = $bd^3/12$, and its mass per unit length is ρ_b. The layered continuum (clayey soil) beneath the foundation comprises a two-phase medium with a solid (soil) skeleton with interconnected pores (voids) that are completely filled with an isotropic, viscous, and incompressible Newtonian fluid (which is water in the case of soil). The two-phase continuum (i.e., fully saturated soil) is considered to have the same width b as that of the beam and consists of n layers with the bottom (n^{th}) layer resting on a rigid substratum (e.g., bed rock or very dense sand). The i^{th} layer extends vertically downward to a depth H_i such that the thickness T_i of the i^{th} layer is H_i - H_{i-1} (with $H_0 = 0$). The total thickness of the continuum (soil deposit) is $H_{Total}(\sum_{i=1}^{n} T_i)$. Each poroelastic layer i is assumed to be isotropic and heterogeneous with spatially varying Young's modulus E_{si},

Poisson's ratio of υ_{si}, porosity f_i, coefficient of permeability $\bar{k_i}$, soil mass density ρ_{Si}, and fluid (water) density ρ_F (Figure 7.1). Further, the multi-layered continuum is assumed to follow Biot's theory of poroelasticity [38]. The beam and poroelastic continuum (soil) are assumed to be in full contact at all times, and the interface friction is neglected.

A Cartesian $x-z$ coordinate system is considered attached to the left end of the beam with x direction positive to the right, and z direction positive vertically downward (Figure 7.1). In order to capture the accurate response of the beam-foundation (soil) system without any boundary effects, the analysis domain is assumed to extend beyond the two-ends of the beam (for beams with free ends) to a length βL (where $\beta \geq 1$ and its value is determined through trial and error) in positive and negative x directions, respectively (Figure 7.1).

It is assumed that the displacements in the beam and continuum are small and occur only in the vertical direction (i.e., the horizontal displacements are assumed to be negligible). Further, fluid flow in the poroelastic continuum (soil) is assumed to occur only in the vertical direction. The fluid pressure in the pores (i.e., the pore pressure) becomes zero at the ground surface (i.e., at the interface of the beam and continuum where $z = 0$). The interface between the bottom (n^{th}) layer and the hard substratum (bed rock) at $z = H_{Total}$ may be permeable allowing free drainage (double-drainage condition) or may be completely impermeable (single drainage condition). Accordingly, the pore pressure at $z = H_{Total}$ may or may not be zero.

7.3.2 External Forces

Simulating the consolidation settlement requires that external loads are applied on the beam-foundation system. The loads acting on the beam may be static in nature or may change in magnitude and/or position over time t such that the quasi-static condition or dynamic condition can modeled, respectively. In this study, the applied loads are vertical, time dependent, and can be distributed spatially ($q(x,\ t)$) or concentrated at different discrete points x_j ($Q_j(x_j,\ t)$) (Figure 7.1).

7.3.3 Coupling of Porous Soil and Water

A two-dimensional (2D) representative element (RE) of the two-phase medium that obey the plane-strain condition is considered (Figure 7.1). The RE is chosen to be large enough compared to the size of the pores such that uniform water pressure can be assumed through out the pores (the consolidation process is sufficiently slow so that the water pressure will

redistribute between pores and the pressure difference vanishes within the RE). At the same time, the RE is chosen small enough compared to the scale of the soil continuum so that it may be considered infinitesimal in the mathematical sense. A stress state is assumed by means of average stress components distributed uniformly on the faces of the RE, as shown in Figure 7.1.

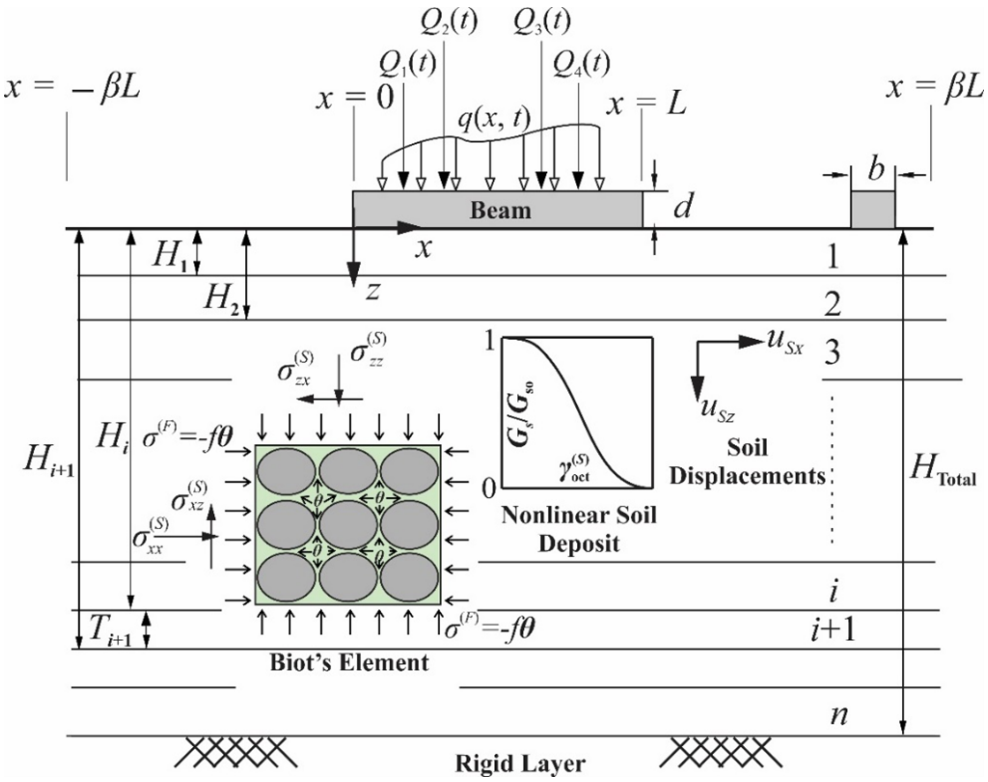

Figure 7.1: Beam resting on nonlinear, poroelastic and multi-layered continuum (soil)

According to Biot's theory, the stresses in a poroelastic solid (soil) RE are composed of two parts: an equivalent fluid stress $\sigma^{(F)}$ and the average stress in the soil skeleton $\sigma^{(S)}$. The equivalent fluid stress $\sigma^{(F)}$ is assumed to be proportional to the excess pore pressure θ (the actual pressure in the fluid occupying the pores) and are related through the volume fraction of the pores with respect the bulk volume such that

$$\sigma^{(F)} = -\left(\frac{V_{pore}}{V_{bulk}}\right)\theta = -f\theta \tag{7.1}$$

where f = porosity of the porous medium (soil) = V_{pore} / V_{bulk}, V_{pore} is the volume of

the pores (voids) and V_{bulk} = bulk volume of the porous medium, and the negative sign indicates that $\sigma^{(F)}$ generates tension on the faces of the RE (Figure 7.1) [38]. The total stress in the RE is a summation of the skeleton stress $\sigma^{(S)}$ and the equivalent fluid stress $\sigma^{(F)}$ (stresses are carried partly by the fluid and partly by the porous solid). Thus, the total stress representative tensor for the RE considering the plane strain problem is given by

$$\sigma^{Total} = \begin{bmatrix} 0 & 0 & \sigma_{xz}^{(S)} \\ 0 & 0 & 0 \\ \sigma_{zx}^{(S)} & 0 & \sigma_{zz}^{(S)} + \sigma_{zz}^{(F)} \end{bmatrix} \tag{7.2}$$

To complete the description of mechanical coupling between the solid and fluid, Biot used the generalized Darcy's law to describe fluid flow through the pores during the consolidation process. The generalized form of Darcy's law for unidirectional vertical flow under plane-strain condition is given by

$$-\bar{k}\left(\frac{\partial\theta}{\partial z} + \frac{\partial\theta}{\partial x}\right) = \left(\frac{\partial u_{Fz}}{\partial t} - \frac{\partial u_{Sz}}{\partial t}\right) \tag{7.3}$$

where u_{Sz} = vertical displacement of the solid skeleton of the RE, u_{Fz} is the vertical displacement of the fluid in the RE. Equations 7.1-7.3 ensure force and momentum balance in the poroelastic continuum in the absence of body forces [37].

7.3.4 Nonlinearity and Damping in Soil

In this chapter, the soil is assumed to be nonlinear elastic characterized by two pair of elastic constants such as E_s and υ_s or G_s and υ_s (E_s = Young's modulus, G_s = shear modulus, and υ_s = Poisson's ratio). It is common in geotechnical engineering to assume υ_s to be a constant (i.e., it is assumed that the nonlinearity has no significant impact on υ_s), and relate G_s with the shear strain to take into account the nonlinearity [213]. It is, in fact, well established that the shear stress-shear strain relationship of soil is nonlinear, hysteretic, and effective stress dependent [204]. Several studies have experimentally established the nonlinearity in soil in terms of modulus reduction curves in which G_s is plotted as a function of the engineering shear strain γ in soil [76]. Alternatively, the reduction of G_s with γ has been expressed as nonlinear elastic hyperbolic constitutive models [266, 244].

In the present thesis, the nonlinear elastic model of Vardanega and Bolton (2013) [244] for clayey soils is adopted, which was developed based on the results of 67 laboratory tests performed on a variety of clayey soils

$$\frac{G_s}{G_{s0}} = \left[1 + \left(\frac{\gamma^{(S)}}{\gamma^{(S)}_{ref}}\right)^{\alpha}\right]^{-1} \tag{7.4}$$

where G_s is the secant shear modulus in clayey soil, G_{s0} is the initial (small-strain) shear modulus in the clayey soil, $\gamma^{(S)}_{ref}$ (= 0.002) is a reference shear strain in the soil or the shear strain at failure or the shear strain at which the initial shear modulus G_0 is reduced to 50% of its initial value [266, 244], α (= 0.736) is a parameter describing the curvature of the nonlinear stress-strain relationship, and $\gamma^{(S)}$ is the engineering shear strain in the soil. For the present plane strain problem, it is reasonable to represent $\gamma^{(S)}$ by the octahedral engineering shear strain of the solid (soil), given by

$$\gamma^{(S)}_{oct} = \frac{2}{3}\left[2\left(\varepsilon^{(S)}_{zz}\right)^2 + 6\left(\varepsilon^{(S)}_{xz}\right)^2\right]^{\frac{1}{2}} \tag{7.5}$$

Two fundamentally different damping phenomena are associated with dynamic soil behavior, namely, radiation damping and material damping. Radiation damping is caused by waves traveling away from the region of interest, which is implicitly incorporated into the present analysis by introducing two decay functions ϕ(z) and ψ(x) for the displacement and the pore pressure, respectively, as described later. Material damping is caused by internal energy dissipation that arises from a complex molecular interaction within the material. The internal energy dissipation in soil is characterized by a hysteretic mode, which is largely dependent on the shear strain level [105].

It is typical in soil dynamics to represent the material damping by the damping ratio ζ. Factors that affect the damping ratio are friction between soil particles, strain rate, and nonlinear stress-strain behaviour [266]. The damping ratio varies with induced soil strain and a nonlinear relationship between ζ and $\gamma^{(S)}$ exists [105]. However, well established functional relationships (equations) applicable to a wide range of clayey soils are not available, because of which the effect of strain-compatible damping is taken into account in this study by adapting the principle of Rayleigh damping [186]. According to Rayleigh, the damping matrix [C] is in part composed of the mass matrix [M] and in part of the stiffness matrix [K], and the contributions of the mass and stiffness matrices are governed by the Rayleigh coefficients α_1 and α_2 as

$$[C] = \alpha_1[M] + \alpha_2[K] \tag{7.6}$$

where α_1 and α_2 are scalars with units of 1/sec and sec, respectively [63], and are given as inputs in the analysis. The stress-strain nonlinearity impacts [M] and [K] because of which the strain-compatible damping is considered in this framework.

7.4 Analytical Framework

7.4.1 Displacements, Strains, and Stresses in Two-Phase Medium

The poroelastic solid (soil) responds to both compression (or extension) and shear stresses, but the Newtonian fluid (water) responds only to normal stresses. The horizontal displacement in the solid is assumed to be negligible and the horizontal displacement in the fluid is zero because the flow is assumed to occur only in the vertical direction. Denoting the vertical displacements in the solid and fluid respectively as u_{Sz} and u_{Fz}, and the strain tensors in the solid and fluid respectively as $\varepsilon^{(S)}$ and $\varepsilon^{(F)}$, the following strain displacement relationships can be obtained

$$\varepsilon^{(S)} = \begin{Bmatrix} \varepsilon_{xx}^{(S)} \\ \varepsilon_{zz}^{(S)} \\ \varepsilon_{xz}^{(S)} \end{Bmatrix} = \begin{Bmatrix} 0 \\ -\dfrac{\partial u_{Sz}}{\partial z} \\ -\dfrac{1}{2}\dfrac{\partial u_{Sz}}{\partial x} \end{Bmatrix} \tag{7.7a}$$

$$\varepsilon^{(F)} = \begin{Bmatrix} \varepsilon_{xx}^{(F)} \\ \varepsilon_{zz}^{(F)} \\ \varepsilon_{xz}^{(F)} \end{Bmatrix} = \begin{Bmatrix} 0 \\ -\dfrac{\partial u_{Fz}}{\partial z} \\ 0 \end{Bmatrix} \tag{7.7b}$$

The elastic constitutive relationship relates the strain tensor $\varepsilon^{(S)}$ at any point within the solid to the stress tensor $\sigma^{(S)}$ as (Figure 7.1)

$$\sigma^{(S)} = \begin{Bmatrix} \sigma_{xx}^{(S)} \\ \sigma_{zz}^{(S)} \\ \sigma_{xz}^{(S)} \end{Bmatrix} = \frac{E_s}{(1+\upsilon_s)(1-2\upsilon_s)} \begin{bmatrix} 1-\upsilon_s & \upsilon_s & 0 \\ \upsilon_s & 1-\upsilon_s & 0 \\ 0 & 0 & 0.5-\upsilon_s \end{bmatrix} \begin{Bmatrix} 0 \\ -\dfrac{\partial u_{Sz}}{\partial z} \\ -\dfrac{1}{2}\dfrac{\partial u_{Sz}}{\partial x} \end{Bmatrix} \tag{7.8}$$

where the Young's modulus E_s of the solid can be interpreted as the secant modulus for nonlinear elastic soil.

It is assumed that, at any given time t, the two state variables u_{Sz} (vertical soil displacement) and θ (excess pore pressure) can be decomposed into products of separable functions [179]

$$u_{Sz}(x,z,t) = w(x,t)\phi(z) \tag{7.9}$$

$$\theta(x,z,t) = p(z,t)\psi(x) \tag{7.10}$$

where $w(x,\, t)$ is the settlement (vertical displacement) of the top surface of the poroelastic continuum (soil), which is the same as the beam displacement for $0 \leq x \leq L$, ϕ(z) is a dimensionless displacement shape function varying with depth, $p(z,\, t)$ is the excess pore pressure at the beam center which varies with depth and time, and $\psi(x)$ is a dimensionless pore pressure shape function varying in the horizontal direction. It is assumed in the analysis that $\phi(0) = 1$, which ensures perfect contact between the beam and the underlying soil, and that $\phi(H_{total}) = 0$, which ensures that the vertical displacement in the continuum arising from applied forces decreases with depth and becomes zero at the interface with the rigid layer. It is also assumed that $\psi = 1$ at the point corresponding to the beam center (typically, the load center), and that $\psi = 0$ at the horizontal boundaries of the problem (away from the beam-ends).

Substituting Equation 7.9 into Equation 7.7(a) and substituting the result in Equation 7.8, the soil (solid skeleton) stress tensor can be expressed as

$$\sigma^{(S)} = \begin{Bmatrix} \sigma_{xx}^{(S)} \\ \sigma_{zz}^{(S)} \\ \sigma_{xz}^{(S)} \end{Bmatrix} = \frac{E_s}{(1+\upsilon_s)(1-2\upsilon_s)} \begin{bmatrix} 1-\upsilon_s & \upsilon_s & 0 \\ \upsilon_s & 1-\upsilon_s & 0 \\ 0 & 0 & 0.5-\upsilon_s \end{bmatrix} \begin{Bmatrix} 0 \\ -w(x,t)\frac{d\phi(z)}{dz} \\ -\frac{1}{2}\frac{\partial w(x,t)}{\partial x}\phi(z) \end{Bmatrix} \tag{7.11}$$

In order to algebraically relate the solid displacement u_{Sz} with the fluid displacement u_{Fz}, Equation 7.3 is convoluted using a unit step function g_r as

$$-\int_0^t \left[\bar{k}\left(\frac{\partial\theta}{\partial z}+\frac{\partial\theta}{\partial x}\right)g_r(\tau-t)\right]dt=\int_0^t\left[\left(\frac{\partial u_{Fz}}{\partial t}-\frac{\partial u_{Sz}}{\partial t}\right)g_r(\tau-t)\right]dt \tag{7.12}$$

Applying the convolution product rule given by

$$\int_0^t f_r(t)g_r(\tau-t)dt=f_r*g_r \tag{7.13}$$

to Equation 7.11 for an arbitrary function f_r (τ is a dummy variable and '*' refers to the convolution product), integrating both sides by parts, and rearranging results in

$$u_{Fz}=u_{Sz}-g_r*\bar{k}\left(\frac{\partial\theta}{\partial z}+\frac{\partial\theta}{\partial x}\right) \tag{7.14a}$$

$$\dot{u}_{Fz}=\dot{u}_{Sz}-\bar{k}\left(\frac{\partial\theta}{\partial z}+\frac{\partial\theta}{\partial x}\right) \tag{7.14b}$$

where $\dot{u}_{Sz}$ and $\dot{u}_{Fz}$ are the solid and fluid velocities, respectively.

Substituting Equations 7.10, 7.9, and 7.14(a) into Equation 7.7(b) results in

$$\varepsilon^{(F)}=\begin{Bmatrix}\varepsilon_{xx}^{(F)}\\ \varepsilon_{zz}^{(F)}\\ \varepsilon_{xz}^{(F)}\end{Bmatrix}=\begin{Bmatrix}0\\ w(x,t)\dfrac{d\phi(z)}{dz}-g_r*\bar{k}\dfrac{\partial^2 p(z,t)}{\partial z^2}\psi(x)-g_r*\bar{k}\dfrac{\partial p(z,t)}{\partial z}\dfrac{d\psi(x)}{dx}\\ 0\end{Bmatrix} \tag{7.15}$$

7.4.2 Energy per Unit Volume

The strain energy density $\Pi_{D-continuum}$ of the poroelastic soil is given by [38]

$$\Pi_{D-continuum}=\frac{1}{2}\left(\sigma_{zz}^{(S)}\varepsilon_{zz}^{(S)}+\sigma_{xz}^{(S)}\varepsilon_{xz}^{(S)}+\sigma_{zz}^{(F)}\varepsilon_{zz}^{(F)}\right) \tag{7.16a}$$

Substituting Equations 7.7(a), 7.1, 7.10, 7.14, 7.15, and 7.11 into Equations 7.16(a), and considering any soil layer i, the strain energy density is given by

$$\begin{aligned}\Pi_{D-continuum,i} = \frac{1}{2}\left[\bar{E_{si}} w^2 \left(\frac{d\phi_i}{dz}\right)^2 + G_{si}\phi_i^2\left(\frac{\partial w}{\partial x}\right)^2\right] \\ +\frac{1}{2} f_i \left[p_i \psi w \frac{d\phi_i}{dz} - p_i \psi \bar{k_i}\left(p_i \frac{\partial^2 p_i}{\partial z^2} + \psi \frac{d^2\psi}{dx^2}\right) * g_r\right]\end{aligned} \tag{7.16b}$$

where ϕ_i and p_i are respectively the functions $\phi(z)$ and $p(z, t)$ in the i^{th} layer; and $\bar{E_{si}} = \bar{E_{si}}(x, z)$ and $G_{si} = G_{si}(x, z)$ are respectively the constrained and shear moduli in the i^{th} layer given by

$$\bar{E_{si}} = \frac{E_{si}(1-\upsilon_{si})}{(1+\upsilon_{si})(1-2\upsilon_{si})} \tag{7.17a}$$

$$G_{si} = \frac{E_{si}}{2(1+\upsilon_{si})} \tag{7.17b}$$

The kinetic energy of the poroelastic continuum per unit volume is given by

$$T_{D-continuum} = \frac{b}{2}\rho_{11}\left(\frac{\partial u_{Sz}}{\partial t}\right)^2 + \frac{b}{2}\rho_{12}\left(\frac{\partial u_{Sz}}{\partial t}\frac{\partial u_{Fz}}{\partial t}\right) + \frac{b}{2}\rho_{22}\left(\frac{\partial u_{Fz}}{\partial t}\right)^2 \tag{7.18a}$$

where the mass coefficients ρ_{11}, ρ_{12}, and ρ_{22} represent the nonuniformity of relative fluid flow through connected pores such that $\rho_{11} + 2\rho_{12}+\rho_{22} = (1\text{-}f)\rho_s+f\rho_F$, $\rho_{11} + \rho_{22} = (1\text{-}f)\rho_s$, and $\rho_{12}+\rho_{22} = f\rho_F$ (Biot 1956). Substituting Equations 7.9, 7.10, and 6.14(b) into Equation 7.18(a), and considering any soil layer i, the kinetic energy per unit volume is given by

$$\begin{aligned}T_{D-continuum,i} = \frac{b}{2}\left(\rho_{11,i} + 2\rho_{12,i} + \rho_{22,i}\right)\left(\frac{\partial w}{\partial t}\right)^2 \phi_i^2 - \frac{b}{2}\rho_{22,i}\bar{k_i^2}\left(\frac{\partial p_i}{\partial z}\right)^2 \psi_i^2 \\ -b\left(\rho_{12,i} + \rho_{22,i}\right)\bar{k_i}\frac{\partial w}{\partial t}\phi_i\psi_i\frac{\partial p_i}{\partial z}\end{aligned} \tag{7.18b}$$

where $\rho_{11,i}$, $\rho_{12,i}$, and $\rho_{22,i}$ are the mass coefficients of the i^{th} layer

7.4.3 Extended Hamilton's Principle

The governing differential equations for the beam-foundation system are obtained using the extended Hamilton's principle of least actions [41], given by

$$\delta \int_{t_1}^{t_2} (-\Pi_{total} + T_{total} + W_{nc}) dt = 0 \tag{7.19}$$

where Π_{total} and T_{total} are the potential and kinetic energies of the system, W_{nc} is the work done by the non-conservative forces, t_1 and t_2 are arbitrary times at which the equilibrium configuration of the system is known, and δ is the variational operator.

Considering the volumes V_{beam} and $V_{continuum,i}$ of the beam and the i^{th} soil (continuum) layer, respectively, the total potential energy of the beam-continuum (soil) system (considering all the n layers) is given by

$$\begin{aligned}
\Pi_{total} &= \int_{V_{beam}} \Pi_{D-beam} dV_{beam} + \sum_{i=1}^{n} \int_{V_{continuum,i}} \Pi_{continuum,i} dV_{continuum,i} \\
&= \int_0^L \frac{E_b I_b}{2} \left(\frac{\partial^2 w}{\partial x^2} \right)^2 dx + \sum_{i=1}^{n} \frac{b}{2} \int_{-\beta L}^{\beta L} \int_{H_{i-1}}^{H_i} \left[\left\{ E_{si} w^2 \left(\frac{d\phi_i}{dz} \right)^2 + G_{si} \phi_i^2 \left(\frac{\partial w}{\partial x} \right)^2 \right\} + \right. \\
&\qquad \left. f_i \left\{ p_i \psi w \frac{d\phi_i}{dz} - p_i \psi \bar{k_i} \left(p_i \frac{\partial^2 p_i}{\partial z^2} + \psi \frac{d^2 \psi}{dx^2} \right) * g_r \right\} \right] dz dx
\end{aligned} \tag{7.20}$$

where $\Pi_{D-beam} \left[= 0.5 E_b I_b \left(\frac{\partial^2 w}{\partial x^2} \right)^2 \right]$ is the strain energy density of the beam.

Similarly, the total kinetic energy T_{total} of the beam-soil system is given by

$$T_{total} = \int_{V_{beam}} T_{D-beam} dV_{beam} + \sum_{i=1}^{n} \int_{V_{continuum,i}} T_{continuum,i} dV_{continuum,i}$$

$$= \int_0^L \frac{\rho_b A_b}{2} \left(\frac{\partial w}{\partial t} \right)^2 dx + \sum_{i=1}^{n} \int_{-\beta L}^{\beta L} \int_{H_{i-1}}^{H_i} \left[\frac{b}{2} \left(\rho_{11,i} + 2\rho_{12,i} + \rho_{22,i} \right) \left(\frac{\partial w}{\partial t} \right)^2 \phi_i^2 \right. \tag{7.21}$$

$$\left. - \frac{b}{2} \rho_{22,i} \bar{k_i^2} \left(\frac{\partial p_i}{\partial z} \right)^2 \psi_i^2 - b \left(\rho_{12,i} + \rho_{22,i} \right) \bar{k_i} \frac{\partial w}{\partial t} \phi_i \psi_i \frac{\partial p_i}{\partial z} \right] dz dx$$

where $T_{D-beam} \left[= 0.5 \rho_b A_b \left(\frac{\partial^2 w}{\partial t^2} \right)^2 \right]$ is the kinetic energy per unit volume of the beam.

The nonconservative forces consist of applied and damping forces so that W_{nc} is given by

$$W_{nc} = - \int_0^L Q_j(t) \delta_d(x_0 - x_j) w dx - \int_0^L q(t) w dx - \frac{1}{2} c \left(\frac{\partial w}{\partial t} \right)^2 \tag{7.22}$$

where δ_d is the Dirac delta function, c is the damping coefficient of the beam-soil system, and x_0 is the initial (or stationary) position of the applied force.

Substituting Equations 7.20, 7.21, and 7.22 in Equation 7.19 results in

$$\delta\int_{t_1}^{t_2}\Bigg[\int_0^L \frac{\rho_b A_b}{2}\left(\frac{\partial w}{\partial t}\right)^2 dx+\sum_{i=1}^{n}\int_{-\beta L}^{\beta L}\int_{H_{i-1}}^{H_i}\Bigg[\frac{b}{2}\left(\rho_{11,i}+2\rho_{12,i}+\rho_{22,i}\right)\left(\frac{\partial w}{\partial t}\right)^2\phi_i^2-$$
$$\frac{b}{2}\rho_{22,i}\bar{k_i^2}\left(\frac{\partial p_i}{\partial z}\right)^2\psi_i^2-b\left(\rho_{12,i}+\rho_{22,i}\right)\bar{k_i}\frac{\partial w}{\partial t}\phi_i\psi_i\frac{\partial p_i}{\partial z}\Bigg]dzdx\Bigg]dt$$
$$-\delta\int_{t_1}^{t_2}\Bigg[\int_0^L \frac{E_b I_b}{2}\left(\frac{\partial^2 w}{\partial x^2}\right)^2 dx+\sum_{i=1}^{n}\frac{b}{2}\int_{-\beta L}^{\beta L}\int_{H_{i-1}}^{H_i}\left(\bar{E_{si}}w^2\left(\frac{d\phi_i}{dz}\right)^2\right.$$
$$\left.+G_{si}\phi_i^2\left(\frac{\partial w}{\partial x}\right)^2+f_i\left\{p_i\psi w\frac{d\phi_i}{dz}-p_i\psi\bar{k_i}\left(p_i\frac{\partial^2 p_i}{\partial z^2}+\psi\frac{d^2\psi}{dx^2}\right)*g_r\right\}\right)dzdx$$
$$-\int_0^L Q_j\delta_d(x_0-x_j)wdx-\int_0^L qwdx\Bigg]dt$$
$$+\delta\int_{t_1}^{t_2}\left[-\frac{1}{2}c\left(\frac{\partial w}{\partial t}\right)^2\right]dt=0 \tag{7.23}$$

Applying the principle of least actions and considering separately the variations of the functions w, p, ψ, and ϕ, the corresponding Euler-Lagrange equations of motions (i.e., the governing differential equations and associated initial and boundary conditions of $w(x, t)$, $p(z, t)$, $\psi(x)$, and $\phi(z)$) are obtained from Equation 7.23. These differential equations satisfy the extended Hamilton's principle and therefore maintain instantaneous equilibrium of the system.

In obtaining the differential equations it is assumed that the soil is heterogeneous within each layer with spatially varying $\bar{E_{si}}$ and G_{si} (i.e., $\bar{E_{si}} = \bar{E_{si}}$(x,z) and $G_{si} = G_{si}$(x,z)), which is necessary to incorporate the effect of soil nonlinearity in the analytical framework because different strains are generated at different points in the soil because of beam displacement, and this results in different reductions of soil modulus at these points rendering the soil heterogeneous (even if the soil is homogeneous prior to loading). Further, f_i, $\bar{k_i}$, $\rho_{11,i}$, $\rho_{12,i}$, and $\rho_{22,i}$ are assumed to vary both in the horizontal and vertical directions (i.e., f_i = f_i(x,z), $\bar{k_i} = \bar{k_i}$(x,z), $\rho_{11,i} = \rho_{11,i}$(x,z), $\rho_{12,i} = \rho_{12,i}$(x,z), and $\rho_{22,i} = \rho_{22,i}$(x,z) although in practice these quantities are usually treated as constants for any soil layer.

7.4.4 Beam and Soil Surface Displacements

For the domain $0 \leq x \leq$ L over which the beam is present, the differential equation governing the beam deflection w(x, t) is obtained as

$$E_b I_b \frac{\partial^4 w}{\partial x^4} - 2t_s \frac{\partial^2 w}{\partial x^2} - 2\frac{dt_s}{dx}\frac{\partial w}{\partial x} + k_s w + c\frac{\partial w}{\partial t} + (\eta_1^{(w)} + \rho_b A_b)\frac{\partial^2 w}{\partial t^2} + r^{(w)}\psi - \eta_2^{(w)}\frac{\partial \psi}{\partial x} = q(t) + Q_j(t)\delta_d(x_0 - x_j) \quad (0 \leq x \leq L) \tag{7.24a}$$

For the domains -$\beta L \leq x \leq 0$ and $L \leq x \leq \beta L$ (i.e., over the soil domains with no beam), the differential equation governing the displacement $w(x, t)$ of the top surface of the continuum (soil) is obtained as

$$-2t_s \frac{\partial^2 w}{\partial x^2} - 2\frac{dt_s}{dx}\frac{\partial w}{\partial x} + k_s w + c\frac{\partial w}{\partial t} + \eta_1^{(w)}\frac{\partial^2 w}{\partial t^2} + r^{(w)}\psi - \eta_2^{(w)}\frac{\partial \psi}{\partial x} = 0 \quad (-\beta L \leq x \leq 0) \;\&\; (L \leq x \leq \beta L) \tag{7.24b}$$

The initial conditions for Equation 7.24(a,b) are $w = 0$ and $\partial w/\partial t = 0$ at $t = 0$. The boundary conditions for Equation 7.24(a,b) for free beams are

$$w\,|_{x=-\beta L} = w\,|_{x=\beta L} = 0 \tag{7.25a}$$

$$w_{Right}\,|_{x=0} = w_{Left}\,|_{x=0} \tag{7.25b}$$

$$w_{Left}\,|_{x=L} = w_{Right}\,|_{x=L} \tag{7.25c}$$

$$\left[-2t_s\tfrac{\partial w}{\partial x}\right]_{Left}|_{x=0} = \left[E_b I_b\tfrac{\partial^3 w}{\partial x^3} - 2t_s\tfrac{\partial w}{\partial x}\right]_{Right}|_{x=0} \tag{7.25d}$$

$$\left[E_b I_b\tfrac{\partial^3 w}{\partial x^3} - 2t_s\tfrac{\partial w}{\partial x}\right]_{Left}|_{x=L} = \left[-2t_s\tfrac{\partial w}{\partial x}\right]_{Right}|_{x=L} \tag{7.25e}$$

(with no concentrated moment acting)

$$E_b I_b \frac{\partial^2 w}{\partial x^2}\,|_{x=0\ \&\ x=L} = 0 \tag{7.25f}$$

$$w\,|_{x=0\ \&\ x=L} = 0 \quad \text{(for fixed end)} \tag{7.26a}$$

$$\frac{\partial w}{\partial x}\,|_{x=0\ \&\ x=L} = 0 \quad \text{(for fixed end)} \tag{7.26b}$$

$$E_b I_b \frac{\partial^2 w}{\partial x^2}\,|_{x=0\ \&\ x=L} = 0 \quad \text{(for hinged end with no applied moment)} \tag{7.26c}$$

(for hinged end with no applied force)

$$\left[E_b I_b \frac{\partial^3 w}{\partial x^3} - 2t_s \frac{\partial w}{\partial x}\right] |_{x=0 \ \& \ x=L} = 0 \tag{7.26d}$$

The parameters in the above equations are given by

$$\eta_1^{(w)}(x) = b \sum_{i=1}^{n} \int_{H_{i-1}}^{H_i} (\rho_{11,i} + 2\rho_{12,i} + \rho_{22,i}) \phi_i^2 dz \tag{7.27a}$$

$$\eta_2^{(w)}(x,t) = b \sum_{i=1}^{n} \int_{H_{i-1}}^{H_i} \bar{k_i} (\rho_{12,i} + \rho_{22,i}) \frac{\partial p_i}{\partial z} \phi_i^2 dz \tag{7.27b}$$

$$k_s(x) = b \sum_{i=1}^{n} \int_{H_{i-1}}^{H_i} \bar{E_{si}} \left(\frac{d\phi_i}{dz}\right)^2 dz \tag{7.27c}$$

$$t_s(x) = \frac{b}{2} \sum_{i=1}^{n} \int_{H_{i-1}}^{H_i} G_{si} \phi_i^2(z) dz \tag{7.27d}$$

$$r^{(w)}(x,t) = \frac{1}{2} \sum_{i=1}^{n} \int_{H_{i-1}}^{H_i} f_i p_i \frac{\partial \phi_i}{\partial z} dz \tag{7.27e}$$

Note that the parameter k_s is analogous to the Winkler spring constant of soil and represents the compressive resistance of the continuum, and the parameter t_s represents the shear resistance of soil and can be interpreted as the shear force acting between adjacent soil springs that are compressed differently because of the applied loads. It is important to note that the two parameters k_s and t_s vary spatially in the x direction, depend on the properties of both the continuum (soil) and beam, and couple the beam displacement and surface soil displacement function w with the soil displacement shape function ϕ. The parameter $r^{(w)}$ depends on the porosity and fluid pressure (pore pressure), and varies horizontally and with time. The effect of variation of pore pressure p with time is reflected in Equation 7.24(a,b) through $r^{(w)}$ (this parameter couples w with p). The parameter $\eta_1^{(w)}$ represents the soil mass contributing to the vibration, while $\eta_2^{(w)}$ is a coupling parameter that depends on soil permeability $\bar{k}$, soil mass density ρ_s, fluid mass density ρ_F, the variation of pore

pressure with depth $\partial p/\partial z$, and the soil displacement shape function ϕ. The function w is also coupled with the pore pressure shape function ψ through the last two terms $r^{(w)}\psi$ and $\eta_2^{(w)}\ \partial\psi/\partial x$ on the left-hand side of Equation 7.24(a,b).

7.4.5 Pore Pressure Shape Function

The differential equation of $\psi(x)$ is obtained as

$$g_r * r_1^{(\psi)}\frac{d^2\psi}{dx^2} + g_r * \frac{\partial r_1^{(\psi)}}{\partial x}\frac{d\psi}{dx} - g_r * r_2^{(\psi)}\psi + \eta_1^{(\psi)}\psi + r^{(w)}w - \eta_2^{(w)}\frac{dw}{dt} = 0 \tag{7.28}$$

with the boundary conditions $\psi = 0$ and $d\psi/dx = 0$ at both $x =$ - βL and $x = \beta L$, where

$$r_1^{(\psi)}(x,t) = \sum_{i=1}^{n}\int_{H_{i-1}}^{H_i} \bar{k_i} f_i p_i^2 dz \tag{7.29a}$$

$$r_2^{(\psi)}(x,t) = \sum_{i=1}^{n}\int_{H_{i-1}}^{H_i} \bar{k_i} f_i p_i \frac{\partial^2 p_i}{\partial z^2} dz \tag{7.29b}$$

$$\eta_1^{(\psi)}(x,t) = b\sum_{i=1}^{n}\int_{H_{i-1}}^{H_i} \bar{k_i^2}\rho_{22,i}\left(\frac{dp_i}{dz}\right)^2 dz \tag{7.29c}$$

Differentiating Equation 7.28 with respect to time and applying the inverse of the unit convolution integral rule (given by Equation 7.13) to the first three terms on the left hand side results in

$$r_1^{(\psi)}\frac{d^2\psi}{dx^2} + \frac{\partial r_1^{(\psi)}}{\partial x}\frac{d\psi}{dx} + \left(\frac{\partial \eta_1^{(\psi)}}{\partial t} - r_2^{(\psi)}\right)\psi + \frac{\partial}{\partial t}\left(r^{(w)}w - \eta_2^{(w)}\frac{\partial w}{\partial t}\right) = 0 \tag{7.30}$$

The parameters $r_1^{(\psi)}$ and $r_2^{(\psi)}$ in Equation 7.30 vary horizontally and with time, and couple the functions ψ and p. Thus, the time dependency of the excess pore pressure in Equation 7.30 is partly captured by the parameters $r_1^{(\psi)}$ and $r_2^{(\psi)}$, and partly by the forcing term $\partial(r^{(w)}w - \eta_2^{(w)}(dw/dt))/\partial t$, which also couples the functions ψ and w. The parameter $\eta_1^{(\psi)}$ changes with time and is a function of $\bar{k}$, ρ_F , and $\partial p/\partial z$.

7.4.6 Soil Displacement Shape Function

The differential equation of $\phi(z)$ within the i^{th} layer is obtained as

$$m_{si}\frac{d^2\phi_i}{dz^2} + \frac{\partial m_{si}}{\partial z}\frac{d\phi_i}{dz} - (\zeta_{1,i}^{(\phi)} - n_{si})\phi_i + (r_i^{(\phi)} - \zeta_{2,i}^{(\phi)})\frac{\partial p_i}{\partial z} = 0 \tag{7.31}$$

with the boundary conditions are $\phi(0) = 1$ (at the beam-soil interface), $\phi(H_{Total}) = 0$ (at the interface with the bedrock), and $\phi_i(H_i) = \phi_{i+1}(H_i)$ (at the interface of the adjacent layers), where

$$m_{si}(z,t) = b\int_{-\beta L}^{\beta L} \bar{E_{si}} w^2 dx \tag{7.32a}$$

$$n_{si}(z,t) = b\int_{-\beta L}^{\beta L} G_{si}\left(\frac{\partial w}{\partial x}\right)^2 dx \tag{7.32b}$$

$$r_i^{(\phi)}(z,t) = \frac{1}{2}\int_{-\beta L}^{\beta L} f_i \psi w dx \tag{7.32c}$$

$$\zeta_{1,i}^{(\phi)}(z,t) = b\int_{-\beta L}^{\beta L} (\rho_{11,i} + 2\rho_{12,i} + \rho_{22,i})\left(\frac{\partial w}{\partial t}\right)^2 dx \tag{7.32d}$$

$$\zeta_{2,i}^{(\phi)}(z,t) = b\frac{\partial p_i}{\partial z}\int_{-\beta L}^{\beta L} \bar{k_i}(\rho_{12,i} + \rho_{22,i})\psi\left(\frac{\partial w}{\partial t}\right) dx \tag{7.32e}$$

The parameters m_{si} and n_{si} vary spatially in the z direction because of the heterogeneity in soil and also change with time. The parameters $r_i^{(\phi)}$, $\zeta_{1,i}^{(\phi)}$, and $\zeta_{2,i}^{(\phi)}$ vary with both depth and time as well, and partially takes into account the time dependency of the soil mass response. The parameters m_{si} and n_{si} couple the functions ϕ and w. The parameter $r_i^{(\phi)}$ couple the functions ϕ and ψ, while the term $(r_i^{(\phi)} - \zeta_{2,i}^{(\phi)})\partial p_i/\partial z$ couple the functions ϕ and p.

7.4.7 Differential Equations for Vertical Distribution of Pore Pressure

The differential equation of $p(z)$ within the i^{th} layer is obtained as

$$g_r * r_{2,i}^{(p)} \frac{\partial^2 p_i}{\partial z^2} + g_r * \frac{dr_{2,i}^{(p)}}{\partial z} \frac{\partial p_i}{\partial z} - g_r * r_{1,i}^{(p)} p_i + \zeta_{1,i}^{(p)} \frac{\partial^2 p_i}{\partial z^2} + (r_i^{(\phi)} - \zeta_{2,i}^{(p)}) \frac{d\phi_i}{dz} = 0 \tag{7.33}$$

with the boundary conditions $p = 0$ at $z = 0$ (at the surface) and $dp/dx = 0$ at $z = H_{total}$ (at the interface of the bedrock) for the single-drainage condition, and $p = 0$ at $z = 0$ and $z = H_{total}$ for the double-drainage condition; and $p_i = p_{i+1}$ at $z = H_i$ (at the interface of adjacent layers), where

$$r_{1,i}^{(p)}(z) = \int_{-\beta L}^{\beta L} \bar{k}_i f_i \psi \frac{\partial^2 \psi}{\partial x^2} dx \tag{7.34a}$$

$$r_{2,i}^{(p)}(z) = \int_{-\beta L}^{\beta L} \bar{k}_i f_i \psi^2 dx \tag{7.34b}$$

$$\zeta_{1,i}^{(p)}(z,t) = b \int_{-\beta L}^{\beta L} \bar{k}_i (\rho_{12,i} + \rho_{22,i}) \psi \left(\frac{\partial w}{\partial t} \right) dx \tag{7.34c}$$

$$\zeta_{2,i}^{(p)}(z,t) = b \int_{-\beta L}^{\beta L} \rho_{22,i} \bar{k}_i^{\,2} \psi^2 dx \tag{7.34d}$$

Differentiating Equation 7.33 with respect to time and applying the inverse of the unit convolution integral rule to the first three terms on the left hand side results in

$$\left[r_{2,i}^{(p)} + \frac{\partial \zeta_{1,i}^{(p)}}{\partial t} \right] \frac{\partial^2 p_i}{\partial z^2} + \frac{dr_{2,i}^{(p)}}{\partial z} \frac{\partial p_i}{\partial z} - r_{1,i}^{(p)} p_i + \zeta_{1,i}^{(p)} \frac{\partial^3 p_i}{\partial z^2 \partial t} + \frac{\partial}{\partial t} \left\{ \left(r_i^{(\phi)} - \zeta_{1,i}^{(p)} \right) \frac{d\phi_i}{dz} \right\} = 0 \tag{7.35}$$

The parameters $r_1^{(p)}$, $r_2^{(p)}$, and $\zeta_{1,i}^{(p)}$ vary with depth and couple the functions p and ψ. The parameter $\zeta_{1,i}^{(p)}$ vary with both depth and time and couple the functions p and w. The term $(r^{(\phi)}\text{-}\zeta_{1,i}^{(p)})d\phi/dz$ capture the coupling between the functions ϕ and p.

7.5 Inputs and Solution Method

The purpose of the developed model is to compute the long-term, time-dependent dynamic consolidation settlement of beams (foundations) by simultaneously solving the differential Equations 7.24(a,b), 7.30, 7.31, and 7.35 of the functions w, ψ, ϕ, and p . The geometric inputs required for the analysis are the beam dimensions b, d, and L, and the thicknesses T_i of the different soil layers. The material inputs include the beam Young's modulus E_b and mass density ρ_b , the soil elastic constants E_{si} and υ_{si} for each layer, the mass density of each soil layer ρ_{si} , the fluid mass density ρ_F , the reference shear strain $\gamma_{ref}^{(S)}$ of each soil layer, and the coefficient of permeability $\bar{k}_i$ and porosity f_i of each layer. The inputs used for the different problems analyzed in this paper are given in Table 7.1.

7.5.1 1D Finite Element Analysis

In order to obtain solutions using the FE method, the problem domain is discretized into horizontal and vertical strips of thickness Δz and Δx, respectively, as shown in Figure 7.2. The entire soil domain is divided into a grid of $(M_3 - 1) \times (N - 1)$ rectangular cells, each with dimensions $\Delta z \times \Delta x$. The discretization step Δz was chosen such that each horizontal strip lies within a particular soil layer and does not overlap adjacent soil layers. The x-coordinate of the centerline of any vertical strip v is x_v, while the z-coordinate of the centerline of any horizontal strip h is z_h. The vth vertical strip and the h^{th} horizontal strip intersect to form the cell (v, h), with the coordinates of its centroid given by (x_v, z_h). Two-noded beam and bar elements of length Δx with linear Lagrangian and cubic Hermitian shape functions, respectively, are used to discretize Equation 7.24(a,b) in the x direction such that these elements seat on top of the vertical strips with the nodes placed on top of the vertical interfaces of the adjacent strips. Equation 7.30 is similarly discretized in the x direction using two-noded bar element of length Δx (with linear Lagrangian shape functions). The v^{th} bar or beam element of length Δx seating on top of the v^{th} vertical strip Δx has the ς^{th} and $(\varsigma + 1)^{th}$ nodes as the first (left) and second (right) nodes, respectively. Equations 7.31 and 7.35 are also discretized with two-noded bar elements (with linear Lagrangian shape functions) such that the elements with length Δz fit in with the horizontal strips and the nodes lie on the interfaces of the adjacent horizontal strips (Figure 7.2). The h^{th} bar element of length Δz fitting into the h^{th} horizontal strip has the g^{th} and $(g + 1)^{th}$ nodes as the first (top) and second (bottom) nodes, respectively (Figure 7.2).

Table 7.1: Details of geometry and properties of the poroelastic continuum (soil) and beam for the different problems analyzed in this study

Problem Number	**Problem Type**	**Associated Figure(s)**	**Soil Properties**	**Layer 1**	**Layer 2**	**Layer 3**	**Beam Properties**	
1	Verification	4	E_s (MPa)	22			E_b (MPa)	2500
			υ_s	0.3			b (m)	1
			T_i (m)	4			d (m)	0.75
			$\gamma_{ref}^{(S)}$	0.002			L (m)	8
			k_i (m/day)	–				
			f_i	–				
			a_1 (1/sec)	0				
			a_2 (1/sec)	0				
			ρ_{si} (kg/m^3)	1800				
2	Verification	5	E_s (MPa)	20			E_b (MPa)	–
			υ_s	0.4			b (m)	–
			T_i (m)	6			d (m)	–
			$\gamma_{ref}^{(S)}$	–			L (m)	–
			k_i (m/day)	0.0015				
			f_i	0.51				
			a_1 (1/sec)	–				
			a_2 (1/sec)	–				
			ρ_{si} (kg/m^3)	–				
3	Verification	6	E_s (MPa)	20			E_b (MPa)	2500
			υ_s	0.3			b (m)	0.91
			T_i (m)	7.3			d (m)	0.3
			$\gamma_{ref}^{(S)}$	0.002			L (m)	30
			k_i (m/day)	0.0075				
			f_i	–				
			a_1 (1/sec)	–				
			a_2 (1/sec)	–				
			ρ_{si} (kg/m^3)	–				
4	Scalability and convergence	7 and 8	E_s (MPa)	20			E_b (MPa)	2000
			υ_s	0.01, 0.1, 0.2, 0.3, 0.4, and 0.49			b (m)	1.0
			T_i (m)	5, 10, and 20			d (m)	0.5
			$\gamma_{ref}^{(S)}$ (applicable to Fig. 8)	0.002			L (m)	10
			k_i (m/day)	0.01				
			f_i	0.5				
			a_1 (1/sec)	0				
			a_2 (1/sec)	0				
			ρ_{si} (kg/m^3)	1700				
5	Illustration	9	E_s (MPa)	20	25		E_b (MPa)	2300
			υ_s	0.4	0.4		b (m)	1.0
			T_i (m)	5	5		d (m)	0.55
			$\gamma_{ref}^{(S)}$	0.002	0.002		L (m)	10
			k_i (m/day)	0.001	0.0015			
			f_i	0.5	0.5			
			a_1 (1/sec)	0	0			
			a_2 (1/sec)	0	0			
			ρ_{si} (kg/m^3)	1800	1800			
			ρ_F (kg/m^3)	1000	1000			
6	Illustration	9	E_s (MPa)	18	27	31.5	E_b (MPa)	2000
			υ_s	0.41	0.41	0.41	b (m)	1.0
			T_i (m)	3	3	4	d (m)	0.4
			$\gamma_{ref}^{(S)}$	0.002	0.002	0.002	L (m)	7
			k_i (m/day)	0.002	0.0024	0.003		
			f_i	0.55	0.55	0.55		
			a_1 (1/sec)	0	0	0		
			a_2 (1/sec)	0	0	0		
			ρ_{si} (kg/m^3)	1800	1800	1800		
			ρ_F (kg/m^3)	1000	1000	1000		

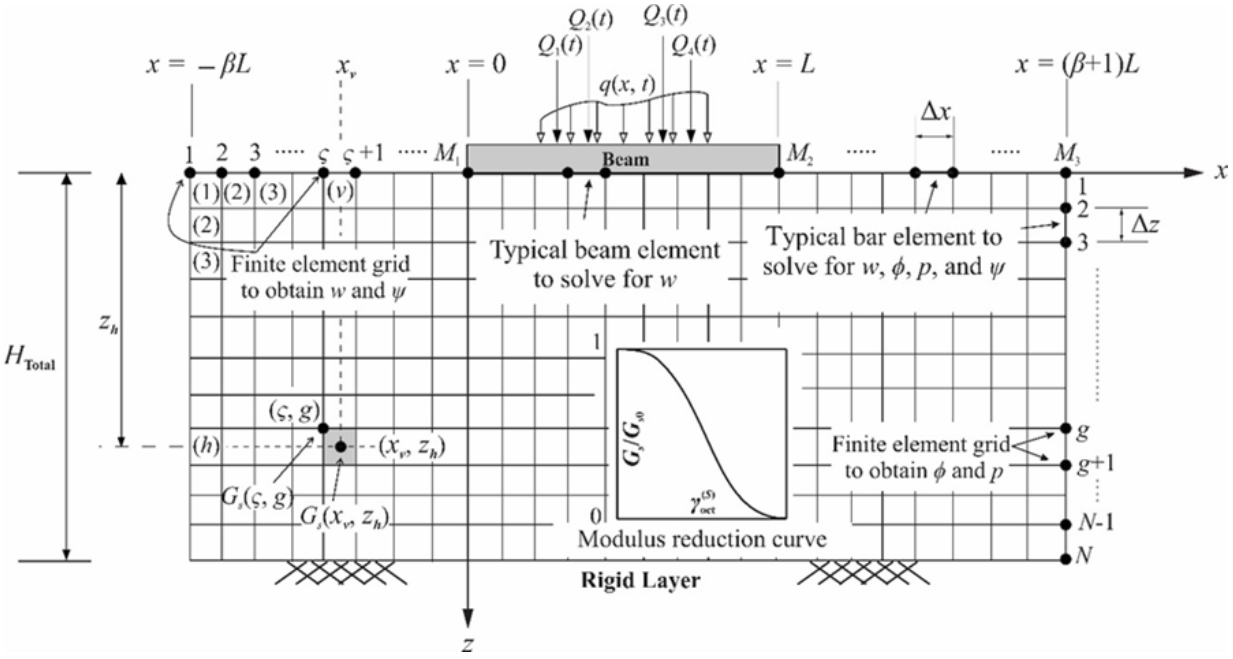

Figure 7.2: Discretization of beam-continuum (soil) system

7.5.2 Solution Algorithm

The coupled differential Equations 7.24(a,b), 7.30, 7.31, and 7.35 are solved simultaneously following an iterative algorithm (Figure 7.3). The unconditionally stable and implicit Wilson-θ method is used as the time integration method [29] to solve the dynamic Equations 7.24(a,b) and 7.35 for w and p, respectively. Equations 7.30 and 7.31 are solved statically to obtain ψ and ϕ, respectively. The four differential equations of w, ψ, ϕ and p are solved at each time step Δt within a specified tolerance for accuracy and convergence. Further, the applied loads $Q_j(x,\ t)$ and/or $q(x,\ t)$ are applied incrementally (i.e., in increasing increments of ΔQ and/or Δq such that the first load step $Q^{(1)} = \Delta Q$ ($q^{(1)} = \Delta q$), the second load step $Q^{(2)} = 2\Delta Q$ ($q^{(2)} = 2\Delta q$) and so on until the total load Q (or q) is applied in Π steps such that $Q^{(\Pi)} = \Pi\Delta Q = Q$ ($q^{(\Pi)} = \Pi\Delta q = q$) within each time step Δt to capture the nonlinearity in the beam-soil system. For each load increment, the displacement functions w and ϕ are used to calculate the soil strain components at the discretized nodes of the grid (Figure 7.2) using Equation 7.7(a). From the calculated strain components, the octahedral shear strains $\gamma_{oct}^{(S)}$ at these nodes are calculated using Equation 7.5. The octahedral strain values are then used in Equation 7.4 to calculate the secant shear modulus $G_s(\varsigma,\ g)$ for any node $(\varsigma,\ g)$, which is subsequently used to calculate

the reduced soil resistances k_s and t_s (Equation 7.27(c,d)) of nonlinear soil.

The iterative solution algorithm consists of two main interior loops (loops 1 and 2) and one exterior loop (loop 3), in addition to one starting loop (loop 0). The first interior loop (loop 1) is used to obtain the excess pore pressure function p and its companion shape function ψ, described by Equations 7.35 and 7.30, respectively, for predetermined sets of values of w and ϕ. The second interior loop (loop 2) is used to obtain beam-soil displacement w and its companion shape function ϕ, described by Equations 7.24(a,b) and 7.31, respectively, for predetermined values of p and ψ. The two interior loops are performed sequentially with iterations between the loops within the exterior loop (loop 3) until convergence on the values of p, ψ, w, and ϕ are obtained.

For computing the immediate (elastic or nonlinear) settlement, loop 0 is used at the initial stage of the algorithm for time $t = 0$ to solve for w and ϕ only described by Equations 7.24(a,b) and 7.31, respectively, after dropping all the poroelastic terms and coefficients associated with p and ψ.

7.6 Results

7.6.1 Accuracy, Computational Efficiency, and Convergence

Three problems are presented in this chapter to verify the accuracy of the present analysis. The results from the present analysis are compared with both the results available from other existing analytical and semi-analytical methods and the results obtained from equivalent two-dimensional (2D) FE analysis. To ensure that the present analysis works for all aspects of the problem, the type of load, the geometry of the problem, the constitutive relation of the soil (linear or nonlinear), the nature of the soil medium (solid or porous), the material properties of the beam, and the material parameters of the soil are varied throughout the verification problems.

The first verification problem (Problem 1 in Table 7.1), is used to check the accuracy of the model in simulating the nonlinear dynamic behavior of the beam-soil system (without poroelasticity). A comparison of beam responses obtained from the present analysis is made with those obtained from equivalent 2D FE analysis (performed using PLAXIS 2D) in which the same nonlinear elastic soil constitutive relationship is used. Figure 7.4 shows the linear and nonlinear displacement time histories of a 8 m long beam with free ends resting on a single-layer continuum and subjected to a 30 kN concentrated sinusoidal load with 5 Hz frequency acting at the mid-span for 0.5 sec. The beam and continuum

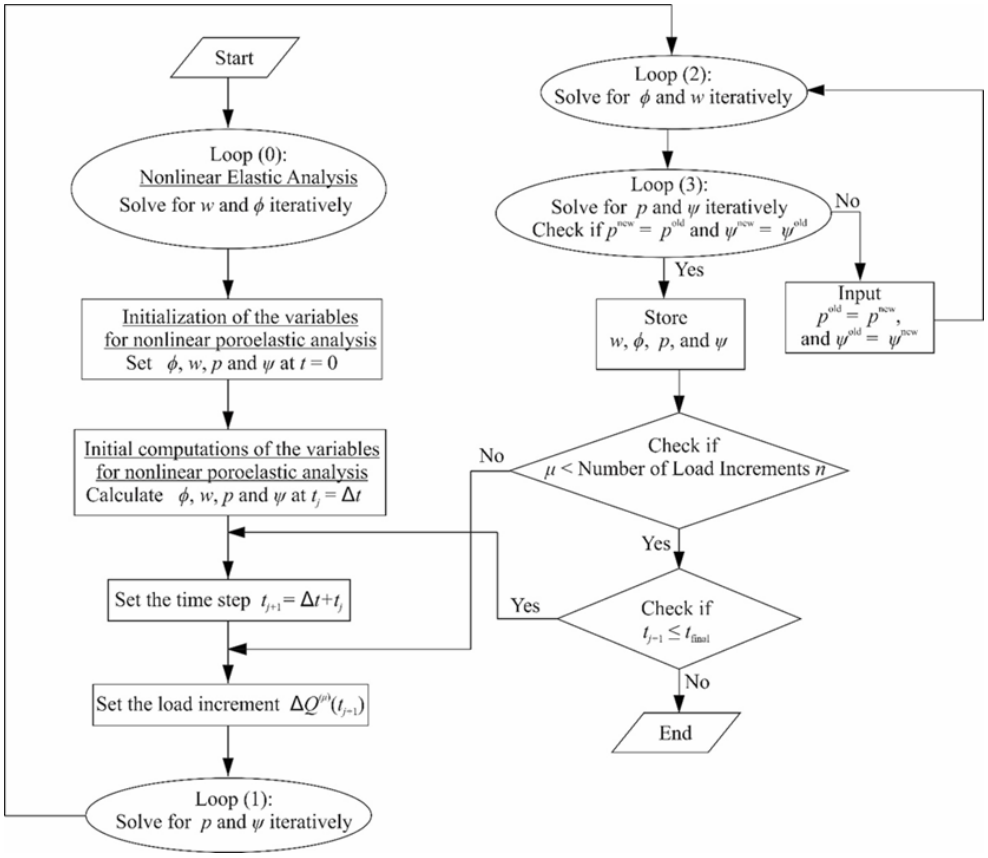

Figure 7.3: Solution algorithm

geometries and properties are given in the figure and in Table 7.1 (Problem 1). The input Young's modulus (given in Table 7.1) is the initial (small-strain) value (E_{s0}) from which the small-strain shear modulus is calculated using the input Poisson's ratio. Equation 7.4 is used to calculate the reduced shear moduli as functions of induced soil strains. The Poisson's ratio is kept constant at the prescribed values for both the beam responses. The plotted linear and nonlinear displacement profiles $w(x)$ obtained from both the present analysis and equivalent 2D FE analysis match well. The maximum difference in the mid-span beam displacements for linear and nonlinear analysis are 4.8% and 7.1%, respectively. Thus, the present framework captures the stress-strain nonlinearity of soil well and simulate the dynamic response quite accurately. The CPU time taken to run the present nonlinear dynamic analysis is 79 sec using a computer with Intel CORE i7 3.6-GHz processor and 16GB DDR3 RAM while the time required to run the 2D nonlinear FE analysis

(in PLAXIS) using the same computer is 658 sec (i.e., 8 times greater).

In the second verification problem (Problem 2 in Table 7.1), the accuracy of simulating the consolidation process using the present analysis is checked against the one-dimensional consolidation theory by Terzaghi for linear elastic soils. A distributed load $q = 15$ kN/m is applied directedly on the surface of a 6 m thick saturated clay layer (with no beam on top), which is a classical Terzaghi's consolidation problem. Single drainage is assumed such that water flows only upward in the negative z-direction. Figure 7.5 shows the variation of the normalized excess pore pressure θ/p_0 ($p_0 = q$= initial excess pore pressure in soil) as a function of the normalized depth z/H_{total} for different values of time factor T_v ($T_v = c_v t/H_d^2$ where c_v = coefficient of consolidation = $\bar{k}\bar{E}_s/\gamma_w$ and H_d = maximum drainage path = H_{total} for this problem) obtained from both the analytical solution by Terzaghi and the present analysis. The details of the soil properties and geometries are given in Figure 7.5 and Table 7.1 (corresponding to Problem 2). The maximum difference in the calculated excess porewater pressure obtained from the present analysis and Terzaghi's theory is 4.2%. It is evident that the present analysis can simulate the consolidation process quite accurately.

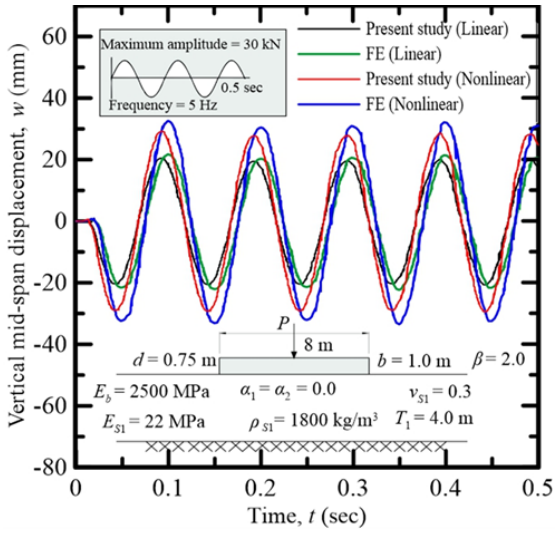

Figure 7.4: Linear and nonlinear time histories of mid-span displacement of a 8 m-long free beam resting on a 4 m thick soil deposit and subjected to a sinusoidal load with a maximum amplitude of 30 kN, frequency of 5 Hz and acting for a duration of 0.5 sec (Problem 1 of Table 7.1)

The third verification problem (Problem 3 in Table 7.1) is used to check the accuracy of the linear poroelastic model. The response of a 30 m long free-free beam resting on

a 7.3 m thick saturated clay layer and subjected to a distributed load $q = 48.6$ kN/m is obtained from the present analysis and compared with that obtained by Pe (1995) [179] using a coupled field theory-based method. The double drainage condition was assumed by Pe (1995) [179] for the problem and is maintained the same in the present analysis. The details of the beam and soil properties and geometries are given in Figure 7.6 and Table 7.1 (Problem 3). Figure 7.6 also shows the total settlement (i.e., elastic plus consolidation settlement) profiles $w(x, t)$ along beam half-span obtained from both the present analysis and by Pe (1995) [179] for $t = 40$ days and 80 days. The maximum difference in total displacement between that obtained from the present analysis and by Pe (1995) [179] is 4.3% occurring at $t = 80$ days. Thus, the present analysis produces accurate beam response in poroelastic continuum.

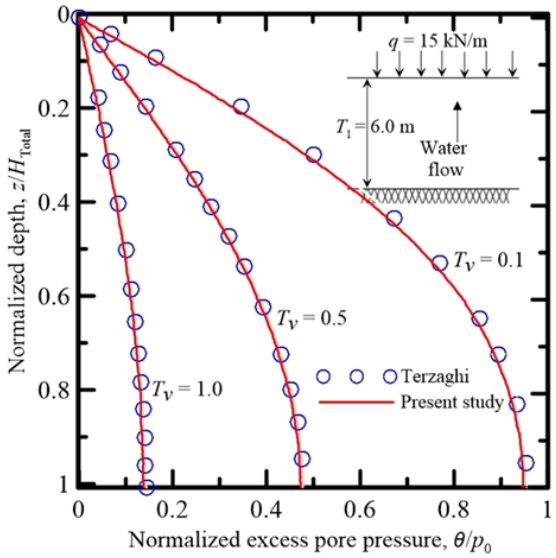

Figure 7.5: Normalized excess pore pressure θ/p_0 versus normalized depth z/H_{total} for different values of time factor T_v obtained from the present analysis and from Terzaghi's theory (Problem 2 of Table 7.1)

A study is further conducted to examine the scalability of the analysis with respect to 2D FE analysis (performed using Plaxis). The soil nonlinearity is not considered in this study to focus on the validity of the model for different static loads and for different depths of the rigid base. A 10 m long beam with free ends is considered resting on a single-layer soil deposit with thickness $T_1 = 5$ m, 10 m, and 20 m, respectively. Two loading cases are considered. In the first loading case, the beam is subjected to a sustained 30 kN point load acting at the mid-span. In the second loading case, the beam is subjected to a sustained

uniform load of 30 kN/m distributed along the beam span (see Figure 7.7(a)-(b) and Table 7.1 corresponding to Problem 4 for details). The soil domain is extended horizontally beyond both the beam ends to a distance equal to the beam span ($\beta = 1$). Figure 7.7(a)-(b) show the maximum difference in mid-span consolidation settlement, obtained from the present analysis and corresponding 2D FE analysis, at $t = 100$ days versus the soil thickness-to-beam span ratio T_1/L for different soil Poisson's ratios, obtained from both the loading cases (point load case shown in Figure 7.7(a) and uniform load case shown in Figure 7.7(b)). The maximum difference increases slightly with an increase in both T_1/L and υ_s but the difference lies within a reasonable limit (less than 10%). The rate of increase in the maximum mid-span consolidation settlement is slightly higher for the point load case. Thus, the present analysis can produce accurate results for a wide range of domain geometries.

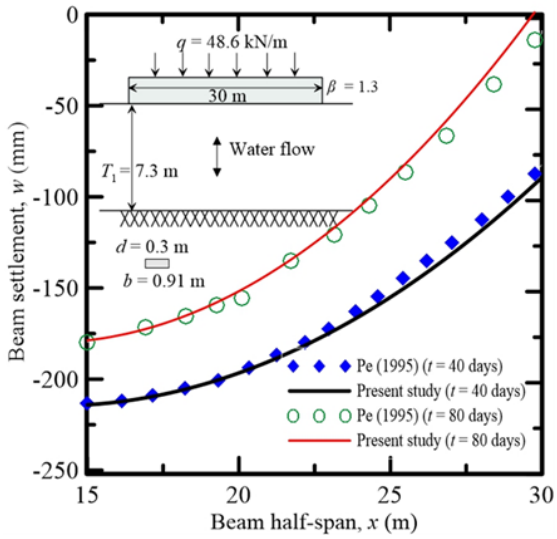

Figure 7.6: Comparison of displacement profiles of a 30 m long beam free at both ends and resting on a linear poroelastic continuum (clay deposit) at time $t = 40$ days and $t = 80$ days (Problem 3 of Table 7.1)

A convergence study is also conducted for the analysis to investigate how the element size and time step impact the results. The beams with $L = 10$ m and 20 m and with soil layer thicknesses $T_1 = 10$ m and 20 m, as described in Problem 4 of Table 7.1, are used for the study. The mid-span consolidation settlement at time $t = 50$ days is selected as the representative beam response for the convergence study. The total number of degrees of freedom $M_3 \times N$ (see Figure 7.2) is used to represent the element size (the same element size l_v is used in both x and z directions, $\Delta x = \Delta z$). Figure 7.8(a) shows that the mid-span

displacement for the 10 m long beam converged for $M_3 \times N = 36{,}991$ corresponding to $l_v/L = 0.0019$. The mid-span displacement for the 20 m long beam converged for $M_3 \times N = 181{,}201$, which corresponds to $l_v/L = 0.0011$. The effect of time step on the convergence of the mid-span consolidation settlement for both the 10 m and 20 m long beams is shown in Figure 7.8(b). The mid-span consolidation settlement converged at an average time step $\Delta t = 0.25$ day and 0.2 day for the 10 m and the 20 m long beams, respectively (for $M_3 \times N = 51{,}201$ and $l_v/L = 0.0017$). Similar convergence studies with respect to element size and time step were performed for other problems before producing the final results.

Clearly, the present analysis produces accurate and reliable results, and takes about 50% less time than 2D FE analysis. The comparisons described above do not include the additional time and expertise required for creating model geometry and meshing in 2D FE analysis. It is pertinent to note that the inputs of geometry and material properties for the present analysis are given in a text file (without requiring any numerical mesh generation), which makes the analysis rather user friendly.

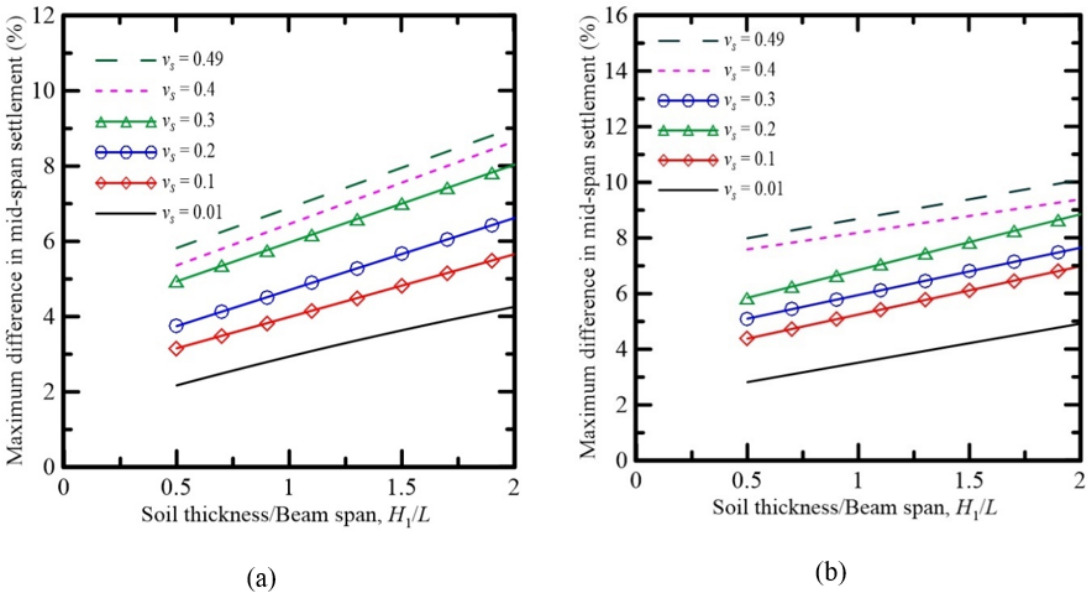

Figure 7.7: Effect of domain size on the accuracy of results with respect to 2D FE (Problem 4 of Table 7.1): (a) sustained uniform load case and (b) sustained point load case

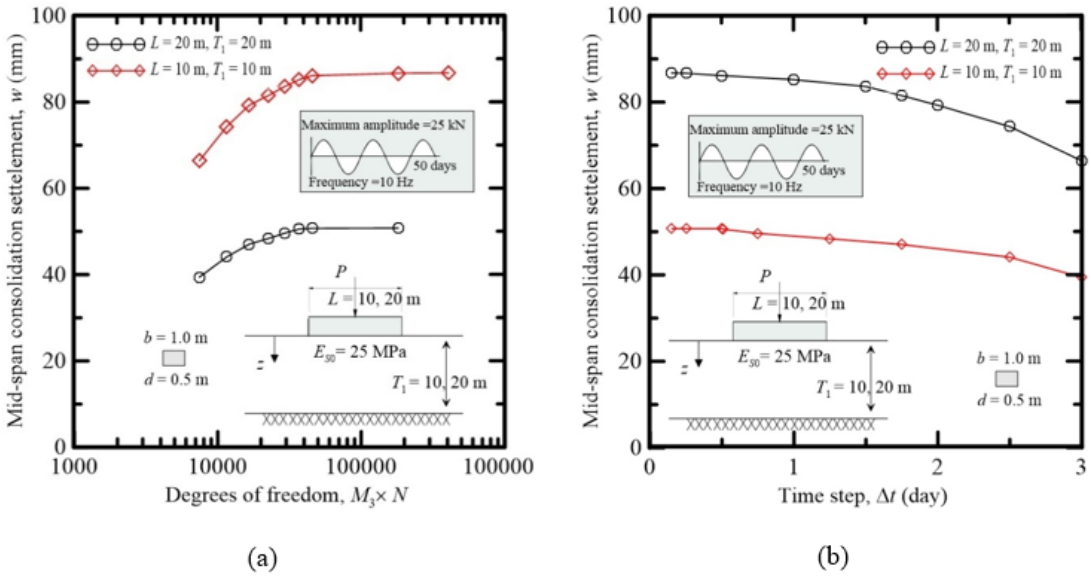

Figure 7.8: FE convergence study (Problem 4 of Table 7.1): (a) convergence with respect to element size and (b) convergence with respect to time step length

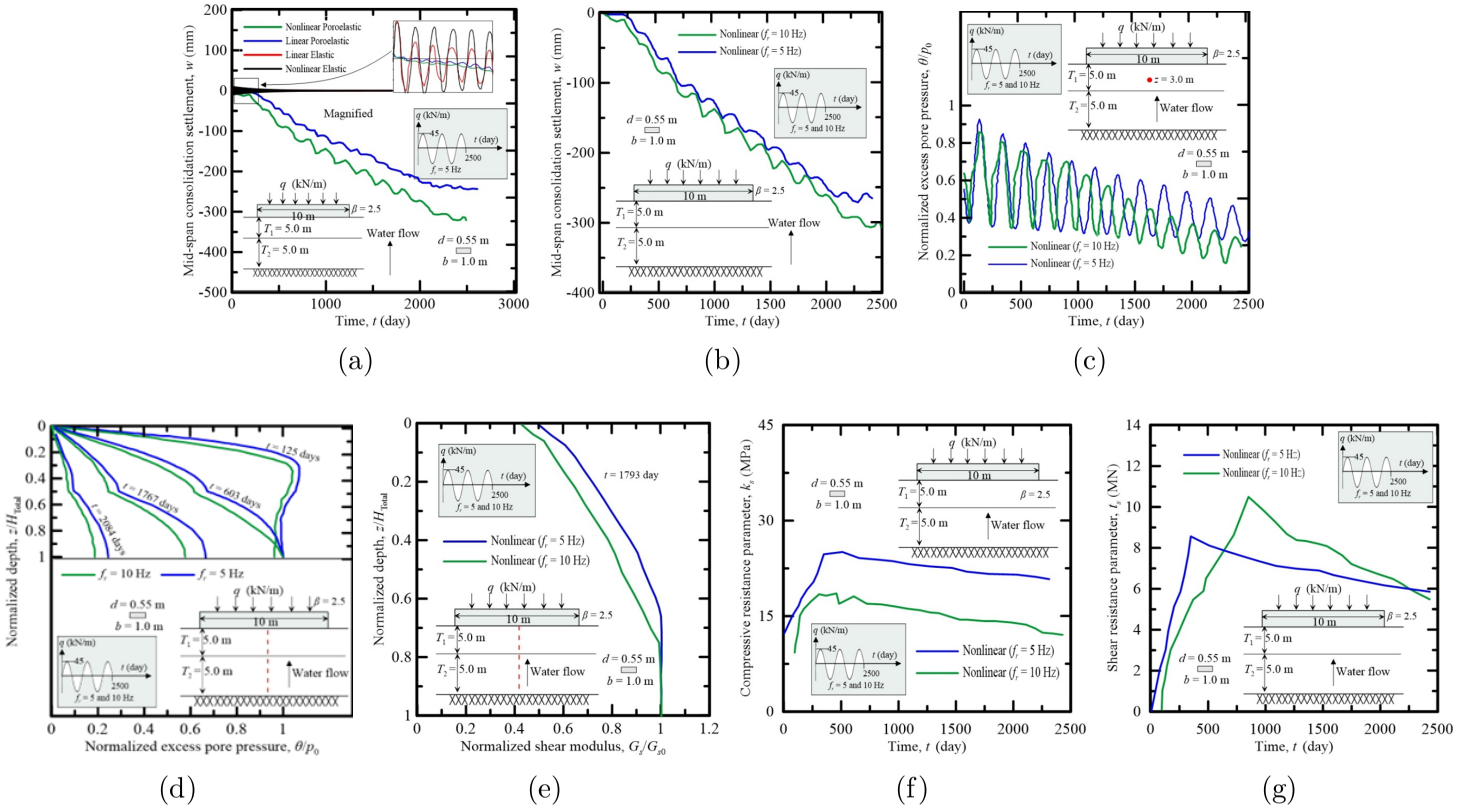

Figure 7.9: Nonlinear poroelastic dynamic response of a 10 m-long free-free strip footing (beam) resting on a two-layer saturated clayey deposit with single drainage and subjected to a uniformly distributed load of sinusoidal variation with an amplitude of 45 kN/m vibrating with two different frequencies 5 Hz and 10 Hz (Problem 5 of Table 7.1): (a) time histories of mid-span linear and nonlinear elastic and consolidation settlements, (b) time histories of mid-span nonlinear consolidation settlement for the two loading frequencies, (c) time histories of the normalized excess pore pressure for a point at 3 m depth below the mid-span for the two loading frequencies, (d) normalized excess pore pressure profiles with normalized depth at the mid-span ($x = 0.5$L) of the beam at $t = 125$ days, $t = 603$ days, $t = 1767$ days, and $t = 2084$ days, (e) variation of normalized soil shear modulus G_s/G_{s0} of soil with depth along the vertical plane at the mid-span of the beam corresponding to $t = 1793$ days; (f) time-history response of soil compression parameter k_s at the beam mid-span ($x = 0.5$L), and (g) time-history response of soil shear parameter t_s at the beam mid-span ($x = 0.5$L)

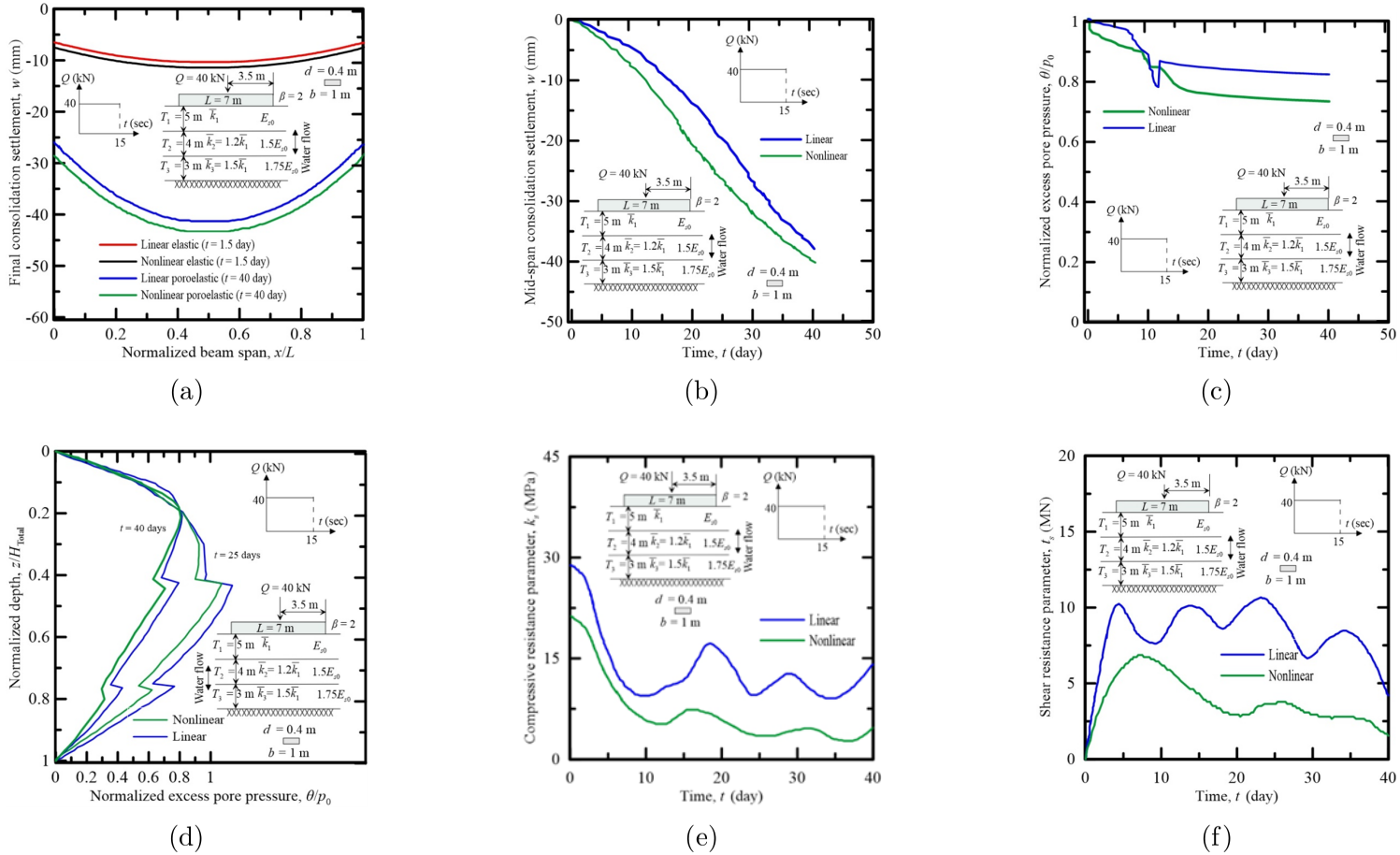

Figure 7.10: Linear and nonlinear poroelastic dynamic response of 7 m-long free-free strip footing resting on a two-layer saturated clayey deposit with double drainage and subjected to a mid-span step point load of 40 kN amplitude acting for a duration of $t = 15$ sec (Problem 6 of Table 7.1): (a) elastic and consolidation settlement profiles of the footing at t =1.5 days and $t = 40$ days, respectively, (b) time history of mid-span consolidation settlement of the footing, (c) time history of excess pore pressure dissipation for a point at 6 m depth below the mid-span, (d) normalized excess pore pressure profiles with normalized depth at the mid-span ($x = 0.5$L) of the beam at $t = 25$ days and $t = 40$ days, (e) time-history response of soil compression parameter k_s at the beam mid-span ($x = 0.5$L), and (f) time-history response of soil shear parameter t_s at the beam mid-span ($x = 0.5$L)

7.6.2 Effect of Consolidation and Loading Frequency

The effect of soil consolidation and loading frequency on the linear and nonlinear responses of the beam continuum system is illustrated through a problem described in Figure 7.9a (Problem 5 of Table 7.1). A 10 m long strip footing with free ends rests on a two-layered saturated clayey deposit with single drainage condition and a uniform coefficient of hydraulic conductivity $\bar{k} = 100 \times 10^{-5}$ m/day and 150×10^{-5} m/day for the first and the second layers, respectively. A power generator is assumed to rest on the top of the strip footing and generate a sustained sinusoidal load of 45 kN/m amplitude applied uniformly over the entire beam. Two different loading frequencies, $f_r = 5$ and 10 Hz, are considered. The power generator is assumed to operate continuously for a very long time. Table 7.1 corresponding to Problem 5 and Figure 7.9a give the details of the inputs for this problem.

Figure 7.9a shows the time histories of mid-span linear and nonlinear elastic and consolidation settlements $w(L/2,\ t)$ for the loading frequency $f_r = 5$ Hz. It is evident that the poroelasticity generates a much higher cumulative settlement in comparison with elastic analysis in which poroelasticity is not considered. The soil nonlinearity increases both elastic and poroelastic settlements. The consolidation settlement corresponding to $t = 2300$ days at the mid-span increased by 20.3% because of soil nonlinearity.

Figure 7.9b shows the time histories of the beam mid-span nonlinear poroelastic consolidation settlements $w(L/2,\ t)$ for two loading frequencies $f_r = 5$ and 10 Hz. A greater load frequency results in a greater displacement and a faster the rate of consolidation. A 21.3% increase in the final mid-span consolidation settlement corresponding to $t = 2300$ days is observed as the loading frequency increased from 5 to 10 Hz.

The time histories of the normalized excess porewater pressure $\theta(3,\ t)$ at a point 3 m below the mid-span of the footing are shown in Figure 7.9c for the two loading frequencies. The normalization is done with respect to the initial excess pore pressure p_0 at the beam-soil interface, which is the same as the contact stress at $t = 0$ day and is given by

$$p_0 = -2t_s \frac{\partial^2 w}{\partial x^2} + k_s w - 2\frac{dt_s}{dx}\frac{\partial w}{\partial x} \tag{7.36}$$

The profiles of normalized excess pore pressure θ/p_0 over normalized depth z/H_{Total} at the mid-span of the footing ($x = 0.5L$) are plotted in Figure 7.9d for $t = 125$ days, $t = 603$ days, $t = 1767$ days, and $t = 2084$ days and for the two loading frequencies. It is clear that a lower loading frequency leads to less dissipation of pore pressure at a given time resulting in slower consolidation rate and a lower settlement.

Figure 7.9e shows the profiles of the normalized secant shear modulus G_s/G_{s0} with normalized depth z/H_{Total} along the vertical section through the mid-span of the beam at time t =1793 days, for the two loading frequencies. It is clear that the extent of nonlinear behavior depends on the load frequency.

The time histories of the parameters k_s and t_s are plotted in Figures 7.9f-7.9g for the vertical section along the mid-span of the footing for the two loading frequencies. It is interesting to note that k_s and t_s change with time. The parameter k_s is lower in magnitude for the higher load frequency than for the corresponding lower load frequency, which explains why displacements are more for higher load frequency than for the lower load frequency.

7.6.3 Effect of Soil Nonlinearity

The following example problem (Figures 7.10a-7.10f) (Problem 6 of Table 7.1) illustrates the influence of soil stress-strain nonlinearity on the consolidation response of the beam-soil system. A free-end strip footing (beam) of length L = 7 m, depth d = 0.4 m and width b = 1 m and resting on a three-layer saturated clayey deposit is considered. A diesel engine is assumed to rest on the top of the mid-span of the footing and generate a sustained step point load of 40 kN amplitude for a period of 15 sec. Table 7.1 corresponding to Problem 6 and Figure 7.10a provide the inputs of the problem. Double drainage condition is assumed with a varying hydraulic conductivity $\bar{k}$ in the three layers.

The linear and nonlinear elastic and consolidation settlement profiles $w(x, t)$ at times t = 15 sec and t = 40 days, respectively, are plotted in Figure 7.10a. It is evident that, for a typical beam-soil geometry and material properties, soil nonlinearity increases both the elastic and consolidation settlements. A respective increase of 3.2% and 5.8% occurs for the mid-span elastic and consolidation settlements at t = 1.5 days because of soil nonlinearity. Figure 7.10b shows the time history of the mid-span consolidation settlement $w(L/2, t)$, which indicates that soil nonlinearity has a strong influence on the rate and magnitude of consolidation settlement.

The time histories of the normalized excess porewater pressure θ/p_0 at a point 6 m below the mid-span of the footing are shown in Figure 7.10c for both the linear and nonlinear analysis. It is clear that soil nonlinearity leads to a faster dissipation of excess porewater pressure, which increases the rate of consolidation. Figure 7.10d shows the normalized excess pore pressure θ/p_0 profiles over normalized depth z/H_{Total} at the mid-span for t = 25 and 40 days. The effect of soil layering (with different values of $\bar{k}$ and E_{s0} in different layers) is clear in the pore pressure profile plots. Further, Figure 7.10d shows that soil

nonlinearity accelerates the excess pore pressure dissipation, as also evident from Figures 7.10a - 7.10c.

The linear and nonlinear time histories of the parameters k_s and t_s for the vertical section along the mid-span of the beam are plotted in Figures 7.10e - 7.10f. The parameters k_s and t_s are lower in magnitude for nonlinear soil than for the corresponding linear soil (this explains why displacements are more for nonlinear soil than for linear soil).

7.7 Conclusions

A new analysis method is developed based on variational principles for calculating the time-dependent consolidation settlement of flexible beams (foundations) resting on nonlinear, multilayered, visco-poroelastic continuums (soils). A simplified continuum model is assumed to represent the poroelastic soil in which the displacements and pore pressures are expressed as products of separable functions. The poroelastic soil is assumed to follow Biot's consolidation theory. The variational principles of mechanics are used in the analysis in which the extended Hamilton's principle is applied to obtain the four Euler-Lagrange differential equations describing the time-dependent dynamic equilibrium of the beam-continuum system.

The differential equations are solved using one-dimensional finite element analysis. As these differential equations are coupled, they are solved simultaneously following an iterative algorithm. The implicit Wilson-θ time integration scheme is used to obtain the displacement and excess pore pressure time histories of the beam-soil system responses. In the analysis, soil nonlinearity is considered by using a nonlinear-elastic soil constitutive model in which the stresses and strains are related through a hyperbolic constitutive equation developed for clayey soils. In the constitutive model, the reduction of the secant shear modulus is expressed as a function of the induced strain in soil, which is considered to be the octahedral shear strain in this analysis. The poroelastic soil domain is discretized into a two-dimensional grid such that the degraded shear modulus is calculated at the grid points and incorporated into the finite element discretized forms of the differential equations to obtain the nonlinear beam response. To capture the nonlinear response as a function of the loading history, the imposed dynamic loads are applied incrementally within each single dynamic time step.

The inputs required for the analysis are the magnitude, duration, nature, frequency, and type of applied loads; geometry and Young's modulus of beam; and layering, initial elastic constants, mass densities of soil and fluid, permeability, porosity, drainage condition, and

an appropriate modulus reduction equation (constitutive model) of soil. These inputs can be conveniently given to the code through a text file without any requirement for generation of the analysis domain and numerical mesh (as is required in finite element analysis). Thus, no specialized knowledge of numerical methods is required for performing the analysis. Further, the results from this analysis are obtained within minutes in a computer with Intel CORE i7 3.6-GHz processor and 16GB DDR3 RAM. The accuracy of the analysis is verified with both the results obtained from existing analytical semi-analytical methods, and with 2D nonlinear finite element analysis (performed using PLAXIS). Systematic studies are performed demonstrating the convergence and scalability of the problem. The analysis framework provides a rigorous, easy-to-use, and quick methodology for analyzing beams and similar flexible foundations (such as strip foundations) resting on nonlinear poroelastic soils subjected to dynamic loads.

Two example problems are analyzed to demonstrate the use of the analysis and highlight the nonlinear dynamic poroelastic characteristics of the beam- soil system. The numerical results presented in the paper indicate that the interaction between the soil and beam depends on the linear and nonlinear behavior of soil and on the frequency of the applied load. The magnitude of beam (foundation) settlement, the rate of consolidation settlement, and the rate of dissipation of excess pore pressure depend on the interaction with the beam. This aspect is not taken into account in the widely used Terzaghi's consolidation theory.

Soil nonlinearity and higher loading frequency accelerate the consolidation process and produce larger consolidation settlements than linear elastic soils and lower loading frequency. The soil modulus degrades gradually over time in nonlinear elastic soils as the consolidation process progresses. The presence of soil layering with different values of soil permeability and modulus in different layers impact the dissipation of excess pore pressure and the consolidation rate. The soil compression and shear parameters, k_s and t_s, are affected by the poroelasticity and nonlinearity of soil. These parameters have lower values in nonlinear soils and for higher loading frequency than in linear soils and for lower loading frequency, and decrease with time as consolidation progresses.

Chapter 8

Conclusions and Recommendations

In this chapter, the conclusions and observations derived from the findings of this research on the behaviour of BOF continuum system subjected to dynamic loads are described. The conclusions are based on the results of the study. Recommendations are also given based on the findings of the research.

8.1 Summary and Conclusions

The research work presented in this thesis was aimed at developing a methodology for the dynamic analysis of beam on nonlinear elastic and poroelastic foundation problems so that the nonlinear time-dependent beam-soil response can be determined. The beam-soil response is important for evaluating both the serviceability and the ultimate state of the beam-soil systems with applications in strip foundations, pavements, and railway tracks. The method proposed in this research is an efficient, dynamic continuum-based framework and it was implemented in a MATLAB code. The inputs required for the analysis are beam geometry (cross-section and length) and material properties (Young's modulus), soil layering (number of soil layers and thickness of each layer), the stress-strain response of each soil layer (small-strain stiffness modulus and a rule describing the degradation of modulus with strain or stress), soil porosity and hydraulic conductivity, and the magnitudes and the type of the applied force. These inputs can be given in a text file without requiring any inputs on geometry or meshing. Thus, the developed method is user friendly. At the same time, the method is computationally more efficient than equivalent finite element analysis. The salient points found in the different chapters of the thesis are summarized below.

In chapter 1, a critical review of the literature on BOF models was performed and research gaps were identified.

In chapter 2, analytical and numerical solutions for dynamic analysis of simply supported beams on two parameter elastic foundations subjected to a moving concentrated load with constant speed was developed. Linear Integral Transforms were used to solve the governing equilibrium equation of motion analytically. The analytical solutions were developed in closed form expressions for different speed and damping cases. The FEM was used to solve the governing equilibrium equation numerically.

- By increasing the span length and hence nullifying the effect of the boundary conditions, the proposed solution has proved to be suitable for handing the steady state response of infinitely long beam resting on two-parameter elastic foundation.
- The foundation compressive stiffness, the moving load speed, and beam span length were found to affect the behaviour of the beam-foundation system with respect to the dynamic amplification factors of the beam deflection.

In chapter 3, an analysis framework is presented for Timoshenko beams resting on multi-layer foundation (soil) in which the foundation is treated as a continuum.

- The resulting governing differential equation of beam deflection resembles that of beam resting on two-parameter foundation characterized with parameters k_s and t_s representing the compressive and shear resistances of soil.
- Systematic parametric studies were performed and used to develop closed form equations of k_s and t_s are obtained as part of the solution, such that are rigorously related to the elastic constants of the multi-layered foundation (continuum). Thus, empiricism is not required in the estimation of the foundation parameters k_s and t_s.
- A closed form solution of the mid-span displacement of both beam resting on single-layer foundation is developed using both Timoshenko and Euler-Bernoulli beam theories, which can be directly used by practitioners in their analysis of beams on foundations.
- A parametric study was conducted on beams resting on multilayered soil, and equations are developed to determine the foundation parameters k_s and t_s.
- The increase in the relative bending stiffness of beam and soil was found to decrease the surface deflection.

- A flexibility index λ is defined in terms of the elastic constants and geometry of the beam-foundation system, and it is shown through a systematic parametric study that, for beams subjected to uniformly distributed load and resting on a single-layer foundation with the thickness T of the foundation layer varies from half to twice the beam length L (i.e., $T/L = 0.5$ to 2), produces rigid beam behavior, $0 < \lambda \leq 0.86$ and $0 < \lambda \leq 1.4$ produce flexible beam behavior for which the Timoshenko beam theory is most appropriate (the limit of 0.86 is applicable for the case of uniformly distributed load and the limit of 1.4 is applicable for the case of mid-span concentrated load), and $\lambda > 0.86$ and $\lambda > 1.4$ produce flexible beam behavior for which both Timoshenko and Euler-Bernoulli beam theories are applicable.

In chapter 4, A new model is developed based on a continuum approach for dynamic analysis of soil structure interaction. The inputs required are the magnitude and frequency or velocity of applied loads; beam geometry, Young's modulus, and density; and soil geometry, density, and elastic constants.

- One of the advantages of the developed model is that it leads to equations similar to beams resting on bed of springs (i.e., the soil is represented by springs, which is commonly termed as the foundation on which the beam rests) characterized by two parameters k_s and t_s representing the compressive and shear resistances of the foundation.

- It is shown in this analysis that, unlike the traditional approach, k_s and t_s are not foundation constants but depend on the beam-foundation interaction and, therefore, are functions of time – this is a novel finding and a significantly different approach for problems related to dynamic interaction of beams with underlying foundations.

- Another advantage of the present model is that the inertial resistance of soil (i.e., the foundation) is explicitly taken into account by a parameter η_s, which is also a function of time (inertia of foundations are not taken into account for traditional spring-based foundation models). Thus, the parameters k_s, t_s and η_s are interaction parameters and change with load frequency and velocity.

- Further, geometric damping is also taken into account in this model through a decay function, which is typically not available in traditional spring-based soil-structure interaction models.

In chapter 5, a new analysis is developed based on variational principles to obtain the time-dependent dynamic response of beams resting on multilayered nonlinear viscoelastic continuum/foundation/soil and subjected to vibrating and moving loads.

- In the analysis, soil nonlinearity is considered by using a nonlinear-elastic soil constitutive model to describe the reduction of secant shear modulus as a function of the induces strain in soil.
- The results from the present analysis are obtained in about 50% of the time required for obtaining the results from 2-D nonlinear dynamic finite element analysis (performed using PLAXIS).
- The convergence and scalability of the present analysis method are also demonstrated. Thus, the analysis framework provides a rigorous, easy-to-use, and quick methodology for analyzing beams resting on nonlinear viscoelastic continuums/foundations/soils subjected to dynamic loads.
- The soil "spring" parameters k_s and t_s are not constants as traditionally assumed but functions of the beam-foundation system (including the nonlinearity) and change with time.
- Further, the analysis automatically calculates the mass (inertial effect) of soil (continuum) participating in the vibration through the parameter η_s,
- The parameters k_s and t_s are found to be lower in magnitude for nonlinear soil than for the corresponding linear soil. Further, both k_s and t_s fluctuate initially and then tend towards more stable values as time increases -k_s is more affected by soil nonlinearity than t_s.

In chapter 6, a new analysis method is developed for calculating the consolidation settlement of flexible beams (foundations) resting on nonlinear, multilayered poroelastic continuums (soils). The poroelastic soil is assumed to follow Biot's consolidation theory. The analysis framework provides a rigorous, easy-to-use, and quick methodology for analyzing beams and similar flexible foundations (such as strip foundation) resting on nonlinear poroelastic soils subjected to sustained loads.

- These inputs required for the analysis can be conveniently given to the code through a text file without any requirement for generation of the analysis domain and numerical mesh (as is required in finite element analysis). Thus, no specialized knowledge of numerical methods is required for performing the analysis.
- The numerical results presented in the paper indicate that the interaction between the linear or nonlinear soil and the beam depends on the beam slenderness (aspect) ratio and the relative stiffness of the beam and soil.

- The magnitude of beam (foundation) settlement, the rate of consolidation settlement, and the rate of dissipation of the excess pore pressure depend on the flexibility (or rigidity) of the beam. This aspect is not taken into account in the widely used Terzaghi's consolidation theory.

- Soil nonlinearity accelerates the consolidation process and produces larger consolidation settlements than linear elastic soils. The soil modulus degrades gradually over time in nonlinear elastic soils as the consolidation process progresses.

- The presence of soil layering with different values of soil permeability and modulus in different layers impact the dissipation of excess pore pressure and the consolidation rate.

- The soil compression and shear parameters, k_s and t_s, are affected by the poroelasticity and nonlinearity of soil. These parameters have lower values in nonlinear soils than in linear soils and decrease with time in an asymptotic manner as consolidation progresses.

In chapter 7, a new analysis method is developed for calculating the time-dependent consolidation settlement of flexible beams (foundations) vibrating on nonlinear, multilayered, visco-poroelastic continuums (soils). The poroelastic soil is assumed to follow Biot's consolidation theory. Thus, the analysis framework provides a rigorous, easy-to-use, and quick methodology for analyzing beams and similar flexible foundations (such as strip foundation) resting on nonlinear poroelastic soils subjected to dynamic loads.

- The numerical results presented in the chapter indicate that the interaction between the soil and beam depends on the linear/nonlinear behaviour of the soil and the frequency of the applied load. The magnitude of beam (foundation) settlement, the rate of consolidation settlement, and the rate of dissipation of the excess pore pressure depend on the interaction with the beam.

- Soil nonlinearity and higher loading frequency accelerate the consolidation process and produce larger consolidation settlements than linear elastic soils and lower loading frequency.

- The soil modulus degrades gradually over time in nonlinear elastic soils as the consolidation process progresses.

- The presence of soil layering with different values of soil permeability and modulus in different layers impact the dissipation of excess pore pressure and the consolidation rate. The soil compression and shear parameters, k_s and t_s, are affected by the poroelasticity and nonlinearity of soil. These parameters have lower values in nonlinear soils and for higher loading frequency than in linear soils and for lower loading frequency and decrease with time as consolidation progresses.

8.2 Recommendations for Future Work

The following recommendations are made for future work:

- More realistic and specific soil constitutive relationships representing different types of soil can be used to investigate the soil structure interaction in different soils.
- The study should be extended to investigate real life applications such as railway-track interaction.
- Many simplified assumptions were made in the presented research such as neglecting the horizontal displacement in soil and assuming the pore water to flow only in the vertical direction. Such assumptions can be relaxed and the model can be further developed with more realistic assumptions.
- In this research, the material nonlinearity is only considered in the soil and not in the beam behavior. Further studies are recommended to investigate the effect of the beam nonlinearity on the response of the beam-soil system.
- Only limited parametric studies have been conducted in the presented research to investigate the accuracy, sensitivity and convergence of the nonlinear dynamic response of the beam-soil system. Extensive parametric studies are recommended to investigate the soil structure interaction further.
- The analysis method assumes perfect contact between the beam and the soil surface during loading. An improvement is recommended to account for tensionless foundation behavior where the separation between the beam and the soil is considered due to uplifting or soil heaving.
- The analysis method could also be improved to account for different loading scenarios such as considering the inertia of the moving loads, prescribed displacements or

acceleration in the soil body (such as earthquake loading), prestressing forces in the beam, pretension from soil reinforcement, and moving distributed loads.

- The beam-soil system in this methodology assumes to represent a plain strain loading condition. The analysis method can be modified to account for axisymmetrical or rectangular plates (three dimensional problems) resting on multilayered soil deposits.
- Small strain material models used in the current study are limited in their ability to capture the progressive failure within soils, as their small strain range is restricted. To simulate the progressive failure of soil, more advanced constitutive models, such as elasto-plastic models (Cap models), can be used in conjunction with failure criteria (such as Mohr-Coulomb or Drucker-Prager).

References

[1] Sondipon Adhikari, D Karličić, and X Liu. Dynamic stiffness of nonlocal damped nano-beams on elastic foundation. *European Journal of Mechanics-A/Solids*, 86:104144, 2021.

[2] Zhi Yong Ai and Jian Bang Cai. Static analysis of timoshenko beam on elastic multilayered soils by combination of finite element and analytical layer element. *Applied Mathematical Modelling*, 39(7):1875–1888, 2015.

[3] Zhi Yong Ai and Ya Dong Hu. The analysis of beams on layered poroelastic soils with anisotropic permeability and compressible pore fluid. *Applied Mathematical Modelling*, 40(11-12):5876–5890, 2016.

[4] Zhi Yong Ai, Zhi Xiong Li, and Yi Chong Cheng. Bem analysis of elastic foundation beams on multilayered isotropic soils. *Soils and Foundations*, 54(4):667–674, 2014.

[5] Zhi Yong Ai, Wen Jie Liu, and Ben Kai Shi. Quasi-static interaction between non-uniform beams and anisotropic permeable saturated multilayered soils with elastic superstrata. *Applied Mathematical Modelling*, 53:400–418, 2018.

[6] Zhi Yong Ai and Guang Peng Ren. Dynamic response of an infinite beam on a transversely isotropic multilayered half-space due to a moving load. *International Journal of Mechanical Sciences*, 133:817–828, 2017.

[7] Wang Ai-qin. Analytic solution of beams loaded vertical force on elastic half space. *Journal of Chang'an University (Natural Science Edition)*, 5(127), 2008.

[8] AY Aköz and F Kadioğlu. The mixed finite element solution of circular beam on elastic foundation. *Computers & structures*, 60(4):643–651, 1996.

[9] Yalcin Akoz and Hale Ergun. Analysis of partially embedded beams in two-parameter foundation. *Structural Engineering and Mechanics*, 42(1):1–12, 2012.

[10] Yalçin Aköz and Fethi Kadioğlu. The mixed finite element method for the quasi-static and dynamic analysis of viscoelastic timoshenko beams. *International Journal for Numerical Methods in Engineering*, 44(12):1909–1932, 1999.

[11] Ihsan Al-Abboodi, TM Toma-Sabbagh, and Ali Al-Jazaairry. Modelling the response of single passive piles subjected to lateral soil movement using plaxis. *International Journal of Engineering Research & Technology*, 4(3):176–180, 2015.

[12] Kazem Alambeigi, Mehdi Mohammadimehr, Mostafa Bamdad, and Timon Rabczuk. Free and forced vibration analysis of a sandwich beam considering porous core and sma hybrid composite face layers on vlasov's foundation. *Acta Mechanica*, 231(8):3199–3218, 2020.

[13] Sofia W Alisjahbana, Irene Alisjahabana, Shota Kiryu, and Buntara S Gan. Semi analytical solution of a rigid pavement under a moving load on a kerr foundation model. *Journal of Vibroengineering*, 20(5):2165–2174, 2018.

[14] SJ Antony and Zuhair Kadhim Jahanger. Local scale displacement fields in grains–structure interactions under cyclic loading: Experiments and simulations. *Geotechnical and Geological Engineering*, 38(2):1277–1294, 2020.

[15] IE Avramidis and Konstantinos Morfidis. Bending of beams on three-parameter elastic foundation. *International Journal of Solids and Structures*, 43(2):357–375, 2006.

[16] Y Ayvaz and K Özgan. Application of modified vlasov model to free vibration analysis of beams resting on elastic foundations. *Journal of Sound and vibration*, 255(1):111–127, 2002.

[17] GS Babu and Vikas Pratap Singh. Simulation of soil nail structures using plaxis 2d. *Plaxis Bulletin*, 25:16–21, 2009.

[18] Roberto Ballarini. The da vinci-euler-bernoulli beam theory. *Mech. Eng. Mag. Online*, 7, 2003.

[19] MR Banan, G Karami, and M Farshad. Finite element analysis of curved beams on elastic foundations. *Computers & structures*, 32(1):45–53, 1989.

[20] Prasanta Kumar Banerjee, Prasanta Kumar Banerjee, and Roy Butterfield. *Boundary element methods in engineering science*. McGraw-Hill (UK), 1981.

[21] Daniele Baraldi and Nerio Tullini. Static stiffness of rigid foundation resting on elastic half-space using a galerkin boundary element method. *Engineering Structures*, 225:111061, 2020.

[22] Daniele Baraldi and Nerio Tullini. Buckling of beams and coatings of finite width in bilateral frictionless contact with an elastic half-space. *International Journal of Solids and Structures*, 228:111104, 2021.

[23] Mohammad Reza Barati and Ashraf Zenkour. Forced vibration of sinusoidal fg nanobeams resting on hybrid kerr foundation in hygro-thermal environments. *Mechanics of Advanced Materials and Structures*, 25(8):669–680, 2018.

[24] James R Barber. *Intermediate mechanics of materials*, volume 175. Springer, 2010.

[25] JR Barber. Beams on elastic foundations. In *Intermediate mechanics of materials*, pages 353–384. Springer, 2011.

[26] Dipanjan Basu and NSV Kameswara Rao. Analytical solutions for euler–bernoulli beam on visco-elastic foundation subjected to moving load. *International Journal for Numerical and Analytical Methods in Geomechanics*, 37(8):945–960, 2013.

[27] KJ Bathe and EL Wilson. Stability and accuracy analysis of direct integration methods. *Earthquake Engineering & Structural Dynamics*, 1(3):283–291, 1972.

[28] Klaus-Jürgen Bathe. *Finite element procedures in engineering analysis*. 1996.

[29] Klaus-Jürgen Bathe. *Finite element procedures*. Klaus-Jurgen Bathe, 2014.

[30] Fred W Beaufait and Peter W Hoadley. Analysis of elastic beams on nonlinear foundations. *Computers & Structures*, 12(5):669–676, 1980.

[31] T Benz, PA Vermeer, and R Schwab. A small-strain overlay model. *International journal for numerical and analytical methods in geomechanics*, 33(1):25–44, 2009.

[32] Xuecheng Bian, Jing Hu, David Thompson, and William Powrie. Pore pressure generation in a poro-elastic soil under moving train loads. *Soil Dynamics and Earthquake Engineering*, 125:105711, 2019.

[33] MA BIOT. Bending of an infinite beam on an elastic foundation. *Zeitschrift fiir Angewandte Maihematik und Mechanik*, 2(3):165–184, 1922.

[34] Maurice A Biot. Bending of an infinite beam on an elastic foundation. 1937.

[35] Maurice A Biot. Consolidation settlement under a rectangular load distribution. *Journal of Applied Physics*, 12(5):426–430, 1941.

[36] Maurice A Biot. Theory of elasticity and consolidation for a porous anisotropic solid. *Journal of applied physics*, 26(2):182–185, 1955.

[37] Maurice A Biot. General solutions of the equations of elasticity and consolidation for a porous material. 1956.

[38] Maurice A Biot. Theory of propagation of elastic waves in a fluid-saturated porous solid. ii. higher frequency range. *The Journal of the acoustical Society of america*, 28(2):179–191, 1956.

[39] Maurice A Biot. Mechanics of deformation and acoustic propagation in porous media. *Journal of applied physics*, 33(4):1482–1498, 1962.

[40] George David Birkhoff. *Dynamical systems*, volume 9. American Mathematical Soc., 1927.

[41] George David Birkhoff. *Dynamical systems*, volume 9. American Mathematical Soc., 1960.

[42] JR Booker. The consolidation of a finite layer subject to surface loading. *International Journal of Solids and structures*, 10(9):1053–1065, 1974.

[43] JR Booker and JC Small. The behaviour of an impermeable flexible raft on a deep layer of consolidating soil. *International Journal for Numerical and Analytical Methods in Geomechanics*, 10(3):311–327, 1986.

[44] Joseph Boussinesq. *Application des potentiels à l'étude de l'équilibre et du mouvement des solides élastiques: principalement au calcul des déformations et des pressions que produisent, dans ces solides, des efforts quelconques exercés sur une petite partie de leur surface ou de leur intérieur: mémoire suivi de notes étendues sur divers points de physique, mathematique et d'analyse*, volume 4. Gauthier-Villars, 1885.

[45] Joseph E Bowles. *Foundation analysis and design*. 1996.

[46] D Bowness, AC Lock, W Powrie, JA Priest, and DJ Richards. Monitoring the dynamic displacements of railway track. *Proceedings of the Institution of Mechanical Engineers, Part F: Journal of Rail and Rapid Transit*, 221(1):13–22, 2007.

[47] David R Brill and I Dennis Parsons. Three-dimensional finite element analysis in airport pavement design. *International Journal of Geomechanics*, 1(3):273–290, 2001.

[48] Yuanqiang Cai, Honglei Sun, and Changjie Xu. Steady state responses of poroelastic half-space soil medium to a moving rectangular load. *International Journal of Solids and Structures*, 44(22-23):7183–7196, 2007.

[49] Yuanqiang Cai, Honglei Sun, and Changjie Xu. Response of railway track system on poroelastic half-space soil medium subjected to a moving train load. *International Journal of Solids and Structures*, 45(18-19):5015–5034, 2008.

[50] Ivo Calio and Annalisa Greco. Free vibrations of timoshenko beam-columns on pasternak foundations. *Journal of Vibration and Control*, 19(5):686–696, 2013.

[51] Zhigang Cao and Anders Boström. Dynamic response of a poroelastic half-space to accelerating or decelerating trains. *Journal of Sound and Vibration*, 332(11):2777–2794, 2013.

[52] Zhigang Cao and Yuanqiang Cai. Isolation of train-induced ground-borne vibration by trenches on a poroelastic half-space. *Journal of Engineering Mechanics*, 139(5):580–593, 2013.

[53] MD Capron and FW Williams. Exact dynamic stiffnesses for an axially loaded uniform timoshenko member embedded in an elastic medium. *Journal of sound and vibration*, 124(3):453–466, 1988.

[54] Z Celep. In-plane vibrations of circular rings on a tensionless foundation. *Journal of sound and vibration*, 143(3):461–471, 1990.

[55] Z Celep and K Güler. Axisymmetric forced vibrations of an elastic free circular plate on a tensionless two parameter foundation. *Journal of Sound and Vibration*, 301(3-5):495–509, 2007.

[56] K Chahour, G Lefeuve-Mesgouez, A Mesgouez, and B Safi. Influence of the railway track components on the dynamic response of a layer resting on a half-space. *International Multidisciplinary Scientific GeoConference: SGEM*, 17(1.4):189–196, 2017.

[57] CS Chang and JM Duncan. Consolidation analysis for partly saturated clay by using an elastic–plastic effective stress–strain model. *International Journal for Numerical and Analytical Methods in Geomechanics*, 7(1):39–55, 1983.

[58] Jen-San Chen and Yung-Kan Chen. Steady state and stability of a beam on a damped tensionless foundation under a moving load. *International Journal of Non-Linear Mechanics*, 46(1):180–185, 2011.

[59] Yuyan Chen, Niki D Beskou, and Jiang Qian. Dynamic response of an elastic plate on a cross-anisotropic poroelastic half-plane to a load moving on its surface. *Soil Dynamics and Earthquake Engineering*, 107:292–302, 2018.

[60] Alexander H-D Cheng. *Poroelasticity*, volume 27. Springer, 2016.

[61] Meshack Chiwanga and AJ Valsangkar. Generalized beam element on two-parameter elastic foundation. *Journal of Structural Engineering*, 114(6):1414–1430, 1988.

[62] Anil K Chopra. Dynamics of structures: Theory and applications to earthquake engineering, prentice hall. *Inc., Upper Saddle River, NJ*, 1995.

[63] Anil K Chopra. *Dynamics of structures*. Pearson Education India, 2007.

[64] Donald P Coduto. Foundation design. *Pomona, California State Polytechnic University*, 1994.

[65] Enrico Conte and Antonello Troncone. Nonlinear consolidation of thin layers subjected to time-dependent loading. *Canadian Geotechnical Journal*, 44(6):717–725, 2007.

[66] İ Coşkun. The response of a finite beam on a tensionless pasternak foundation subjected to a harmonic load. *European Journal of Mechanics-A/Solids*, 22(1):151–161, 2003.

[67] Pedro Alves Costa, Aires Colaço, Rui Calçada, and António Silva Cardoso. Critical speed of railway tracks. detailed and simplified approaches. *Transportation Geotechnics*, 2:30–46, 2015.

[68] Ayse T Daloglu and CV Girija Vallabhan. Values of k for slab on winkler foundation. *Journal of Geotechnical and Geoenvironmental Engineering*, 126(5):463–471, 2000.

[69] Mehmet Baris Darendeli. *Development of a new family of normalized modulus reduction and material damping curves*. The university of Texas at Austin, 2001.

[70] Robert W Day. *Foundation engineering handbook: design and construction with the 2009 international building code*. McGraw-Hill Education, 2010.

[71] Fabio De Angelis and Donato Cancellara. On the influence of the elastic medium stiffness in the buckling behavior of compressed beams on elastic foundation. In *Applied Mechanics and Materials*, volume 166, pages 776–783. Trans Tech Publ, 2012.

[72] MA De Rosa. Free vibrations of timoshenko beams on two-parameter elastic foundation. *Computers & structures*, 57(1):151–156, 1995.

[73] Arindam Dey and Prabir Kr Basudhar. Parameter estimation of four-parameter viscoelastic burger model by inverse analysis: case studies of four oil-refineries. *Interaction and multiscale mechanics*, 5(3):211–228, 2012.

[74] Honggui Di, Shunhua Zhou, Zhe Luo, Chao He, Junhua Xiao, and Xue Li. A vehicle-track-tunnel-soil model for evaluating the dynamic response of a double-line metro tunnel in a poroelastic half-space. *Computers and Geotechnics*, 101:245–263, 2018.

[75] Hu Ding, Yan Yang, Li-Qun Chen, and Shao-Pu Yang. Vibration of vehicle–pavement coupled system based on a timoshenko beam on a nonlinear foundation. *Journal of Sound and Vibration*, 333(24):6623–6636, 2014.

[76] Ricardo Dobry. Dynamic properties and seismic response of soft clay deposits. In *Proc. of the Int. Symp. on Geotech. Engrg. of Soft Soils*, volume 2, pages 51–86. Sociedad Mexicana de Mecanica de suelos, 1987.

[77] Ricardo Dobry, RS Ladd, Felix Y Yokel, Riley M Chung, and D Powell. *Prediction of pore water pressure buildup and liquefaction of sands during earthquakes by the cyclic strain method*, volume 138. National Bureau of Standards Gaithersburg, MD, 1982.

[78] J Michael Duncan. Limitations of conventional analysis of consolidation settlement. *Journal of geotechnical engineering*, 119(9):1333–1359, 1993.

[79] James M Duncan and Chin-Yung Chang. Nonlinear analysis of stress and strain in soils. *Journal of the soil mechanics and foundations division*, 96(5):1629–1653, 1970.

[80] J Dundurs and M Hetényi. The elastic plane with a circular insert, loaded by a radial force. *Journal of Applied Mechanics*, 28(1):103, 1961.

[81] Sekhar Chandra Dutta and Rana Roy. A critical review on idealization and modeling for interaction among soil–foundation–structure system. *Computers & structures*, 80(20-21):1579–1594, 2002.

[82] Ini B Edem. The exact two-node timoshenko beam finite element using analytical bending and shear rotation interdependent shape functions. *International Journal for Computational Methods in Engineering Science and Mechanics*, 7(6):425–431, 2006.

[83] M Eisenberger. Vibration frequencies for beams on variable one-and two-parameter elastic foundations. *Journal of Sound and Vibration*, 176(5):577–584, 1994.

[84] M El-Mously. Fundamental frequencies of timoshenko beams mounted on pasternak foundation. *Journal of Sound and Vibration*, 228(2):452–457, 1999.

[85] Hesham Elhuni and Dipanjan Basu. Dynamic response of simply supported beams on two-parameter foundations. In *19th International Conference on Soil Mechanics and Geotechnical Engineering, ICSMGE 2017*, 2017.

[86] Hesham Elhuni and Dipanjan Basu. Dynamic soil structure interaction model for beams on viscoelastic foundations subjected to oscillatory and moving loads. *Computers and Geotechnics*, 115:103157, 2019.

[87] Hesham Elhuni and Dipanjan Basu. Novel nonlinear dynamic beam–foundation interaction model. *Journal of Engineering Mechanics*, 147(4):04021012, 2021.

[88] Hesham Elhuni and Dipanjan Basu. Interaction of beams with consolidating nonlinear poroelastic layered soil. *Journal of Engineering Mechanics*, 148(3):04021167, 2022.

[89] Hesham Elhuni, Bipin K Gupta, and Dipanjan Basu. A new analysis of circular raft on layered elastic soil. In *Geo-Congress 2019: Foundations*, pages 509–520. American Society of Civil Engineers Reston, VA, 2019.

[90] Coenraad Esveld and Coenraad Esveld. *Modern railway track*, volume 385. MRT-productions Zaltbommel, 2001.

[91] Martin Fahey and John P Carter. A finite element study of the pressuremeter test in sand using a nonlinear elastic plastic model. *Canadian Geotechnical Journal*, 30(2):348–362, 1993.

[92] MM Filonenko-Borodich. A very simple model of an elastic foundation capable of spreading the load. *Sb. Tr. Mosk. Elektro. Inst. Inzh. Trans*, 53, 1945.

[93] Z Friedman and John B Kosmatka. An improved two-node timoshenko beam finite element. *Computers & structures*, 47(3):473–481, 1993.

[94] L Frỳba, S Nakagiri, and N Yoshikawa. Stochastic finite elements for a beam on a random foundation with uncertain damping under a moving force. *Journal of sound and vibration*, 163(1):31–45, 1993.

[95] Ladislav Frỳba. *Vibration of solids and structures under moving loads*, volume 1. Springer science & business media, 2013.

[96] Vivek Garg and MS Hora. A review on interaction behaviour of structure-foundation-soil system. *system*, 2(6), 2012.

[97] CV Girija Vallabhan and YC Das. Modified vlasov model for beams on elastic foundations. *Journal of geotechnical engineering*, 117(6):956–966, 1991.

[98] MI Gorbunov-Posadov. Beams and plates on elastic foundation. *Gostroiizdat, Moscow*, 1949.

[99] DV Griffiths and G Bee. Analytical and numerical observations on the hetenyi solution for buckling of beams on elastic foundations. *Journal of Engineering Mechanics*, 141(1):06014014, 2015.

[100] F Gruttmann and W Wagner. Shear correction factors in timoshenko's beam theory for arbitrary shaped cross-sections. *Computational mechanics*, 27(3):199–207, 2001.

[101] Kadir Güler. Circular elastic plate resting on tensionless pasternak foundation. *Journal of engineering mechanics*, 130(10):1251–1254, 2004.

[102] S Haldar and D Basu. Analysis of beams on heterogeneous and nonlinear soil. *International Journal of Geomechanics*, 16(4):04016004, 2016.

[103] Bing Han, Jianwen Liang, Jia Fu, and Run Liu. 3d dynamic soil-structure interaction in layered, fluid-saturated, poroelastic half-space. *Soil Dynamics and Earthquake Engineering*, 120:113–126, 2019.

[104] Chad W Harden and Tara C Hutchinson. Beam-on-nonlinear-winkler-foundation modeling of shallow, rocking-dominated footings. *Earthquake Spectra*, 25(2):277–300, 2009.

[105] Bobby O Hardin and Vincent P Drnevich. Shear modulus and damping in soils: design equations and curves. *Journal of the Soil mechanics and Foundations Division*, 98(7):667–692, 1972.

[106] Xiping He, Manqing Xu, Xiaoqiang Huang, and Zhaoting Yang. Dynamic interaction between the infinite beam and the the saturated poro-elastic soil foundation due to moving loads. In *2014 International Conference on Mechatronics, Electronic, Industrial and Control Engineering (MEIC-14)*, pages 1330–1333. Atlantis Press, 2014.

[107] M Hetenyi. Beams on elastic foundations. the university of michigan press. *Ann Arbor, Michigan*, 1946.

[108] T Hong, JG Teng, and YF Luo. Axisymmetric shells and plates on tensionless elastic foundations. *International Journal of Solids and Structures*, 36(34):5277–5300, 1999.

[109] A. Hornberg. *Handbook of machine foundation*. John Wiley & Sons, 2006.

[110] Zdzislaw Hryniewicz. Dynamics of rayleigh beam on nonlinear foundation due to moving load using adomian decomposition and coiflet expansion. *Soil Dynamics and Earthquake Engineering*, 31(8):1123–1131, 2011.

[111] Yu-Jia Hu, Yuan-Yuan Zhu, and Chang-Jun Cheng. Dqm for dynamic response of fluid-saturated visco-elastic porous media. *International Journal of Solids and Structures*, 46(7-8):1667–1675, 2009.

[112] Izzat M Idriss, Ricardo Dobry, and Ram D Singh. Nonlinear behavior of soft clays during cyclic loading. *Journal of the Geotechnical Engineering Division*, 104(12):1427–1447, 1978.

[113] Isao Ishibashi and Xinjian Zhang. Unified dynamic shear moduli and damping ratios of sand and clay. *Soils and foundations*, 33(1):182–191, 1993.

[114] Subrat Kumar Jena, Snehashish Chakraverty, and Mohammad Malikan. Application of shifted chebyshev polynomial-based rayleigh–ritz method and navier's technique for vibration analysis of a functionally graded porous beam embedded in kerr foundation. *Engineering with Computers*, 37(4):3569–3589, 2021.

[115] Bo Jin. Dynamic displacements of an infinite beam on a poroelastic half space due to a moving oscillating load. *Archive of Applied Mechanics*, 74(3):277–287, 2004.

[116] R Jones and J Xenophontos. The vlasov foundation model. *International Journal of Mechanical Sciences*, 19(6):317–323, 1977.

[117] P Castro Jorge, A Pinto da Costa, and FMF Simões. Finite element dynamic analysis of finite beams on a bilinear foundation under a moving load. *Journal of Sound and Vibration*, 346:328–344, 2015.

[118] P Castro Jorge, FMF Simões, and A Pinto Da Costa. Dynamics of beams on non-uniform nonlinear foundations subjected to moving loads. *Computers & Structures*, 148:26–34, 2015.

[119] Alev Kacar, H Tugba Tan, and Metin O Kaya. Free vibration analysis of beams on variable winkler elastic foundation by using the differential transform method. *Mathematical and Computational Applications*, 16(3):773–783, 2011.

[120] S Kaewunruen and AM Remennikov. Dynamic properties of railway track and its components: recent findings and future research direction. *Insight-Non-Destructive Testing and Condition Monitoring*, 52(1):20–22, 2010.

[121] MH Kargarnovin and D Younesian. Dynamics of timoshenko beams on pasternak foundation under moving load. *Mechanics research communications*, 31(6):713–723, 2004.

[122] MH Kargarnovin, D Younesian, DJ Thompson, and CJC Jones. Response of beams on nonlinear viscoelastic foundations to harmonic moving loads. *Computers & Structures*, 83(23-24):1865–1877, 2005.

[123] Eduardo Kausel and José Manuel Roësset. Stiffness matrices for layered soils. *Bulletin of the seismological Society of America*, 71(6):1743–1761, 1981.

[124] PE Kavitha, KS Beena, and KP Narayanan. A review on soil–structure interaction analysis of laterally loaded piles. *Innovative Infrastructure Solutions*, 1:1–15, 2016.

[125] AD KERR. Elastic and viscoelastic foundation models. *J. of Applied Mechanics*, 31, 1964.

[126] Arnold D Kerr. *Fundamentals of railway track engineering*. 2003.

[127] Arnold D Kerr and Douglas W Coffin. Beams on a two-dimensional pasternak base subjected to loads that cause lift-off. *International journal of solids and structures*, 28(4):413–422, 1991.

[128] Behrooz Keshtegar, Mohsen Motezaker, Reza Kolahchi, and Nguyen-Thoi Trung. Wave propagation and vibration responses in porous smart nanocomposite sandwich beam resting on kerr foundation considering structural damping. *Thin-Walled Structures*, 154:106820, 2020.

[129] Jueun Kim and APS Selvadurai. A note on the consolidation settlement of a rigid circular foundation on a poroelastic halfspace. *International Journal for Numerical and Analytical Methods in Geomechanics*, 40(14):2003–2016, 2016.

[130] Pyol Kim, Yong-Gun Kim, Chung-Hyok Paek, and Jun Ma. Lattice boltzmann method for consolidation analysis of saturated clay. *Journal of Ocean Engineering and Science*, 4(3):193–202, 2019.

[131] Seong-Min Kim and Jose M Roesset. Dynamic response of a beam on a frequency-independent damped elastic foundation to moving load. *Canadian Journal of Civil Engineering*, 30(2):460–467, 2003.

[132] Sunita Kumari, Pragyan P Sahoo, VA Sawant, et al. Dynamic response of railway track using two parameter model. *International Journal of Science and Engineering Applications*, 1(2):143–147, 2012.

[133] Anneke Labuschagne, NF Janse van Rensburg, and AJ2480028 Van der Merwe. Comparison of linear beam theories. *Mathematical and Computer Modelling*, 49(1-2):20–30, 2009.

[134] Yew Chin Lai, Bing Yuan Ting, Woon-Sung Lee, and Bryan R Becker. Dynamic response of beams on elastic foundation. *Journal of Structural Engineering*, 118(3):853–858, 1992.

[135] HP Lee. Dynamic response of a timoshenko beam on a winkler foundation subjected to a moving mass. *Applied Acoustics*, 55(3):203–215, 1998.

[136] Jin Ho Lee, Jae Kwan Kim, and John L Tassoulas. Dynamic analysis of a layered halfspace subjected to moving line loads. *Soil Dynamics and Earthquake Engineering*, 47:16–31, 2013.

[137] Gaëlle Lefeuve-Mesgouez and Arnaud Mesgouez. Three-dimensional dynamic response of a porous multilayered ground under moving loads of various distributions. *Advances in Engineering Software*, 46(1):75–84, 2012.

[138] Xiaoyan LEI. *High speed railway track dynamics*. Springer, 2022.

[139] Dingqing Li, James Hyslip, Ted Sussmann, and Steven Chrismer. *Railway geotechnics*. CRC Press, 2015.

[140] Dingqing Li and Ernest T Selig. Method for railroad track foundation design. i: Development. *Journal of geotechnical and geoenvironmental engineering*, 124(4):316–322, 1998.

[141] Dingqing Li and ET Selig. Evaluation of railway subgrade problems. *Transportation research record*, 1489:17, 1995.

[142] Dingqing Li and Stephen Wilk. Recent studies on railway-track substructure at ttci. *Transportation Safety and Environment*, 3(1):36–49, 2021.

[143] S-R Li and RC Batra. Thermal buckling and postbuckling of euler-bernoulli beams supported on nonlinear elastic foundations. *AIAA journal*, 45(3):712–720, 2007.

[144] Xiaojiao Li, Fuyou Xu, and Zhe Zhang. Symplectic eigenvalue analysis method for bending of beams resting on two-parameter elastic foundations. *Journal of Engineering Mechanics*, 143(9):04017098, 2017.

[145] Xiaojiao Li, Fuyou Xu, and Zhe Zhang. Symplectic method for natural modes of beams resting on elastic foundations. *Journal of Engineering Mechanics*, 144(4):04018009, 2018.

[146] Xudong Li and Sai K Vanapalli. Simulation of progressive shear failure in railway foundation. *Transportation Geotechnics*, 29:100550, 2021.

[147] Robert Y Liang and JX Zhu. Dynamic analysis of infinite beam on modified vlasov subgrade. *Journal of transportation engineering*, 121(5):434–442, 1995.

[148] Leonid Libkin. *Elements of finite model theory*, volume 41. Springer, 2004.

[149] Suchart Limkatanyu, Woraphot Prachasaree, Nattapong Damrongwiriyanupap, Minho Kwon, and Wooyoung Jung. Exact stiffness for beams on kerr-type foundation: the virtual force approach. *Journal of applied mathematics*, 2013, 2013.

[150] Gao Lin, Zejun Han, and Jianbo Li. An efficient approach for dynamic impedance of surface footing on layered half-space. *Soil Dynamics and Earthquake Engineering*, 49:39–51, 2013.

[151] Y-H Lin and MW Trethewey. Finite element analysis of elastic beams subjected to moving dynamic loads. *Journal of sound and vibration*, 136(2):323–342, 1990.

[152] Jinyu Liu, Ruiyun Jiao, Jing Wang, Zhendong Yang, and Kaiyun Zhan. Propagation dynamics of cosh-airy beams in kerr nonlinear media. *Journal of Nonlinear Optical Physics & Materials*, 28(03):1950030, 2019.

[153] Qijian Liu and Jianjun Ma. Analytical model for beams on elastic foundations considering the coupling of horizontal and vertical displacements. *Journal of Engineering Mechanics*, 139(12):1757–1768, 2013.

[154] Domenico Lombardi, Subhamoy Bhattacharya, and David Muir Wood. Dynamic soil–structure interaction of monopile supported wind turbines in cohesive soil. *Soil dynamics and earthquake engineering*, 49:165–180, 2013.

[155] Chunfang Lu and Chaoxun Cai. Overview on safety management and maintenance of high-speed railway in china. *Transportation Geotechnics*, 25:100397, 2020.

[156] Zheng Lu, Ran Fang, Hailin Yao, Zhi Hu, Jie Liu, et al. Evaluation and analysis of the traffic load–induced settlement of roads on soft subsoils with low embankments. *Int. J. Geomech*, 18(6):04018043, 2018.

[157] Jianjun Ma, Fengjun Liu, Mengqiang Nie, and Junbo Wang. Nonlinear free vibration of a beam on winkler foundation with consideration of soil mass motion of finite depth. *Nonlinear Dynamics*, 92(2):429–441, 2018.

[158] X Ma, JW Butterworth, and GC Clifton. Static analysis of an infinite beam resting on a tensionless pasternak foundation. *European Journal of Mechanics-A/Solids*, 28(4):697–703, 2009.

[159] XH Ma, Yung Ming Cheng, SK Au, YQ Cai, and CJ Xu. Rocking vibration of a rigid strip footing on saturated soil. *Computers and Geotechnics*, 36(6):928–933, 2009.

[160] Tutorial Manual. Plaxis 2d. *Deft University of Technology & PLAXIS, Netherlands*, 2016.

[161] H Matsunaga. Vibration and buckling of deep beam-columns on two-parameter elastic foundations. *Journal of sound and vibration*, 228(2):359–376, 1999.

[162] Eleni Minga and HJ Burd. Validation of the plaxis modeto 1d model for dense sand, 2019.

[163] SC Mohanty, RR Dash, and T Rout. Parametric instability of a functionally graded timoshenko beam on winkler's elastic foundation. *Nuclear Engineering and Design*, 241(8):2698–2715, 2011.

[164] Jacques Monnet. Numerical validation of an elastoplastic formulation of the conventional limit pressure measured with the pressuremeter test in cohesive soil. *Journal of Geotechnical and Geoenvironmental Engineering*, 133(9):1119–1127, 2007.

[165] Konstantinos Morfidis and IE Avramidis. Generalized beam-column finite element on two-parameter elastic foundation. *Structural engineering and mechanics: An international journal*, 21(5):519–537, 2005.

[166] Alan Morris. *A practical guide to reliable finite element modelling*. John Wiley & Sons, 2008.

[167] Zissimos P Mourelatos and Michael G Parsons. A finite element analysis of beams on elastic foundation including shear and axial effects. *Computers & structures*, 27(3):323–331, 1987.

[168] JS Mundrey. *Railway track engineering*. McGraw-Hill Education, 2009.

[169] Lohitkumar S Nainegali, Prabir Kumar Basudhar, and Priyanka Ghosh. Interference of two asymmetric closely spaced strip footings resting on nonhomogeneous and linearly elastic soil bed. *International Journal of Geomechanics*, 13(6):840–851, 2013.

[170] BABATOPE Omolofe. Deflection profile analysis of beams on two-parameter elastic subgrade. *Latin American Journal of Solids and Structures*, 10:263–282, 2013.

[171] K Ono and M Yamada. Analysis of railway track vibration. *Journal of sound and vibration*, 130(2):269–297, 1989.

[172] AS Osman, DJ White, AM Britto, and MD Bolton. Simple prediction of the undrained displacement of a circular surface foundation on non-linear soil. *Géotechnique*, 57(9):729–737, 2007.

[173] Korhan Ozgan. Dynamic analysis of thick plates including deep beams on elastic foundations using modified vlasov model. *Shock and Vibration*, 20(1):29–41, 2013.

[174] Aydın Özmutlu. Response of a finite beam on a tensionless pasternak foundation under symmetric and asymmetric loading. *Structural Engineering and Mechanics*, 30(1):21–36, 2008.

[175] Duhee Park and Youssef MA Hashash. Soil damping formulation in nonlinear time domain site response analysis. *Journal of Earthquake Engineering*, 8(02):249–274, 2004.

[176] S Parkash and VJ Puri. Foundations for machines: Analysis and design. *A Wily-Inter Science Publication*, 1988.

[177] PL Pasternak. On a new method of analysis of an elastic foundation by means of two-constants [dissertation]. *Moscow, USSR: Gosudarstvennoe Izdatelstvo Literaturi po Stroitelstvu I Arkhitecture*, 1954.

[178] VA Patil, Vishwas Abhimanyu Sawant, and Kousik Deb. 3d finite-element dynamic analysis of rigid pavement using infinite elements. *International Journal of Geomechanics*, 13(5):533–544, 2013.

[179] Win Pe. *Beam on poroelastic foundation*. PhD thesis, Texas Tech University, 1995.

[180] SE Perkins, LV Alexander, and JR Nairn. Increasing frequency, intensity and duration of observed global heatwaves and warm spells. *Geophysical Research Letters*, 39(20), 2012.

[181] PK Pradhan, A Mandal, DK Baidya, and DP Ghosh. Dynamic response of machine foundation on layered soil: cone model versus experiments. *Geotechnical and geological engineering*, 26:453–468, 2008.

[182] Jean H Prevost. Wave propagation in fluid-saturated porous media: an efficient finite element procedure. *International Journal of Soil Dynamics and Earthquake Engineering*, 4(4):183–202, 1985.

[183] VS Protsenko and VL Rvachev. Plate in the form of an infinite strip on an elastic half-space: Pmm vol. 40, n 2, 1976, pp. 298–305. *Journal of Applied Mathematics and Mechanics*, 40(2):273–280, 1976.

[184] Ioannis G Raftoyiannis, Tassos P Avraam, and George T Michaltsos. A new approach for loads moving on infinite beams resting on elastic foundation. *Journal of Vibration and Control*, 18(12):1828–1836, 2012.

[185] Sunita Rani, Raman Kumar, and Sarva Jit Singh. Consolidation of an anisotropic compressible poroelastic clay layer by axisymmetric surface loads. *International Journal of Geomechanics*, 11(1):65–71, 2011.

[186] John William Strutt Baron Rayleigh. *The theory of sound*, volume 2. Macmillan & Company, 1896.

[187] Junuthula Narasimha Reddy. *Energy and variational methods in applied mechanics: with an introduction to the finite element method*. Wiley New York, 1984.

[188] Lymon C Reese, William M Isenhower, and Shin-Tower Wang. *Analysis and design of shallow and deep foundations*, volume 10. John Wiley & Sons, 2005.

[189] E Reissner. Stationary, axially symmetric vibrations of a homogeneous elastic halfspace excited by a vibrating mass. *Arch Appl Mech*, 7(6):381–96, 1936.

[190] Eric Reissner. Symmetric bending of shallow shells of revolution. *Journal of Mathematics and Mechanics*, pages 121–140, 1958.

[191] Alex M Remennikov and Sakdirat Kaewunruen. A review of loading conditions for railway track structures due to train and track vertical interaction. *Structural Control and Health Monitoring: The Official Journal of the International Association for Structural Control and Monitoring and of the European Association for the Control of Structures*, 15(2):207–234, 2008.

[192] John R Rice and Ronald F Boisvert. From scientific software libraries to problem-solving environments. *IEEE Computational Science and Engineering*, 3(3):44–53, 1996.

[193] Cristiano Rodrigues, Fernando MF Simões, A Pinto da Costa, Diego Froio, and Egidio Rizzi. Finite element dynamic analysis of beams on nonlinear elastic foundations under a moving oscillator. *European Journal of Mechanics-A/Solids*, 68:9–24, 2018.

[194] J Ryue, DJ Thompson, PR White, and DR Thompson. Investigations of propagating wave types in railway tracks at high frequencies. *Journal of Sound and Vibration*, 315(1-2):157–175, 2008.

[195] Javad Sadeghi, Hajar Heydari, and Elaheh Amiri Doloei. Improvement of railway maintenance approach by developing a new railway condition index. *Journal of Transportation Engineering, Part A: Systems*, 143(8):04017037, 2017.

[196] H Saito and T Terasawa. Steady-state vibrations of a beam on a pasternak foundation for moving loads. *Journal of Applied Mechanics*, 47(4):879, 1980.

[197] Rodrigo Salgado. *The engineering of foundations, slopes and retaining structures.* CRC Press, 2022.

[198] Ranbir S Sandhu and Karl S Pister. A variational principle for linear, coupled field problems in continuum mechanics. *International Journal of Engineering Science*, 8(12):989–999, 1970.

[199] A Santana, JJ Aznarez, LA Padron, and O Maeso. A bem–fem model for the dynamic analysis of building structures founded on viscoelastic or poroelastic soils. *Bulletin of Earthquake Engineering*, 14(1):115–138, 2016.

[200] EJ Sapountzakis and AE Kampitsis. Nonlinear dynamic analysis of timoshenko beam-columns partially supported on tensionless winkler foundation. *Computers & structures*, 88(21-22):1206–1219, 2010.

[201] EJ Sapountzakis and AE Kampitsis. Nonlinear response of shear deformable beams on tensionless nonlinear viscoelastic foundation under moving loads. *Journal of Sound and Vibration*, 330(22):5410–5426, 2011.

[202] EJ Sapountzakis and AE Kampitsis. Inelastic analysis of beams on two-parameter tensionless elastoplastic foundation. *Engineering Structures*, 48:389–401, 2013.

[203] Ronald F Scott. Foundation analysis. Technical report, Prentice-Hall New Jersey, 1981.

[204] Harry Bolton Seed. Soil moduli and damping factors for dynamic response analysis. *EERC*, 1970.

[205] Jackson Sekasi, Asst Prof Berhe, and Tensay Gebremedhin. Railway track substructure failures, a critical literature review. *Railway Track Substructure Failures, a Critical Literature Review (April 20, 2021)*, 2021.

[206] Antony PS Selvadurai. *Elastic analysis of soil-foundation interaction*. Elsevier, 2013.

[207] APS Selvadurai and Li Shi. Biot's problem for a biot material. *International Journal of Engineering Science*, 97:133–147, 2015.

[208] T Senjuntichai, S Mani, and RKND Rajapakse. Vertical vibration of an embedded rigid foundation in a poroelastic soil. *Soil Dynamics and Earthquake Engineering*, 26(6-7):626–636, 2006.

[209] Teerapong Senjuntichai, Suraparb Keawsawasvong, and RKND Rajapakse. Vertical vibration of a circular foundation in a transversely isotropic poroelastic soil. *Computers and Geotechnics*, 122:103550, 2020.

[210] X Sheng, CJC Jones, and M Petyt. Ground vibration generated by a harmonic load acting on a railway track. *Journal of sound and vibration*, 225(1):3–28, 1999.

[211] Li Shi and APS Selvadurai. Dynamic response of an infinite beam supported by a saturated poroelastic halfspace and subjected to a concentrated load moving at a constant velocity. *International Journal of Solids and Structures*, 88:35–55, 2016.

[212] LM Shirima and MW Giger. Timoshenko beam element resting on two-parameter elastic foundation. *Journal of engineering mechanics*, 118(2):280–295, 1992.

[213] Raj Siddharthan, Zia Zafir, and Gary M Norris. Moving load response of layered soil. i: Formulation. *Journal of engineering mechanics*, 119(10):2052–2071, 1993.

[214] Scott A Simson, Luis Ferreira, and Martin H Murray. Rail track maintenance planning: An assessment model. *Transportation Research Record*, 1713(1):29–35, 2000.

[215] TG Sitharam. *Advanced foundation engineering*. Taylor & Francis, a CRC title, part of the Taylor & Francis imprint, a ..., 2018.

[216] Hari M Srivastava and Robert G Buschman. *Theory and applications of convolution integral equations*, volume 79. Springer Science & Business Media, 2013.

[217] Honglei Sun, Yimin Yang, Li Shi, and Xueyu Geng. The equivalent stiffness of a saturated poroelastic halfspace interacting with an infinite beam under a moving point load. *Soil Dynamics and Earthquake Engineering*, 107:83–95, 2018.

[218] Lu Sun and Feiquan Luo. Steady-state dynamic response of a bernoulli–euler beam on a viscoelastic foundation subject to a platoon of moving dynamic loads. *Journal of Vibration and Acoustics*, 130(5), 2008.

[219] Iancu-Bogdan Teodoru and Vasile Muşat. The modified vlasov foundation model: an attractive approach for beams resting on elastic supports. *EJGE*, 15:1–13, 2010.

[220] Karl Terzaghi. Evalution of conefficients of subgrade reaction. *Geotechnique*, 5(4):297–326, 1955.

[221] Karl Terzaghi, Ralph B Peck, and Gholamreza Mesri. *Soil mechanics in engineering practice*. John Wiley & Sons, 1996.

[222] Enrico Tezzon, Nerio Tullini, and Fabio Minghini. Static analysis of shear flexible beams and frames in adhesive contact with an isotropic elastic half-plane using a coupled fe–bie model. *Engineering Structures*, 104:32–50, 2015.

[223] David Thambiratnam and Yan Zhuge. Dynamic analysis of beams on an elastic foundation subjected to moving loads. *Journal of sound and vibration*, 198(2):149–169, 1996.

[224] Stephen Timoshenko. *History of strength of materials: with a brief account of the history of theory of elasticity and theory of structures*. Courier Corporation, 1983.

[225] Stephen P Timoshenko. Lxvi. on the correction for shear of the differential equation for transverse vibrations of prismatic bars. *The London, Edinburgh, and Dublin Philosophical Magazine and Journal of Science*, 41(245):744–746, 1921.

[226] Bing Y Ting and Eldon F Mockry. Beam on elastic foundation finite element. *Journal of Structural Engineering*, 110(10):2324–2339, 1984.

[227] S Tirnoshenko, DH Young, and W Weaver. Vibration problems in engineering, 1974.

[228] VN Tishchenko. Models of layer deformation of an elastic half space. *Journal of Soviet Mathematics*, 65(1):1396–1402, 1993.

[229] Maria I Todorovska and Yousef Al Rjoub. Plain strain soil–structure interaction model for a building supported by a circular foundation embedded in a poroelastic half-space. *Soil Dynamics and Earthquake Engineering*, 26(6-7):694–707, 2006.

[230] Chris Tofallis. A better measure of relative prediction accuracy for model selection and model estimation. *Journal of the Operational Research Society*, 66(8):1352–1362, 2015.

[231] AM Trochanis, R Chelliah, and J Bielak. Unified approach for beams on elastic foundations under moving loads. *Journal of geotechnical engineering*, 113(8):879–895, 1987.

[232] Nien-chien Tsai and Russell A Westmann. Beam on tensionless foundation. *Journal of the Engineering Mechanics Division*, 93(5):1–12, 1967.

[233] GC Tsiatas. Nonlinear analysis of non-uniform beams on nonlinear elastic foundation. *Acta Mechanica*, 209(1):141–152, 2010.

[234] Edward Tsudik. *Analysis of structures on elastic foundations*. J. Ross Publishing, 2012.

[235] Nerio Tullini and Antonio Tralli. Static analysis of timoshenko beam resting on elastic half-plane based on the coupling of locking-free finite elements and boundary integral. *Computational Mechanics*, 45(2):211–225, 2010.

[236] Ayse Turhan. *A consistent Vlasov model for analysis of plates on elastic foundations using the finite element method*. PhD thesis, Texas Tech University, 1992.

[237] Katarína Tvrdá. Foundation plate on the elastic half-space, deterministic and probabilistic approach. In *MATEC web of conferences*, volume 107, page 00058. EDP Sciences, 2017.

[238] Kristianto Usman, Michael Burrow, and Gurmel Ghataora. Railway track subgrade failure mechanisms using a fault chart approach. *Procedia Engineering*, 125:547–555, 2015.

[239] Rajib Ul Alam Uzzal, Rama B Bhat, and Waiz Ahmed. Dynamic response of a beam subjected to moving load and moving mass supported by pasternak foundation. *Shock and Vibration*, 19(2):201–216, 2012.

[240] CV Vallabhan and YC Das. Beams on elastic foundations: a new approach. In *Foundation engineering: Current principles and practices*, pages 613–624. ASCE, 1989.

[241] CV Girija Vallabhan and A Turhan Daloglu. Consistent fem-vlasov model for plates on layered soil. *Journal of Structural Engineering*, 125(1):108–113, 1999.

[242] CV Girija Vallabhan and YC Das. A refined model for beams on elastic foundations. *International Journal of Solids and Structures*, 27(5):629–637, 1991.

[243] JN Varandas, A Paixão, E Fortunato, B Zuada Coelho, and P Hölscher. Long-term deformation of railway tracks considering train-track interaction and non-linear resilient behaviour of aggregates–a 3d fem implementation. *Computers and Geotechnics*, 126:103712, 2020.

[244] Paul J Vardanega and Malcolm D Bolton. Stiffness of clays and silts: Normalizing shear modulus and shear strain. *Journal of Geotechnical and Geoenvironmental Engineering*, 139(9):1575–1589, 2013.

[245] Aleksandar B Vesić. Bending of beams resting on isotropic elastic solid. *Journal of the Engineering Mechanics Division*, 87(2):35–53, 1961.

[246] Gregor Vilhar, Anita Laera, Federico Foria, Abhishek Gupta, and Ronald BJ Brinkgreve. Implementation, validation, and application of pm4sand model in plaxis. In *Geotechnical Earthquake Engineering and Soil Dynamics V: Numerical Modeling and Soil Structure Interaction*, pages 200–211. American Society of Civil Engineers Reston, VA, 2018.

[247] Vasilii Zakharovich Vlasov. Beams, plates and shells on elastic foundations. *Israel Program for Scientific Translations, Jerusalem*, 1966.

[248] Mladen Vucetic and Ricardo Dobry. Effect of soil plasticity on cyclic response. *Journal of geotechnical engineering*, 117(1):89–107, 1991.

[249] Chenting Wang and Bin Zhen. The study for the influence of nonlinear foundation on responses of a beam to a moving load based on volterra integral equations. *Journal of Vibration Engineering & Technologies*, 9(5):939–956, 2021.

[250] GX Wang and J Kuwano. Modeling of strain dependency of shear modulus and damping of clayey sand. *Soil Dynamics and Earthquake Engineering*, 18(6):463–471, 1999.

[251] Lihua Wang, Lujun Wang, and Chunlin Liu. Analytical model for vertical dynamic interaction between circular raft and saturated soils. *International Journal of Geomechanics*, 21(4):06021005, 2021.

[252] YH Wang, LG Tham, and YK Cheung. Beams and plates on elastic foundations: a review. *Progress in Structural Engineering and Materials*, 7(4):174–182, 2005.

[253] Yechiel Weitsman. Onset of separation between a beam and a tensionless elastic foundation under a moving load. *International Journal of Mechanical Sciences*, 13(8):707–711, 1971.

[254] Krzysztof Wilmanski. A few remarks on biot's model and linear acoustics of poroelastic saturated materials. *Soil Dynamics and Earthquake Engineering*, 26(6-7):509–536, 2006.

[255] Emil Winkler. Theory of elasticity and strength, 1867.

[256] Asrat Worku. Winkler's single-parameter subgrade model from the perspective of an improved approach of continuum-based subgrade modeling. *Zede Journal*, 26:11–22, 2009.

[257] Asrat Worku. Calibrated analytical formulas for foundation model parameters. *International Journal of Geomechanics*, 13(4):340–347, 2013.

[258] Bin Xu, Jian-Fei Lu, and Jian-Hua Wang. Dynamic response of an infinite beam overlying a layered poroelastic half-space to moving loads. *Journal of Sound and Vibration*, 306(1-2):91–110, 2007.

[259] MH Yas and N Samadi. Free vibrations and buckling analysis of carbon nanotube-reinforced composite timoshenko beams on elastic foundation. *International Journal of Pressure Vessels and Piping*, 98:119–128, 2012.

[260] Jian-Hua Yin. Closed-form solution for reinforced timoshenko beam on elastic foundation. *Journal of Engineering Mechanics*, 126(8):868–874, 2000.

[261] T Yokoyama. Vibration analysis of timoshenko beam-columns on two-parameter elastic foundations. *Computers & Structures*, 61(6):995–1007, 1996.

[262] WANG Yong, KONG Ling-Wei, and WANG Yan-Li. Mechanism and control of subgrade mud pumping under the cyclic load of train. In *2014 International Conference on Mechanics and Civil Engineering (icmce-14)*, pages 369–374. Atlantis Press, 2014.

[263] Davood Younesian, Ali Hosseinkhani, Hassan Askari, and Ebrahim Esmailzadeh. Elastic and viscoelastic foundations: a review on linear and nonlinear vibration modeling and applications. *Nonlinear Dynamics*, 97(1):853–895, 2019.

[264] Yan Yu, Ivan P Damians, and Richard J Bathurst. Influence of choice of flac and plaxis interface models on reinforced soil–structure interactions. *Computers and Geotechnics*, 65:164–174, 2015.

[265] Jabbar Ali Zakeri and He Xia. Application of 2d-infinite beam elements in dynamic analysis of train-track interaction. *Journal of Mechanical Science and Technology*, 23(5):1415–1421, 2009.

[266] Jianfeng Zhang, Ronald D Andrus, and C Hsein Juang. Normalized shear modulus and material damping ratio relationships. *Journal of geotechnical and geoenvironmental engineering*, 131(4):453–464, 2005.

[267] Feng Zhaohua and Robert D Cook. Beam elements on two-parameter elastic foundations. *Journal of Engineering Mechanics*, 109(6):1390–1402, 1983.

[268] Ding Zhou. A general solution to vibrations of beams on variable winkler elastic foundation. *Computers & structures*, 47(1):83–90, 1993.

[269] OC Zienkiewicz, C Emson, and P Bettess. A novel boundary infinite element. *International Journal for Numerical Methods in Engineering*, 19(3):393–404, 1983.